Université de Montréal

Biogenesis of the *C. elegans* germline syncytium: from nucleation to maturation

par
Rana Amini

Programme de Biologie Moléculaire
Faculté de Médicine

Thèse présentée à la Faculté de Médicine
en vue de l'obtention du grade de Doctorat
en Biologie Moléculaire
option Biologie des System

Juillet, 2015

Résumé

La vie commence par la fusion des gamètes pour générer un zygote, dans lequel les constituants à la fois de l'ovocyte et des spermatozoïdes sont partagés au sein d'un syncytium. Le syncytium consiste en des cellules ou tissus dans lesquels des cellules nucléées individuelles distinctes partagent un cytoplasme commun. Alors que l'avantage du syncytium durant la fécondation est tout à fait évident, les syncytia se produisent également dans de nombreux contextes de développement différents dans les plantes, les champignons et dans le règne animal, des insectes aux humains, pour des raisons qui ne sont pas immédiatement évidentes. Par exemple, la lignée germinale de nombreuses espèces de vertébrés et d'invertébrés, des insectes aux humains, présente une structure syncytiale, suggérant que les syncytia constituent des phases conservées de développement de la lignée germinale. Malgré la prévalence commune des syncytia, ces derniers ont cependant confondu les scientifiques depuis des décennies avec des questions telles que la façon dont ils sont formés et maintenus en concurrence avec leurs homologues diploïdes, et quels sont les avantages et les inconvénients qu'ils apportent.

Cette thèse va décrire l'utilisation de la lignée germinale syncytiale de *C. elegans* afin d'approfondir notre compréhension de l'architecture, la fonction et le mode de formation des tissus syncytiaux. Les cellules germinales (CGs) dans la lignée germinale de *C. elegans* sont interconnectées les unes aux autres par l'intermédiaire de structures appelées des anneaux de CG. En utilisant l'imagerie des cellules vivantes, nous avons d'abord analysé l'architecture syncytiale de la lignée germinale au long du développement et démontré que la maturation de l'anneau de CG se produit progressivement au cours de la croissance des larves et que les anneaux de CG sont composés de myosine II, de l'anilline canonique ANI-1, et de la courte isoforme d'anilline ANI-2, qui n'a pas les domaines de liaison à l'actine et à la myosine, depuis le premier stade larvaire, L1. Parmi les composants de l'anneau de CG, ANI-2 est exprimé au cours du développement et exclusivement enrichi entre les deux CGs primordiales (CGPs) au cours de l'embryogenèse de *C. elegans*, indiquant qu'ANI-2 est un composant *bona fide* des anneaux de CG. Nous avons en outre montré que les anneaux de CG sont largement

absents dans les animaux mutants pour *ani-2*, montrant que leur maintien repose sur l'activité d'ANI-2. Contrairement à cela, nous avons trouvé que la déplétion d'ANI-1 a augmenté à la fois le diamètre des anneaux de CG et la largeur du rachis. Fait intéressant, la déplétion d'ANI-1 dans les mutants d'*ani-2* a sauvé les défauts d'anneaux de CG des gonades déficientes en *ani-2*, ce qui suggère que l'architecture syncytiale de la lignée germinale de *C. elegans* repose sur un équilibre de l'activité de ces deux protéines Anilline. En outre, nous avons montré que lors de leur entrée à l'âge adulte, les mutants *ani-2* présentent de sévères défauts de multinucléation des CGs qui découlent de l'effondrement des membranes de séparation des CGs individuelles. Cette multinucléation a coïncidé avec le début de la diffusion cytoplasmique, dont le blocage réduit la multinucléation des gonades mutantes pour *ani-2*, suggérant que les anneaux de CG résistent au stress mécanique associé au processus de diffusion cytoplasmique. En accord avec cela, nous avons trouvé aussi que la gonade peut soutenir la déformation élastique en réponse au stress mécanique et que cette propriété repose sur la malléabilité des anneaux de CGs.

Dans une étude séparée afin de comprendre le mécanisme de formation du syncytium, nous avons suivi la dynamique de division de la cellule précurseur de la lignée germinale, P4 en deux CGP dans l'embryon de *C. elegans*. Nous avons démontré que les CGPs commencent la cytocinèse de manière similaire aux cellules somatiques, en formant un sillon de clivage, qui migre correctement et transforme ainsi l'anneau contractile en anneau de « midbody ring » (MBR), une structure qui relie de manière transitoire les cellules en division. Malgré cela, les CGPs, contrairement à leurs homologues somatiques, ne parviennent pas à accomplir la dernière étape de la cytocinèse, qui est la libération abscission-dépendante du MBR. Au lieu de cela, le MBR persiste à la frontière entre les CGPs en division et subit une réorganisation et une maturation pour se transformer finalement en structures en forme d'anneau qui relient les cellules en division. Nous montrons en outre que les composants du MB/MBR; UNC-59^{Septin}, CYK-7, ZEN-4^{Mklp1}, RHO-1^{RhoA} sont localisés à des anneaux de CG au long du développement de la lignée germinale du stade L1 à l'âge adulte, ce qui suggère que les anneaux de CG sont dérivés des MBR.

Bien qu'il reste encore beaucoup à faire pour comprendre pleinement le mécanisme précis de la formation du syncytium, le maintien, ainsi que la fonction du syncytium, nos résultats appuient un modèle dans lequel la stabilisation du MBR et la cytocinèse incomplète pourraient être une option conservée dans l'évolution pour la formation du syncytium. En outre, notre travail démontre que les régulateurs de la contractilité peuvent jouer un rôle dans la maturation et l'élasticité de l'anneau de CG au cours du développement de la lignée germinale, fournissant un ajout précieux pour une plus ample compréhension de la syncytiogenèse et de sa fonction.

Mots-clés: cytocinèse incomplète, syncytium, lignée germinale de *C. elegans*, anilline, abscission, « midbody », CGP, formation du syncytium

Abstract

Life begins by the union of oocyte and sperm to generate a zygote, in which the constituents of both gametes are shared within a single cytoplasm in a syncytium. Syncytium is referred to cells or tissues wherein discrete single nucleated cells share a common cytoplasm. While the purpose of a syncytium in fertilization is quite evident, syncytia occur in many different developmental settings in plants, fungi and throughout the animal kingdom for reasons that are not immediately obvious. For instance, germline of many vertebrate and invertebrate species, from insects to humans exhibit syncytial structure, suggesting that syncytia are conserved phase of germline development. Despite the common prevalence of syncytia however, syncytia have confounded scientist for decades with questions such as how they are formed and maintained in competition with their diploid counterparts, and what advantages and disadvantages they bear.

This thesis will describe the use of the *C. elegans* syncytial germline to further our understanding of the architecture, function and mode of formation of the syncytial tissues. Germ cells (GCs) in germline of *C. elegans* are interconnected to one another via structures here referred to as GC rings. Using live-cell imaging, we first analyzed the germline syncytial architecture throughout development and demonstrated that GC ring maturation occurs progressively during larval growth and that the GC rings are composed of Myosin II, the canonical anillin ANI-1 and ANI-2 the short isoform of anillin that lacks the actin- and myosin- binding domains, since the first larval stage, L1. Among GC ring components, ANI-2 is developmentally expressed and exclusively enriched between the two primordial GCs (PGCs) during *C. elegans* embryogenesis, indicating that ANI-2 is a *bona fide* component of GC rings. We further showed that the GC rings are largely absent in *ani-2* mutant animals, showing that their maintenance relies on the activity of ANI-2. Contrary to this, we found that ANI-1 depletion increased both the diameter of GC rings and the width of the rachis. Interestingly, depletion of ANI-1 partially rescued the GC ring defects of *ani-2*-deficient gonads, suggesting that the *C. elegans* germline syncytial architecture relies on a balance between activities of these two Anillin proteins. Moreover, we showed that adult *ani-2*

mutants exhibit severe GC multinucleation defects that arise from a collapse of the membranes separating individual GCs. This GC multinucleation initiated at the transition from L4 to adult, which coincided with the onset of oogenesis and cytoplasmic streaming in the rachis. We found that multinucleation is dependent on oogenesis, as GC multinucleation was reduced in conditions where oogenesis was absent. In consistent with this, we further found that the gonad can sustain elastic deformation in response to mechanical stress and that this property relies on malleability of GC rings provided by ANI-2.

In a separate study to understand the mechanism of syncytium formation, we monitored the dynamics of the germline founder cell (P_4) cytokinesis into Z_2 and Z_3 during embryogenesis. We found that P_4 accomplishes the first phase of cytokinesis, cytoplasmic isolation. In support of this, we found that there is no cytoplasmic exchange of a fluorescent marker between Z_2 and Z_3 shortly after birth, suggesting that they are not syncytial at this stage. Interestingly however, P_4 fails to complete the last phase of cytokinesis, abscission wherein the midbody-ring (MBR) is released from the cell-cell boundary and eventually disappears. Instead, the MBR connecting Z_2 and Z_3 remains tightly associated to the cortex throughout embryogenesis, forming a stable structure. Interestingly, we found that components of persisting MBRs are all stable constituents of GC rings of the syncytial gonad, suggesting that GC rings are derived from stabilized MBRs.

While much remains to be done to fully understand the precise mechanism of syncytium formation, maintenance and function, our findings support a model in which MBR stabilization and incomplete cytokinesis could be an evolutionary conserved feature for syncytium formation. In addition, our work demonstrates that contractility regulators may play a role in GC ring maturation and GC ring elasticity during germline development, providing a valuable addition for further understanding syncytiogenesis and its function.

Keywords: abscission, anillin, germline development, incomplete cytokinesis, midbody, syncytiogenesis

Table of Contents

List of Figures and Tables

1. Introduction:

3.1. Article 1:

3.2. Article 2:

4. Discussion:

Tables:

List of abbreviations

ACT-4: ACTin-4

ACT-5: ACTin-5

AHD: Anillin homology domain

AKAP4: A-kinase anchor proteins

ALG-2: Argonaute (plant)-Like Gene

ALIX: ALG-2–interacting protein X (ALIX)

ANI-1: ANIllin-1

ANI-2: ANIllin-2

ANI-3: ANIllin-3

ANK: N-terminal ankyrin repeats

AP: anteroposterior axis

APC: Anaphase promoting complex

ARF6: ADP-ribosylation factor 6

C-terminal: Carboxy-terminal

C. elegans: Caenorhabditis elegans

Cdc42: Cell division control protein 42 homolog

CENP-E: Centromere-associated protein E

CEP55: Centrosomal protein of 55 kDa

CHMP-4B: charged multivesicular body (MVB) protein 4B

CHMP-4C: charged multivesicular body (MVB) protein 4C

CPC: chromosomal passenger complex

CR: Contractile ring

CYK-4: CYtoKinesis defect-4

CYK-7: CYtoKinesis defect-7

DIC: differential interference contrast

DMYPT: Drosophila Myosin Phosphatase Targeting Protein

DNA: Deoxyribonucleic acid

DTC: distal tip cell

ECM: extracellular matrix

ECT-2: epithelial cell transforming 2

ESCRT: endosomal sorting complex required for transport

F-actin: filamentous actin

FCM: fusion-competent myoblasts

fGSCs: female germline stem cells

fli-1: Drosophila FLIghtless

GAP: GTP-ase activating protein

GC: germ cell

GDP: Guanosine triphosphatase

GEF: GDP-GTP Exchange

GEF-H1: GDP-GTP Exchange-H1

GFP: green fluorescent protein

GnRH: gonadotropin-releasing hormone

GSCs: germline stem cells

GTP: Guanosine-5'-triphosphate (GTP

GTPase: guanine triphosphatase

hGH: human growth hormone

him-4: High Incidence of Males

HP: human parthenogenetic

HSF2: Heat shock transcription factors

HSFs: Heat shock transcription factors

Hts: hu-li tai shao

ICB: intercellular bridge

Ig: immunoglobulin

IGF: insulin-like growth factor 1

INCENP: inner centromeric protein

kDa: kilo Dalton

KIF4: Kinesin-4

LET-21: LEThal-21

LET-502: LEThal-502

MB: midbody

MBR: midbody ring

MDCK: Madin–Darby canine kidney cells

MEL-11: Maternal Effect LethaL-11

MgcRacGAP: male germ cell Rac GTPase-activating protein

Mid1p: mating pheromone-induced death protein 1

Mid2p: mating pheromone-induced death protein 2

MKLP-1: Mitotic Kinesin-Like Protein 1

MLC: myosin light chain

MRLC: myosin II regulatory light chain

Mucin-D: Mucin- *Drosophila*

MYPT: myosin phosphatase-targeting subunit

N-terminal: amino-terminal

NLS: nuclear localization sequences

NMY-II: Non-muscle myosin II

PAR-4: abnormal embryonic PARtitioning of cytoplasm

Pav-Klp: pavarotti, a *Drosophila* kinesin-like protein

PGC: primordial germ cell

PH: pleckstrin-homology

PH domain: Pleckstrin homology domain

PIP: Phosphatidylinositol phosphate

PIP2: Phosphatidylinositol 4,5-bisphosphate

PLC: phospholipase C

PRC1: protein regulator of cytokinesis 1

pTyr proteins: phosphotyrosine-containing protein(s)

Rac1: ras-related C3 botulinum toxin substrate 1

RacGAP1: Rac GTPase-activating protein

RBD: RhoA-binding domain

RC: ring canal

RFP: red fluorescence protein

Rho-1: Rho family GTPase Rho-1

RhoA: Ras homolog gene family, member A

RNAi: RNA interference

ROCK: Rho-dependent kinase

S. pombe: Schizosaccharomyces pombe

S2: Schneider 2 cells

SDS-PAGE: sodium dodecyl sulphate polyacrylamide gel electrophoresis

SEPT: septin

SGP: somatic gonad precursor

SH3: Src homology

SIM: structured illumination microscopy

SPh: somatic gonad primordium

TEX14: testis-expressed gene 14

TSG101: tumor susceptibility gene 101

TZ: transition zone

UNC-45: UNCoordinated-45

UNC-59: UNCoordinated-59

ZEN-4: Zygotic epidermal ENclosure defective-4

α-spectrin: alpha-spectrin

δ Tubulin: gamma-tubulin

WASp: Wiskott-Aldrich syndrome protein

SCAR/WAVE:

CAM: calmodulin 1

To Baya and Papa

Acknowledgement

First and foremost, I would like to thank my advisor, Jean-Claude Labbé. Jean-Claude has been and, I sincerely hope, will continue to be a great mentor. I am especially grateful to Jean-Claude for teaching me the essence of critical thinking, scientific integrity and for all the insightful discussions that improved my scientific outlook. I have been amazingly fortunate to have an advisor who gave me the freedom to explore on my own, while being a source of constructive input, encouragement, unconditional support and understanding throughout my PhD.

Moreover, I owe a profound thank you to Nicolas Chartier, a great friend and a former colleague, who in addition to patiently walking me through his project before leaving the Labbé laboratory provided indispensible source of scientific motivation and inspiration with his passion during the course of my PhD. Merci Kiki!

Thanks to all the Labbé lab members, past and present, particularly Abby Gerhold, for reading the two manuscripts and providing very useful suggestions and perceptive inputs and more importantly for kindly and patiently sharing her time and knowledge with me. I would also like to thank Alexia Rabilotta-Faure for her advice, support, problem-solving skills and friendship over these years. Thanks to Patrick Narbonne for helping me understand the *C. elegans* genetics and for his advice. I would also like to thank members of Amy and Paul Maddox laboratories, in particular Benjamin Lacroix and Joel Ryan, for being generous with their time and patient with their explanations that have certainly enriched my ideas. My special thanks goes to my former colleagues and office mates: Anne-Marie Laduceure, Rajesh Ranjan Vincent Hyenne, Ramraj Velmurugan, Ken Lam and Laura Benkemoun, I couldn't ask for better colleagues and friends. The majority of my thesis relied on having access to the imaging facility in IRIC, so I would like to thank Christian Charbonneau for being very patient and helpful throughout the years.

My thesis committee guided me through all these years. Thank you to Dr. Sébastien Carréno,

Dr. Jean-François Côté and Dr. Alisa Piekny for their helpful advice on my research project.

Thanks to my amazing mom and my sister Mitra for their unconditional love and support throughout my life. Thanks to my best friends Gloria Assaker and Sanaz Rassouli for always being there for me. And thanks to the rest of my family and friends near and far. You all made this time all the more pleasant.

Finally, I would like to dedicate this thesis to my lovely grandparents, Baya Azarpour and Papa Anousheh, the greatest mentors and friends, source of inspiration who passed away during the course of my PhD.

Preface

Cytokinesis failure has been proposed to be the most frequently used mode of syncytiogenesis across the animal kingdom. Surprisingly, while accidental failures of cytokinesis in normal tissues cause pathological disorders such as cancer, regulated cytokinesis failure is a physiological element of syncytial tissues. Hence, to be most effective in understanding cytokinesis failure and its influence on syncytium formation, we must first obtain an exhaustive description of how cytokinesis normally progresses. Accordingly, in the following pages, I first provide a summary of what is currently known about cytokinesis and one of its key regulators; anillin. Then, I will describe different types of syncytia and their structure, followed by two chapters on mechanisms of syncytium formation and its function. Lastly, I will introduce the system we used to study syncytiogenesis; the *C. elegans* germline. Importantly, the story of syncytiogenesis and its exact roles and benefits is not complete; there are many unknowns and confusing results, but if we could only figure out how syncytia pull it off, maybe we could gain some insights on potential underlying mechanism of cytokinesis failure and their associated disorders.

1. Introduction

1.1. Cytokinesis, the final stage of cell division, is a multi-step event

Cytokinesis is the final and irreversible stage of animal cell division during which one cell is physically separated into two distinct cells (Glotzer, 1997a; Glotzer, 1997b). To ensure the faithful propagation of the genome, cytokinesis must be spatiotemporally coordinated with chromosome segregation. This coordination is partly achieved by a tight regulation of a well-orchestrated chain of events involving the establishment of the division plane, furrow ingression through contraction of an actomyosin ring, formation of the midbody (MB) and midbody ring (MBR) and cell separation in a process called abscission (Figure 1.1).

The proper execution of each stage depends on its prior stage and thus defects at any step of this cascade may result in cytokinesis failure, the consequence of which could result in problems such as aneuploidy, centrosome amplification and genetic instability, which are characteristics of many cancers. Here, I will overview the different stages of cytokinesis in animal cells, as we currently understand them.

1.1.1. Stage I: Positioning of the Division Plane

To ensure that each of the two daughter cells receives a complete and single copy of the genetic and cytoplasmic materials upon completion of cytokinesis, the cleavage furrow must form in the accurate place in a dividing cell (Figure 1.1 B). This accuracy is gained by specification of the site of cleavage furrow, through assembling a structure known as the central spindle during anaphase (Reviewed in Eggert et al., 2006; Glotzer, 1997a; Glotzer, 1997b; Glotzer, 2001; Glotzer, 2005; Green et al., 2012).

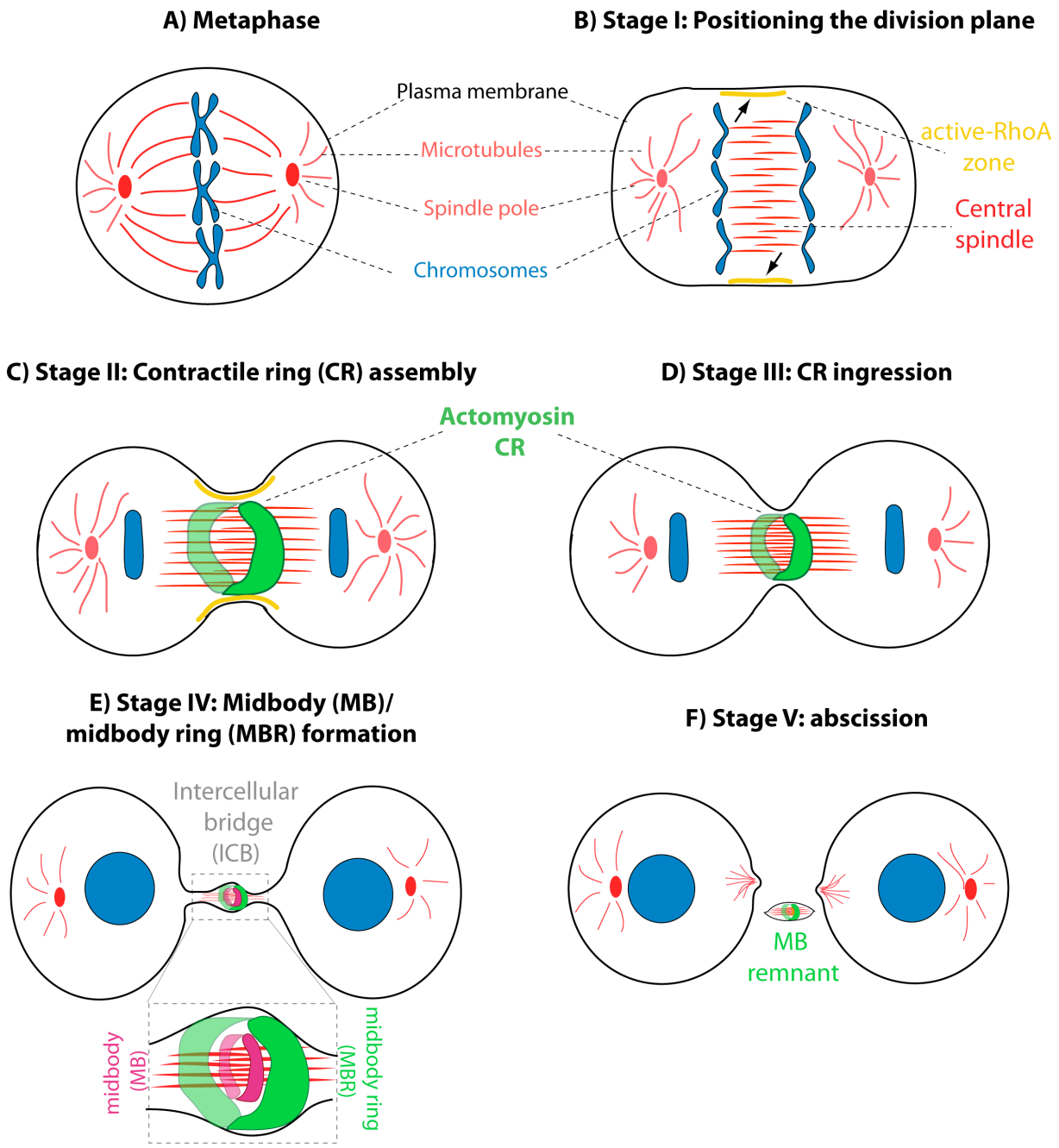

Figure 1.1: Cytokinesis is a multistep process.

Schematic diagram of the progression through cytokinesis. **(A)** metaphase **(B-F)** Different stages of cell division. Black arrows in (B) point to cues from the central spindle that activate RhoA and astral microtubules that reinforce the localization of active RhoA the upstream regulator of the contractile ring (CR).

The central spindle is composed of anti-parallel microtubules, the microtubule binding and bundling protein PRC1 and a kinesin KIF4 (kinesin-4) (Glotzer, 2009a; Glotzer, 2009b; Green et al., 2012), two protein complexes; centralspindlin (composed of two molecules of MKLP1 (known as ZEN-4 in *C. elegans*) the motor component of the centralspindlin complex and two molecules of MgcRacGAP (known as CYK-4 in *C. elegans*)) (Mishima et al., 2002) and the chromosomal passenger complex (CPC) composed of the kinase Aurora B, Incenp, Borealin and Survivin (Carmena et al., 2012; Glotzer, 2009b; Ruchaud et al., 2007). Central spindle assembly and thereby specification of the division plane site are subject to both temporal regulation (coupling to cell cycle) and spatial regulation (coupling to spindle position) (Reviewed in Eggert et al., 2006; Glotzer, 1997a; Glotzer, 1997b; Glotzer, 2001; Glotzer, 2005; Green et al., 2012). Here I will only describe current understanding on the spatial regulation aspect of the first stage of cytokinesis to understand how the cleavage furrow is localized to a single, defined place at the cell cortex.

1.1.1.1. Mitotic spindle microtubules

In 1985, Ray Rappaport, a pioneer in the field of cytokinesis, performed his classic physical micromanipulation experiments that were aimed to tackle how cleavage furrow is placed in an appropriate place during division. He observed that the cleavage furrow site is determined by the position of the mitotic spindle (the microtubule-based structure that forms during mitosis) in late metaphase or early anaphase of the cell cycle and concluded that the positioning of the cleavage furrow involves continuous communication between the mitotic spindle and the cell cortex (Pollard, 2004; Rappaport, 1985).

The precise mechanism by which microtubules position the division plane between the segregated chromosomes is still elusive, however different models have been proposed to explain this. One well-established model is that the mitotic spindle contributes to establishment of cleavage furrow positioning. But which part of the mitotic spindle functions in this process? The answer to this question is a subject of perhaps one of the oldest debates in

the field. While some experiments are in favor of *"the astral stimulation hypothesis"* which postulates that the non-spindle astral microtubules that radiate from centrosomes to the cell periphery, are essential for determining the cleavage furrow site (Rappaport, 1961; Rappaport and Rappaport, 1985), others contradicted this view by proposing the second hypothesis, "*the central spindle hypothesis*", arguing that midzone microtubules are key regulators of this process (Bonaccorsi et al., 1998; Cao and Wang, 1996).

While abundant evidence from many species supports the latter hypothesis, a third hypothesis, "*the astral relaxation hypothesis"* postulates that astral microtubules generate a negative signal that enhances cortical relaxation in their immediate vicinity close to the pole (White, 1985; Wolpert, 1960). In addition, Antony Hyman's group using laser micro-dissection, spatially separated aster and midzone microtubules and showed that the furrow is first positioned by an astral signal and subsequently by a second midzone-derived signal, suggesting that both arrays send signals to the cortex (Bringmann and Hyman, 2005). Perhaps the simplest explanation for these contradictory results is that different factors and mechanisms or a combination of different mechanisms are likely to determine the cleavage furrow site depending on the cell types, sizes and organism. Alternatively, the critical determinant for the specification of cleavage furrow positioning may not be evolutionarily conserved. Nevertheless, in all cases, regardless of the exact source, it is evident that the positional cue for the site of division plane comes from the microtubule-rich mitotic spindle, either through a traditionally believed model of "direct microtubule/cortical contact" or through the novel "diffusion-based" mechanism of transport along microtubules (Canman, 2009; von Dassow et al., 2009).

1.1.1.2. Rho GTPase signaling

Clues to the molecular basis of cleavage furrow positioning may be found in proteins that accumulate at the equator in a microtubule-dependent manner and their function to deliver signal(s) from microtubules to specify the site of the presumptive furrow. One such molecule

is the small GTPase RhoA that has been shown to contribute to specifying the plane of cell division in animal cells (Bement et al., 2005; Nishimura and Yonemura, 2006; Piekny et al., 2005; Yonemura et al., 2004; Yuce et al., 2005). Members of the Rho family guanosine triphosphatases or GTPases (including RhoA, Rac1, and Cdc42) (Piekny et al., 2005) spatiotemporally regulate various distinct cellular processes, including cytokinesis. Rho GTPases are activated by RhoGEF (guanine nucleotide exchange factors or GEFs) that catalyze the exchange of GDP for GTP (Rossman et al., 2005) and are inactivated by GTPase activating proteins (GAPs) which promote GTP hydrolysis (Tcherkezian and Lamarche-Vane, 2007). It has been shown that both GEFs (e.g. ECT-2/Pebble) (Yuce et al., 2005) and GAPs (e.g. MgcRacGAP) respectively control RhoA activation and inactivation, and as such help cells progress through cytokinesis (Bement et al., 2005; Nishimura and Yonemura, 2006; Yonemura et al., 2004; Yuce et al., 2005). For example, disruption of the RhoGEF ECT2 leads to a failure in cytokinesis (Tatsumoto et al., 1999).

Previous work proposed that the proper localization and activation of the RhoGEF ECT2 (Pebble in *Drosophila melanogaster,* and LET-21 or ECT-2 in nematodes) to the presumptive site of division depends on the centralspindlin complex (Nishimura and Yonemura, 2006; Somers and Saint, 2003). The activated RhoGEF ECT2 then triggers the localized activation and accumulation of RhoA at the site of cell division (Kimura et al., 2000; Prokopenko et al., 1999; Tatsumoto et al., 1999). Contrary to this, others suggested that ECT-2 only functions to restrict the already-active RhoA to a tightly focused region at the equatorial cortex, while another GEF, GEF-H1, is required for RhoA activation (Birkenfeld et al., 2007). Besides ECT-2, Anillin has been also shown to stabilize restricted RhoA localization at the furrow, suggesting that there is feedback between downstream components of cytokinesis and RhoA (Piekny and Glotzer, 2008; Zhao and Fang, 2005).

While RhoA is activated at the equatorial cortex, its activation is inhibited by astral microtubules at the polar cortex (Werner et al., 2007). Active RhoA at the equatorial cortex in turn promotes assembly and contraction of the actomyosin ring and thereby helps to initiate

cytokinetic ring ingression (Bement et al., 2006; Piekny et al., 2005). However, there is also compelling evidence that in Rat1A cell lines of embryonic rat fibroblasts, RhoA is dispensable for specification of the cleavage furrow positioning and that RhoA inactivation does not abrogate successful cytokinesis (Yoshizaki et al., 2004). In addition, it was found that RhoA requirement during cytokinesis might depend on the degree of cell adhesion in mammalian NIH 3T3 isolates (O'Connell et al., 1999). Altogether, these data suggest that cytokinesis may proceed by a RhoA-independent mechanism in some cell types.

1.1.2. Stage II: contractile ring assembly

In animal cells, attachment of the contractile ring (CR) to the plasma membrane creates a cleavage furrow that ultimately partitions the dividing cell into two (Figure 1.1 C). Accumulation of active RhoA at the equatorial cortex (Bement et al., 2005) promotes the recruitment of actin and myosin and thus assembly of the actomyosin-based contractile ring (CR) beneath the plasma membrane via two regulatory pathways. First, active RhoA stimulates polymerization of unbranched F-actin filaments through recruiting and activating an actin nucleator, formin (Diaphonous in *Drosophila*, CYK-1 in *C. elegans*) (Castrillon and Wasserman, 1994; Piekny et al., 2005; Watanabe et al., 1999). On the other hand, RhoA also indirectly promotes non-muscle myosin II (NMY-II) activity by activating kinases such as Citron kinase (Shandala et al., 2004) and Rho kinase (ROCK), which act on myosin either by phosphorylation of the myosin light chain (MLC) or by inhibiting the myosin phosphatase-targeting subunit (MYPT) (Amano et al., 1996; Matsumura, 2005). In addition to this pathway, several other mechanisms have been also shown to function in actin and myosin assembly at the cortex (Yumura et al., 2008; Zhou and Wang, 2008). For instance during pseudocleavage in the *C. elegans* embryo, signaling by astral microtubules, through an unknown mechanism functions in asymmetric CR assembly by locally inhibiting myosin recruitment to the posterior pole, a region with high microtubule densities (Werner et al., 2007).

The CR is composed of a parallel array of actin filaments (Maupin and Pollard, 1986) and myosin, two essential CR components. Besides these two components, the CR also contains other proteins assembled in an ordered fashion, including septin filaments (Eggert et al., 2006; Estey et al., 2010; Joo et al., 2007; Maddox et al., 2007), the scaffold protein anillin (Field and Alberts, 1995; Piekny and Maddox, 2010) and actin crosslinking proteins (Reichl et al., 2008). Among these, anillin plays an important scaffolding role by binding to membrane, actin, myosin, RhoA and CYK-4/MgcRacGAP and thus links the equatorial cortex to the signals coming from the mitotic spindle and to the CR (D'Avino, 2009; Hickson and O'Farrell, 2008a; Piekny and Maddox, 2010; Sun et al., 2015). I will further expand on anillin in *Section 1.2*.

1.1.3. Stage III: contractile ring ingression

Once the CR is assembled, it initiates constriction (Figure 1.1 D), which progressively draws the plasma membrane inward until it closes the gap between the two dividing cells, forming two separated cells. In addition to cytokinesis, CR ingression has been shown to function in several other processes, including wound closure (Mandato and Bement, 2001), epithelial morphogenetic movements (Bloor and Kiehart, 2002) and epithelial cell delamination (Rosenblatt et al., 2001), suggesting that the CR has been adapted to serve different functions. Despite the importance of CR ingression during cytokinesis, the exact mechanisms generating tension to draw the constriction of the CR remain elusive. The limitation to the current knowledge is in part due to the lack of high-resolution images that depict the ingression and rare measurements of tension *in vivo*. Nevertheless, several different models have been proposed to explain actomyosin contractility, on the basis of ultrastructural studies and biophysical considerations.

A classic model for CR constriction is the *"sliding filament"* model (Schroeder, 1972), which is based on the mechanism of muscle contraction and assumes that the interactions of bipolar myosin motor filaments with actin filaments generate the contractile force required to invaginate the plasma membrane furrow between the segregating cells during cytokinesis

(Mierzwa and Gerlich, 2014; Salmon, 1989). Consistent with this concept, several ultrastructural studies reported presence of a layer of actin filaments arranged circumferentially beneath the plasma membrane (Arnold, 1969; Maupin and Pollard, 1986; Schroeder, 1972; Selman and Perry, 1970), resembling the organization of actin in striated muscle cells. In parallel to this, several other studies reported presence of filamentous myosin at the CR (Vale et al., 2009; Yumura et al., 2008; Zhou and Wang, 2008). In addition, evidence supporting a force-generating role for myosin in this model came from studies showing that mutations that disturb myosin filament assembly result in CRs that are unable to contract (Egelhoff et al., 1993). Despite these, over the years, several other ultrastructural studies revealed principal discrepancies between CR structure in dividing cells and muscle sarcomeres. For instance, while myosin was proposed to drive the major force-generating element during CR constriction, experimental evidence showed that the presence or proper function of myosin is not needed for cytokinesis in some cells and/or under specific conditions (Lord et al., 2005; Ma et al., 2012; Mendes Pinto et al., 2013; Neujahr et al., 1997; Zang et al., 1997). Another major difference is that the CR in animal cells gets disassembled and releases material during constriction and, as such, its volume decreases over time. Despite this, the function of the CR is not affected (Schroeder, 1972). Altogether, these dissimilarities suggest the existence of alternative force-generating mechanisms that would not require muscle-like filament organizations.

Several other mechanisms have been proposed to explain how force is generated during CR constriction. For many years, the leading theory was the *"purse-string"* model, wherein the alignment of actin filaments with the division plane is an essential element. In this model, the bipolar myosin filaments walk along antiparallel actin filaments using their motor activity, drawing the F-actin strands together in a purse-string-like fashion (Satterwhite and Pollard, 1992). Because the plasma membrane is anchored to the F-actin filaments, constriction of the actomyosin ring pulls the membrane inside. However, several experimental evidences have challenged this model, mainly based on lack of a highly organized structure of concentric actin filaments in mammalian NRK cells, Swiss 3T3 cells and *Dictyostelium* cells (Fishkind and

Wang, 1993; Reichl et al., 2008). Another model proposes that randomly distributed myosin filaments within homogenous bundles of actin, generate the force needed for CR constriction (Carlsson, 2006). Altogether, these findings highlight the importance of new efforts to investigate force-generating mechanism underlying CR ingression during cytokinesis, perhaps by examining the exact arrangement of the filaments in CR and their function.

1.1.4. Stage IV: The biogenesis and architecture of MB and MBR formation

1.1.4.1. Maturation of the central spindle to form the MB

Constriction of the CR squeezes the cytoplasm at the center of the central spindle, generating an intercellular bridge (ICB) that transiently interconnects the two daughter cells (Glotzer, 2005; Green et al., 2012). The CR constricts until it reaches the central spindle and compacts its antiparallel microtubule into a single large bundle, forming a structure called midbody (MB) (Figure 1.1 E). The MB was first described in 1891 by Walther Flemming using light microscopy and histochemical methods, as a specialized structure conjoining the divided daughter cells in the lung epithelium of the salamander larva (Chen et al., 2013; Paweletz, 2001). He speculated that these structures are derived from spindle midzone between the segregating chromosomes and described them as densely stained bodies of 1-1.5 μm in size and named them "Zwischenkörper" ("Zwischen" and "körper" mean "between" and "body", respectively). Despite this, the MB has been only sporadically studied since its discovery and, as such, remained a mysterious structure for more than 100 years. In fact, the MB was so much ignored that some scientists considered it a "remnant", "scar", and even "cell garbage can" (Schicktanz and Schweda, 2009). But this was changed by advanced microscopy techniques and methods to dissect protein functions.

Structural composition of the MB

The MB is derived from the central spindle and, as such, its most prominent structural component is a densely packed array of anti-parallel microtubules (Figure 1.2 A). Along the

microtubules, the MB contains microtubule interacting proteins that co-localize to the central spindle (e.g., the centralspindlin complex) (Figure 1.2 A). For instance, MKLP-1, is one of the earliest centralspindlin components that was found to be associated with the MB (Sellitto and Kuriyama, 1988). Functional proteomic and comparative genomic approaches showed that MBs contain many different components, which are not only cytoskeleton-related proteins but also proteins involved in other pathways, such as secretory, or, membrane-associated, lipid rafts and vesicle trafficking (Skop et al., 2004). However, this is certainly an underestimation of the structural complexity of the MB, given the fact that its structural composition changes during cytokinesis progression.

Central spindle proteins relocate to different regions of the MB (Figure 1.2 A): *1) Bulge*, a region that is surrounded by the plasma membrane and develops at the center of the MB during central spindle maturation and microtubule compaction. Proteins including ECT-2 and MKLP-1 the motor component of the centralspindlin complex, centrosomal protein of 55 kDa (CEP55), ARF6 and RacGAP1 are released from the MB microtubules and re-localized to the bulge, which has a ring-like structure and wraps tightly around the MB (Elia et al., 2011; Hu et al., 2012). *2) Dark zone*, a narrow region on the microtubule bundles at the center of the MB. PRC1 and KIF4 remain associated with the microtubules in this zone (Elia et al., 2011; Hu et al., 2012). *3) Flanking regions*, two bands on microtubules at the periphery of the dark zone. CENPE, MKLP2, and Aurora B localize with microtubules at these regions (Hu et al., 2012). This re-localization pattern suggests that different regions probably serve distinct functions in the MB formation as well as abscission. In addition to this concept, the Mitchison group proposed that the MB core, wherein the antiparallel microtubules overlap, provides architectural integrity to the midzone while the flanking regions function to position abscission sites (Hu et al., 2012). Before proceeding, it is important to mention that despite attempts to map the central spindle proteins to different subregions of the MB, researchers are still confounded by the exact molecular composition and biophysical nature of the MB.

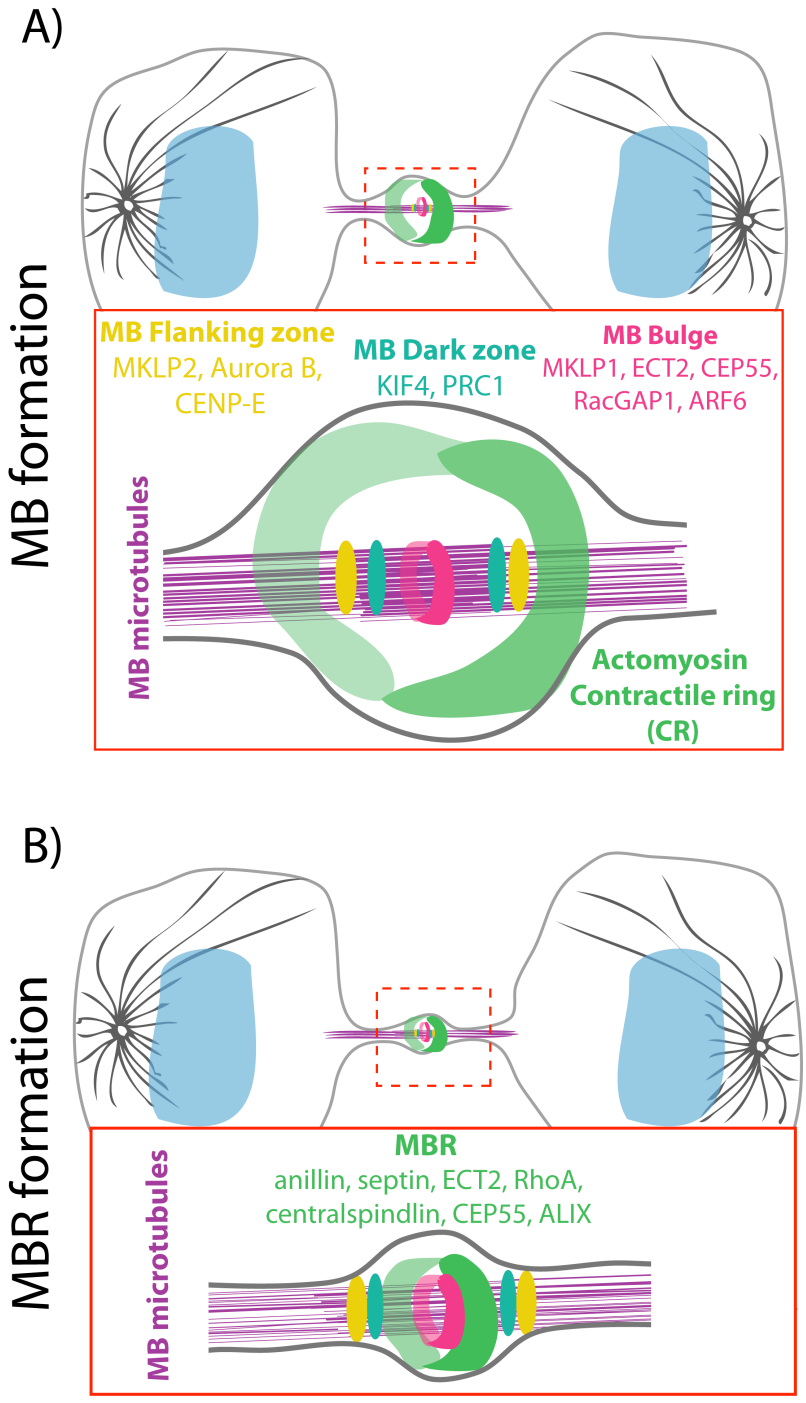

Figure 1.2: Illustrations of midbody (MB) and midbody ring (MBR) structural components.

Figure inspired from Green et al, 2012.

Another interesting question is how these components are targeted to the MBs and how ultimately the MBs are formed. In almost all systems, central spindle is essential for the MB formation (Matuliene and Kuriyama, 2002) and several of the proteins that localize to the central spindle play key roles in the MB formation (Matuliene and Kuriyama, 2002; Matuliene and Kuriyama, 2004). In fact, it has been shown that the centralspindlin complex besides being important for stage I of cytokinesis (Positioning of the division plane), is also necessary for the MB formation, and ultimately for completion of cytokinesis (Matuliene and Kuriyama, 2002; Matuliene and Kuriyama, 2004). Thus, it is not surprising to assume that the central spindle directly orchestrates re-localization of its components to form the MB.

Moreover, conversion of the central spindle to the MB is positively correlated with ingression of the CR, as either blocking CR ingression (Straight et al., 2003) or actin depolymerization (Hu et al., 2012), perturbs the MB formation. The CR ingression has been shown to contribute to the MB formation, perhaps through directing the re-localization of the MB components to different zones of the MB. It has been reported that without CR ingression, proteins that are normally partitioned into three distinct subregions of the MB; PRC1 and KIF4, Aurora B and MKLP-1, remain co-localized at the center of microtubule bundles, suggesting that furrow ingression is required for relocation of central spindle components in order to form the MB (Hu et al., 2012).

Function of the MB

Originally, the MB, together with its associated membranes and its compact microtubules had been proposed to serve as a diffusion barrier to limit cytoplasmic exchange between the dividing daughter cells, a process that is also known as cytoplasmic solation (Green et al., 2013). Indeed, monitoring the diffusion of fluorescent probes between the two dividing daughter cells upon photoactivation confirmed that the dividing cells undergo cytoplasmic isolation in different systems (Guizetti et al., 2011; Sanger et al., 1985; Steigemann et al., 2009). Currently, however, there is no consensus in the field regarding the timing of cytoplasmic isolation. While previous work in HeLa cells showed that cytoplasmic isolation occurs ~60 min after the completion of CR constriction and coincides with

endosomal sorting complex required for transport (ESCRT)–mediated scission (more details in *Section 1.1.5.*) (Guizetti et al., 2011; Steignemann et al., 2009), recent work in the *C. elegans* 1-cell stage embryo, revealed that the cytoplasmic isolation occurs upon completion of furrowing in an ESCRT-independent manner (Green et al., 2013).

Despite these unequivocal evidences and despite the compact appearance of MB microtubules, some other work suggest that this barrier might function selectively, as some proteins can still diffuse through the MB and transverse from one dividing daughter cell to the other, while others are not (Chen et al., 2013; Guizetti et al., 2011; Sanger et al., 1985; Schmidt and Nichols, 2004; Steigemann et al., 2009). Perhaps, the simplest way to explain this selective barrier would be that there is a space between the MB and the plasma membrane at the interface of the dividing cells that only allows proteins with a certain size to pass. Another possibility is that the microtubule-based MB is not capable of closing the bridge between the dividing cells. In fact, whether MB microtubules are required for cytoplasmic isolation during cytokinesis is a controversial subject. Recently, Karen Oegema group showed that cytoplasmic isolation occurs in the absence of MB microtubules in the *C. elegans* 1-cell stage embryo, suggesting the microtubules are not essential to block cytoplasmic diffusion between the dividing daughter cells (Green et al., 2013). In consistent with this, it has been shown that the germline stem cells (GSCs) of the *Drosophila* testis accomplish cytoplasmic isolation hours after microtubule disassembly, suggesting that a diffusion barrier is formed in the absence of MB microtubules (Lenhart and DiNardo, 2015). Undoubtedly, further studies are required to more thoroughly parse the MB structure and its role as a barrier, particularly in cells within different tissues and at carefully defined times during cytokinesis, to determine the function of the MB as a barrier and timing of cytoplasmic isolation.

Another widely accepted role of the MB and its microtubule bundles is its role as a platform to bring together a large number of abscission-related components (Schiel and Prekeris, 2013). Given that MBs are composed of various proteins with several distinct roles, it is not surprising that they would function as such a binding platform for abscission regulators. Recent progress on the molecular mechanism of abscission showed that the MB and its

microtubules serve as platform to coordinate the cytoskeleton and plasma membrane rearrangements and recruit functional complexes including microtubule severing enzyme spastin and the endosomal sorting complex required for transport (ESCRT) needed for abscission (more details in *Section 1.1.5.*). Despite this, work in the *C. elegans* embryo has provided convincing evidence that depletion of the MB microtubules does not affect abscission. Similar to this, it has been reported that the MB microtubules in HeLa cells are not directly required for abscission (Guizetti et al., 2011), suggesting that at least in some cell types, the MB microtubules are not critical for abscission. Moreover, domain analysis of three MB components in HeLa cells, namely MKLP1, KIF4 and PRC1 showed that they can still localize to the MB even when they lack their microtubule-interacting regions, suggesting that microtubules are not even essential for the MB assembly (Hu et al., 2012).

Besides functioning as a diffusion barrier and/or as a platform several other distinct non-cytokinetic roles have been attributed to the MB including signaling events (Skop et al., 2004), communication with centrosomes (Piel et al., 2001), polarity specification (Pollarolo et al., 2011), dorso-ventral axis formation in the *C. elegans* embryo (singh and Pohl, 2014), cell fate determination (Ettinger et al., 2011; Kuo et al., 2011) and cell fate specification (Dubreuil et al., 2007).

1.1.4.2. Maturation of the CR to form the MBR

As the constriction nears completion, the CR becomes progressively tighter until it reaches a diameter of ~1 μm (Mullins and Biesele, 1977) and subsequently transforms itself into the midbody ring (MBR), a dense structure that forms around the center of the MB (Figure 1.2 B). The MBR contains no or very few microtubules while several CR components, including myosin (Green et al., 2013), anillin (El Amine et al., 2013; Fields and Alberts, 1995; Hickson and O'Farrell, 2008a; Hu et al., 2012; Kechad et al., 2012; Straight et al., 2005) septin (Green et al., 2013), Citron kinase (Hu et al., 2012; Madaule et al., 1998), and RhoA (Hu et al., 2012) localize to it. Work using *Drosophila* S2 cells showed that the CR-to-MBR transition, requires the scaffolding protein, anillin (Kechad et al., 2012). Interestingly, a recent paper revealed that this anillin-dependent CR-to-MBR transformation occurs via opposing

mechanisms of membrane removal from the nascent MBR and anillin maintenance at the mature MBR (El Amine et al., 2013). On one hand, septin acts on the C-terminus of anillin to locally remove membrane from the nascent MBR through internalization, shedding and extrusion. On the other hand, Citron kinase acts on N-terminus of anillin to maintain anillin at the mature MBR through acting on, suggesting that the removal of membrane is coordinated with the CR disassembly, a process that is coupled to the formation of the MBR (El Amine et al., 2013).

MBR function

Most of the actin filaments that are found in the CR are disassembled following its complete constriction (Guizetti et al., 2011). While this is essential to allow for abscission, it could weaken the stability of the furrow and thereby its link to the membrane, leading the furrow to retract. To prevent this, the MBR has been proposed to mechanically stabilize the furrow and tether it to the plasma membrane at the division plane. This model has been confirmed by recent studies from Gilles Hickson's group (El Amine et al., 2013). They demonstrated that to prevent furrow regression during abscission, the MBR acts as an anchor to the plasma membrane. This anchor then persists until the complete separation of the two dividing cells. Cortical anchoring of the MBR depends on anillin, which localizes to the MBR. Anillin being a scaffolding protein interacts with both membrane (Sun et al., 2015) and the plasma membrane–associated septins (D'Avino et al., 2008; Oegema et al., 2000) and thereby tethers the MBR and its adjacent regions to the cell cortex.

Alternatively, the MBR has been proposed to serve as the platform that brings together the abscission-related components to specify the place and timing of abscission (Green et al., 2012; Steigemann and Gerlich, 2009). As described in *Section 1.1.4.1 Functions of MB*, a recent study from Karen Oegema's group provided evidence supporting this model by demonstrating that abscission-related events including membrane shedding, ESCRT machinery recruitment and MB/MBR release all occur normally in the absence of MB microtubules (Green et al., 2013). Another evidence supporting the microtubule-independent abscission recruitment model comes from a recent study from DiNardo's group wherein they

showed that the ESCRT-III components are delivered to the abscission site in GSCs of the *Drosophila* testis in the absence of microtubules (Lenhart and DiNardo, 2015), suggesting that in the absence of MB microtubules, the MBR is sufficient to orchestrate abscission and abscission-related events.

1.1.5. Stage V: Abscission a multistep event

CR constriction dynamically narrows the cell to the point where abscission can take place (Figure 1.1 F). Abscission represents the final stage of cytokinesis and is referred to the severing of membrane and the MB connecting the two dividing daughter cells at the end of cytokinesis. The small size of the MB (diameter of ~1 μm), its transient nature and the unsynchronized timing of abscission are only a few of the obstacles in the field of abscission research. Thus, it is not surprising that abscission is the least well-understood stage of cytokinesis. Nevertheless, advent of sophisticated super-resolution live and ultrastructural imaging techniques in combination with high-throughput genomics screening and proteomics analysis of the late MB/MBR enabled scientists to study and monitor the structural and molecular dynamics of different steps of abscission (Figure 1.3).

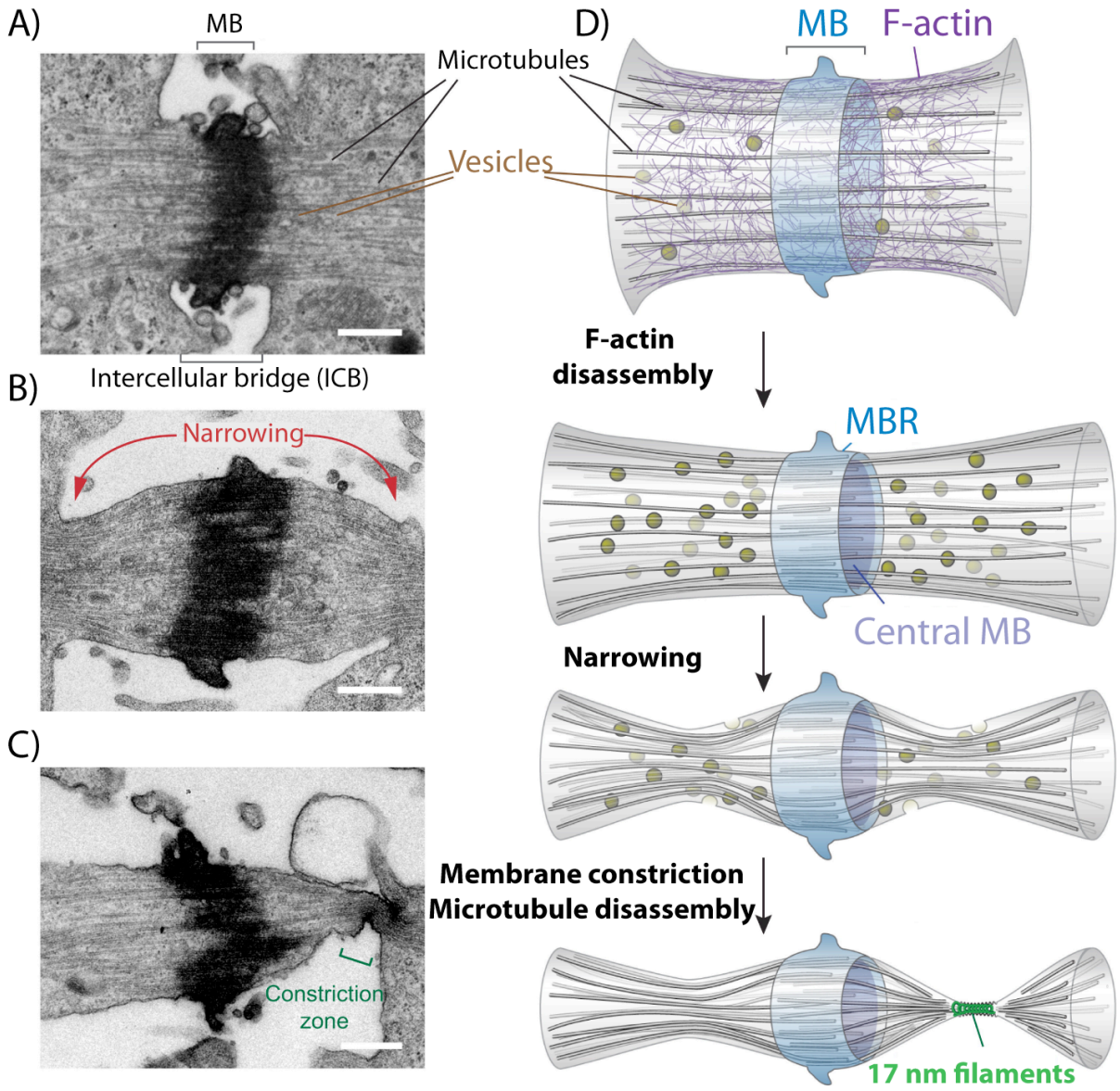

Figure 1.3: Different steps of abscission.

(A-C) Transmission electron micrographs of ICBs of HeLa cells at different stages of abscission. **(A)** Early-stage ICB appears short with bundles of straight microtubules. **(B)** Mid-stage, elongated ICB. Microtubule bundles appear compressed at either end, where the ICB has a reduced diameter. **(C)** Late-stage ICB with rippled, electron-dense cortex at a constriction zone. Microtubules at the constriction zone appear curved and highly compressed. **(D)** Schematics of abscission. Complete ingression of the cleavage furrow is followed by disassembly of cortical F-actin. Fusion of vesicles correlates with gradual narrowing of the ICB on both sides of the MB. Abscission proceeds by assembly and constriction of 17 nm filaments adjacent to the MB and simultaneous disassembly of the microtubules lateral to the MB. (Mierzwa and Gerlich, 2014).

To ensure that abscission undergoes properly, several events must occur in a temporally and spatially concerted manner. The first step is to prime the cell for assembly of the abscission machinery. Next, microtubule bundles, the MB/MBR and other cellular materials are removed during abscission. During this step, the plasma membrane and MB/MBR are budding away from the cytoplasm of the dividing cells, a process that results in the membrane and MB/MBR release also known as shedding. The final stage is sealing of the plasma membrane between the dividing daughter cells that ultimately results in their physical separation. Over the past few years, based on the topology of the membrane at the boundary of the two dividing daughter cells, different models have been proposed to explain the mechanisms of membrane deformation and severing including the mechanical rupture model (Burton and Taylor, 1997; Steigemann and Gerlich, 2009), the Golgi and endocytosis vesicle-mediated model (Gromley et al., 2005) and the ESCRT-mediated membrane fission model (Carlton and Martin-Serrano, 2007; Elia et al., 2011; Guizetti et al., 2011; Steigemann and Gerlich, 2009). Below I will give a concise overview of the sequence of main events occurring during abscission with a focus on the ESCRT-mediated plasma membrane fission model (Figure 1.3). Before proceeding however, for the sake of clarity, I will first give a brief overview of the ESCRT machinery and its function.

1.1.5.1. Background on ESCRTs

Although the endosomal sorting complex required for transport (ESCRT) complex has been only discovered in 2001, it is evolutionarily conserved from Archaea to animals (Wollert et al., 2009b). ESCRTs were named initially for their role in sorting membrane proteins from endosomes to lysosomes (Katzmann et al., 2001) but ESCRTs are also known for their role in membrane remodeling, constriction, scission and fission events during different cellular processes. One example is the ESCRT-dependent biogenesis of viral buddings and membrane severing that function in the release of viruses including HIV-1 from the plasma membrane of the infected cells (von Schwedler et al., 2003). Interestingly, extensive research during the past few years has led to discovering novel functions for ESCRT machinery from plasma membrane wound repair (Jimenez et al., 2014) to membrane scission of axons and dendrites

during neuron pruning (Issman-Zecharya and Schuldiner, 2014; Loncle et al., 2015; Zhang et al., 2014a). It worth mentioning that most, if not all, of both classic and novel ESCRT-dependent functions involve membrane severing. Based on the similar topology of the budding virus and the membrane at the ICB prior to abscission, it has been proposed that the membrane and MB/MBR breakage might be analogous to virus release from the infected cell and thus abscission may require similar ESCRT-dependent fission strategies.

The ESCRT machinery is comprised of five protein components, including ESCRT-0, ESCRT-I, ESCRT-II, ESCRT-III, and vacuolar protein sorting 4 (Vps4) and several other ESCRT-associated proteins such as the apoptosis-linked gene 2-interacting protein X (ALIX) (Wollert et al., 2009b). It has been shown that depletion of any of these ESCRT or ESCRT-related components result in cytokinesis failure (Carlton et al., 2008; Carlton and Martin-Serrano, 2007). Altogether, these features make ESCRTs attractive candidates to mediate abscission.

1.1.5.2. I: The MB/MBR as a platform to recruit abscission machinery

Prior to abscission, the MB and the MBR play a critical role as an anchorage to provide mechanical stability to the bridge and thus prevent furrow regression and subsequently abscission failure. However, the main function of MB/MBR during abscission is presumably to create the preconditions for abscission by performing as an assembly platform for the abscission-relevant machinery. In parallel with this, high-resolution structured illumination microscopy (SIM) of Madin–Darby canine kidney cells (MDCK) revealed that CEP55 (Zhao et al., 2006), the ESCRT-I subunit tumor-susceptibility gene 101 (TSG101) and the charged multivesicular body (MVB) protein 4B (CHMP4B) an ESCRT-III related protein are all sequentially assembled into ring-like structures at the center of MB (Elia et al., 2011). Currently, the model for ESCRT recruitment to the MB/MBR is that ALIX and TSG101 loading to the MB/MBR takes place by their binding to CEP55 (Mierzwa and Gerlich, 2014).

In addition, it was shown that prior to abscission, different types of vesicles including the recycling endosomes accumulate along microtubules with the highest concentration near the MB, wherein they play crucial role in abscission (Fielding et al., 2005; Wilson et al., 2005). These results indicate that the MB may serve as an anchoring scaffold for molecules and complexes that facilitate vesicle accumulation at or near MB during abscission. Despite this, the membrane-fission event during abscission does not occur at the MB (Elia et al., 2011; Guizetti et al., 2011), further confirming the notion that the MB rather than being an abscission site, functions as a platform for initiation of abscission by recruiting proteins necessary for abscission.

1.1.5.3. II: Abscission site formation

For a proper abscission to take place, a functional abscission site must be first formed. Approximately 10-20 minutes before membrane fission, in HeLa cells for instance, the cortex adjacent to the MB (0.95 ± 0.41 μm away from the center of MB) undergoes a secondary ingression and forms two narrow wave-like structures termed cortical secondary constriction zones (Figure 1.3 C), one at each side of the MB (Elia et al., 2011; Guizetti et al., 2011; Mullins and Biesele, 1977). Interestingly, at this time, ESCRT-III is redistributed from the MB to these two constriction sites (Figure 1.3 C, cartoon) (Elia et al., 2011). The narrow rippled constriction zones have been previously observed and proposed to mature into abscission sites (Mullins and Biesele, 1977). This concept is supported by studies depicting that in human cells, proteins believed to drive abscission, including ESCRTs and microtubule severing enzyme spastin, are recruited to these sites only after the MB formation (Elia et al., 2011; Guizetti et al., 2011; Morita et al., 2007). In addition, these rippled zones are composed of tightly compressed bundles of microtubules as well as spiral-shaped filaments of 17 nm diameter (Figure 1.3 C, cartoon). Based on septin ability to form filamentous structures (Cao et al., 2009) and their role in cytokinesis, Schiel and Prekeris, proposed that these 17 nm filaments might be composed of septins (Schiel and Prekeris, 2011), however studies from Gerlich laboratory suggest that ESCRT-III could be a more attractive candidate. These 17 nm

spiral-shaped filaments correspond to locations at which the ESCRT-III complex interacts with the plasma membrane and, as such, have been speculated to be composed of ESCRT-III filaments, an assumption that needs to be experimentally validated (Guizetti et al., 2011). In consistent with this hypothesis, it was previously shown that while cortical constriction of abscission sites in HeLa cells does not require microtubule severing enzymes, F-actin or Golgi-derived secretion (Guizetti et al., 2011), ESCRT-III is required for both the membrane deformations at the constriction zones and formation of spiral-shaped filaments (Guizetti et al., 2011).

But ESCRTs are not the only components present at the abscission site. Previous studies depicted that during the MB formation in HeLa cells, the furrow regulator RhoA (Hu et al., 2012) and the two furrow components anillin and septin (Hu et al., 2012; Renshaw et al., 2014) selectively relocate to the ruffled constriction sites (Hu et al., 2012), suggesting that they both might have roles in cytokinesis beyond regulating furrow ingression, perhaps in either preparing the abscission site prior to ESCRT recruitment or in formation of these sites (Renshaw et al., 2014). However, due to early requirement of these proteins for cytokinesis, this possibility could not be directly tested by knockdown assays, and thus other approaches were devised. In one such attempt, an anillin truncation that lacks the C-terminal septin-interacting domain in HeLa cells was shown to disturb septin recruitment to the abscission site and ultimately inhibit abscission site formation (Renshaw et al., 2014), suggesting that the anillin-septin interaction is required for biogenesis of abscission sites. Consistent with this, septins were shown to regulate abscission in HeLa cells (Estey et al., 2010), *Drosophila* S2 cells and *C. elegans* (Green et al., 2013).

1.1.5.4. III: ESCRT-III recruitment to the abscission sites

Of particular interest is the question of how ESCRTs, and in particular ESCRT-III, are directed to the abscission sites. In human cells, for instance, it was shown that ESCRT recruitment to the abscission site is only feasible once septin and anillin have been removed

from these regions (Renshaw et al., 2014). Persistence of anillin at the abscission site in HeLa cells, blocks ESCRT-III recruitment to these regions and, ultimately leads to abscission failure (Renshaw et al., 2014). In the same study, it was shown that, ESCRT-III recruitment to abscission sites is blocked in *septin*-depleted HeLa cells. However, depletion of septin in the *C. elegans* embryo does not affect ESCRT recruitment (Green et al., 2013), suggesting that different strategies are used to assemble ESCRTs to the abscission site.

Furthermore, as mentioned in *Section 1.1.5.2.,* in human cells, the centrosomal protein CEP55 is the key protein directing ESCRT recruitment. During late stages of cytokinesis, CEP55 binds to the centralspindlin component MKLP-1 (Bastos and Barr, 2010; Carlton and Martin-Serrano, 2007) and then interacts with and recruits the ESCRT-associated protein, ALIX and the ESCRT-I component TSG101 to the MB (Carlton et al., 2008; Carlton and Martin-Serrano, 2007; Mierzwa and Gerlich, 2014; Morita et al., 2007). Once at the MB, TSG101 recruits ESCRT-III to two cortical abscission zones at both sides of the MB (Elia et al., 2011; Guizetti et al., 2011; Lafaurie-Janvore et al., 2013). Organisms including *C. elegans* and *Drosophila* lack homologues of CEP55 and thus must have developed other ways to recruit the ESCRT machinery to the abscission site. This could happen through direct interaction of the ESCRTs with the centralspindlin. Altogether, coordination between assembly and/or disassembly of different factors, membrane deformation and ESCRT recruitment to abscission sites is a necessary prerequisite for membrane scission and thereby abscission.

1.1.5.5. IV: ESCRT-mediated microtubule and membrane scission

Completion of cytokinesis requires both microtubule and membrane severing. In addition, abscission also relies on a coordinated membrane trafficking to deliver new membrane between the dividing cells. ESCRT-III localization to the abscission zone induces constriction that is followed by breakage of the intercellular bridge, leading to complete separation of the two daughter cells (Figure 1.3 C, cartoon). Upon cortical constriction at abscission sites, the MB diameter, as assessed by the diameter of microtubule bundles,

gradually narrows to about half of its initial width (Figure 1.3 B), until the first microtubule bundle disassembles at one side adjacent to the MB, 49 ± 10 min after complete furrow ingression, while the 2nd microtubule bundle disassembles ~20 min after the first one (Guizetti et al., 2011). This microtubule disassembly step requires spastin, a microtubule-severing enzyme. Interestingly, it was shown that in dividing HeLa cells, the N-terminal region of spastin, binds to the ESCRT-III protein and that knockdown of CHMP1B reduces the amount of spastin at the MB (Yang et al., 2008). Ultimately, abscission is achieved through the membrane scission event (Yang et al., 2008). ESCRT-III, as mentioned before is assumed to be the key factor that directs membrane scission, leading to the MB release and the complete separation of the two daughter cells (Elia et al., 2011; Guizetti et al., 2011). It is shown that the spiral-shaped filaments made by ESCRT-III components drive membrane deformation and scission (Hanson et al., 2008; Wollert et al., 2009a). These results indicate that while ESCRTs could interact with spastin to direct microtubule severing (Yang et al., 2008), they also form spiral filaments to direct the membrane scission (Elia et al., 2011; Guizetti et al., 2011), suggesting that ESCRT function is to coordinated the microtubule disassembly and severing at the MB, followed by plasma membrane constriction and, ultimately, fission.

Despite these, it is still not completely understood how ESCRTs act as a molecular scissor during abscission. For instance, while the ESCRT-deformed membranes in eukaryotes were shown to be typically 50-100 nm in diameter (McDonald and Martin-Serrano, 2009), the diameter of the MB is significantly larger (Gromley et al., 2005; Guizetti et al., 2011; Mullins and Biesele, 1977), raising an interesting question of how ESCRT filaments are able to induce MB narrowing and ultimately the plasma membrane and the MB severing during abscission. Given that different types of vesicles (endosomal and Golgi-derived) accumulate at the MB prior to abscission, one possibility is that they set the stage ready for ESCRT-mediated abscission by narrowing the MB to a diameter sufficient for ESCRT-mediated events. Recycling endosomes have emerged as important players in mediating abscission (Schiel et al., 2013; Schiel et al., 2012; Wilson et al., 2005). Alternatively, ESCRTs and vesicle trafficking machinery could function together to accomplish abscission (Chen et al., 2013).

Before proceeding, it is important to mention that the fate determination of the post-abscission MB depends on cell-type and status, as in some cases such as stem cells the MB are retained and accumulated within the cell after release (Kuo et al., 2011), while in others they are released extracellularly as a remnant to the surrounding medium (Ettinger et al., 2011). Nonetheless, it was shown that post-abscission MBs have important roles and are major regulators of different cellular events including the embryonic patterning in *C. elegans* (Singh and Pohl, 2014a; Singh and Pohl, 2014b).

Altogether, despite considerable progress have been made in the last few years that shed light on the cellular structures and dynamics occurring during abscission, the mechanism of abscission still remains unclear. Development of new imaging strategies and genetically encoded biosensors will hopefully enable scientists to observe the dynamics and localization of various components during abscission to provide a better understanding of the mechanism of abscission.

1.2. Anillin

Classical genetic or biochemical inhibition of proteins, as well as large-scale RNAi screens, generated a list of proteins essential for cytokinesis, the majority of which are evolutionarily conserved. Some of these serve scaffolding functions in order to properly organize cytokinesis in a spatiotemporally manner. Anillin is one such protein and its multi-domain structure allows it to interact with other essential cytokinesis components in establishing the CR. In this section I will summarize what is currently known about anillin, its structure and function, as well as, its expression and localization pattern in diverse organisms. I will begin with an overview of anillin protein structure, highlighting conserved and non-conserved regions across species.

1.2.1. History and background

In 1982, Bruce Alberts' group, using F-actin affinity chromatography and immunofluorescence techniques, identified an F-actin-binding protein in *Drosophila* embryo extracts (Miller et al., 1989) and later named this novel protein anillin (from the Spanish "anillo", for ring), "in recognition of its ring-shaped distribution in dividing cells, where it is part of the cleavage furrow" (Field and Alberts, 1995). In addition, in the same study Christine Field showed that besides binding to F-actin, anillin is able to bundle these filaments and that its localization alternates between the nucleus during S phase and the cytoplasmic cortex during cytokinesis (Field and Alberts, 1995), suggesting that it might be a structural component of the cleavage furrow that functions in cytokinesis.

1.2.2. Anillin is a highly conserved protein

Anillin homologues have been also identified in numerous organisms other than *Drosophila*, from yeast to humans (D'Avino, 2009; Hickson and O'Farrell, 2008a; Piekny and Maddox, 2010). These homologues are in humans (ANLN) (Oegema et al., 2000), mice (Anln), *C. elegans* (ANI-1, ANI-2 and ANI-3) (Maddox et al., 2005) and anillin-related proteins in *Schizosaccharomyces pombe* (Mid1p and Mid2p) and *Saccharomyces cerevisiae* (Boi1p and Boi2p) (Zhang and Maddox, 2010), indicating that anillin is conserved among organisms and that some may have more than one protein with homology to anillin.

1.2.3. Interactions of anillin multidomain scaffolding protein

Anillin is a multi-domain protein that was reported to physically interact with several components of the cleavage furrow in biochemical and *in vivo* assays. For example, anillin has been shown to interact with several components of the CR including, F-actin (Field and Alberts, 1995; Miller et al., 1989), active Myosin II (Straight et al., 2005), septins (Field et al., 2005; Kechad et al., 2012; Kinoshita et al., 2002; Oegema et al., 2000), plasma membrane lipids (Sun et al., 2015), astral microtubules in HeLa cells (Triplet et al., 2014), as well as

contractility regulators including active RhoA (D'Avino et al., 2008), RacGAP50c (MgcRacGAP/CYK-4) (D'Avino et al., 2008; Gregory et al., 2008) and the phosphorylated form of myosin regulatory light chain (MRLC) (Straight et al., 2005), suggesting that anillin acts as a scaffold for regulatory proteins as well as for the actomyosin and microtubule cytoskeletons. Below, I will provide list of different anillin domains and proteins interact with them.

1.2.3.1. N-terminus

Actin- and myosin-binding domains

The N-terminus of some but not all anillin proteins contains a region that binds F-actin (Field and Alberts, 1995; Oegema et al., 2000), and a region that binds phosphorylated cytoplasmic myosin (Straight et al., 2005). Despite these interactions, anillin and myosin in *C. elegans* and *Drosophila* (Hickson and O'farrell, 2008; Maddox et al., 2005; Piekny and Maddox, 2010; Straight et al., 2005) and anillin and actin in *Drosophila* and human cultured cells are independently recruited to the CR (Piekny and Glotzer, 2008; Piekny and Maddox, 2010). The actin- and myosin-binding domains seem to rather function in organizing myosin and actin during cytokinesis (see *Section 1.2.5.1.*) (Maddox et al., 2005, Piekny and Maddox, 2010; Werner and Glotzer, 2008). Moreover, as described in *Section 1.1.4.2.*, truncation analysis of anillin in *Drosophila* S2 cells revealed that these domains contribute to the formation and integrity of the MBR during later stages of cytokinesis (Kechad et al., 2012).

1.2.3.2. C-terminus

The Anillin homology domain (AHD)

The C-terminal region of anillin consists of the AHD and PH domains. AHD was named for its conservation among metazoan anillins. Recent crystal structure and functional analysis of human anillin and *S. pombe* Mid1 revealed that they both contain two novel

domains within their AHD (Sun et al., 2015). The first domain is a conserved anti-parallel coiled-coil domain, which has been named the *RhoA-binding domain (RBD)*, for its ability to bind to RhoA (Figure 1.4, human). This finding supports a previous study showing that anillin directly binds to RhoA in humans (Piekny and Glotzer, 2008). The second domain is a cryptic lipid-binding *C2 domain*, adjacent to the pleckstrin-homology (PH) domain (Figure 1.4, human) (Sun et al., 2015). The C2 domains are known as either calcium-dependent or – independent membrane-binding sites of many cellular proteins involved in various processes including signal transduction and membrane trafficking (Cho, 2001) and are found in many proteins that bind lipids. Consistent with this the L3 loop region of C2 domain of human anillin binds to a cell membrane phospholipid phosphatidylinositol 4,5-bisphosphate ($PI_{4,5}P2$) *in vitro*, and its deletion completely abolishes lipid binding of AHD as well as anillin anchorage to the cytokinetic furrow (Sun et al., 2015). A linker sequence (Figure 1.4, human, white dashed line) further connects the PH domain to the C2 domain in human anillin (Sun et al., 2015).

The Pleckstrin-homology domain (PH)

Another characteristic sequence feature of all anillin family members is their C-terminal PH domain, which serves a common role of mediating interactions with the plasma membrane via phosphoinositides (Lemmon, 2004; Lemmon et al., 2002; Liu et al., 2012) or cortical septins (Kinoshita et al., 2002; Oegema et al., 2000) or both (Field et al., 2005). In many systems, the PH domain is required for anillin targeting to the CR; examples include human anillin (Liu et al., 2012; Oegema et al., 2000; Piekny and Glotzer, 2008) and the *S. pombe* anillin-related protein Mid2 (Berlin et al., 2003). In HeLa cells, the anillin PH domain targets both anillin and septin to the cleavage furrow via binding to $PI_{4,5}P2$, (Liu et al., 2012).

1.2.4. Anillin domain structure in animals

1.2.4.1. Drosophila

Drosophila anillin contains 1239 amino acids and has an apparent mobility of

approximately 190 kDa on SDS-polyacrylamide gel electrophoresis (SDS-PAGE) (Field and Alberts, 1995). It contains a PH domain near its C-terminal region (Rebecchi and Scarlata, 1998) (Figure 1.4 *Drosophila*). Upstream of the PH domain, within the C-terminal, is the AHD (Oegema et al., 2000), with a binding domain for the central spindle protein RacGAP50C (D'Avino et al., 2008; Gregory et al., 2008; Straight et al., 2005). Myosin-binding, actin-binding and actin-bundling domains are located at its N-terminus (Straight et al., 2005). It also contains two consensus sequences for an SH3 binding domain, which are thought to mediate protein-protein interactions, and at least three nuclear localization sequences (NLS) (Field and Alberts, 1995).

1.2.4.2. human

Human genome encodes a single anillin homologue with a domain organization similar to that of *Drosophila* anillin. It contains a PH and an AHD domain at its C-terminus, an actin- and myosin-binding region toward the N-terminus and one consensus SH3-binding motif and NLSs. As described in *Section 1.2.3.2.*, the AHD domains consists of a C2 domain and an RBD domain (Figure 1.4, human). In contrast to *Drosophila* anillin, an N-terminal region of human anillin containing three putative NLSs is responsible for nuclear localization (Oegema et al., 2000).

1.2.4.3. C. elegans

C. elegans genome encodes three isoforms of anillin, ANI-1, ANI-2 and ANI-3. All three homologues contain the C-terminal AHD and PH domains, whereas only ANI-1 contains the actin- and myosin-binding domains at its N-terminus, making ANI-1 the likely canonical *C. elegans* anillin. The other two *C. elegans* anillins are short isoforms that are not observed in *Drosophila*, humans and vertebrates (Figure 1.4, *C. elegans*) (Maddox et al., 2005).

Identification of anillin structure in many animals revealed that while the general structure of anillin and anillin-related proteins has been relatively well conserved in metazoans, there are also some discrepancies in anillin structure among animals. For instance, pairwise alignments indicate that the human and *Drosophila* sequences are highly identical along their entire

lengths, with the highest level of identity in the C-terminal region of the protein (Tatusova and Madden, 1999), suggesting that the PH domain exhibits an essential role in different systems. In the next section, I will provide a summary of proteins that interact with each of these regions of anillin.

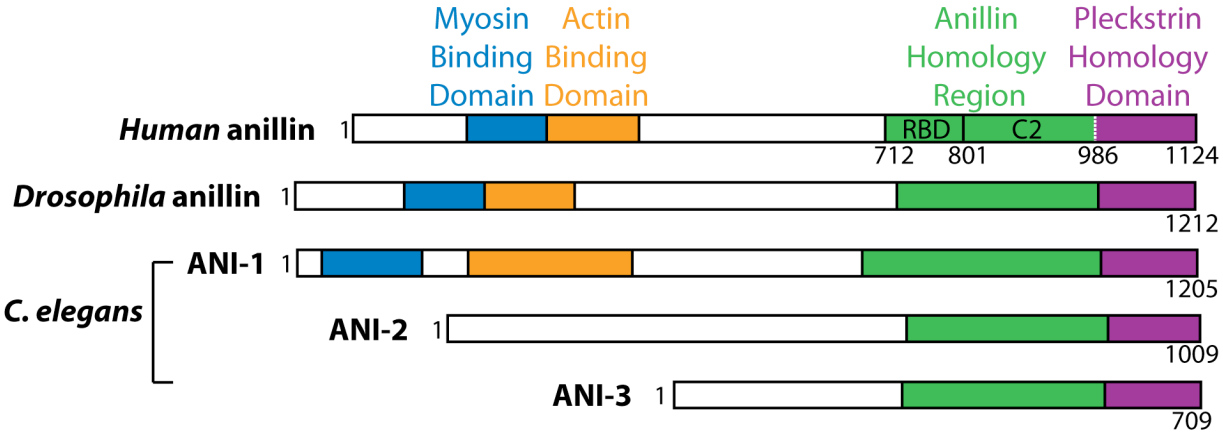

Figure 1.4: Anillin structure in different organisms.

1.2.5. Functions of Anillin

Although anillin was initially considered as a scaffold in cytokinesis in several different tissues and organisms (D'Avino, 2009; Piekny and Maddox, 2010; Werner and Glotzer, 2008), recent evidence unraveled the importance of anillin outside of cytokinesis. Examples include ventral enclosure during epidermal morphogenesis of the *C. elegans* embryo (Fotopoulos et al., 2013), cell–cell junction integrity in the epithelia of *Xenopus* embryos (Reyes et al., 2014) and neuron migration and neurite growth via linking RhoG to the actin cytoskeleton at the leading edge in the Q neuroblast lineage of *C. elegans* (Tian et al., 2015).

From the day of its discovery, the specific localization of anillin to the CR during cytokinesis and not to other contractile, actin-rich structures such as stress fibers or the apical side of the

constricting epithelial cells, hinted at potentially specific role of anillin in cytokinesis. Nevertheless, the significance of anillin in cytokinesis was first shown in a study by Karen Oegema in 2000. In that study, she showed that monkey cells injected with an affinity-purified antibody against human anillin fail to accomplish cytokinesis (Oegema et al., 2000). Since then, several other studies demonstrated an essential role for anillin in cytokinesis in different cell types and organisms (Echard et al., 2004; Eggert et al., 2004; Field et al., 2005; Piekny and Glotzer, 2008; Somma et al., 2002), reflecting a highly conserved role for anillin during cytokinesis. Given anillin's interaction with multiple conserved furrow proteins, anillin might function at different stages of cytokinesis. Below, I will provide examples to describe how anillin could mediate and facilitate different stages of cytokinesis in different systems.

1.2.5.1. Anillin as an organizer of contractility components to CR

Given anillin's multidomain structure and its ability to interact with several proteins, anillin has been proposed to organize contractility by coordinated targeting of the contractility proteins to the CR (Piekny and Maddox, 2010). For instance, in HeLa cells, anillin-$PI_{4,5}P2$ interaction, via its PH domain, is required for the assembly of septins at the cleavage furrow (Liu et al., 2012). In agreement with this, analysis of *Drosophila* embryos mutant for *anillin* revealed that the localization of myosin and septin at the cleavage furrow are disrupted (Field et al., 2005; Thomas and Wieschaus, 2004). In addition, several studies have that anillin is required for the spatial and/or temporal organization of myosin filaments during cytokinesis (Piekny and Maddox, 2010) in different systems, including the *Drosophila* embryo undergoing cellularization (Field et al., 2005), *Drosophila* S2 cells (Hickson and O'farrell, 2008b; Straight et al., 2005), human cultured cells (Straight at al., 2005) and the *C. elegans* zygote (ANI-1) (Maddox et al., 2005). Anillin-dependent actin organization has also been reported. For instance, in *Drosophila* S2 cells, loss of anillin function leads to F-actin disorganization at the furrow, which in turn results in cytokinesis failure (Echard et al., 2004). Could it then be that in *anillin* mutants, structural disorganization of the CR generates nonfunctional CRs that are not capable of ingression?

Although in some cases, anillin depletion leads to failure in CR ingression, in many others it does not. For instance, in human cells, anillin depletion by RNAi does not prevent CR ingression *per se*. Instead, the anillin-depleted cells exhibit ectopic localization of myosin at their polar cortices, resulting in extensive lateral oscillations, which ultimately lead to cytokinesis failure, suggesting that anillin specifies the position of the cleavage furrow in part by restricting the localization of myosin at the equatorial cortex (Piekny and Maddox, 2010; Triplet et al., 2014). Likewise, while *C. elegans* ANI-1, the canonical isoform of anillin, is required to organize foci containing myosin and septins in the early embryo (Maddox et al., 2005), it is otherwise dispensable for successful cytokinesis (Maddox et al., 2007). Instead, *C. elegans* ANI-1 is required for asymmetric furrowing and organizing cortical contractility during ruffling and meiotic cytokinesis (Maddox et al., 2005).

One possibility to explain non-essential role of anillin for CR ingression in the mentioned systems is that one or more cytokinesis regulators replace anillin during CR ingression. Alternatively, anillin could function redundantly with one or more proteins to regulate CR ingression. In support of this hypothesis, depletion of human anillin results in failure in furrowing only when the central spindle is perturbed (Piekny and Glotzer, 2008). Simultaneous depletion of ANI-1 and the central spindle component MKLP-1/ZEN-4 has been shown to impair full ingression of the cytokinetic furrow (Werner and Glotzer, 2008), suggesting that anillin is only required for CR ingression in embryos with compromised central spindle. This also leads to another notion in the field that anillin might serve a role to couple the CR to microtubules during cytokinesis. I will expand on this concept in the following section.

1.2.5.2. Specification of the division plane by anillin

As mentioned before, one critical step for a reliable cytokinesis is specification of the division plane (see *Section 1.1.1.*), a process that is directed by signals from the central spindle as well as astral microtubules (Eggert et al., 2006; Glotzer, 2005). This is achieved through the

opposite action of astral and central spindle microtubules. While signals from the central spindle lead to the accumulation of contractility proteins at the equatorial furrow, inhibitory signals from astral microtubules prevent contractile proteins from accumulating on the polar cortex, and thereby spatially position the division plane.

Based on functional redundancy of MKLP-1 (a central spindle component) and anillin in furrow ingression in HeLa cells (Piekny and Glotzer, 2008) and the *C. elegans* embryo (Tse et al., 2011), it has been previously proposed that anillin is part of the astral microtubule pathway in these two systems. Recent evidence supporting this hypothesis came from Alisa Piekny's lab, wherein they demonstrated that anillin localizes to and interacts with astral microtubules in HeLa cells to limit myosin assembly to the equatorial cortex, and hence specify the position of the division plane (Triplet et al., 2014). In addition, Mid-1, the anillin homologue in *S. Pombe* is required for interaction of astral microtubules with the cortex (Gachet et al., 2004), suggesting that anillin stabilizes the alignment of the mitotic spindle.

1.2.5.3. Anillin as an anchor of the CR and/or MBR to the membrane during late cytokinesis

Throughout all stages of cytokinesis, the CR must be anchored at the proper position to the plasma membrane and be stabilized at the division plane to ensure the faithful segregation of the genetic and cytoplasmic material. This anchoring could be important for maintaining the structural integrity of the CR during furrow ingression. Given anillin's multidomain structure and capacity to bind to various distinct elements of the contractile machinery as well as plasma membrane, a long-standing model has posited that anillin acts to anchor the CR to the membrane during cytokinesis (Oegema et al., 2000). In this model, anillin mediates interactions between the CR components and the membrane cytoskeleton to ultimately link the CR to the plasma membrane (Sun et al., 2015). Recent structural and functional studies confirmed this model by showing that human anillin and *S. pombe* Mid1 anchor the CR to the plasma membrane at the division plane. In human cells, this anchoring occurs via the

synergistic actions of the RBD, C2 and PH domains, through binding to RhoA and phospholipids at anillin C-terminus (Sun et al., 2015), along with its N-terminus actin- and myosin-binding domains which enable stable linking of anillin at the cleavage furrow with the membrane of the division plane, to help to maximize the efficiency of CR dynamics and ingression.

Likewise, anillin could function to prevent the MBR from regressing during later stages of cytokinesis, so as to stabilize the close connection between the daughter cells. It has been shown that anillin not only orchestrates the CR to MBR transition, but it also links the MBR to the membrane in *Drosophila* S2 cells (El Amine et al., 2013; Kechad et al., 2012). On one hand, it binds to the CR via its N-terminal region and thus supports CR-to-MBR maturation. On the other hand, it recruits septin to the equatorial cortex. By doing so, it links the MBR to the plasma membrane, a connection that is probably lost in the anillin-depleted cells, resulting in furrow oscillation and cytokinesis failure (Kechad et al., 2012). Altogether, these findings uncover a potential conserved role of anillin in providing anchorage to the ingressed CR or to the MBR during cytokinesis.

1.2.5.4. Anillin as a potential regulator of abscission

In *Drosophila* S2 cells that are depleted of anillin by RNAi, the CR is formed and undergoes ingression, however the membrane surrounding the MB undergoes blebbings, which ultimately result in cytokinesis failure (Echard et al., 2004). Because the MB is formed in these conditions, it was argued that anillin perhaps functions after furrow formation and furrow ingression, during later stages of cytokinesis, to facilitate abscission. This model has been partially supported by several studies in HeLa cells, showing that anillin besides being localized to the cleavage furrow is also localized to the presumptive abscission sites (Elia et al., 2011; Hu et al., 2012; Renshaw et al., 2014), where it regulates ESCRT-III recruitment (see *Section 1.1.5.3.*) (Renshaw et al., 2014). In support of the role of anillin in abscission, anillin-depleted cells were reported to fail to display the narrowing step of ICB (Kechad et al.,

2012), a step that normally happens prior to abscission.

Altogether, although anillins have conserved functions among organisms, discrepancies in anillin function in different organisms or sometimes even within the same animal has been observed. A good example for the latter discrepancy has found in *C. elegans*, in which one of its three homologues, the short anillin ANI-3 has no known function, whereas its two other anillin homologues, the canonical anillin ANI-1 and the short isoform of anillin AN-2 exhibit different localizations, structures as well as functions. The canonical isoform of anillin, ANI-1 contributes to the organization of the cortical cytoskeleton during cytokinesis (Lord et al., 2005) and asymmetric furrow ingression in the embryo (Maddox et al., 2007), while the short isoform ANI-2 contributes to the syncytial organization of the gonad (Green et al., 2011, Maddox et al., 2005). Our lab has previously showed that during polarity establishment in the *C. elegans* embryo, PAR-4 positively regulates actomyosin contractility by inhibiting ANI-2 activity, which in turn has been proposed to inhibit ANI-1, possibly by acting as a competitor (Chartier et al., 2011). In *par-4* mutant embryos, ectopic accumulation of ANI-2 negatively regulates actomyosin contractions during polarity establishment by competing with ANI-1 (Chartier et al., 2011), suggesting that ANI-2 acts a dominant negative regulator of contractility. Altogether, these suggest that anillins undergo adaptations that enable them to meet the specific requirements of different cellular contexts.

1.3. Introduction to syncytial tissues

1.3.1. Historical background

The term syncytium is used to describe any tissue that lacks membrane barriers between adjacent nuclei. In summarizing the history of the studies of syncytia, it is important to note that remarkably various cell biologists from different eras have contributed to the progress in this field. Before tissues could be viewed by electron microscopy, they were all thought to be cellular (or composed of single-nucleated cells). A syncytial architecture was described for the first time in 1865 in teased preparations of fresh testis by Von La Valette St. George wherein he observed that daughter cells remain attached to each other during division and thus form a chain of connected cells (Dym and Fawcett, 1971). To explain this novel feature, he claimed:

> *"The proliferation (of the germ cells) takes place in two ways. The nucleus may divide and with it the cytoplasm so that two separate daughter cells arise from a single cell. This is the usual mode of increase in cell numbers. However, it also may happen that the second cell produced by division remains attached to the first, and this, in turn, may divide and in this way a chain of cells is formed. If the divisions do not take place in a consistent direction, a cluster (pile) of interconnected cells arise"* (quoated in Dym and Fawcett, 1971)

In 1872, Ernst Haeckel, used the term *"syncytium"*, for the first time, to describe the non-cellular ectoderm of the *Calcispongia* also known as calcareous sponges (Haeckel, 1872). In 1888, Adam Sedgwick observed syncytia in germ layers of *Peripatus Capensis* ("A Monograph of the Development of Peripatus Capensis", 1888). Other cell biologists working with fixed and sectioned tissues reported similar observations in the 19th century (Dym and

Fawcett, 1971). Among them was James Howard McGregor who, studying spermatogenesis in amphiuma in 1899, stated that:

> *"As the division proceeds, the central spindle persists as a delicate bridge, its fibers showing the thickenings which later fuse to form a ring-shaped midbody".* (From "The spermatogenesis in Amphiuma" McGregor 1899)

He further claimed that it was the first time that such a bridge was ever observed in post-telophase spermatids. Other scientists including Sertoli (1877) and von Ebner (1888) observed and depicted similar interconnecting bridges between spermatogonia during spermatogenesis (Figure 1.5).

Although these observations suggested that bridges exist and connect the cells during spermatogenesis, they left several details ambiguous as to whether they are stable structures or if they commonly occur during spermatogenesis and throughout the animal kingdom. In addition, some scientists assumed that the mere presence of these structures might be the result of poorly prepared samples. Hence, it is perhaps not surprising that these interesting observations were overlooked and thus for a long time spermatocytes were illustrated as separate cells in academic textbooks.

The development of electron microscopy in the 1920s, swept away these quandaries by allowing cell biologists to revisit germline tissues to elucidate their structural details. Much of the early work was performed by Don Fawcett, who made a landmark contribution to the field. Fawcett and others repeatedly described and depicted in various studies presence and persistence of intercellular bridges (here referred to as ICBs) and their fine structural details in the male germline of a wide variety of animals, including *Drosophila melanogaster*, *Drosophila virilis,* opossum, pigeon, rat, hamster, guinea pig, rabbit, cat, monkey and human, all of which are syncytial (Figure 1.6) (Burgos and Fawcett, 1955; Dym and Fawcett, 1971;

Fawcett, 1970; Fawcett, 1973; Fawcett et al., 1959; Weber and Russell, 1987).

A) **B)**

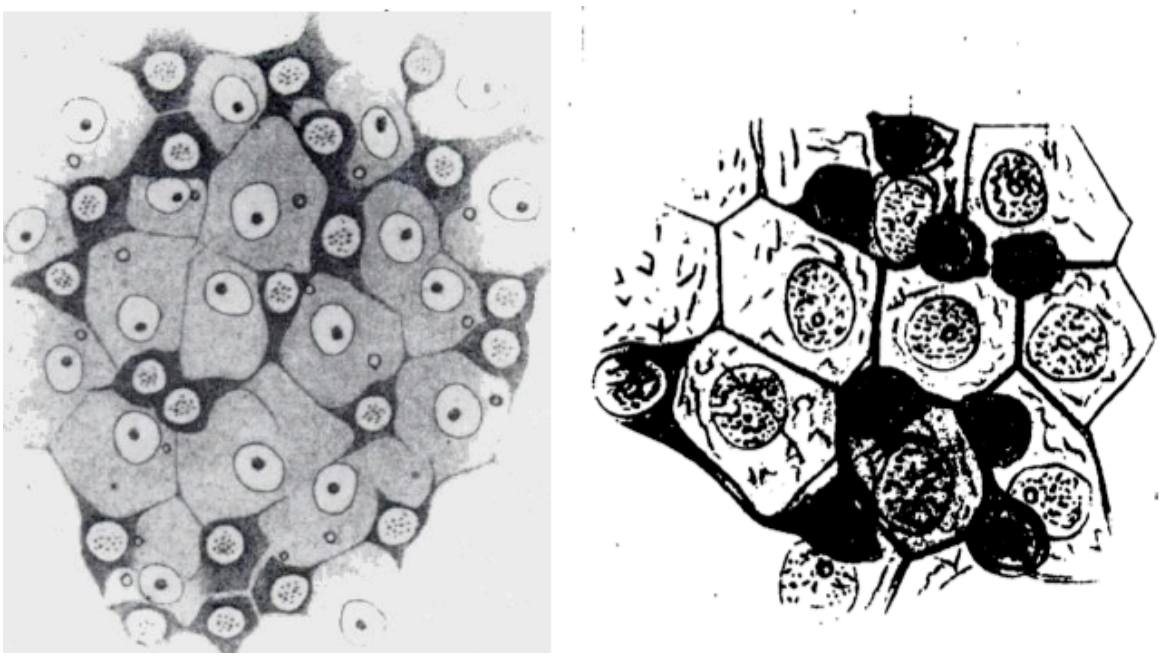

Figure 1.5: Drawings of mammalian germline bridges by nineteenth-century scientists.

(A) Sertoli (1877) and **(B)** von Ebner (1888). The darker cells are spermatogonia, which are interconnected by cytoplasmic bridges. The lighter cells are Sertoli cells. (Adapted from Fawcett and Dym, 1971, (A) originally published in Sertoli E. Sulla struttura dei canalicoli seminiferi dei testicoli studiata in rapporto allo sviluppo dei nemaspermi. *Arch Sci Med* 1877; 2:107-146; 267-295 and (B) originally published in von Ebner Zur Spermatogenese bei den Saugethieren. *Arch Mikrosk Anat* 1888; 31:236-292.

Thanks to these achievements, scientists discovered that ICB occurrence is not only limited to the male germline. As it turned out, female germ cells (GCs) from *Drosophila*, rabbit, mouse, rat, hamster and human exhibit syncytial organizations, similar to their male counterparts (Anderson and Huebner, 1968; Brown and King, 1964; Foor, 1967; Gondos and Conner, 1973; Zamboni and Gonndos, 1968). Classically, syncytia have been studied in male and female germline tissues of various animals. Slautterback et al. (1959) and Fawcett (1961)

provided the first evidence of the natural occurrence of ICBs in the somatic tissues of hydra (Fawcett, 1961; Slautterback and Fawcett, 1959).

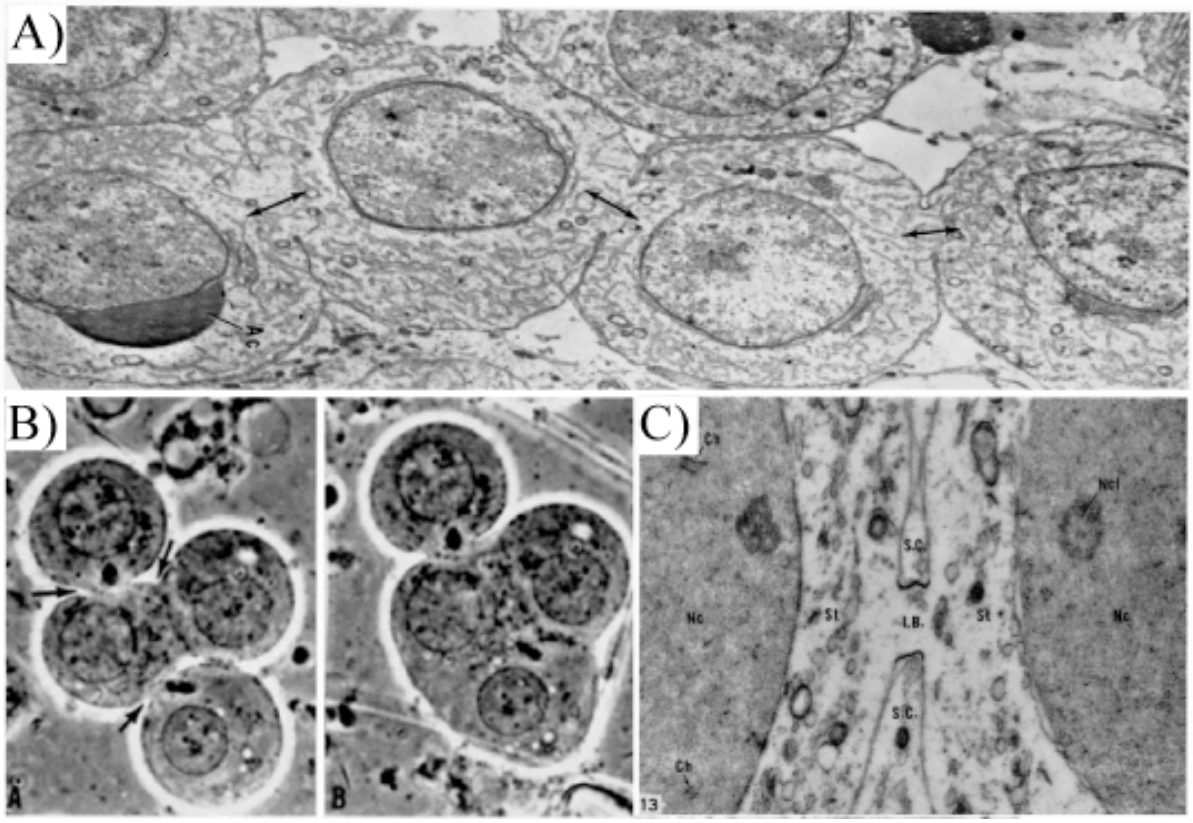

Figure 1.6: Mammalian male germline of various species are syncytial.

(A) Electron micrographs of testis in guinea pig. Arrows point to three ICBs connecting four spermatids. **(B)** Phase contrast photomicrographs of a group of rat spermatids. Arrows point to the site of ICB connecting the spermatids. **(C)** Electron micrographs of human primary spermatocytes (St) joined by a bridge (I.B.). Images are from (Fawcett et al., 1959), originally published in *Journal of Biophys Biochem Cytol,* reprinted in *Journal of Cell Biology*.

Electron microscopy has been extremely fruitful in the discovery of ICBs and their ultrastructure in various tissues, but ironically this approach has been also a limiting factor to elucidate the molecular composition, mode of division and behavioral dynamics of these structures during animal development. In over a half century that have passed since these

seminal studies, the implementation of new preparative techniques and the development of more powerful optical instruments enabled scientists to demonstrate the presence of syncytial organizations in numerous other tissues, of both germ and somatic lineages (Airoldi et al., 2011; Arnold, 1974; Greenbaum et al., 2011; Haglund et al., 2011; Huckins and Oakberg, 1978; Ren and Russell, 1991; Robinson and Cooley, 1996).

For instance, we now know that ICB occurrence and syncytium formation is far more extensive than a single case of somatic cells in hydra. Syncytia are a common phenomenon widely found in multicellular organisms including fungi (Salles-Passador et al., 1991), plants (Plachno and Swiatek, 2011) and animals (Lacroix et al., 2012). In addition, further progress in transgene technology, including the characterization and isolation of various fluorescent proteins, *in vivo* cell imaging techniques and biochemical analysis have opened new insights into these phenomena, their detailed morphological and compositional description, their function and even mechanisms of formation. In the following pages, I will focus on how and why syncytia are formed to provide the current status of the field.

1.3.2. The structural features of syncytia

Syncytia are found in diverse taxa from broadly present in plants (De Veylder et al., 2011) to several different tissues in multicellular animals and even in bacteria (Mendell et al., 2008). These examples highlight the incredible biological diversity and molecular repertoire of syncytial tissues. Resolving what syncytia are made of might provide some valuable insight into their role and mechanism of formation. Given the prevalent nature of syncytial tissues, several group of scientists were encouraged to unravel the structural and molecular details of syncytia in various animals. To date, comparisons of syncytia among species have uncovered several of their striking features. In addition, molecular and structural properties of syncytia are often thought to play a central role in the formation and behavior of these tissues during development. Here, I will first highlight the structure of the germline syncytia in *Drosophila*

and mouse male as we currently understand them and then I will give a brief overview of one example of somatic syncytia in a still growing list of syncytial tissues across the animal kingdom. I will further compare the two systems as a first mean to address whether structural properties of germline syncytia serve a corresponding role to those in the somatic syncytia.

1.3.2.1. Germline Syncytia

Most male and female GCs in a wide variety of vertebrate and invertebrate animals develop, at least for a period of time and as part of their differentiation program, within a cluster of interconnected cells in a syncytium, also known as cyst (Figure 1.7). The common prevalence of germline cysts provides strong evidence that syncytial organization is a conserved feature of germline development across species (reviewd in de Cuevas et al., 1997; Haglund et al., 2011; Pepling et al., 1999; Robinson and Cooley, 1996). In the following pages, I describe the structure and properties of germline cysts in female and male *Drosophila* and male mice.

Drosophila germline

The *Drosophila* male and female germline are perhaps the most-studied and the best-understood syncytial structures. Comparing these two systems and their structures in detail contributed to the understanding of syncytia in general. Before proceeding, for the sake of clarity, I will first briefly describe the development of the *Drosophila* female and male germline from a syncytial organization and formation perspective and then I will describe their various molecular constituents.

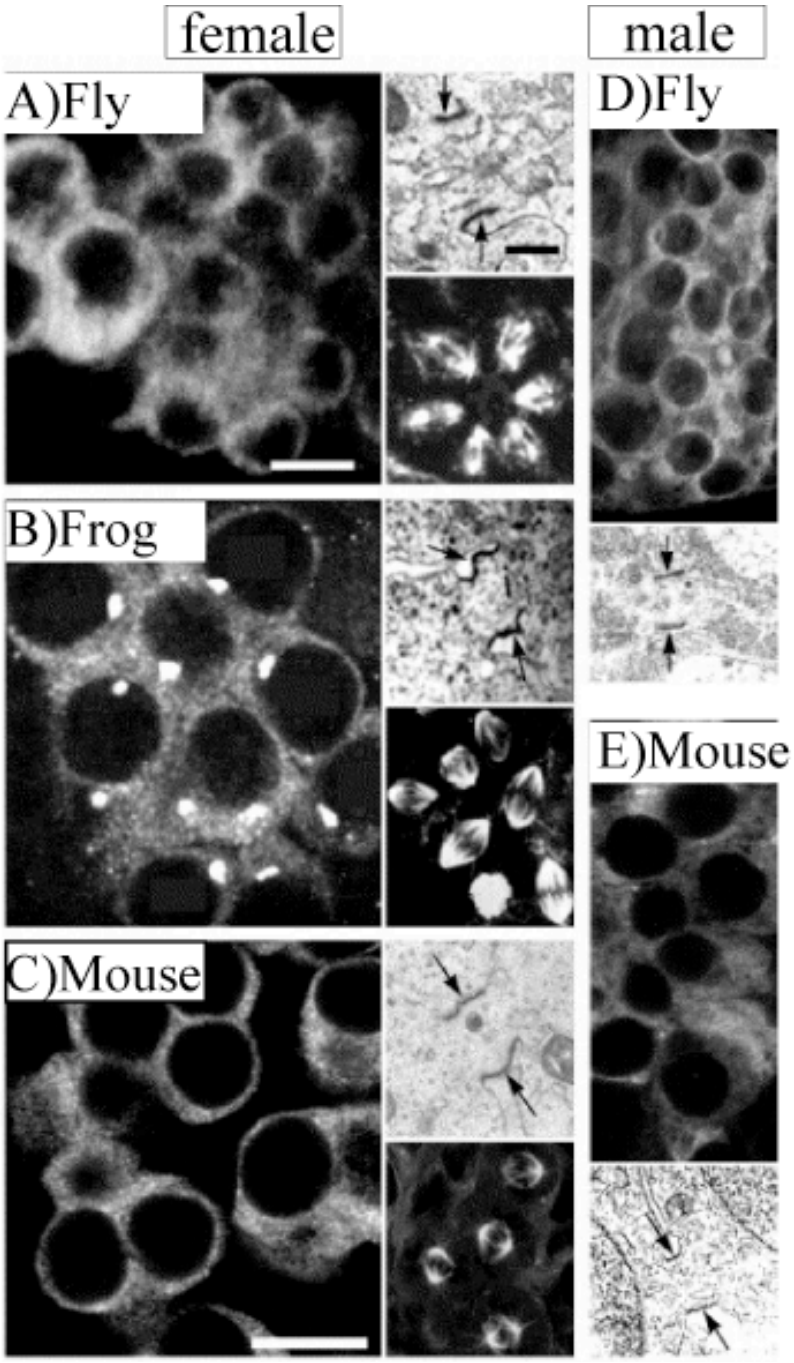

Figure 1.7: Syncytium is a conserved phase of germline development.

(A) *Drosophila* ovary **(B)** *Xenopus* ovary **(C)** mouse ovary **(D)** *Drosophila* testis and **(E)** mouse testis. (A, C, D and E) stained with a GC marker and **(B)** stained with gamma-tubulin. Top insets (A-C) and insets in (D and E), are electron micrographs from each species. Arrows point to ICBs. Bottom insets (A-C) show synchronous GC division for each species. Adapted from (Pepling et al., 1999).

Oogenesis occurs continuously in the *Drosophila* ovary. An ovary is composed of 16-20 ovarioles, each of which contains 14 different egg chambers at different developmental stages with increasing size and age from the anterior towards the posterior. At the anterior tip of each ovariole lies the germarium, which consists of different regions based on morphology (Figure 1.8 A) (Mahajan-Miklos and Cooley, 1994; Mahowald and Strasshe.Jm, 1970 and reviewed in ; Robinson and Cooley, 1997). In region 1 of the germarium, the female germline stem cells (fGSCs) undergo successive asymmetric cell divisions that give rise to two unequal daughter cells; another stem cell and a cystoblast (Haglund et al., 2011; Mahajan-Miklos and Cooley, 1994). The cystoblast then undergoes four synchronous mitotic divisions, characterized by incomplete cytokinesis, to generate a syncytium in region 2a, wherein 15 arrested cleavage furrows join 16 GCs. At this stage the arrested cleavage furrows begin maturing into stable ring canals. The 16-cell cyst later enters region 2b where the cyst will be enveloped by a monolayer of somatic epithelial follicular cells (which is also a syncytium, see *Section 1.3.2.2.*) to complete the formation of the egg chamber and oocyte specification. Among the 16 GCs, only 1 is specified to become the oocyte while the other 15 become nurse cells (reviewd in Haglund et al., 2011; Lin et al., 1994; Pepling et al., 1999; Robinson and Cooley, 1996). The formed stage 1 egg chamber eventually moves into region 3, which is the last region of the germarium (Figure 1.8 A).

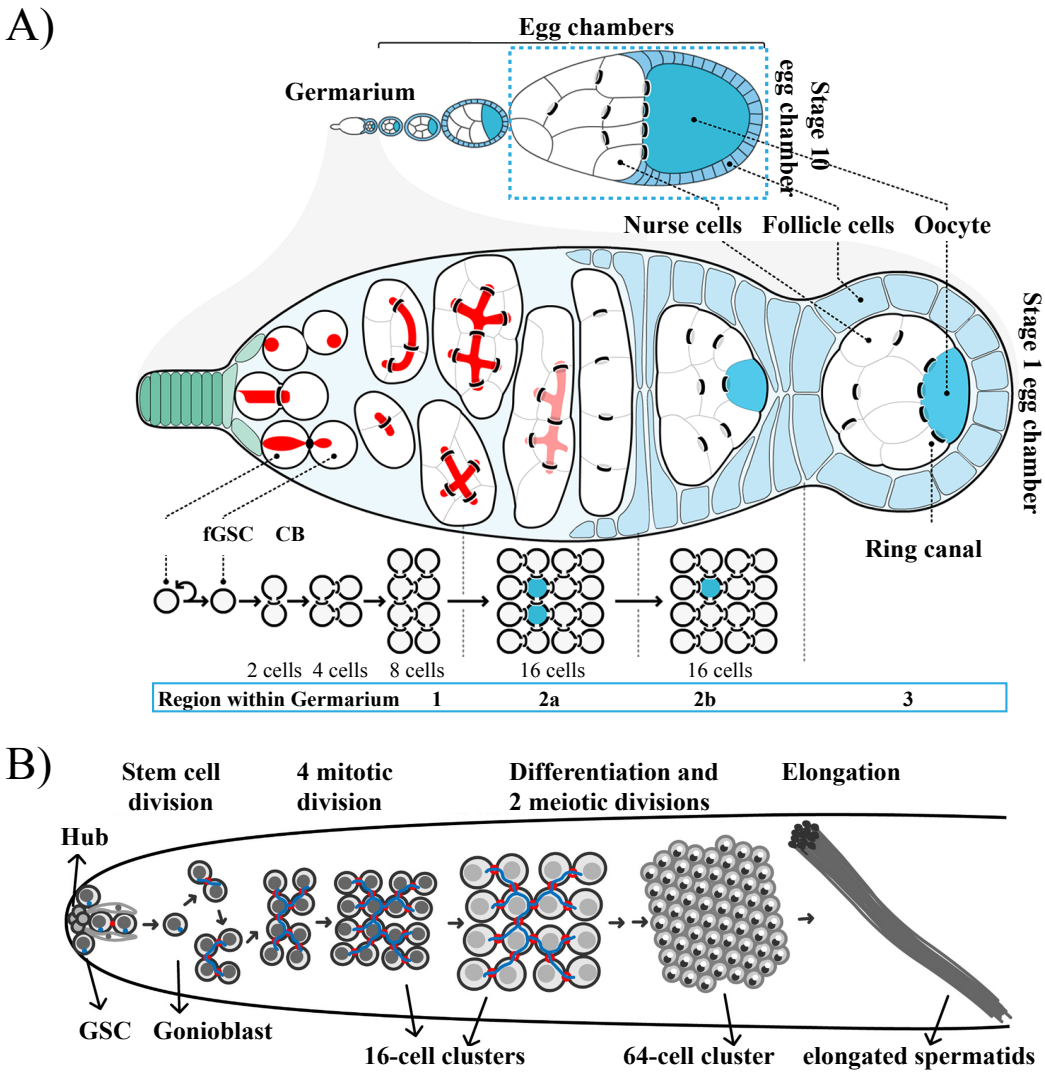

Figure 1.8: Schematic overview of germline development during *Drosophila* oogenesis and spermatogenesis.

(A) Scheme showing an ovariole with a germarium linked to four growing egg chambers (top) and a close-up on a germarium (bottom). The germarium is divided into regions 1, 2a, 2b, and 3. Region 1 contains fGSC (Female germline stem cell) and mitotically active 2-, 4-, and 8-cell clusters. Eventually, 16 GCs will be formed that are initially interconnected by the fusome (red). In 2a, gradually one of the two GCs with 4 ICBs (turquoise) is selected to become the oocyte. Meanwhile the fusome break down (light red) and follicle cells (blue) begin to migrate around the cyst. Young egg chambers completely surrounded by follicle cells flatten into a lens shape in region 2b. The stage-1 egg chamber reaches region 3 of the germarium where it becomes spherical and prepares for departure from the germarium as a stage-2 egg chamber (Adapted from Eikenes et al., 2015) **(B)** Ring canals are colored in red and the fusome is shown in blue (Adapted from Eikenes et al., 2013).

The initial steps of the germline development in male *Drosophila* are quite similar to female germline development, where the GSCs divide asymmetrically to produce a daughter stem cell and a founder gonial cell (Hime et al., 1996). In males, as in females, the founder gonial cell initiates four consecutive rounds of synchronous and incomplete mitotic divisions resulting in 16 interconnected spermatocytes. However, in males, the 16-cell cyst undergoes enlargement and differentiation before two extra rounds of meiosis with incomplete cytokinesis further occur to form a total of 63 ring canals interconnecting 64 haploid spermatids within the cyst (Figure 1.8 B) (Hime et al., 1996). In contrast to the *Drosophila* oogenesis, in the *Drosophila* male program of spermatogenesis, both mitosis and meiosis occur symmetrically and thus all the GCs within the syncytia equally mature into sperms. A remarkable series of events and structural alterations results in the formation of ring canals during *Drosophila* germline development:

Formation of the fusome:

One striking feature of both female and male ring canals in the *Drosophila* germline is the appearance of an unusual spherical intracellular GC-specific organelle known as the fusome in the female cystoblast (Figure 1.8 A, shown in red) or the male founder gonial cell (Figure 1.8 B, shown in blue). The fusome was initially described by Platner as "Verbindungsbrücken" meaning "bridging connections" in spermatocytes of numerous insects (reviewd in de Cuevas et al., 1997). In 1901, another example of a remarkably similar structure has been recognized during oogenesis of the diving beetle (Dytiscus) where it has been proposed to be a remnant of the mitotic spindle (de Cuevas et al., 1997; Lin et al., 1994). However, studies of the fusome in Drosophila ovaries argue against this, showing that the small spherical fusome in cystoblasts arises from merging of the newly formed fusome at the cleavage furrow and the fusome from the previous division (see Figure 1.11) (deCuevas et al., 1996; Lin and Spradling, 1995; Lin et al., 1994).

Despite the fusome appearance in both sexes, the female and male fusome in *Drosophila* exhibit structural and behavioral differences (Hime et al., 1996). For example, during *Drosophila* oogenesis, each round of cystoblast mitosis is accompanied by fusome elongation

and branching along the ring canals to physically connect individual GCs within the cyst (Figure 1.8 A) (reviewd in de Cuevas et al., 1997; Haglund et al., 2011; Pepling et al., 1999; Robinson and Cooley, 1996). As a result of these divisions, 2 out of 16 GCs contain four ring canals. Eventually, among these 2 cells, the one retaining the most fusome material becomes the oocyte (de Cuevas and Spradling, 1998). Subsequent to this and upon formation of the 16-cell cyst in region 2a of the germarium (Figure 1.8 A), fusomes break down and disappear (Figure 1.8 A, in light red) and open the ring canals, thus allowing the transport of organelles and molecules into the oocyte (Figure 1.8 A) (more details are described in *Section 1.4.1.2.*) (de Cuevas et al., 1997; Pepling et al., 1999). Contrary to this, fusomes in males do not break down and instead persist and grow during meiosis and spermatogenesis (Hime et al., 1996). One explanation for the persistence of the fusome in males is that it could play a role in organizing and aligning the elongated spermatids flagella within the cyst (Hime et al., 1996). In addition to this behavioral difference, some dissimilarities in the molecular composition of the *Drosophila* male and female fusomes have also been documented (Hime et al., 1996). A series of studies from Allan Spradling group have shown that the female fusomes are composed of membrane skeleton components including α-spectrin and the adducin-like hu-li tai shao (Hts) and that they play an important role in cyst formation and oocyte differentiation (de Cuevas and Spradling, 1998; deCuevas et al., 1996; Lin and Spradling, 1995; Lin et al., 1994; Yue and Spradling, 1992), whereas in males, only α-spectrin has been observed in fusomes (Hime et al., 1996).

Development of ring canals:

Germline ring canals in male and female *Drosophila* are initially formed from modified cytokinetic furrows. Following this, through a series of defined steps of protein recruitment and removal, ring canals mature into stable structures. As such, formation and maturation of *Drosophila* germline ring canals are two spatiotemporally distinct events that happen during different phases. Below, I will give a brief summary of the structural alterations and the order in which different proteins join and leave the ring canals in both sexes.

The cleavage furrows of GCs contain a number of proteins, many of which are identified components of cytokinetic rings such as actin (Hime et al., 1996; Robinson and Cooley, 1997), the centralspindlin component Pav-Klp (Carmena et al., 1998; Haglund et al, 2010; Hime et al., 1996; Minestrini et al., 2002), the actomyosin-binding protein Anillin (Field and Alberts, 1995; Haglund et al., 2010; Hime et al., 1996), the scaffolding protein Cindr (Eikenes et al., 2013; Haglund et al., 2010; Haglund et al., 2011) and the glycoprotein Mucin-D (Kramerova and Kramerov, 1999). One central feature of both male and female germlines during early stages of ring canal formation is the appearance of 0.5-1 μm rings of phosphotyrosine-containing protein(s) (pTyr proteins) in the cleavage furrow (Cooley and Theurkauf, 1994; Hime et al., 1996; Robinson et al., 1994; Robinson et al., 1994; Robinson and Cooley, 1996). Except for these parallels between male and female ICBs throughout initial periods of building a ring canal, subsequent processes that occur during later stages of ring canal development and their molecular composition vary between the two sexes (Hime et al., 1996).

During *Drosophila* oogenesis, for instance, upon formation of the 16-cell cyst and its entry into region 2a of the germarium, the fusome breaks down (de Cuevas and Spradling, 1998) and Cindr disappears from the cleavage furrows (Haglund et al., 2010; Haglund et al., 2011). Once the oocyte becomes specified, actin filaments and Hts, an essential protein for female ring canal growth, begin to accumulate at the inner rims of the female ring canals (Robinson et al., 1994). Addition of these two proteins is accompanied by an increase in the amount of phosphotyrosine staining on the ring canal at region 2a (Robinson et al., 1994). In region 3 of the germarium, wherein the stage-1 egg chamber is ready to leave the germarium (Figure 1.8 A), Anillin gets dissociated from the outer rim of the female ring canals, while Kelch (an actin filament cross-linking protein) is recruited to the inner edge of the ring canals (Field and Alberts, 1995; Robinson et al., 1994; Robinson and Cooley, 1997). At this point, the bridge diameter increases from < 1 μm to 3-4 μm (Robinson and Cooley, 1997), forming what is considered to be a mature ring canal, which contains Pav-Klp, bundles of actin, Hts, Cheerio and Kelch (reviewed in Greenbaum et al., 2011; Haglund et al., 2011; Robinson and Cooley, 1996). Mature ring canals continue to expand in diameter, during which Hts, Kelch and Cheerio promote the bundling of actin filaments along the inner rim of the ring canal.

Similar to female GCs, *Drosophila* male ring canals initially loose their Cindr (Eikenes et al., 2013; Haglund et al., 2010). Loss of Cindr has been proposed to be a critical step to promote incomplete cytokinesis at the transition from mitosis to differentiation in both male and female germline tissues (Eikenes et al., 2013). Despite this similarity, actin disappears from the male *Drosophila* GCs (Greenbaum et al., 2011; Haglund et al., 2011; Hime et al., 1996; Robinson and Cooley, 1996). Proteins such as pTyr proteins, Anillin, Mucin-D, Pav-Klp and at least three *Drosophila* Septin proteins (Peanut, Sep1 and Sep2) remain stably associated to the ring canals throughout spermatogenesis (Greenbaum et al., 2011; Haglund et al., 2011; Hime et al., 1996; Robinson and Cooley, 1996). Moreover, unlike in females, neither Kelch nor Hts were detected in male ring canals (Hime et al., 1996). Altogether, these studies reveal that the major component of the mature GC ring canals in females is actin whereas male ring canals have a septin-based cytoskeleton.

Mammalian germline

The first studies of syncytia were reported in testes of various male animals, yet mammalian ICBs, compared to their *Drosophila* counterparts, are significantly less explored and thus the structural and compositional properties of mammalian ICBs still remains not fully understood. This could be in part due to the technical difficulties of performing in vivo live imaging in the mammalian germline. Nevertheless, for several years electron microscopy enabled scientists to perform considerable ultrastructural analyses on ICBs in a variety of mammalian species. Among these studies, Weber and Russell, 1987, provided the first systematic investigation of the structural morphology of ICBs throughout different stages of rat spermatogenesis and demonstrated that both the ICB diameter and length undergo changes during spermatogenesis (Weber and Russell, 1987). For example, they observed that as cells progress through spermatogenesis, the diameter of their connecting ICBs increase (Weber and Russell, 1987).

Later, Russell et al. 1987 identified actin as an ICB component in male germline of rat and ground squirrel (Russell et al., 1987). Moreover, they demonstrated that upon using

cytochalasin D (an actin-depolymerizing drug), the ICBs of male squirrel collapse resulting in a multinucleated cell, further highlighting that actin is an essential component of mammalian germline ICBs and is required for their maintenance (Russell et al., 1987). In 1998, in a study that aimed to establish the cell type-specific expression of Heat shock transcription factors (HSFs) in the rat seminiferous epithelium, immunoelectron microscopic analyses revealed that HSF2 is localized to the membranes of the interconnecting ICBs of rat spermatocytes and spermatids (Alastalo et al., 1998). Until quite recently, actin and HSF2 were the only identified components of the ICBs during spermatogenesis and the molecular composition of the mammalian ICBs remained unidentified. Currently, much of our understanding of mammalian germline syncytia has come from studies in male mice, from a series of papers from Martin Matzuk's laboratory in which they showed that the molecular composition of the ICBs in male mice testes is quite distinct from the ring canals in *Drosophila* (Greenbaum et al., 2009; Greenbaum et al., 2007; Greenbaum et al., 2006; Iwamori et al., 2010).

One key component of human and mice GC ICBs that has not been identified in male or female *Drosophila* germline is TEX14 (testis-expressed gene 14) (Greenbaum et al., 2007). TEX14 was first identified as a protein with 3 N-terminal ankyrin repeats (ANK), a central kinase-like domain (KL) and several coiled-coil motifs localized to male GC ICBs and required for male fertility in mice (Greenbaum et al., 2006). Using biochemical and proteomic analyses, Matzuk's group further revealed that TEX14 has an essential role in ICB formation (Greenbaum et al., 2006) and that its recruitment to the midbody is required for transforming the midbody matrix into a stable ICB (Greenbaum et al., 2007). To date this study remains the first and only observation reporting an essential role for an ICB component in syncytium formation in mammals. In addition to TEX14, Matzuk's group has also identified several cytokinetic components including the two centralspindlin proteins MKLP-1 (Mitotic Kinesin-Like Protein 1, a homolog of Pav-Klp in *Drosophila*) and MgcRacGAP (male germ cell Rac GTPase-activating protein) to be localized to ICBs in mice testes (Greenbaum et al., 2007).
The more detailed analysis of GC ICBs and their composition allowed the Matzuk group to describe different molecular steps of ICB development throughout mice spermatogenesis in a

model shown in Figure 1.10 C. Male GCs start as diploid spermatogonia, proceed through meiosis as spermatocytes, and complete development as haploid spermatids. During early stages of telophase in the spermatogonia, TEX14 is recruited to the cleavage furrow that contains MKLP-1, MgcRacGAP, Anillin and one of thirteen functional genes of mammalian Septin (SEPT7) (Greenbaum et al., 2007; Kinoshita, 2003). Upon midbody formation, TEX14 rings are localized in the inner rim, wherein they perfectly colocalize with the centrosomal proteins CEP55 (CEntrosomal Protein 55kDa) and Pericentrin (Chang et al., 2010; Iwamori et al., 2010). MKLP-1 and CYK-4/MgcRacGAP remain in the outer rim of the midbody (Greenbaum et al., 2007). At this time, Anillin and SEPT7 have relocated from the outer rim of the bridge to the sides of the midbody (Greenbaum et al., 2007). During early stages of ICB formation, Anillin is removed from the ICB whereas SEPT7 returns to the outer rim of the ICB, wherein two other mammalian Septins, SEPT2 and SEPT9, are also added (Greenbaum et al., 2007). Thus unlike *Drosophila*, Anillin is not a component of mature ICBs. Eventually as the ICB undergoes maturation, Septins get dissociated from them, whereas TEX14, MKLP-1, CYK-4/MgcRacGAP (Greenbaum et al., 2007) and centrosomal proteins CEP55 and Pericentrin 2 (Chang et al., 2010; Iwamori et al., 2010) remain tightly associated to the bridges. Similar to a ICB expansion shown in earlier studies of rat spermatogenesis (Weber and Russell, 1987), TEX14 rings also grow in diameter during the transition from midbody to a mature ICB in male mice. The maturation is further accompanied by extensions of TEX14 rings toward the outer rim of the bridge until the two rims unite. Meanwhile, proteins such as HSF2, δ Tubulin, actin and Plectin are added to the enlarging matured ICBs (Greenbaum et al., 2007). Moreover, it has been reported that TEX14 is also an essential component of embryonic GC ICBs in male and female mice (Greenbaum et al., 2009).

1.3.2.2. Overview of somatic syncytia

Across the animal kingdom, several different somatic tissues have been reported to have syncytial architecture. Examples include hydra (Fawcett et al., 1959), seam cells in *C. elegans*, ovarian epithelial follicle cells (Airoldi et al., 2011; de Cuevas and Spradling, 1998; Giorgi, 1978; Haglund et al., 2010; Kramerova and Kramerov, 1999; Minestrini et al., 2002;

Woodruff and Tilney, 1998), larval imaginal discs, pupal legs and larval brain (Kramerova and Kramerov, 1999) in *Drosophila* (Giorgi, 1978; Kramerova and Kramerov, 1999; Larsen, 1989; Poodry and Schneiderman, 1970), mammalian cardiomyocytes (Clubb and Bishop, 1984; Engel et al., 2006; Lacroix and Maddox, 2012; Li et al., 1997), ~30% of human hepatocytes (Gentric and Desdouets, 2014; Gentric et al., 2012; Gupta, 2000; Kudryavtsev et al., 1993; Lacroix and Maddox, 2012; Seglen, 1997), megakaryocytes and vascular smooth muscle cells in humans. In addition tissue layers within several different organs can be also composed of a syncytial structure. Examples include human trophoblast giant cells (TGCs) of the placenta, which provide a barrier between the maternal blood supply and the fetus (Watson and Cross, 2005) or the subperineurial glia (SPG) of the *Drosophila* nervous system that functions as a blood-brain barrier in *Drosophila* (Unhavaithaya and Orr-Weaver, 2012). Despite the frequency of syncytia occurrence among somatic tissues, their structure, function and mechanism of formation remain poorly understood. Here I will focus on somatic syncytium of the ovarian follicular epithelium in *Drosophila* and briefly describe their molecular structure and morphology.

Drosophila follicular ring canals

During *Drosophila* oogenesis, the follicle cells form a single epithelial layer around germline cysts within the egg chamber. The follicle cells are positioned in such a way that their apical ends face the GCs within the cyst and their basal end are adjacent to the basement membrane forming the outer surface of the egg chamber. Ultrastructural analyses of the epithelial tissues surrounding the germline cysts in various insects have revealed the presence of ICBs, also known as somatic ring canals, in these tissues (Fiil, 1978; Meola et al., 1977; Ramamurty and Engels, 1977). Later, Giorgi (1978) reported that the epithelial follicle cells in *Drosophila*, similar to other insects, are also linked to each other via somatic ring canals and described them as being “of unusual morphology” (Giorgi, 1978). More studies of these tissues by other scientists further confirmed the existence of ring canals containing F-actin in the *Drosophila* follicle cells, similar to *Drosophila* female germline ICBs (Woodruff and Tilney, 1998). Despite this similarity, however, it has been shown that the ICBs of follicle

cells are much smaller in diameter than the germline ring canals. Consistent with this, unlike the female germline ring canals, the amount of F-actin filaments in each ring as well as the diameter of ring canals in *Drosophila* follicle cells remain unchanged throughout the course of oogenesis (Woodruff and Tilney, 1998). Further attempts to investigate the molecular composition of somatic ring canals revealed that in addition to F-actin (Woodruff and Tilney, 1998), they contain Pav-KLP (Minestrini et al., 2002), visgun (Airoldi et al., 2011; Buszczak et al., 2007; Nystul and Spradling, 2007), Anillin (de Cuevas and Spradling, 1998), Mucin-D (Kramerova and Kramerov, 1999), Cindr (Haglund et al., 2010) (Figure 1.9). In addition, Nasrat and Polehole, two *Drosophila* cell surface molecules, localize to the ring canals between the follicle cells at the oocyte periphery and they were initially proposed to be ring canal components of somatic follicle cells in *Drosophila* (Jimenez et al., 2002). However, further investigations by Lynn Cooley's group, revealed that neither of these cell surface proteins co-localize with a known component of follicle ring canals, Pav-KLP, demonstrating that they are not among the somatic ring canal constituents of *Drosophila* follicle cells (Airoldi et al., 2011).

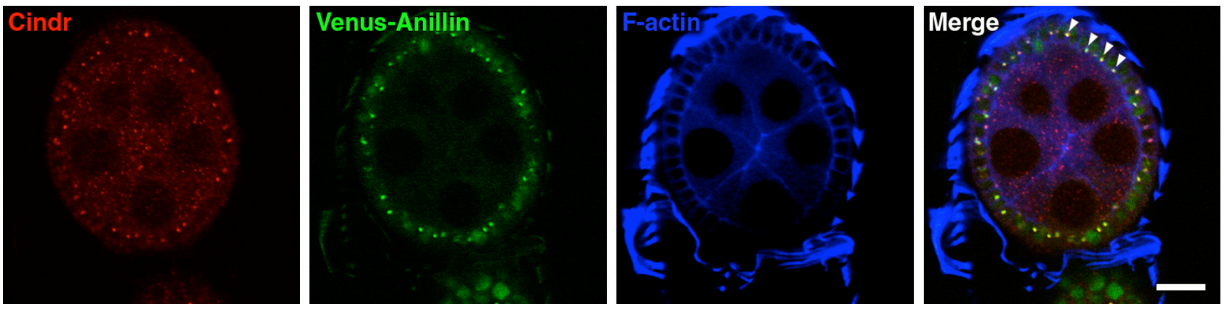

Figure 1.9: Follicle cells of the *Drosophila* ovary are syncytial.

Venus-tagged Anillin (green), stage-8 egg chambers of *Drosophila* were fixed and stained with anti-Cindr (red) and phalloidin (blue). Cindr (red) localizes with Anillin (green) at follicle cell's ICBs (arrowhead) (Adapted from Haglund et al., 2010).

1.3.3. Comparing the syncytial systems

Comparison of the cytoskeletal architecture of germline and somatic ICBs in *Drosophila* and mammals reveals some similarities in the development of these common traits as well as divergent features between them (Airoldi et al., 2011; de Cuevas et al., 1997; Greenbaum et al., 2007; Haglund et al., 2010; Haglund et al., 2011; Mahowald and Strasshe.Jm, 1970; Robinson and Cooley, 1996). Dissimilarities in dynamics and structure might in fact reflect the different roles each one of these tissues is playing during development. Here I will first overview the common and then the differences among diverse syncytial tissues (Figure 1.10).

1.3.3.1. Common features of syncytia

The most prominent landmark of the germline and somatic ICBs is the presence of an electron-dense layer that lines the inner walls of the bridge (Haglund et al., 2011; Woodruff and Tilney, 1998). This property has been proposed to provide rigidity and stability to the bridge by protecting its plasma membrane from events that normally promote completion of cytokinesis (This will be further expanded in section 4). The second parallel between all germline and somatic syncytia is the early recruitment of some key regulators of cytokinesis including Pavarotti/MKLP1 (Carmena et al., 1998; Greenbaum et al., 2007; Minestrini et al., 2002), suggesting that these components may have a unique structural function during ring canal assembly and maintenance throughout syncytium formation in various tissues and in different animals. Future efforts will no doubt discover other common features of syncytial tissues and will further highlight conserved properties required for the proper formation and/or function of syncytia.

1.3.3.2. Dissimilarities among syncytia

One property that has been only seen in germline syncytia is the ICB diameter enlargement that occurs depending on the developmental stage of the gametogenesis in germline of mammalian males and both sexes in *Drosophila* (from 1μm to 10μm during

Drosophila oogenesis, from 1.8μm to 3μm during *Drosophila* spermatogenesis and from 1μm to 3μm during mammalian spermatogenesis), while the ICB size remains unchanged in somatic follicle cells.

Another difference is the absence of actin filaments in male ring canals, while their presence is required for integrity of the female ICBs and their function at least in *Drosophila* germline. For instance, it has been shown that in *hts* mutants, actin filaments fail to accumulate at the female ring canals resulting in ring canal collapse, a defect which in turn blocks the material transport from the nurse cells into the oocytes, resulting in sterility (Yue and Spradling, 1992). One explanation for these compositional dissimilarities could be that the female ring canals expand during development to reach approximately 10 μm in diameter, whereas their male counterparts do not expand as much (Hime et al., 1996; Hudson and Cooley, 2002; Robinson and Cooley, 1996; Tilney et al., 1996; Weber and Russell, 1987). Consistent with this, Hime et al, 1996 proposed that the presence of proteins such as actin and kelch in female ring canal might be an adaptation for the female-specific role of ring canals in transport of cytoplasmic materials from 15 nurse cells into the oocyte during *Drosophila* oogenesis (Hime et al., 1996). Overall, the differences between *Drosophila* female and male germline suggest that GCs use distinct methods to stabilize their ring canals during germline development. Furthermore, in contrast to male and female *Drosophila,* anillin is not in the ICB in mammals. While Tex14 is an essential component of germline ICBs in mice (Greenbaum et al., 2006) and humans (Greenbaum et al., 2007), its homolog has not yet identified in germline of *Drosophila* or other species.

On one hand, compositional differences of ICBs among different syncytial structures suggest that there are variations in their mode of formation. On the other hand, ICBs, particularly during early steps of formation, appear to contain a group of core components of cytokinesis, suggesting a common molecular process underlying their formation, a process that is perhaps coupled with modifications in cytokinesis.

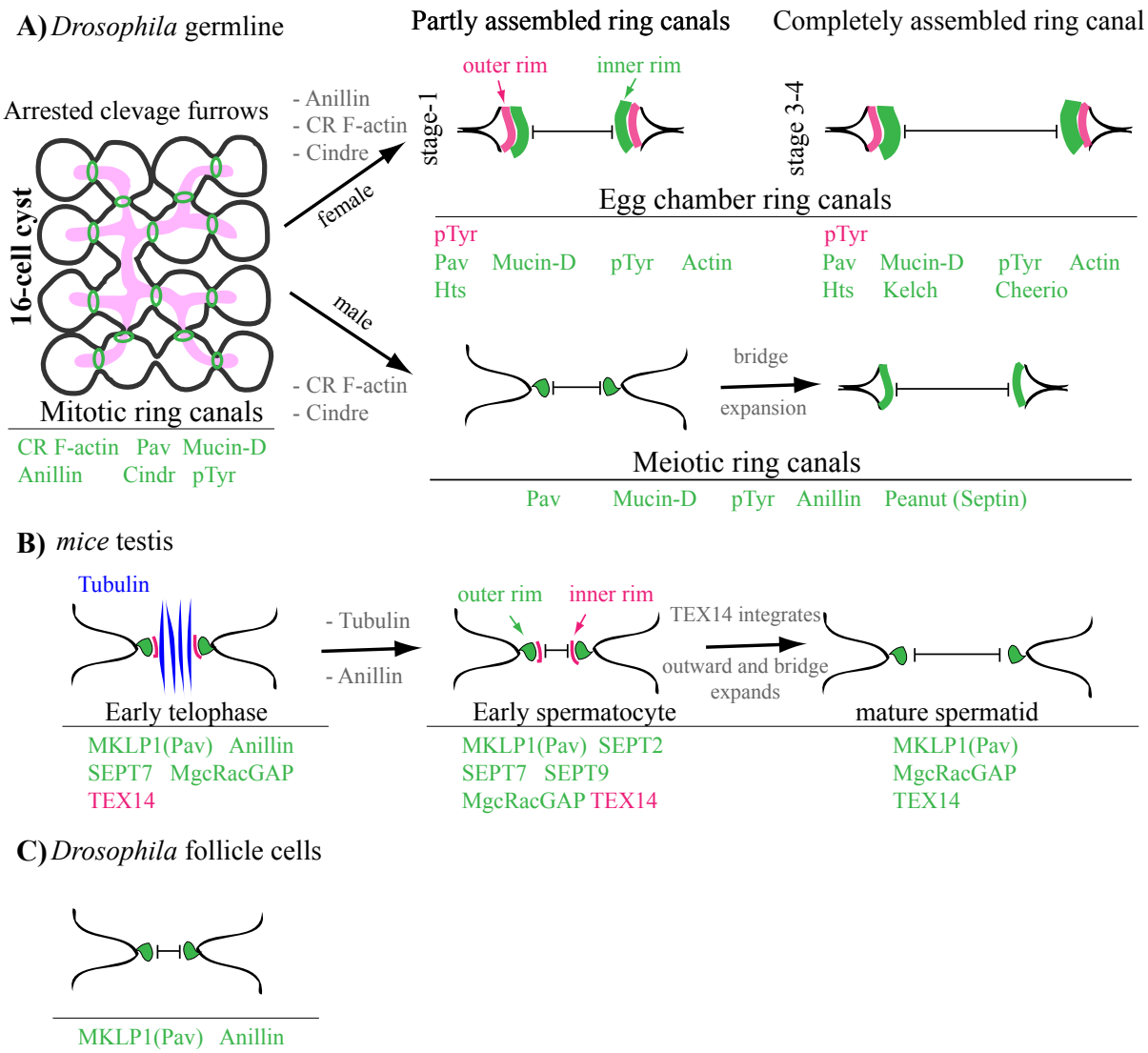

Figure 1.10: Comparison of syncytial tissues in different organisms.

(A) *Drosophila* female (top) *Drosophila* male (bottom), **(B)** mice testis and **(C)** *Drosophila* somatic ovarian follicle cells. Figure inspired from Robinson et al., 1997.

1.4. How are syncytia formed?

As explained in the previous pages, syncytia are normal developmental and physiological state of several different tissues (and in some cases the entire organism) in different taxa. To understand the purpose of syncytia, we must first understand how these fascinating structures are formed. Although, syncytiogenesis could occur via several routes: genomic doubling, gametic nonreduction, and polyspermy (Otto and Whitton, 2000), a general term often used to describe the generation of a syncytial structure is endoreplication, which refers to multiple genome duplications without division/cytokinesis (Figure 1.11 A). In general, syncytia, as Wilhelm His stated in his 1898 paper "*Ueber Zellen und Syncytienbildung"*, may occur either through delayed formation of the cell membranes or incomplete cytokinesis (also refer to as cytokinesis failure) (Figure 1.11 B) or from fusion of already formed cells (Figure 1.11 C) (Hardesty, 1904).

Nonetheless, regardless of mode of syncytium formation, there are two distinct types of syncytia: **1) Physiologically/developmentally-programmed syncytia**: tissues in which syncytium is part of a tightly controlled normal developmental or physiological program with beneficial roles to serve special functions throughout or at least during particular developmental stages of the plant or animal life and **2) Pathological syncytia**: tissues in both animals and plants that are normally composed of single-nucleated diploid cells but are switched to the polyploid state during pathological or viral infection (e.g., in animals measles virus, a respiratory syncytial virus and HIV) (Gao and Zheng, 2011; Pastey et al., 2000; Weng et al., 2009) or in response to injury or environmental changes including the mechanical and metabolic stress (Pandit et al., 2013; Davoli and de Lange, 2011). This type of syncytium is accidentally formed and in most cases, but not always is correlated with problems such as chromosome instability, aneuploidy and carcinogenesis (Nguyen and Ravid, 2006).

For the purpose of this work I will emphasize on how physiologically/developmentally programmed-syncytia are formed. It is clear that syncytial tissues have evolved frequently, via

a variety of pathways. Remarkably, programmed cytokinesis failure seems to be the most widely used strategy to form this type of syncytia. Thus, here I will first focus on and provide examples on how different tissues, across the animal kingdom, achieve their syncytial state by altering different stages of cytokinesis. Then, I will briefly describe the fusion mechanism of syncytium formation by providing a brief summary of skeletal muscle formation.

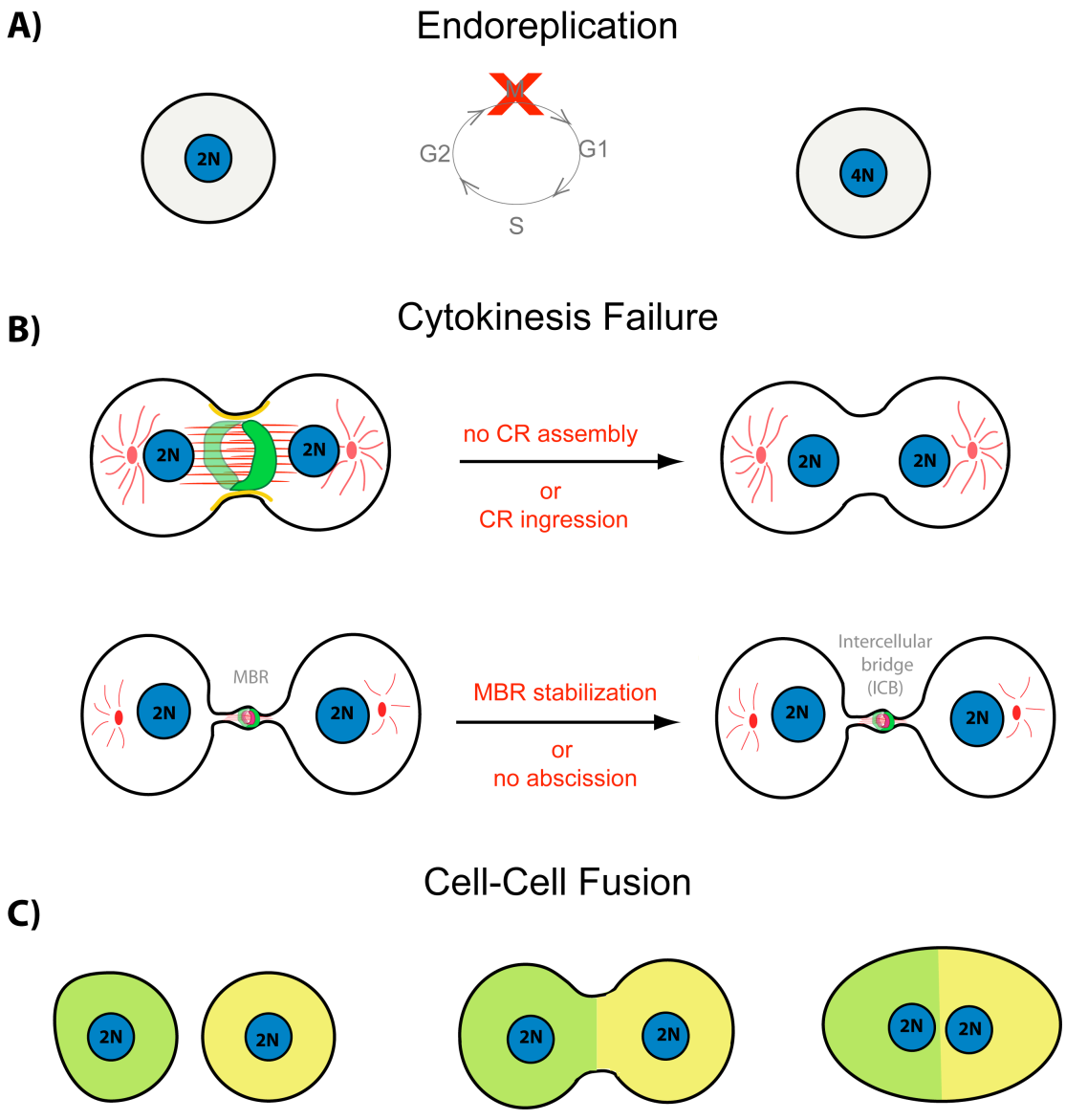

Figure 1.11: Schematic showing different mechanism of syncytium formation

1.4.1. Syncytium formation through modifications in cytokinesis

As described in *Section 1.1.*, cytokinesis is a highly ordered and spatiotemporally regulated process, despite this regulation, cytokinesis can sometimes fail. Cytokinesis failure leads to both centrosome amplification and production of tetraploid cells, which may set the stage for tumorogenesis. Paradoxically, it has been repeatedly proposed that a programmed cytokinesis failure is the most prominent mechanism for syncytiogenesis during normal development of several different syncytial tissues, such as cardiomyocytes, and in particular germlines of various animals (reviewed in Greenbaum et al., 2011; Haglund et al., 2011; Pepling et al., 1999). In this scenario, different events could directly or indirectly target and modify distinct stages of the conventional process of cytokinesis, from positioning of the division plane and furrow ingression to abscission, in order to generate the same final product; a syncytium (Figure 1.11 B). In this section, I provide a brief overview of our current understanding of the mechanisms of syncytiogenesis, highlighting steps in the pathway that may be regulated or prone to failure.

1.4.1.1. Syncytium formation via failure of cytokinesis during CR assembly/formation or CR ingression

Here I provide examples of how perturbing the first three stages of cytokinesis; spindle positioning, CR assembly/formation and CR ingression could result in cytokinesis failure by providing single examples for each (Figure 1.11 B).

Post-natal rat liver cells

As described in *Section 1.1.1.1.*, microtubules play crucial roles in delivering signals that lead to localized activation of RhoA in the furrow, which in turn leads to recruitment and activation of effector proteins that organize and stimulate furrow ingressions. Recent studies suggest that cytokinesis failure may occur in cells in which defects in spindle positioning perturbs delivery of activation signals to the cortex. One example of cytokinesis failure at the stage of cleavage-plane specification occurs during rat postnatal liver development (Margall-

Ducos et al., 2007). Upon weaning, postnatal hepatocytes in rat undergo an atypic developmental cell division program during which DNA is duplicated without accomplishing cytokinesis, through a series of events. First, although microtubule network dynamics is normal until early anaphase, during elongation the astral microtubules fail to contact the equatorial cortex and as a result the spindle collapses in telophase. This in turn abolishes delivery of RhoA activators and subsequently active RhoA at the equatorial zone, leading to an absence of activation of RhoA downstream signals in these cells. As such, these cells, unlike their hepatocyte counterparts that complete cytokinesis, fail to elongate and to recruit actin and myosin to the CR and hence lack a functional CR (Guidotti et al., 2003; Margall-Ducos et al., 2007).

Cardiomyocytes

As mentioned before, similar to liver, the heart also contains a large number of tetraploid cells that arise through cytokinesis failure. While during rat prenatal development, cardiomyocytes accomplish cytokinesis, soon after birth (at post-natal day 4) (Li et al., 1996), they undergo nuclear divisions accompanied by cytokinesis failures, resulting in the formation of binucleated myocytes (Clubb and Bishop, 1984; Li et al., 1997). It has been shown that the CR is formed during the binucleation process of cardiomyocytes, suggesting that defects in cytokinesis steps other than CR formation are likely to give rise to binucleated cardiomyocytes. One explanation proposed by different groups is that the incomplete disassembly and persistence of myofibrils, the heart-specific contractile apparatus required for heart beating and blood pumping, physically impedes CR ingression at the furrow during postnatal development of rat cardiomyocytes (Li et al., 1996; Li et al., 1997; Rumyantsev, 1977; Zak, 1974). Despite these, it still remains unclear whether myofibrils are not disassembled from the furrow and how their persistence at the furrow could account for the cytokinesis failure in postnatal rat cardiomyocytes (Engel et al., 2006). Instead, it was shown that while morphology of the centralspindle and its formation, as assessed by localization of Aurora B, appeared to be normal, inappropriate anillin localization and recruitment to the cortex results in an asymmetric furrow ingression and eventually failure of proper CR

contraction, forming a syncytium (Engel et al., 2006), suggesting that earlier steps in cytokinesis may also be affected in these cells.

Megakaryocytes

Megakaryocyte differentiation is also accompanied by generation of a large nuclear mass and cytoplasmic volume within a syncytium (Geddis and Kaushansky, 2006; Vitrat et al., 1998). Megakaryocytes are myeloid cells that reside within the bone marrow and produce and release platelets (thrombocytes) into blood stream which are required for blood clotting (Nakeff and Maat, 1974). To achieve the capacity to release platelets, a megakaryocyte enlarges considerably and undergoes multiple rounds of DNA duplication without cytokinesis which progressively increase its ploidy to ultimately produce a giant polyploid cell (up to 128N). Studies with primary megakaryocytes has revealed that the cleavage furrow is properly formed and undergo ingression, however cytokinesis fails due to regression of the well-formed furrow, arising the 4N cells (Geddis and Kaushansky, 2006; Gentric and Desdouets, 2014; Lacroix and Maddox, 2012; Lordier et al., 2008; Ravid et al., 2002). In consistent with this, it was shown that while the central spindle is normally formed, as assessed by localization of essential cytokinetic components such as Aurora B, INCENP, Survivin, PRC1, MKLP1, MKLP2, MgcRacGAP, and microtubules (Geddis and Kaushansky, 2006; Lordier et al., 2008), during polyploidization the megakaryocytes CR lacks NMY-II and has lower levels of both actin and RhoA at the transition from 2N-to-4N (Geddis and Kaushansky, 2006; Lordier et al., 2008). Reduced level of RhoA activation at 2N-to-4N transition was shown to occur through downregulation of GEF-H1 a RhoA GEF, at the mRNA and protein level during megakaryocyte polyploidization (Gao et al., 2012). Interestingly however, downregulation of ECT-2 another RhoA GEF is required for polyploidization beyond 4N, indicating that two distinct mechanisms may be regulating the 2N-to-4N *vs.* polyploidy events beyond 4N (Gao et al., 2012).

Drosophila egg chambers

Another example of syncytiogenesis involving cytokinesis failure at stage III, CR ingression occurs in the *Drosophila* egg chambers. A series of papers reported that the CR constriction stage of cytokinesis is blocked in *Drosophila* egg chamber syncytial GCs (Ong et al., 2010; Ong and Tan, 2010; Tan et al., 2003; Yamamoto et al., 2013). It is known that phosphorylation of Non-muscle Myosin II (NMY-II) leads to its activation and thereby contraction of the furrow, while myosin activity is negatively regulated by myosin light chain phosphatase (MLCP) (Asano et al., 2009). Interestingly, one of the three subunits of MLCP, known as DMYPT (*Drosophila* Myosin Phosphatase Targeting Protein), is highly enriched in the ovarian *Drosophila* GCs (Ong et al., 2010). It has been demonstrated that loss of DMYPT function causes over-constriction of contractile rings and ring canals in the *Drosophila* ovarian GCs, which in turn results in formation of smaller rings and sterility (Ong et al., 2010; Tan et al., 2003).

1.4.1.2. Syncytium formation via abscission failure

Alternatively, cytokinesis failure could occur via either indirect or direct inhibition of abscission. For example, syncytiogenesis could be initiated by factors that stabilize MB/MBRs in syncytium-forming cells as opposed to discard them in cells undergoing conventional cytokinesis. In this scenario, stabilized MB/MBR could play as a physical burden to indirectly inhibit abscission. For instance, the MB connecting the ovarian follicle cells in *Drosophila*, persist hours after their mitoses are completed, showing that they are stable structures (Lin and Spradling, 1993). One key question that arises concerning this mechanism is whether MB/MBR stability is the cause or consequence of incomplete cytokinesis. But the biggest challenge is perhaps to directly test this model. Most known MB/MBR proteins are also required for furrow site specification and furrow ingression and, as such, knocking them down causes earlier defects that preclude analysis of their specific roles on subsequent MB/MBR formation. Perhaps this explains why many studies have instead relied on the molecular and structural features of ring canals to test this hypothesis.

First, several components of mature ring canals are in fact core components of MBRs, suggesting that ring canals are stable structures that are derived from modified the MBRs. For instance, de Cuevas et al. showed in 1998 that while anillin moves from the cleavage furrow to the nucleus upon completion of cytokinesis in *Drosophila* fGSCs and tissue culture cells (Figure 1.12 A), it persists in ring canals of the cyst-forming cells, confirming the hypothesis of MBR stabilization in syncytium-forming cells (de Cuevas and Spradling, 1998). In parallel to this, monitoring and comparing the fusome behavior in fGSCs undergoing complete cytokinesis with cystoblasts undergoing incomplete cytokinesis, during divisions in the *Drosophila* ovaries, provided evidence supporting this hypothesis (de Cuevas and Spradling, 1998). During asymmetric fGSC division, the fusome is only inherited by one of the daughter cells, but eventually a new fusome is born at the transient ring canal, which later merges with the original fusome. The ring canal shrinks in diameter until it ultimately closes, resulting in a physical separation of the two cells and equal partitioning of the fusome (Figure 1.12 A) (de Cuevas and Spradling, 1998). In the cyst-forming cystoblast however, the ring canal remains open after the old and the new fusome have merged and, as such, the resulting single new fusome is kept between the two daughter cells, wherein it facilitates conversion of the MB/MBR into ring canal. The fusome subsequently extends and branches out to further interconnect the two cells through the ring canal (Figure 1.12 B and C) (reviewed in Pepling et al., 1999).

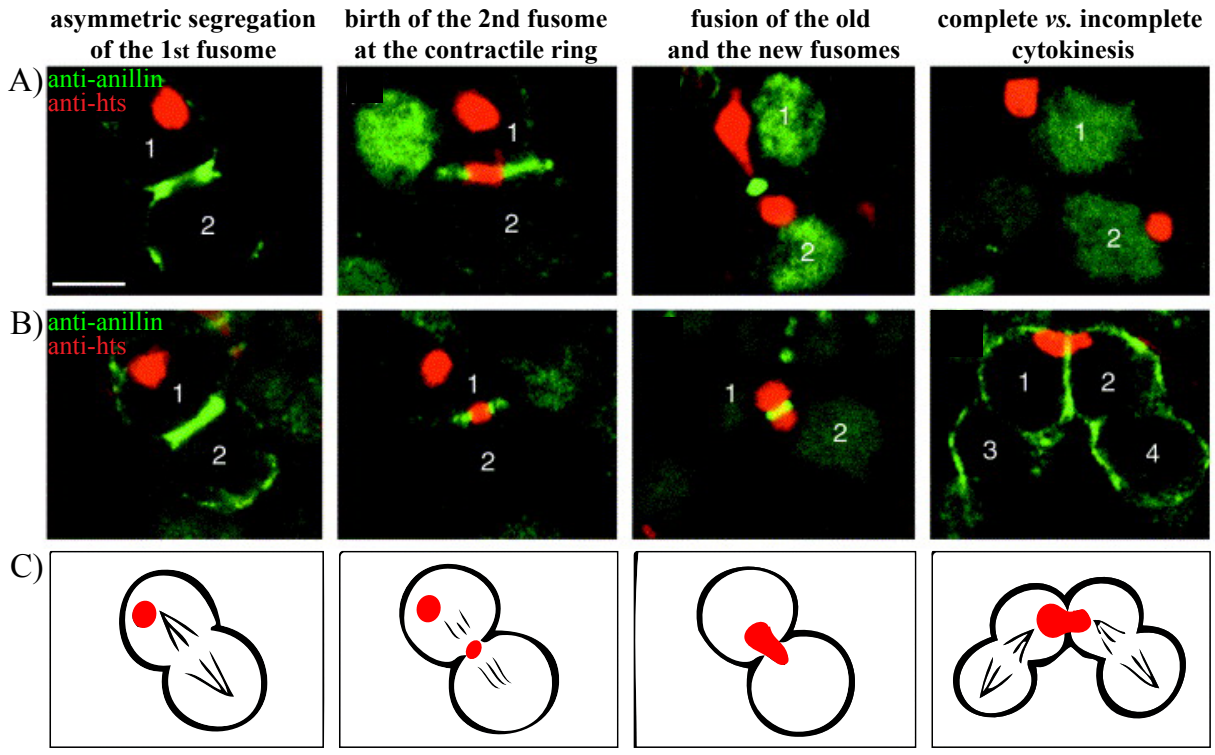

Figure 1.12: Dynamics of the fusome in the *Drosophila* ovary during mitosis.

(A) The female germline stem cell (fGSC) and **(B)** the cystoblast (CB) stained with anti-anillin (green), which labels the CR and anti-hts (red), which marks the fusome. The fusome (red) is asymmetrically divided between the daughter cells during both GSC and cystoblast divisions. In early-interphase, a 'plug' of fusomal material is formed in the nascent contractile ring (green) and later the original fusome moves towards it. Later on, as anillin becomes enriched at the nuclei of both daughter cells, the two fusomes fuse forming a bar-shaped structure through the contractile ring. While the contractile ring closes and pinches the fusome into two parts in the GSC via complete cytokinesis (A, right), the ring remains open in the CB and thereby maintains the fusome between the two daughter cells (B, right). **(C)** The schematic representation of the fusome dynamics during the mitotic division of the cystoblast. Note that in GSCs, anillin moves to the nuclei upon abscission (A), whereas it remains at the ring canals of the cyst-forming cells (B) (modified from Pepling et al., 1999).

Controlled exclusion of the abscission components or abscission-dependent events from the ICBs of syncytial tissues could be a direct mode of syncytiogenesis. In this scenario, MBs of syncytial tissues, unlike those of non-syncytial tissues, are exempt from getting discarded

through the final step of cytokinesis, abscission. While this conceptual framework seems rather plausible, evidence supporting it only came recently from the Matzuk group in a series of studies on mammalian testes (Greenbaum et al., 2009; Greenbaum et al., 2007; Greenbaum et al., 2006; Iwamori et al., 2010). They showed that TEX14, a GC-specific protein localized to the MB, stabilizes it, and converts it into an ICB that is not discarded by abscission (Greenbaum et al., 2007). As mentioned before (*Section 1.3.2.1. mammalian germline*) TEX14 is an ankyrin repeat-containing protein and may thus play a scaffolding role. Indeed, TEX14 localizes to the ring canal and is important for recruitment of central spindle components, such as MacRacGAP and MKLP1, to form stable intracellular bridges

Through compelling biochemical and *in vivo* evidence, they further demonstrated that TEX14 blocks abscission by binding strongly to CEP55 another component of stable ICBs (Iwamori et al., 2010). In the somatic cells that lack TEX14, CEP55 is recruited from the centrosomes to the MB and locally interacts with and recruits two ESCRT-I proteins; TSG101 and ALIX. In GCs, the interaction of TEX14 with CEP55 inhibits the recruitment of TSG101 and ALIX to the MB. This in turn prevents an ALIX-dependent recruitment of ESCRT-III to the midbody, and herby blocks the completion of cytokinesis (Greenbaum et al., 2007). While TEX14 is required for mammalian male GC syncytiogenesis, the mechanism of regulated abscission failure could not be easily considered as a mode of syncytium formation in other syncytial tissues as TEX14 homologs have not yet been identified in germline of other animals. Further efforts will tell us if complexes with similar function to TEX14/CEP55 also exist in other syncytial structures.

1.4.2. Syncytium formation through fusion

Not all syncytia are formed through alterations in cytokinesis. In fact, several tissues in plants and animals use cell-cell fusion as a strategy to form multinucleated tissues, wherein adjacent cells from the same lineage merge their membrane and cytoplasm and fuse to generate a syncytium (Figure 1.11 C). Cell-cell fusion has been repeatedly observed in various

somatic tissues including the syncytiotrophoblast (the placental layer separating maternal and fetal blood supplies) (Huppertz et al., 1998; Plachno et al., 2013; Potgens et al., 2002), muscles in species ranging from *Drosophila* to human cells (Chen et al., 2007), filamentous fungi (Glass et al., 2000; Oren-Suissa and Podbilewicz, 2010), lens of the eye in mice (Shi et al., 2009), embryo of the glass sponge (Leys et al., 2006) and bone (multinucleated osteoclasts). In addition, various non-syncytial tissues undergo fusion to transform into syncytia in response to stress or environmental changes (Pandit et al., 2013). Cell-cell fusion is one of the most fundamental processes in life of multicellular organisms that is required for several different developmental and physiological processes as diverse as fertilization, feeding, immunity, transport and sensory perception. Cell-cell fused syncytia are also known to play important roles in organ formation in different animals including *C. elegans*, wherein about one third of its somatic cells are found in syncytial tissues that are formed by cell fusion (Podbilewicz, 2006). These tissues are diverse and include the hypodermis (the worm's "skin"), vulva (Sapir et al., 2007), hymen, uterus, pharynx, excretory system, male tail and glands (Oren-Suissa and Podbilewicz, 2010). Despite the diversity of the cell types that undergo fusion, the cellular events that are involved in this process are in general common to all of these cell types and include cell recognition, adhesion and membrane fusion. This mode of syncytium formation has been never reported to occur in germline syncytia and thereby is not directly relevant for my research project. Nevertheless, I will briefly describe mechanisms of myoblast fusion during muscle development.

1.4.2.1. Myoblast fusion during muscle development in Drosophila

In *Drosophila*, the larval body wall muscles start to develop during embryogenesis and are composed of large bundles of multinucleated muscle fibers also known as myofibers or myotubes. Each myofiber is formed through fusion of tens of thousands of mononucleated muscle cells known as myoblasts (Bate, 1990; Rushton et al., 1995). Given the importance of muscles during animals' life, a tight regulation of fusion is required to direct spatiotemporal fusion of appropriate number of myoblasts. Myoblast fusion, similar to other cell-cell fusion events, occurs in different steps of: 1) Finding a fusion partner: recognition, migration and

adhesion, 2) enhancing cell membrane proximity and ultimately 3) membrane fusion and formation of a syncytium (Doberstein et al., 1997).

Finding a fusion partner: recognition, migration and adhesion

In *Drosophila*, fusion occurs between two types of mononucleated muscle cells, muscle founder cells and fusion-competent myoblasts (FCMs) (Abmayr et al., 2008; Bate and Rushton, 1993; Baylies et al., 1998). For a proper myoblast fusion to occur, the two fusing partners are brought to intimate proximity to facilitate their fusion. Hence, initially the founder cells recognize and attract the migratory FCMs (Ruiz-Gomez et al., 2000). In response to this, FCMs migrate toward the founder cells and subsequently the two cells adhere to each other in a Ca^{+2}-dependent manner (Knudsen and Horwitz, 1977). Moreover, it was shown that recognition and adhesion between founder cells and FCMs are mediated by immunoglobulin (Ig) domain-containing CAMs (type I transmembrane protein) at contact sites between the two cells (Ruiz-Gomez et al., 2000).

Enhancing cell membrane proximity, membrane fusion and formation of a syncytium

Although cell adhesion brings membranes of the two fusion partners into close proximity, cytoskeleton and actomyosin network-dependent remodeling of the two fusion partners (FCMs and founder cells) provides the sufficient proximity required for fusion of the two cells. For this to happen, first adhesion molecules via their cytoplasmic domains send signals to and recruit the actin cytoskeleton-associated proteins including the actin nucleation–promoting factors SCAR/WAVE and Wiskott-Aldrich syndrome protein (WASp) to sites of fusion (Kim et al., 2007; Kocherlakota et al., 2009; Massarwa et al., 2007; Richardson et al., 2007; Schafer et al., 2007). This in turn leads to a transient and asymmetric F-actin enrichment at the tip of FCMs (Richardson et al., 2007; Sens et al., 2010), and formation of a thin sheath of F-actin along the membrane of the apposing myoblast founder cell (Sens et al., 2010). The enriched F-actin at the FCM tip is composed of several finger-like protrusions that invade the founder cell to promote formation of fusion pores at the fusion site between the two cells

(Sens et al., 2010). In response to FCM invasive force, Myosin II-mediated mechanosensory response on one hand and chemical signaling from cell adhesion molecules such as Rho and Rok on the other hand increases and accumulates the amount of activated Myosin II at the fusion site. The enriched Myosin II in turn generates further cortical tension required for resisting the invasion, thereby promoting cell membrane proximity and fusion (Kim et al., 2015). Altogether, these results suggest that both FCMs-induced protrusive and founder cell-induced resisting forces are required to bring the membranes of fusion partners into close enough proximity to drive fusion. Ultimately, the multiple finger-like protrusions, lead to formation of a single-channel macro fusion pore between the two fusing muscle cells (Sens et al., 2010). Lastly, to facilitate fusion pore formation the lipid bilayers between the two cells need to be destabilized and ultimately fuse in order to form a syncytium.

1.5. The known function of syncytia

Nearly, all mammalian species are diploid and as such it is not surprising that accidental tetraploidy causes early defects such as spontaneous abortion or lethality of the embryo (Kaufman, 1991). Despite this, as described in the previous pages, syncytia are found, as part of differentiation program, from plants (De Veylder et al., 2011; Masterson, 1994; Otto and Whitton, 2000) to several different tissues in multicellular animals (both germline and somatic tissues) (Haglund et al., 2011; McLean and Cooley, 2014) and even in bacteria (Mendell et al., 2008). The prevalence of syncytia in diverse taxa highlights the biological diversity and molecular repertoire of syncytiogenesis and argues in favor of their evolutionary significance during tissue development and/or homeostasis. In fact, syncytiogenesis have been proposed to promote evolutionary diversification of animals and plants by increasing the adaptability of syncytial tissues and organisms (Otto and Whitton, 2000). In addition, it was shown that environmental circumstances and in particular sever climate change could increase the rate of syncytiogenesis in plants and animals (Bogart et al., 1989; Otto and Whitton, 2000), suggesting that syncytia could confer resistance to environmental stresses that are not tolerated by diploid cells. Besides this, during the last 60 years, several distinct functions have been

ascribed to syncytial organizations during development. Nevertheless, their exact role still remains an intriguing question to scientists. This is mainly because the potential and proposed functions of syncytial organizations and probably even the circumstances that trigger their formation depend on the tissues and developmental stage in which syncytiogenesis occurs.
The purpose of this section is to revisit some of the classical views about the function of syncytia in animals.

1.5.1. Synchronous behaviors

One of the most established hypotheses posits that ICBs are a means of maintaining the behavioral synchrony of interconnected cells at critical stages during development (Guo and Zheng, 2004; Robinson and Cooley, 1996). These behaviors could range from coordinated cell cycle or other cellular functions, such as migration or hormone release, to ensure developmental synchrony (Robinson and Cooley, 1996). In a seminal study, Fawcett et al. (1959) initially proposed that ICBs account for synchronous differentiation of cells within syncytial tissues. Some indirect support for this interpretation came from studies in the syncytial cnidoblasts of *Hydra* wherein synchronous differentiation have been also observed (Fawcett, 1961).

Several other studies accumulated evidence to support this scenario. First, in an electron microscopy-based study in 1968, Zamboni and Gonndos showed that during rabbit oogenesis, conjoined GCs within each group in the ovary have close morphological similarities and, depending on the developmental stage, they either all undergo coordinated mitosis, meiosis or subsequent events such as differentiation or even GC degeneration (Zamboni and Gonndos, 1968). In another study, Pepling et al. (1998) demonstrated that the interconnected female GCs of the mouse germline are mitotically synchronous (Pepling and Spradling, 1998). Similar synchronous mitoses, differentiation or other cell-cycle dependent coordinated events have been also reported during spermatogenesis in several other species (Fawcett et al., 1959). Furthermore, it has been proposed that the dendritic interconnections between gonadotropin-

releasing hormone (GnRH) neurons in the adult mouse brain could contribute to the synchronous pulsatile release of GnRH, a critical factor for mammalian fertility (Campbell et al., 2009). In line with this, it has been also suggested that the ICBs formed by fusion of neuronal extensions between the adjoining GnRH neurons of rat and monkey brains are involved in the synchronous hormonal release behavior of GnRH neurons (Witkin et al., 1995).

While the " synchronous behavior" is an attractive explanation for the purpose of ICBs in a variety of syncytial tissues, some aspects of other syncytial tissues do not fit with this theory. For instance during *Drosophila* oogenesis, initially all 16 GCs develop synchronously. However as development proceeds, despite the persistence of ICBs, only one of the 16 GC undergoes meiosis and differentiates as the oocyte, while the other 15 cells develop as nurse cells. Another example is the syncytial germline of male and hermaphrodite *C. elegans*, which is not obviously synchronous: development of GC clusters, for example, is not synchronous, and so clusters at various stages of mitosis, meiosis and spermiogenesis/oogenesis can be found within the syncytial germline. Despite the mentioned flaws, this model proposes that ICBs are required for GC synchronization and subsequently for the progression of gametogenesis.

1.5.2. Cytoplasmic exchange

The above exceptions gave rise to a well-supported hypothesis of "cytoplasmic exchange" that was ironically developed to explain the synchronous behavior of spermatids (Fawcett et al., 1959). In this model, the function of ICBs is proposed to enhance intercellular transport by providing direct cytoplasmic contact between cells. The ICBs are often large enough to allow essential signals, large molecules, proteins, mRNA, ribosomes and other organelles to be exchanged and shared among cells (Greenbaum et al., 2011; Haglund et al., 2011; Mahajan-Miklos and Cooley, 1994; Robinson and Cooley, 1996; Ventela et al., 2003). For instance, it has been demonstrated that during *Drosophila* oogenesis, ICBs also known as

ring canals facilitate flow and directed transport of particles from 15 supporting nurse cells into the oocyte in the syncytial egg chamber (Bohrmann and Biber, 1994; Mahajan-Miklos and Cooley, 1994). Similarly, in the syncytial germline of the adult *C. elegans* hermaphrodite, GCs within the transcriptionally-active pachytene area transfer their cytoplasmic content, including mitochondria and P granules (more details are in *Section 1.7.3.*), toward the transcriptionally-quiescent oocytes (Wolke et al., 2007). The exchange of cytoplasmic content is not only limited to the germline syncytia. Recently, the use of a combination of genetic tools in live and fixed samples of the *Drosophila* ovarian follicular epithelium provided compelling evidence that somatic ICBs also permit a robust and rapid transfer of material between the cells, providing a balance of protein levels between transcriptionally different interconnected cells (Airoldi et al., 2011). This could be a strategy that follicular cells use to compensate for epigenetic or other transcriptional changes that cause variations in gene expression (McLean and Cooley, 2014). Likewise, mammalian germline ICBs in males are thought to equilibrate their cytoplasmic content in a similar way.

1.5.3. Haploid gene sharing

Another interesting hypothesis is that ICBs allow genetically segregated haploid cells to share diploid gene products (Greenbaum et al., 2011; Guo and Zheng, 2004; Haglund et al., 2011; Robinson and Cooley, 1996; Ventela et al., 2003). It is important to note that this model would only explain the role of ICBs in heterogametic spermatids (XY) while it fails to explain role of ICBs in self-fertilizing hermaphrodites (XX) such as *C. elegans*, where meiotic segregation does not produce sex-chromosomal disbalance between gametes. In the male germline of heterogametic animals after meiosis, two genetically distinct types of spermatids are formed; one class with X-chromosome and another with Y-chromosome. Differences in post-meiotic X- and Y-linked gene expression within these two classes could cause phenotypic-imbalance between haploid spermatids. It has been proposed that spermatids remain “phenotypically diploid” after meiosis by sharing the X- and/or Y-linked essential gene products via ICBs (Guo and Zheng, 2004). This strategy ensures that both kinds of developing

spermatids can use diploid gene products to mature normally within the syncytial germline. In support of this scenario, it has been reported that the mRNA expressed from a single copy transgene encoding human growth hormone (hGH) that is solely expressed by post-meiotic cells is distributed equally between the connected spermatids in male mice (Braun et al., 1989; Greenbaum et al., 2011; Guo and Zheng, 2004). Another experimental evidence that is consistent with this hypothesis is that an X chromosome-linked protein kinase A anchoring protein, AKAP4, which is required for sperm motility and is only expressed in post-meiotic cells in mice germline, is transferred between genetically distinct spermatids via ICBs (Morales et al., 2002). Despite the significance of ICBs in male gamete equivalence in mammals, as mentioned above not all haploid gametes require genetic equilibrium, suggesting that this is not the main and conserved function of ICBs in male germline syncytia (Guo and Zheng, 2004).

1.6. Benefits of syncytia in naturally diploid cells

It is traditional to view organisms as either unicellular or multicellular. The diverse examples of syncytia imply that there are several selective advantages for evolving multinucleation. At first sight, it sounds rational to define a physiological role for syncytia in tissues wherein syncytiogenesis occurs as a normal developmental process. However, this does not offer us the whole picture, as accidental failures of cytokinesis could also convert a non-syncytial tissue into a syncytial one, an event that for long was known to be associated with several different disadvantages including aneuploidy and polyploidy linked with disorders. Strikingly however, more recently uncovered functions and beneficial roles for syncytia have begun to emerge from recent studies. Here I will give a brief overview on two recently discovered advantageous functions of syncytia. Before proceeding, it is important to mention that one common theme that is emerging is that syncytia are associated with adaptations to external stresses. In other words, syncytia may be more resistant to the unexpected functional and/or environmental stresses and that syncytial organizations may facilitate tissue adaptations to changes that otherwise are not tolerated by single-nucleated

diploid cell.

1.6.1.Wound healing

Following injury, tissues must activate a repair response that involves in both sensing the injury and restoring the lost tissue in order to return the tissue to its steady-state function. Interestingly, one function that was recently shown to benefit from a syncytial organization is wound healing. It has been reported that upon puncture wounding in the adult abdominal epidermis of adult *Drosophila*, epithelial cells form mononucleated polyploid cells. In addition, following wounding, cells at the wound margin begin to elongate and orient toward the site of injury and subsequently fuse to each other to form a large syncytium. The generated syncytial tissue not only compensates for the cell mass loss, it also provides mechanical stability to the scar tissue, leading to re-epithelialization of the wounded tissue to restore the tissue integrity required for healing (Galko and Krasnow, 2004; Losick et al., 2013).

1.6.2. Survival

Parthenogenesis is development of an unfertilized-oocyte into an embryo, with no genetic contribution from a sperm (Hipp and Atala, 2004). *In vitro* made human parthenogenetic (HP) cells can form blastocytes with morphological resemblance to those generated from fertilization. These embryos show aneuploidy and other defects such as chromosomal abnormalities, which are normally detrimental to the survival of the cells. Despite this, HPs are able to proliferate similar to their fertilized counterparts. It has been recently proposed that this unexpected survival feature of HPs is due to their syncytial structure which provides them with missing cellular components and thus allow them to proliferate and survive (Pennarossa et al., 2015).

1.7. *C. elegans* as a model to study syncytiogenesis

It is becoming evident that an important step toward understanding the complex biological processes is the use of simple model systems in which diverse experimental approaches can be easily utilized to analyze different cellular and molecular mechanisms. *C. elegans*, in particular has been a very powerful model of study in various biological fields, including stem cell biology. In this study, we used *C. elegans* as model to study germline syncytial architecture, formation and function.

1.7.1. History and background

In 1897, Emile Maupas, a French zoologist and botanist, provided the first description of nematode *Caenorhabditis elegans* as a species of nematode (Pazdernik and Schedl, 2013) that is found in rotten plant material including fruits and stems (Felix and Duveau, 2012). But it would be many years before Sydney Brenner, in the 1960s, introduced the free-living *C. elegans* as a model to study development and neurobiology (Brenner, 1974). Since then, it has rapidly established itself as a powerful model system to study a broad spectrum of biological questions. In large part this is due to a unique combination of favorable features, including small cell and body size, short and prolific life cycle, mode of reproduction and most importantly ease of manipulation and maintenance. For instance, because the animal produces a large number of progeny in a short time, the function of a gene can be quickly identified through large-scale genetic analysis. In addition, the relatively small genome of *C. elegans* was the first amongst multicellular organisms to be fully sequenced and shows significant level of sequence conservation with that of humans (Wilson, 1999). Work with *C. elegans* has led to many seminal discoveries including RNA interference (RNAi) and the green fluorescent protein (GFP), molecular mechanism of programmed cell death (Conradt and Xue, 2005) . Given this, it has become relatively easy to knockdown/knockout any given predicted gene either through RNAi (Fire et al., 1998) or targeted mutation, rendering this animal amenable to efficient reverse genetic approaches.

In addition to the attractive properties mentioned above, the animal's transparency allows *in vivo* imaging using differential interference contrast (DIC) microscopy. In fact, using this method, investigators monitored cellular aspects of development during embryogenesis (Sulston et al., 1983), gondogenesis (Sulston and Horvitz, 1977) and in neurons (Sulston, 1983) and mapped the complete cell lineage of the animal. Transgenic animals are also easily generated using both classic methods and novel genome-editing techniques (Dickinson et al., 2013; Paix et al., 2014) and the use of various fluorescent protein tags allows labeling of specific proteins or cells to monitor them *in vivo* (Chalfie et al., 1994; Mello et al., 1991).

1.7.2. The *C. elegans* germline

Propagation of sexually reproducing metazoans depends critically on the formation of functional gametes. This is partly achieved through a highly regulated development of germline tissue. In *C. elegans*, for instance, successful germline development and proper gamete formation involves completion of a choreographed series of events involving specification of GCs as distinct from somatic cells, coordination between germline development and somatic gonad, sex determination, GC mitosis *vs.* meiosis decision, GC apoptosis, recombination/progression through meiotic prophase and many other processes.

1.7.2.1. Germline development in the embryo: P_4 divides into Z_2 and Z_3

The *C. elegans* germline is established and set apart from somatic lineages early during embryogenesis, giving rise to a gonadal primordium that contains two somatic gonad precursors (SGPs) and two primordial germ cells (PGCs). The SGPs (called Z_1 and Z_4) give rise to all somatic cells of the gonad in the adult, whereas the PGCs (called Z_2 and Z_3) build the entire germline (Kimble and Hirsh, 1979; Sulston et al., 1983). An important question is how PGCs and SGPs are formed and how they establish the gonadal primordium. Below is a brief summary of gonadal primordium formation (Figure 1.13).

The first steps of germline proliferation, occur in the early *C. elegans* embryo (P_0), wherein a series of asymmetric cell divisions ensure that proper cell fate determinants, such as the transcription factor PIE-1 and the P granules (ribonucleoproteic material critical for germline specification), are segregated to the germ lineage. The last asymmetric division of the embryonic germ lineage generates a somatic blastomere (D) and the embryonic precursor blastomere termed P_4 that lies at the posterior-most ventral region of the embryo. Around the 28-cell stage, P_4 moves into the embryo during gastrulation. P_4 does not divide however until about the 100-cell stage, when it divides symmetrically and parallel to the antero-posterior axis (AP) to give rise to two PGCs; Z_2 at the posterior and Z_3 at the anterior of the embryo (Sulston et al., 1983). At this stage, the two PGCs are adjacent to one another and are positioned at the posterior-ventral side of the embryo. The PGCs eventually undergo a 90° dorsal-oriented rotation and become perpendicular to antero-posterior axis (Sulston et al., 1983).

At around this time, the two SGPs (Z_1 and Z_4), which are born in more anterior regions within the embryo, migrate independently of each other toward the PGCs at the posterior (Rohrschneider and Nance, 2013; Sulston et al., 1983). Later, when SGPs become adjacent to PGCs, they send protrusions around the PGCs and wrap over their surface, forming the gonadal primordium (Rohrschneider and Nance, 2013). Z_1 and Z_4, reside adjacent to the Z_2 and Z_3 cells respectively. Together with their surrounding basement membrane, these four cells constitute the gonad primordium. Electron micrographs show that Z_2 and Z_3 extend bleb-like lobes towards the intestine within the gonad primordium (Figure 1.13, red arrowhead) (Sulston et al., 1983). Although the exact role of these attachments are not known, similar PGC-endodermal associations have been also reported in other animals including *Drosophila* (Jaglarz and Howard, 1995), suggesting that it might be a conserved feature of gonad formation. The gonad primordium does not undergo division during embryogenesis and remain quiescent until the larva hatches. This quiescence is not a passive consequence of nutrient deprivation, but rather is regulated via components of insulin/IGF-like signaling pathway (Fukuyama et al., 2006).

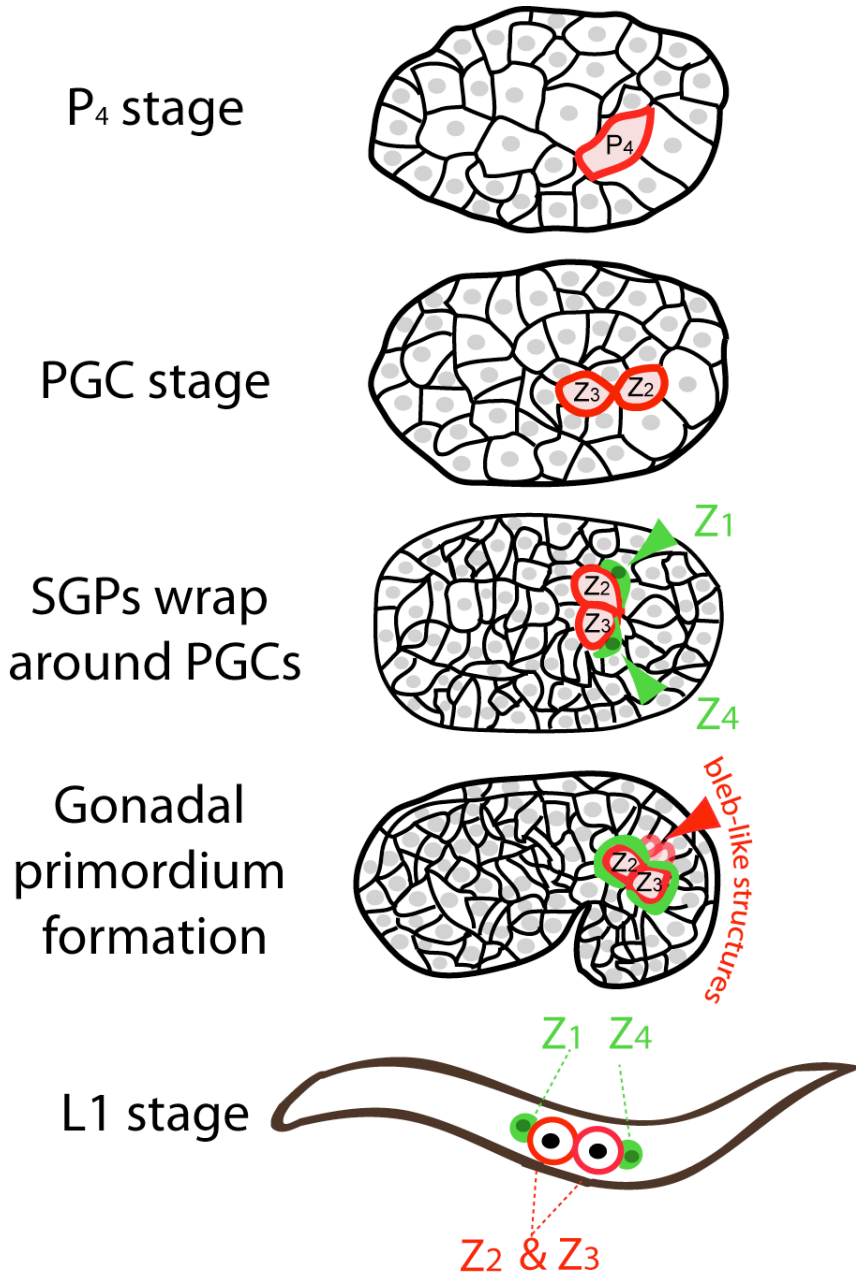

Figure 1.13: Illustration of SGP and PGC morphogenetic behavior during gonadal primordium formation in the *C. elegans* embryo.

SGPs are green and PGCs are red. The P_4 divides once to generate the two PGCs: Z_2 and Z_3. SGPs initially extend long projections posterior to the PGCs and subsequently expand over to cover the ventral and anterior surfaces of PGCs and finally wrap completely around the PGCs. PGCs eventually exhibit bleb-like protrusions (red arrowhead). Figure inspired from Rohrschneider et al., 2013.

1.7.2.2. Development of the C. elegans germline

There are two *C. elegans* sexes, a self-fertilizing hermaphrodite (genotype XX) and a male (genotype XO), Hermaphrodites can produce progeny through self-fertilization or when supplied with sperm by males. However, due to the infrequent developmental occurrence of males, propagation of *C. elegans* primarily relies on self-fertilization of hermaphrodites. Although, most aspects of the germ lineage developmental program are shared between the two sexes, there are some discrepencies in somatic gonad development and thereby germline structure between the male and the hermaphrodite. One such difference is that the hermaphrodite adult has two U-shaped gonad arms, while the male has a single J-shaped gonad arm (Hubbard and Greenstein, 2000; Kimble and Hirsh, 1979). For the sake of simplicity, I will not describe the male gonad development and will focus on hermaphrodites instead.

In both hermaphrodites and males, after hatching, PGCs and SGPs undergo coordinated divisions during larval stages (L1-L4) and into adulthood, to produce respectively the entire germ lineage and the entire somatic gonad which, in hermaphrodites, is composed of two distal tip cells (DTCs), sheath cells, spermathecae, and uterus (Figure 1.14 Adult) (Hubbard and Greenstein, 2000; Kimble and Hirsh, 1979). Below is a brief summary of the development and morphology of the hermaphrodite gonad during the four larval stages as well as adults (Figure 1.14).

L1

At hatching, the two PGCs are flanked by two SGPs and are separated from the non-gonadal soma by a basal lamina (Hubbard and Greenstein, 2000). Midway through the first larval stage, Z_2 and Z_3 undergo their first mitotic division.

L2

In L2, the SGPs divide to generate 12 cells, among which are the two DTCs (Kimble and Hirsh, 1979). Initially, these 12 somatic cells partially surround the centrally located GCs,

forming a ball-like gonad. In late-L2, 10 somatic cells reorganize to form a central somatic gonad primordium (SPh), while each DTC lies at and caps each end of the gonad and remain at the distal tip throughout animal life. In hermaphrodites, DTCs play two important roles: 1) promoting the proliferative GC fate and 2) controlling the morphogenetic outgrowth by migratory behavior or the gonad (Kimble and White, 1981).

L3

At early L3, the two DTCs on opposite sides of SPh migrate away from each other and ultimately segregate GCs on each side into two equivalent gonad arms, one in the anterior and the other in the posterior (Figure 1.14 early L3). In the mid-to-late L3, the GCs at the most proximal ends of the two gonad arms enter meiosis (Kimble and White, 1981). Meiosis onset, also called initial meiotic entry (Pepper et al., 2003), is essential to establish the distal-proximal polarity in the germline, limiting the mitotic cells at the distal end of the gonad and meiotic cells at the proximal end of each gonad arm. It is important to mention that the first GCs that undergo meiosis later develop as sperm. In addition, during late L3, the DTCs make their first turn away from the ventral basement membrane and migrate toward the dorsal membrane, which determines the U-shaped pattern of gonad (Figure 1.14 late L3).

L4

During the L3-L4 transition, the DTCs turn for the second time to migrate back towards the central region of the animal, along the dorsal membrane. Moreover the animal continues to increase in size and cell number and ultimately forms two equivalent U-shaped gonad arms (Figure 1.14 L4). By late L4, sperm production stops and the subsequent adult GCs in the proximal region of the gonad begin to differentiate as oocytes.

Adult

The global architecture of the hermaphrodite adult gonad, as well as the cell cycle state of the nuclei within it, are similar to the hermaphrodite L4 gonad (Figure 1.14), except that the adult gonad is bigger and contains oocytes and embryos. While the regions close to the DTCs contain proliferative GCs, more proximally located GCs loose contact with the DTC and

thereby exit the mitosis and enter early stages of meiotic prophase I in a transition zone (TZ), wherein nuclei exhibit a polarized organization and crescent-shaped DNA morphology that corresponds to the earlier stages of meiosis (leptotene and zygotene) (Lui and Colaiacovo, 2013). After moving through the TZ, the meiotic GCs are arrested at the pachytene stage in the distal arm (Crittenden et al., 1994). Later, as GCs enter the loop region, they exit from pachytene and enter into diplotene and expand in size and differentiate into oocytes that form a single row of transcriptionally quiescent oocytes. The more proximally located oocytes progress to diakinesis of prophase I before undergoing meiotic maturation and finally severing (Kimble and White, 1981) their connection to a shared cytoplasmic space at the center of the germline called the rachis.

Surprisingly, approximately 85% of late pachytene-stage GCs, as assessed by the number of GC corpses observed at a given time relative to the number of laid oocytes within the same time, are eliminated by regulated physiological apoptosis (Bailly and Gartner, 2013; Jaramillo-Lambert et al., 2007). One well-established hypothesis is that the apoptotic GCs act as nurse cells to provide nutrients and cytoplasmic material to the oocytes (Bailly and Gartner, 2013). Arguing against this notion, it was shown that transcriptionally active pachytene GCs deliver material (including RNA and proteins) into the rachis, and this material is transported toward the enlarging transcriptionally inactive oocytes in an actin-dependent process termed cytoplasmic streaming or proximal streaming (Wolke et al., 2007), suggesting that GCs do not necessarily have to die to act as nurse cells. The most proximal oocyte that lies next to the spermatheca undergoes meiotic maturation and then is ovulated into the speramatheca, where it gets fertilized and generates an embryo, a process that repeats itself approximately every 20 minutes (McCarter et al., 1999).

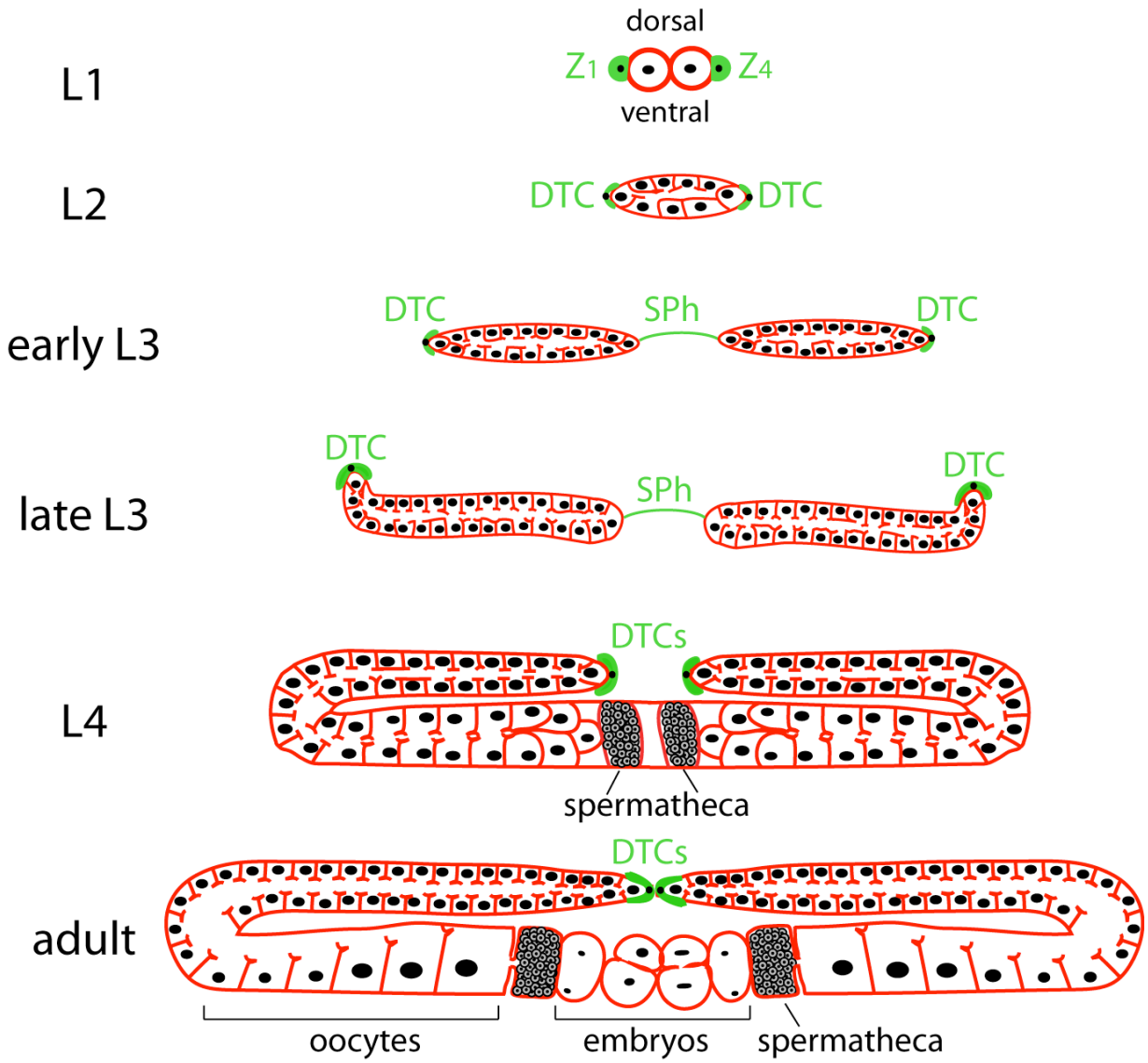

Figure 1.14: Illustration of germline development during *C. elegans* larval stages and adulthood.

Somatic germline is shown in green. L1 is only composed of two PGCs and two SGPs, division of which forms the rosette-shaped L2 gonad. SPh proliferation (Somatic gonad primordium) in early L3 separates the two gonad arms. By late L3, the DTC turns and migrates toward its final position. The GC division continues in L4 to ultimately form an adult gonad within which sperms and oocytes exist.

1.7.3. *C. elegans* adult germline has a syncytial architecture

The adult hermaphrodite germline is a syncytial tube-like organ, wherein individual GC nuclei, except those of mature oocytes, are partially enclosed by cell membranes and are arranged circumferentially around the central anucleate cytoplasmic rachis (Hirsh et al., 1976). The rachis extends through most of the adult gonad, interconnecting hundreds of GCs at various stages of mitosis, meiosis and oogenesis through stable intercellular bridges, here referred to as GC rachis bridges (Figure 1.15). The bridges are stabilized and remained open by Actin/ANI-2-rich structures referred to as GC rachis rings.

As discussed previously (see *Section 1.3.2.*) this property of the *C. elegans* germline is analogous to germlines in other species, wherein syncytia is a conserved phase of germline development (Haglund et al., 2011; Pepling et al., 1999; Urbisz et al., 2015). As such, similar to other syncytial germlines, the *C. elegans* GC rachis rings exhibit structural similarities to the CR, as they retain at least a subset of proteins typically found at the CR during cytokinesis. Foremost among them is the scaffold protein anillin that is a common component of *Drosophila* male and female germlines as well as the mouse testis (Haglund et al., 2011). Its short isoform in *C. elegans* is highly enriched to the GC rachis rings in the adult hermaphrodite germline (Maddox et al., 2005; Zhou et al., 2013). Besides ANI-2, other regulators of cytokinesis including NMY-2 (Maddox et al., 2005b; Zhou et al., 2013), UNC-59^{Septin} (Maddox et al., 2005), two centralspindlin components CYK-4^{MgcRacGAP} (Jantsch-Plunger et al., 2000; Zhou et al., 2013) and ZEN4^{MKLP-1} (Strome, 1986; Zhou et al., 2013) are also enriched at GC rachis rings of the hermaphrodite adult germline. In addition, while F-actin (Strome, 1986; Zhou et al., 2013), RHO-1^{RhoA} (Zhou et al., 2013) and Syntaxin-4 (Zhou et al., 2013) localize to both the GC membranes and GC rachis ring, others including MEL-11 and LET-502 are mainly concentrated to GC membranes (Piekny and Mains, 2002). Hemicentin, a conserved extracellular matrix (ECM) protein (Hodgkin et al., 1979), is another protein that localizes to GC rachis rings (Vogel and Hedgecock, 2001; Xu and Vogel, 2011).

Previous studies have shown that the cytoskeleton is important for maintaining the germline architecture and carrying out its function. For example, RNAi depletion of conserved contractility regulators such as, NMY-2^{myosin}, LET-502, ACT-4, ACT-5, Rho-1^{RhoA}, UNC-45 (Green et al., 2011; Kachur et al., 2008), ECT-2 and ANI-2 (Green et al., 2011; Maddox et al., 2005) and CYK-7 (a novel component of the MB) (Green et al., 2013) as well as mutations in *cyk-4*^{MgcRacGAP} (Jantsch-Plunger et al., 2000; Zhou et al., 2013), *zen-4*$^{mklp-1}$ (Zhou et al., 2013), *him-4* (a gene that encodes a conserved extracellular matrix protein) (Vogel and Hedgecock, 2001) and *fli-1* (a gene that encodes an actin severing protein (Lu et al., 2008)), result in severe defects in syncytial organization of the gonad, such as absence of GC partitions, multinucleation and sterility .

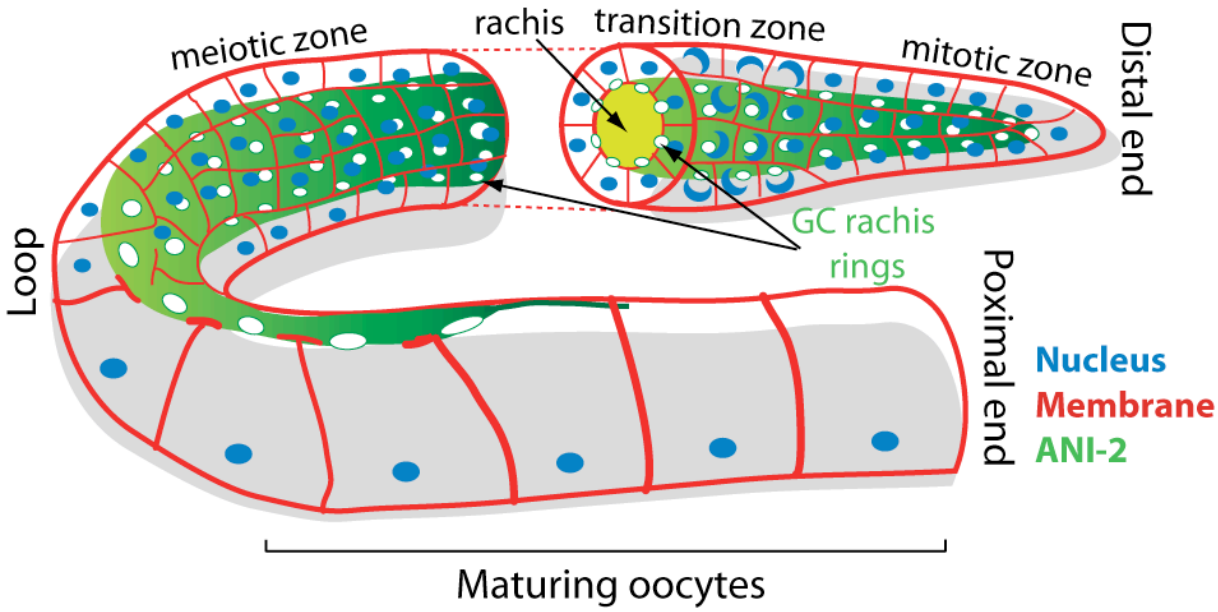

Figure 1.15: 3D illustration of the adult hermaphrodite *C. elegans* gonad.

Figure adapted from Amini et al., 2015.

2. OBJECTIVES

As previously mentioned, despite frequent occurrence of syncytia, there is still much to understand about how they are formed and maintained. Moreover, the exact role of syncytia is a subject of so many debates. In this thesis we took advantage of the syncytial *C. elegans* germline as a model to further our understanding of the structure of, the mechanism of formation and maintenance, and function of germline syncytium. Although we know that several contractility regulators are enriched at the syncytial *C. elegans* germline, their spatial and temporal organization within the *C. elegans* germline and their role in regulating germline architecture and function has not yet been systematically investigated. The goal of this work is to use the C. *elegans* hermaphrodite gonad as a model to investigate cytoskeletal organization in a complex muticellular system, and to probe the molecular mechanisms that establish and maintain this unique architecture.

2.1. Article 1

The objective of "Article 1" was to determine what regulates syncytium formation and maintenance during gonad development. In this work, we focus on role of an ideal candidate protein, the scaffolding ANI-2 in regulating syncytium formation/maintenance. Given ANI-2 enrichment in the GC rachis rings of the hermaphrodite adult germline and its lack of actin- and myosin- binding domains, we hypothesized that ANI-2 is a dominant-negative regulator of cytokinesis that competes with the canonical ANI-1 and uncouples it from other contractility regulators and thereby promotes syncytium formation.

This article addresses several specific objectives:

1. Investigate ANI-2 localization throughout two distinct stages of germline development; in the embryo and throughout successive developmental larval stages.
2. Examine if ANI-2 is differentially expressed in germline *vs.* soma.
3. Develop an assay to identify GC rachis rings to assess syncytium formation and maintenance.
4. Determine timing of syncytium formation and maturation during gonad development.

5. Assess if ANI-2 contributes to syncytium formation/ maintenance and maturation.
6. Determine if and how ANI-2 functions as a dominant-negative regulator of cytokinesis by competing with ANI-1 during germline development.
7. Investigate function of the *C. elegans* germline syncytium and assess if ANI-2 contributes to this.

2.2. Article 2

The objective of "Article 2" was to understand by what mechanisms the syncytium is formed in the *C. elegans* germline. In Article 1, we showed that ANI-2 is exclusively enriched in the PGCs, whereas it is undetectable in somatic blastomeres during *C. elegans* embryogenesis. In addition, our spatiotemporal analysis of three contractility regulators, NMY-II, ANI-1 and ANI-2 localization throughout larval development revealed that while GC rachis ring maturation occurs progressively throughout successive larval stages, GC rachis ring formation and maturation are two independent events. Altogether, we hypothesized that the germline syncytium nucleation occurs upon P_4 division in the *C. elegans* embryo, wherein unlike in somatic blastomeres failure at one or more stages of cytokinesis, results in failure of complete cytokinesis, leading to syncytium formation. To understand this, we used the *C. elegans* primordial germ cells (PGCs) as model and monitored their cytokinesis during embryogenesis.

This article addresses the following main objective:

Investigate whether and how germline syncytium formation is nucleated during C. elegans embryogenesis through a regulated cytokinesis failure.

3. RESULTS

3.1. Article 1

C. elegans Anillin proteins regulate intercellular bridge stability and germline syncytial organization

Rana Amini, Eugénie Goupil, Sara Labella, Monique Zetka, Amy S. Maddox, Jean-Claude Labbé, and Nicolas T. Chartier, 2014.

The following chapter is a reproduction of a published paper in *Journal of Cell Biology* 206(1):129-43. doi: 10.1083/jcb.201310117.

N.T.C. initiated this project in 2010. I Joined this project in May 2011 and jointly conceived the study with N.T.C and J.C.L. N.T.C. designed and conducted the core experiments of this project: Figure 3.1.1, 3.1.3 I, 3.1.3 J, 3.1.5, 3.1.7 D, 3.1.9 D, 3.1.9 E and 3.1.12. (Performed and analyzed by N.T.C., Université de Montréal). I designed and executed all remaining experiments and data analysis except for the Figure 3.1.9 A (Dr. S.L., McGill University). Dr. N.T.C. and I wrote the first draft of the manuscript together and I executed solely in performing experiments and data analysis of its subsequent revision. Dr. E.G. contributed in performing two crosses to make two strains, during revision of this work at *JCB*.

C. elegans Anillin proteins regulate intercellular bridge stability and germline syncytial organization

Running title: ANI-2 regulates germline syncytial organization

Authors: **Rana Amini** [1], Eugénie Goupil [1], Sara Labella [3], Monique Zetka [3], Amy S. Maddox [1,2,4], Jean-Claude Labbé [1,2] and Nicolas T. Chartier [1,5]

[1] Institute of Research in Immunology and Cancer, Montréal, QC, Canada and [2] Department of Pathology and Cell Biology, Université de Montréal, QC, Canada.[3] Department of Biology, McGill University, Montréal, QC, Canada.[4] Present address: Department of Biology, The University of North Carolina at Chapel Hill, Chapel Hill, NC, USA.[5] Present address: Université Joseph Fourier-Grenoble, Institut Albert Bonniot, Grenoble, France.

Corresponding authors: Nicolas Chartier and Jean-Claude Labbé

eTOC Summary Statement: ANI-2 promotes germ cell syncytial organization and allows for compensation of the mechanical stress associated with oogenesis by conferring stability and elasticity to germ cell intercellular bridges.

Keywords: Cytokinesis, Syncytial organization, Intercellular bridge formation, Germline development, Anillin

Abstract

Cytokinesis generally produces two separate daughter cells, but in some tissues daughter nuclei remain connected to a shared cytoplasm, or syncytium, through incomplete cytokinesis. How syncytia form remains poorly understood. We studied syncytial formation in the *C. elegans* germline, in which germ cells connect to a shared cytoplasm core (the rachis) via intercellular bridges. We found that syncytial architecture initiates early in larval development, and germ cells become progressively interconnected until adulthood. The short Anillin family scaffold protein ANI-2 is enriched at intercellular bridges from the onset of germ cell specification, and ANI-2 loss resulted in destabilization of intercellular bridges and germ cell multinucleation defects. These defects were partially rescued by depleting the canonical Anillin ANI-1 or blocking cytoplasmic streaming. ANI-2 is also required for elastic deformation of the gonad during ovulation. We propose that ANI-2 promotes germ cell syncytial organization and allows for compensation of the mechanical stress associated with oogenesis by conferring stability and elasticity to germ cell intercellular bridges.

Introduction

Cytokinesis, the last step of cell division, allows the physical separation of two daughter cells by abscission. Accordingly it is precisely controlled, and cytokinetic failure can lead to aneuploidy, which can cause developmental alterations or have pathological consequences. Interestingly, during the development of certain tissues, some cells are programmed to undergo incomplete divisions to form a syncytium, wherein multiple nuclei remain connected by stable cytoplasmic intercellular bridges (Haglund et al, 2011; Lacroix and Maddox, 2012). For instance, in many species, including humans, germ cells are connected by intercellular bridges that were proposed to regulate germ cell development by facilitating nutrient sharing, and the absence of these bridges is associated with infertility (Brill et al., 2000; Greenbaum et al., 2011; Greenbaum et al., 2006). While many actin-associated proteins and cytokinetic regulators are enriched at intercellular bridges (Greenbaum et al, 2011; Haglund et al., 2011; Lacroix and Maddox, 2012), the mechanisms that regulate their timely formation, maintenance and disassembly remain poorly understood.

The *C. elegans* germline comprises a powerful model system in which to study syncytial organization. Hermaphrodite adult animals possess two U-shaped gonad arms, each containing ~1000 germ cells that are radially arranged around a central rachis, to which they are connected by an intercellular bridge (termed rachis bridge; (Zhou et al., 2013), thus comprising a syncytium (Hirsh et al., 1976). Each gonad arm is organized in a polarized manner, from distal to proximal, such that germ cells at various stages of gametogenesis are physically segregated (see Figure 3.1.3 A; reviewed in (Kimble and Crittenden, 2007). The most distal portion of the gonad contains ~200 mitotic germline stem cells. Germ cells that leave the distal region stop proliferating and begin meiotic differentiation, successively going through stages of meiotic prophase as they progress toward the proximal region. Differentiation culminates in the most proximal part of the gonad where oocyte growth is primarily sustained by an actin-dependent streaming of cytoplasm in the central rachis (Kim et al., 2013; Wolke et al., 2007). Mature oocytes lose their connection with the rachis and become cellularized, ready for ovulation and fertilization by sperm stored in the spermatheca

(Maddox t al., 2005; McCarter et al., 1999). This structural organization ensures that oocytes are constantly produced in a conveyor belt-like fashion.

All germ cells in *C. elegans* originate from a common precursor (reviewed in (Wang and Seydoux, 2013). After fertilization, the zygote contains germline determinants and is referred to as the P_0 germline blastomere. During embryogenesis, germline determinants are progressively compartmentalized through four successive asymmetric divisions, resulting in the generation of a single germline blastomere termed P_4 (Figure 3.1.1 A; (Deppe et al., 1978). The P_4 blastomere divides symmetrically (at around the embryonic 100-cell stage) to give rise to the primordial germ cells Z_2 and Z_3, which do not undergo further division during the remainder of embryogenesis (Deppe et al., 1978; Sulston et al., 1983). As animals hatch in their first larval stage (L1) and begin to feed, Z_2 and Z_3 initiate proliferation and, through successive larval developmental stages (L2, L3 and L4), generate all germ cells in both gonad arms of the adult (Figure 3.1.2 B; (Hirsh et al., 1976).

Germline organization in *C. elegans* depends on a number of conserved actin-binding proteins that are enriched at the rachis bridge of germ cells (Maddox et al., 2005; Zhou et al., 2013). Among these proteins is ANI-2, a homolog of the actomyosin scaffold protein Anillin (Maddox et al., 2005a). While a cannonical *C. elegans* Anillin homolog (termed ANI-1) is enriched in the cytokinetic furrow and predicted to bind non-muscle myosin, F-actin and septins (Field and Alberts, 1995; Oegema et al., 2000; Paoletti and Chang, 2000; Straight et al., 2005), ANI-2 is a shorter Anillin isoform that lacks the N-terminal domains predicted to bind myosin and actin, and was thus proposed to function as a competitive negative regulator of contractility (Chartier et al, 2011). ANI-2 decorates the surface of the rachis and is enriched at rachis bridges in adult hermaphrodites (Maddox et al., 2005). In the proximal gonad, gametes progressively cellularize and detach from the rachis, so that mature oocytes and fertilized embryos contain very little ANI-2 protein (Chartier et al, 2011; Maddox et al., 2005). Partial depletion of ANI-2 by RNAi causes precocious oocyte cellularization, whereas more thorough depletion results in severe germline disorganization, germ cell multinucleation and

adult sterility (Green et al., 2011; Maddox et al, 2005).

How the syncytial architecture of the *C. elegans* germline arises during development is unknown. Here we present the first characterization of the genesis and topology of gonad syncytial architecture throughout development. We find that ANI-2 is expressed early in germline development and is required for the stabilization of the intercellular bridges that connect germ cells to the rachis, in part by opposing ANI-1 activity. Loss of ANI-2 leads to germ cell multinucleation, which can be rescued by blocking cytoplasmic streaming in the rachis. Our results support a model in which ANI-2 stabilizes intercellular bridges and makes them robust to mechanical stress at the onset of oogenesis.

Results

ANI-2 is enriched at the rachis bridge of all germ cells throughout gonad development

To address how the germline syncytium is formed and maintained, we first sought to identify a marker that would enable the monitoring of syncytial organization throughout development. As ANI-2 was previously reported to localize to the rachis of adult animals (Maddox et al., 2005), we analyzed its spatio-temporal localization throughout *C. elegans* development. In wild-type embryos, endogenous ANI-2 was present in very low amounts throughout early embryogenesis, as previously reported (Chartier et al, 2011), but appeared specifically in the P_4 germline blastomere (Figure 3.1.1 B). ANI-2 accumulated at the cell equator during cytokinesis as P_4 divided to produce Z_2 and Z_3, and remained enriched at the midbody that was formed between the two primordial germ cells (Figure 3.1.1 C and Figure 3.1.1 D). The timing of *ani-2* expression is similar to that reported for many germline-specific genes that are controlled by the transcriptional repressor PIE-1 (Wang and Seydoux, 2013). We perturbed germline specification by depleting PIE-1 and found that ANI-2 was undetectable in these embryos (Figure 3.1.1 E). In contrast, when we depleted MEP-1 to deregulate germline gene expression, ANI-2 was present in multiple cells (Figure 3.1.1 E). This indicates that ANI-2 is a *bona fide* germline-enriched protein that is expressed early during germ cell specification and stably accumulates between the two primordial germ cells.

We next monitored ANI-2 distribution throughout germline development in animals co-expressing ANI-2 fused to GFP (GFP::ANI-2) and a membrane marker, an mCherry-tagged probe previously shown to decorate the plasma membrane (Green et al., 2011; Kachur et al, 2008). Similar to endogenous ANI-2 (Maddox et al., 2005), GFP::ANI-2 localized between Z_2 and Z_3 in newly hatched L1 larvae and was present in all germ cells during larval development and into adulthood (except in the most mature oocytes), lining the rachis and becoming progressively enriched at rachis bridges (Figure 3.1.2 A). These results indicate that ANI-2 is present in all germ cells and enriched at rachis bridges throughout germline development, from the birth of primordial germ cells to the completion of oocyte maturation, making it an ideally suited marker to monitor syncytium organization during development.

The syncytial architecture of the C. elegans gonad arises progressively during larval development

To determine how the syncytial architecture of the germline arises during development, we developed a fluorescence microscopy-based assay to monitor the organization of rachis bridges. We measured the cortical fluorescence intensity in multiple optical sections of germ cells co-expressing GFP::ANI-2 and the membrane marker (Figure 3.1.3 B). A given germ cell was considered to be open to the rachis when a minimum in membrane marker fluorescence intensity was detected between two distinct fluorescence intensity peaks of GFP::ANI-2 (Figure 3.1.3 C and D; see Materials and Methods). Rachis bridge diameter was assessed by measuring the distance between the peaks of intensity for each marker, and bridges were considered to be open when their diameter was >0.8 μm.

We first applied this assay to the germ cells of adult animals, as germline syncytial organization is well described for this developmental stage (Hall et al., 1999; Hirsh et al., 1976). All germ cells examined (28/28), including the most distal cells, had a characteristic minimum in membrane marker intensity between two peaks of GFP::ANI-2 intensity (Figure 3.1.3 G) indicating, as expected, that all cells have an open (>0.8 μm) connection to the rachis at this stage.

Analysis of rachis bridge organization during larval development revealed that many germ cells are also open to the rachis at the L4 stage (128/130), late L3 stage (96/117), early L3 stage (71/106) and L2 stage (29/53) (Figure 3.1.3 G). However, for other germ cells at these larval stages, only a single peak of GFP::ANI-2 intensity was detected (Figure 3.1.3 E and F), suggesting that these germ cells are not connected to the central rachis through an open bridge. The proportion of germ cells with this latter GFP::ANI-2 distribution was highest in L2 animals, decreased progressively throughout larval development, and was zero in adult animals (Figure 3.1.3 G). Moreover, we observed that rachis bridge diameter (when open) increased gradually as animals progressed through larval development (Figure 3.1.3 H). Similar results were obtained when we measured rachis bridge organization in animals

expressing GFP-tagged versions of the canonical Anillin ANI-1 or non-muscle myosin II (NMY-2), two contractility regulators that, like ANI-2, accumulate at germ cell rachis bridges (Figure 3.1.4; (Maddox et al., 2007; Nance et al., 2003)). These results indicate that germline syncytial organization occurs progressively during larval development.

We next applied this assay to test whether primordial germ cells in newly hatched L1 larvae are interconnected. According to the localization pattern of GFP::ANI-2 and the membrane marker, Z_2 and Z_3 did not appear to share a cytoplasmic connection (5/5; Figure 3.1.3 G). However, we reasoned that the small measurable zone between these germ cells could confound the fluorescence intensity assay. To independently verify that these cells indeed lacked a cytoplasmic connection, we monitored the diffusion of cytoplasmic, exogenously supplied photo-convertible rhodamine-dextran in the primordial germ cells Z_2 and Z_3. While photo-activation of rhodamine-dextran resulted in its rapid diffusion within a single germ cell (Figure 3.1.5; see also (Green et al., 2013)), we did not detect significant fluorescence accumulation in the sister germ cell up to 30 minutes after photo-activation (Figure 3.1.3 I and J). Together, these results indicate that the two primordial germ cells Z_2 and Z_3 are linked by an intercellular bridge that has a small diameter and allows little or no cytoplasmic exchange, and that rachis bridge opening occurs progressively during larval development, culminating at the adult stage in a germline that is fully syncytial.

ANI-2 is required for rachis bridge stability

ANI-2 is found in all germ cells of larvae and adult animals (except for the cellularized oocytes), suggesting that it regulates rachis bridge formation and/or maintenance. To test this possibility, we measured rachis bridge organization in the germline of living *ani-2(ok1147)* mutant animals co-expressing the fluorescent membrane marker and GFP::ANI-1. *ok1147* is a presumptive null allele of *ani-2*, and homozygous mutant embryos develop into sterile adult animals with a very disorganized germline containing multinucleated, abnormally sized germ cells, similar to the phenotype reported after ANI-2 depletion by RNAi (see below and Figure 3.7. A; (Green et al., 2011). Surprisingly however, the germline morphology of *ani-2* mutant

L4 stage larvae was largely normal, with regularly-sized and -spaced mononucleated germ cells lining the gonad wall (Figure 3.1.6. A and C). Despite these aspects of morphology being normal, rachis bridge organization in *ani-2* mutant L4 stage animals was abnormal. While nearly all control germ cells had open rachis bridges (i.e. >0.8 μm; Figure 3.1.6. B and E) the majority of germ cells (46/68) in L4 stage *ani-2* mutant animals lacked a defined opening to the rachis and a single peak of GFP::ANI-1 intensity was detected (Figure 3.1.6. D and E). In the minority of germ cells in which an open rachis bridge was detected (22/68), the diameter of the bridge was significantly smaller than that measured in control animals (Figure 3.1.6. F). Rachis bridges were also largely absent from the germ cells of younger larvae (early L3; Figure 3.1.6. E). Similar results were obtained from strains co-expressing the membrane marker with either NMY-2::GFP or GFP::PGL-1, a germline P granule component that decorates the surface of germ cell nuclei (Kawasaki et al., 1998; Merritt et al., 2008) (Figure 3.1.8) . We conclude that ANI-2 is required for the formation and/or maintenance of germ cell rachis bridges during germline development.

ANI-2 stabilizes the membrane partitions between germ cells from the late L4 larval stage

Animals lacking ANI-2 fail to form rachis bridges during larval development and become sterile adults with multinucleated germ cells (Figure 3.1.7. A), suggesting that multinucleation is a consequence of defects in rachis bridge formation. To address this possibility, we monitored germline development in animals co-expressing the membrane marker fused to GFP and histone H2B fused to mCherry (Green et al., 2011). We found that until *ani-2* mutant animals reached the L4 larval stage, germline expansion proceeded largely normally; the number of germ cells was comparable to that of control animals at all stages and most germ cells contained a single nucleus (Figure 3.1.7. A). In addition, immunofluorescence analysis of gonads from young adult animals revealed that the germ cells of *ani-2* mutants can enter meiotic differentiation and form sperm, although male mating assays revealed that the sperm are not functional (Figure 3.1.9. A and data not shown). The primary defect of *ani-2* mutant gonads during early larval development was a marked decrease in rachis diameter (Figure 3.1.9. B). Thus, cell proliferation and entry into meiosis are not grossly impaired in *ani-2*

mutants and germline development is largely normal during early larval stages.

In contrast, in the proximal gonad of late L4 stage *ani-2* mutant animals, abnormal multinucleated germ cells were present, albeit at low frequency (Figure 3.1.7. A and B). In young adult animals, multinucleated germ cells increased in proportion, and were observed in progressively more distal regions of the gonad (Figure 3.1.7. A and B). In the gonads of older adult *ani-2* mutant animals (20-48h post L4), most germ cells were multinucleated and the number of nuclei per compartment was higher than in previous developmental stages (Figure 3.1.7. C). Furthermore, the germ cells of *ani-2* mutant animals did not complete meiosis and showed a defect in diakinesis (Figure 3.1.9. A). Multinucleation and diakinesis defects were never observed in the gonads of control animals (n>100). Loss of ANI-2 therefore results in abnormal germ cell multinucleation, initially in the proximal gonad region of late L4 stage animals but progressively affecting the entire germline.

Multinucleation, together with the abnormal execution of diakinesis, is likely key to the sterility of *ani-2* mutant animals. Multinucleation could arise from cumulative cytokinetic failures of dividing germline stem cells in the distal region of the gonad. However, time-lapse analysis of germline stem cell division in *ani-2* mutants revealed that they undergo normal cytokinesis (Figure 3.1.9. D). Likewise, multinucleation did not arise from germ cells abnormally re-entering mitosis, as depletion of the mitotic regulators CDK-1 or PLK-1 by RNAi did not prevent this defect (Figure 3.1.9. D, unpublished data). These results indicate that the multinucleation defect of *ani-2* mutant germ cells is not a consequence of inappropriate cell division.

Because ANI-2 localizes to rachis bridges in wild-type animals, we considered the possibility that multinucleation in *ani-2* mutants arises from a collapse of membrane partitions between germ cells. Time-lapse analysis of the proximal gonad of late L4 stage and young adult *ani-2* mutants revealed two clearly-defined instances of germ cell partition collapse, resulting in

multinucleation (Figure 3.1.7. D). This is likely an underestimation of the frequency of this defect, as our experimental imaging conditions may have masked several more of these events (see Materials and Methods). Together with our finding that germ cells do not enter mitosis inappropriately, these results indicate that ANI-2 is required starting at the L4 larval stage to maintain proper organization of the germline, at least in part by preventing the collapse of germ cell partitions.

ANI-2 and ANI-1 have opposing activities in germline organization

ANI-2 was previously proposed to regulate contractility by competing with the canonical Anillin ANI-1 for one or more contractility regulators (Chartier et al, 2011), suggesting that the defects observed in *ani-2* mutants may result from ANI-1 hyperactivation. To test this, we first characterized the phenotype of *ani-1*(RNAi) animals co-expressing GFP::ANI-2 and the membrane marker (Figure 3.1.10. A). We found that depleting ANI-1 by RNAi did not cause prominent gonad disorganization in adult hermaphrodites and that all germ cells had an intercellular bridge open to the rachis (Figure 3.1.10. B). However, we observed several defects that were opposite to those observed in *ani-2* mutants. In *ani-1*(RNAi) animals, the diameter of rachis bridges was larger and the diameter of the rachis was increased as compared to the control (Figure 3.1.9. C and Figure 3.1.10. C). Additionally, oocyte cellularization was delayed (Figure 3.1.10. A and data not shown). Animals depleted of ANI-1 also showed a number of other defects not observed in *ani-2* mutants, such as a low frequency of bi-nucleated cells (data not shown), consistent with ANI-1's function in regulating cytokinesis. These results indicate that ANI-1 is active in the germline and that its depletion results in defects opposite to those of *ani-2* mutants.

We next asked if the phenotypes observed in the gonad of *ani-2* mutants are a consequence of increased ANI-1 activity. To test this, we measured germline organization in *ani-2* mutant animals in which ANI-1 was depleted by RNAi (Figure 3.1.10. D). While the germline of these *ani-2*(-); *ani-1(RNAi)* animals remained severely disorganized, we found that several

ani-2-related defects were slightly but significantly rescued. As compared to control *ani-2* mutant L4 hermaphrodites, we found that depleting ANI-1 resulted in an increase in the number of germ cells that were open to the rachis and an increase in rachis bridge diameter (Figure 3.1.10. E and F). Furthermore, while the number of multinucleated germ cells was not different from control, we measured a significant decrease in the number of nuclei per multinucleated compartment in the proximal and meiotic regions of young adult hermaphrodite gonads (20h post-L4; Figure 3.1.10. G and H). Altogether, these results indicate that the defects observed in *ani-2* mutants are partly due to an increase in ANI-1 activity and that proper germline organization and function requires a balance between the activity of these two Anillin proteins.

Cytoplasmic streaming in the rachis contributes to germline disorganization in ani-2 mutants

Germ cell multinucleation in *ani-2* mutants is first observed in late L4 stage animals, near the time when the proximal-most germ cells begin to grow and mature as oocytes. Oocyte growth results largely from an actin-dependent distal-to-proximal movement of cytoplasm in the rachis, which initiates as animals enter adulthood (Kim et al., 2013; Wolke et al., 2007). We reasoned that cytoplasmic streaming could cause mechanical stress in the gonad and lead to a collapse of germ cell partitions and germline multinucleation in gonads lacking full ANI-2 function. To test this hypothesis, we first determined whether cytoplasmic streaming occurs in the rachis of *ani-2* mutant animals. We found that streaming initiates properly in the gonads of *ani-2* mutant hermaphrodites (Figure 3.1.11. A and B), although velocity is slightly reduced compared to wild-type adult animals (Figure 3.1.11. C). In addition, while streaming is unidirectional toward the proximal end of the gonad in wild-type animals, the trajectory of cytoplasmic streaming in *ani-2* mutants was variable (Figure 3.1.11. B). This indicates that cytoplasmic streaming, although disorganized, initiates properly in the gonads of *ani-2* mutants.

We then tested whether ANI-2 is required to stabilize the membrane partitions between germ cells and prevent multinucleation in the absence of cytoplasmic streaming. We first tested this by examining the gonad of male animals, which are naturally devoid of cytoplasmic streaming (Wolke et al., 2007). Similarly to the germ cells of adult hermphrodites, we confirmed that the germ cells of adult wild-type males form rachis bridges and that ANI-2 is required for the maintenance of these bridges (Figure 3.1.11. D, E and F). However, unlike in *ani-2* mutant hermaphrodites, the germ cells in *ani-2* mutant males were largely mononucleated (Figure 3.1.11. G). We also inhibited streaming in the rachis of *ani-2* mutant hermaphrodites by depleting GLD-1 and GLD-2, which blocks germ cells from entering meiosis and results in a germline devoid of gametes, filled with mitotically-competent cells (Francis et al., 1995). We found that both the number of multinucleated germ cells and the number of nuclei per multinucleated compartment were significantly lower in adult *ani-2* mutant hermaphrodites depleted in GLD-1 and GLD-2 compared with control *ani-2* mutant animals (Figure 3.1.11. H). Similar results were obtained using *gld-1*(-); *gld-2*(-); *ani-2*(-) triple mutant animals (data not shown). Thus, the absence of cytoplasmic streaming largely rescues the multinucleation phenotype observed in *ani-2* mutant germlines. Together, these results support the notion that the collapse of germ cell partitions and multinucleation of *ani-2* mutant germlines is caused by cytoplasmic streaming in the rachis.

ANI-2 permits elastic deformation of the adult hermaphrodite gonad and rachis bridges

Our results support a model in which ANI-2 stabilizes rachis bridges and prevents collapse of germ cell partitions by counter-balancing the mechanical stress caused by cytoplasmic streaming in the rachis. ANI-2 could compensate for mechanical stress by conferring plasticity to germ cell rachis bridges. To test whether ANI-2 can compensate for mechanical stress, we performed time-lapse imaging of the hermaphrodite gonad during ovulation, when the movement of a mature oocyte into the spermatheca causes deformation of the proximal gonad, and is therefore likely to cause mechanical stress on the gonad and rachis bridges (Figure 3.1.12. A). The proximal ANI-2-enriched rachis in control animals displayed elastic properties, as it stretched to reach a maximum at the moment when the oocyte entered the

spermatheca and decreased rapidly thereafter (Figure 3.1.12. A and B, and Movie S1 can be found on *JCB* website). Interestingly, the diameter of the proximal-most rachis bridge also reached its maximum upon ovulation (Figure 3.1.12. C). This indicates that the proximal gonad undergoes elastic deformation during ovulation and further suggests that changes in rachis bridge diameter permit this deformation.

As ANI-2 is enriched at rachis bridges and is required for their stability, we tested whether ANI-2 is required for deformation of the proximal gonad. In ovulating hermaphrodites partially depleted of ANI-2 by RNAi, the length of the proximal rachis remained stable and did not reach a maximum at the time of oocyte passage into the spermatheca (Figure 3.1.12. B and Movie S2 can be found on *JCB* website). Accordingly, rachis bridges did not display a transient increase in diameter and remained constant throughout ovulation in these animals (Figure 3.1.12. C). This indicates that ANI-2 is required for elastic deformation of the gonad during ovulation and further supports the notion that its enrichment at rachis bridges stabilizes these structures by permitting their deformation.

Discussion

In this study we showed that the primordial germ cells Z_2 and Z_3 do not share cytoplasmic connection and that the syncytial architecture of the *C. elegans* germline arises progressively during larval development. The short Anillin ANI-2 is found in every germ cell, from birth of the two primordial germ cells during embryogenesis to oocyte cellularization when oogenesis completes. We demonstrated that ANI-2 is required to promote rachis bridge organization and that its absence leads to a collapse of membrane partitions between germ cells, and thus germ cell multinucleation, in part due to an increase in ANI-1 activity. We further provided evidence that this defect may be a consequence of cytoplasmic streaming in the rachis that initiates at the onset of oogenesis and that ANI-2 can confer elastic properties to the rachis bridges when they are subjected to deformation. Based on these results, we propose a model (Figure 3.1.12. D) in which the balance of activity between ANI-2 and ANI-1 at rachis bridges stabilizes these structures and provides them with the capacity to sustain the mechanical stress that results from cytoplasmic streaming in the gonad (and perhaps also ovulation), thus ensuring proper germline stability and organization.

Our finding that germ cell rachis bridges are not fully formed at the first larval stage and open progressively during larval development is consistent with observations made by electron microscopy that syncytial organization of the germline only becomes apparent at the L2 stage (Hirsh et al., 1976). Yet, we detected specific accumulation of ANI-2 in the P_4 blastomere and at the midbody between the two primordial germ cells. This supports a view in which the cortical loading and stabilization of ANI-2 upon division of P_4 contributes to prevent the completion of cytokinesis and serves as a nucleating event for intercellular bridge formation. The bridge between Z_2 and Z_3 would initially have a small diameter that would preclude cytoplasmic exchange between the two cells but would progressively increase its diameter during larval development. However, some of our results suggest that other regulators may contribute to intercellular bridge formation independently of ANI-2. First, while most germ cells in *ani-2* mutant L4 larvae have no detectable rachis bridge, 30% of them displayed a smaller but yet measurable opening to the rachis, indicating that some bridge formation can

occur independently of ANI-2. Second, while rachis bridge diameter increased during larval development in wild-type animals, it remained small in these 30% of *ani-2* mutant germ cells, suggesting that ANI-2 promotes the opening of rachis bridges. Finally, we observed actin-dependent cytoplasmic streaming in the rachis of *ani-2* mutants, suggesting that actin cables, which are typically nucleated in the cytoplasm, can reach the central rachis, again arguing for the existence of at least small rachis bridges in *ani-2* mutants. This suggests that ANI-2 does not control the formation of rachis bridges *per se* but is required to promote their opening during larval development. Further experiments will be needed to resolve whether ANI-2 functions at one or more level of germline syncytial organization.

How does ANI-2 coordinate rachis bridge organization? ANI-2 is predicted to possess the C-terminal domains found in canonical Anillin and required for binding to RhoA, RacGAP50C (*Drosophila* MgcRacGAP), septins and lipids of the plasma membrane, but to lack the N-terminal actin- and myosin-binding domains (Maddox et al., 2005). Accordingly it was previously proposed to function as a negative regulator of contractility, by competing with the canonical Anillin ANI-1 for one or more contractility regulators (Chartier et al, 2011). In support of this, we found that depletion of ANI-1 results in a number of germline defects opposite to those observed in ANI-2-depleted animals: when compared to wild-type animals, oocyte cellularization is delayed (as opposed to precocious in *ani-2*(RNAi) animals), the diameter of rachis bridges is larger (it is smaller in *ani-2* mutants) and rachis diameter is increased (it is decreased in *ani-2* mutants). Furthermore depleting ANI-1 partially suppressed the defects observed in *ani-2* mutants. ANI-1 and ANI-2 did not control their respective loading at rachis bridges, suggesting that they function by locally balancing each other's activity. A balance of activity between ANI-1 and ANI-2 at rachis bridges could maintain the organization of these structures by locally controlling the engagement of contractility regulators, and thus regulate rachis bridge diameter. The progressive depletion of ANI-2 from rachis bridges would then promote oocyte cellularization, perhaps by allowing for more ANI-1 activity. However, depleting ANI-1 from *ani-2* mutant animals did not fully rescue their germ cell multinucleation phenotype, indicating that this defect does not arise solely from increased

ANI-1 activity but likely involves other contractility regulators. Interestingly, ANI-2 was recently reported to promote the rachis bridge localization of the contractility regulators CYK-4/MgcRacGap and ZEN-4/MKLP1 (forming the centralspidlin complex), whose depletion results in a germline organization defect similar to that of *ani-2* mutants (Green et al., 2011; Zhou et al., 2013). We propose that ANI-2 regulates the lability of rachis bridges by locally controlling the activity of one or more contractility regulators, either by itself or by competing for their binding with the canonical Anillin ANI-1.

Intercellular bridges between germ cells are found in multiple organisms and were previously proposed to serve a number of possible functions, such as equilibrating gene products between haploid cells, synchronizing germ cell development, enabling the rapid transport of nutrients between cells and homogenizing gamete quality (Dym and Fawcett, 1971; Guo and Zheng, 2004). Our findings that rachis bridge diameter increases as the rachis is stretched during ovulation and that ANI-2 is important to mediate elastic deformation suggests that intercellular bridges may additionally function to resist sustained mechanical stress. For instance, resistance to mechanical stress could be important for mammalian spermatogonia that migrate as germ cysts across Sertoli cell tight junctions during their maturation (Smith and Braun, 2012), (Smith and Braun, 2012), a process that is likely to face great mechanical constraint. Actin-binding proteins, including Anillin, are found at intercellular bridges in many species but it is currently unclear if a role for Anillin in regulating bridge stabilization is conserved. Interestingly, while a single gene encoding Anillin is present in humans, a shorter spliced isoform lacking the actin-binding domain is expressed in certain tissues (N.T.C. and J.C.L., unpublished). Shorter isoforms such as these could have a function similar to ANI-2 at intercellular bridges and thus play a role in regulated cytokinesis failure and/or intercellular bridge elasticity.

Materials and Methods

Strains and alleles

All strains were maintained as described by Brenner (Brenner, 1974) and were grown at 20°C unless otherwise stated. The strains and alleles used in this study are listed in Table S1. Protein depletion by feeding RNAi was performed as previously described (Kamath et al., 2001) using the following individual clones from Julie Arhinger's library: sjj_K10B2.5 (ani-2), sjj_Y49E10.19 (ani-1), sjj_T05G5.3 (cdk-1), sjj_K06H7.1 (plk-1), sjj_T23G11.3 (gld-1), sjj_ZC308.1 (gld-2), sjj_M04B2.1 (mep-1), sjj_Y49E10.14 (pie-1). Briefly, each clone was grown up to log phase and plated overnight on NGM plates containing 50 μM carbenicillin and 1 mM IPTG. All assays were performed on animals grown in the presence of a dsRNA-expressing clone from the L1 stage (*ani-1* and *gld-1/2*) or the L4 stage (all other clones). All clones were verified by sequencing. A vector targeting a gene with no obvious function in embryogenesis or (sjj_C32E12.1; Chartier et al, 2011) was used as control.

Transgenic animals expressing ANI-2 fused to GFP under the control of the *pie-1* promoter were generated by microparticle bombardment of a vector containing the complete *ani-2* coding region (amplified by PCR from genomic DNA) inserted in frame downstream of sequence coding for GFP, a cleavage site for the TEV protease and S-peptide, as previously described (Cheeseman et al., 2004). The germline localization pattern of this fusion protein is indistinguishable from that observed on fixed specimen using anti-ANI-2 antibodies (Maddox et al, 2005, data not shown).

The staging of animals during larval development was done according to growth parameters and gonad morphology (Figure 3.1.2 B), using the following criteria. L1 stage: 2 germ cells (Z_2 and Z_3). L2 stage: multiple germ cells in a single gonad after 15-18 hours of growth at 20ºC. Early L3 stage: the gonad has split into anterior and posterior regions but the distal arms have not yet started to turn dorsally. Late L3 stage: both distal arms have turned dorsally but not yet initiated looping. Early L4 stage: both distal arms have looped but the length of the

distal arm is shorter than half that of the proximal arm. Mid L4 stage: the length of the distal arm equals half that of the proximal arm. Late L4 stage: the distal arm and proximal arms have the same length, yet no oocyte is visible. Twenty and 48 hours post L4 stages: 68h and 96h, respectively, after providing food to synchronized L1 larvae at 20ºC (animals were confirmed to be in late L4 stage by visual inspection after 48h of feeding).

Immunofluorescence

To monitor ANI-2 localization, embryos were obtained after cutting open gravid hermaphrodites in 6 µl of M9 buffer with two 25-gauge needles on a 14x14mm-patterned cel-line slide (Thermo Fisher Scientific) coated with 0.1% poly-L-lysine. A coverslip was placed on the sample and the slide was placed for at least 5 min on a metal block cooled in dry ice. The coverslip was then removed and the slide was placed immediately in fixative (–20ºC methanol) for 20 min. The slide was rehydrated twice with 1X PBS for 5 min, then once with 1X PBST (PBS with 0.1% Tween-20) for 5 min, and then incubated in blocking buffer (1X PBST containing 10% goat serum) for 30 min at room temperature. Antibodies were then applied in blocking buffer and incubated overnight at 4ºC (primary) or 1h at room temperature (secondary), each followed by 4 washes of 5 min in PBST. The fixed specimens were mounted in 90% glycerol containing 1% N-propylgalate and a coverslip was sealed. Embryos were visualized with a Zeiss LSM 510 laser-scanning confocal microscope equipped with a 63X/1.4 Plan-Apochromat objective (Carl Zeiss Canada Ltd., Toronto, ON, Canada). The following antibodies were used: rat anti-PAR-4 (1:50) (Narbonne et al., 2010), rabbit anti-ANI-2 (1:1000) (Maddox et al., 2005), mouse clone DM1A anti-alpha-tubulin (1:500, Sigma) and mouse clone OIC1D4 anti-P granules (1:300, Developmental Studies Hybridoma Bank, University of Iowa). Secondary antibodies were Alexa488-coupled goat anti-rabbit, Alexa647-coupled donkey anti-mouse (1:500 each, Invitrogen) and Cy3-conjugated donkey anti-rat (1:500, Jackson Laboratories).

To visualize germ cell meiotic progression, gonads were extruded by cutting open young adult

animals behind the pharynx in 1X PBS on poly-L-lysine-coated slides and immediately fixed in 1% paraformaldehyde for 5 min. A coverslip was placed on the sample and the slide was snap-frozen in liquid nitrogen. The coverslip was then removed and the slide was immerged in methanol at –20ºC for 1 min. The slide was rehydrated with 1X PBST and incubated in blocking buffer (1X PBST containing 1% bovine serum albumin) for 1h at room temperature. Primary and secondary antibodies were applied in blocking buffer and incubated overnight at room temperature, each followed by 4 washes of 5 min in PBST. The fixed specimens were mounted in Vectashield (Vector Laboratories Inc, Burlington, ON, Canada) containing 1µg/µl of DAPI and a coverslip was sealed. Images were acquired with CoolSnap HQ camera (Photometrics, Tucson, AZ, USA) mounted on a DeltaVision Image Restoration System (Applied Precision, Mississauga, ON, Canada). A 100X/1.35 NA Plan-Apochromat objective was used to acquire sections (separated by 0.2 µm) of the gonad and image processing and deconvolution was done with the softWoRx 3.0 software (Applied Precision). The primary antibodies were rabbit anti-HTP-3 (1:200) (Goodyer et al., 2008) and guinea pig anti-SYP-1 (1:800) (MacQueen et al., 2002). Secondary antibodies were Alexa488-coupled goat anti-rabbit and Alexa555-coupled goat anti-guinea pig (1:1000 each, Invitrogen).

Fluorescence imaging of living animals

To analyze rachis length and rachis bridge diameter during ovulation, animals were mounted individually on a coverslip coated with 0.1% poly-l-lysine and were anaesthetized in 10 µl of egg buffer (Edgar, 1995) containing 0.1% tetramisole (Sigma). The coverslip was placed on a 3% agarose pad and the edges were sealed with petroleum jelly. Time-lapse movies were acquired with a CoolSnap HQ^2 camera (Photometrics) mounted on a Nikon Swept Field Confocal microscope (Nikon Canada, Mississauga, ON, Canada; and Prairie Technologies, Madison, WI, USA), using the 70 µm slit setting. A 60X/1.4 NA Plan-Apochromat objective was used to acquire 29 confocal sections (separated by 0.5 µm) of the gonad, each exposed for 200 milliseconds at 30-second intervals and with minimal laser power to avoid phototoxicity. All acquisition parameters and settings were controlled by Elements

software (Nikon). Confocal sections are presented as maximal intensity projections of the entire stacks. The length of the proximal rachis, from gonad turn to the proximal tip, and the diameter of the most proximal rachis bridge were measured for each time point using Image J software (NIH).

For analysis of rachis bridge formation, synchronized animals of a desired developmental stage were mounted and visualized with a Nikon swept field microscope as described above, except that the 35 μm slit and 60X/1.4 NA or 100X/1.4 NA objectives were used to acquire confocal sections (separated by 0.5 μm) spanning the entire rachis. When required, different regions of the gonad were acquired separately and reconstructed in a single image using the Photomerge function in Adobe Photoshop. To monitor rachis bridges, 6 consecutive confocal sections were analyzed independently using Image J, by measuring fluorescence intensity of expressed fluorescent markers along a 3 pixel-thick line drawn along the lateral and apical cortex, as depicted in Figure 3.1.2 D. Mean fluorescence intensity profiles of each marker were represented along the cortical perimeter. Rachis bridge diameter was determined by measuring the maximal distance between the peaks of fluorescent markers in all analyzed confocal sections. For GFP::ANI-2, GFP::ANI-1 and NMY-2::GFP, peaks were defined as pixels with maximum intensity across the whole fluorescence profile. Distinct peaks were defined as two distinct intensity maximums separated by at least 0.8 μm. For the membrane marker, the fluorescence intensity minimum was defined as the single pixel in the curve with the lowest fluorescence intensity. Peaks were defined as the first measured local maximums of fluorescence intensity, on each side of the minimum, that were maintained over three consecutive pixels and separated by at least 0.8 μm.

To visualize membrane partition collapse between germ cells, L4 stage or young adult animals were mounted and visualized with a Nikon swept field microscope as described above, and the 60X/1.4 NA objective was used to acquire 29 confocal sections (separated by 0.75 μm) every 30 seconds. We could only ascribe 2 clear membrane collapse events, largely due to several limitations in our experimental conditions: 1) we carried out imaging in every region of the

gonad, however imaging was done at high-magnification and each time-lapse acquisition encompassed only a small portion of a gonad arm, thus excluding collapse events occurring in regions not being examined during the analysis; 2) while time-lapse acquisitions were done in multiple confocal sections, we felt confident to ascribe a collapse event only when it occurred in germ cells with their nuclei in the same mid-section plane of the gonad; we observed 6 additional collapse events but the fact that they were occurring more or less along the z-plane made it more difficult to unambiguously ascribe them as such; this is even more exacerbated by the fact that the germline of *ani-2* mutants is disorganized and therefore many germ cell nuclei are not found in a single mid-section plane; and 3) membrane collapsing is an event that is likely very rapid and may occur at a frequency beyond the duration of our acquisition time (40 minutes).

Kymograph analysis of cytoplasmic streaming in the rachis

Living animals were mounted and immobilized as described above. Cytoplasmic movement in the rachis was visualized by Differential Interference Contrast microscopy, using a Zeiss HRM camera mounted on a Zeiss Axioimager Z1 microscope (Carl Zeiss Canada Ltd). Mid-section images of the rachis were acquired with a Plan Apochromat 63x/1.4 NA objective at 15 seconds intervals. Kymographs of cytoplasmic movement in the rachis were generated using the multiple kymograph plug-in available for Image J, by visualizing particle displacement over time along a 7 pixel-wide line drawn from the pachytene region to the proximal end of the gonad. The velocity of cytoplasmic streaming was obtained by averaging the speed of at least 25 particles moving around the loop region of each gonad.

Rhodamine-dextran photo-activation

Tetramethylrhodamine-labelled dextran (10 kDa, Molecular Probes) was reconstituted to 1 mg/ml in injection buffer (1 mM potassium citrate, 6.7 mM KPO4, pH 7.5, 0.67% PEG) and injected into the gonad of adult JH2107 animals (expressing GFP::PGL-1, to visualize the primordial germ cells). After 12h, embryos were obtained by cutting open the injected gravid hermaphrodites using two 25-gauge needles and mounted individually on a coverslip coated

with 0.1% poly-l-lysine in 10 µl of egg buffer. The coverslip was placed on a 3% agarose pad and the edges were sealed with petroleum jelly. Photo-activation in one of the two primordial germ cells was performed with a 405 nm laser mounted on a Zeiss LSM 510 confocal microscope equipped with a 63X/1.4 NA Plan-Apochromat objective, and fluorescence was monitored after excitation with a 543 nm laser. Fluorescence intensities were measured using Image J software in the photo-activated primordial germ cell, its non-photo-activated sister and a control neighbouring somatic cell.

Statistical analysis

Statistical significance between samples was performed by applying Student's *t*-test using Microsoft Excel. Assumptions of normality and equal variance were met for all data analyzed. A two-tailed *p* value smaller than 0.05 was considered significant. All results are expressed as average ± standard deviation. Sample size (n) and *p* values are given on each figure panel or in the figures legends.

Online supplemental material

Table 3.1.1 lists the strains and alleles used in this study. Movie S1 shows time-lapse analysis of gonad elastic deformation during ovulation in a wild-type hermaphrodite. Movie S2 shows time-lapse analysis of gonad elastic deformation during ovulation in a hermaphrodite partially depleted of ANI-2.

Acknowledgments

We are grateful to Karen Oegema, Patrick Narbonne, the Japanese *C. elegans* Gene Knockout Consortium and the *Caenorhabditis* Genetics Center for strains and reagents. We also thank Paul Maddox, Abby Gerhold, Jonas Dorn, Joel Ryan, Benjamin Lacroix, and members of the Maddox and Labbé laboratories for helpful discussions and comments on the manuscript, and Christian Charbonneau of IRIC's Bio-imaging Facility for technical help with image acquisition. A.S.M. was supported by salary awards from the Fonds de Recherche du Québec en Santé (FRQS) and the Canadian Institutes of Health Research (CIHR). N.C. was a

research fellow of the FRQS and holds a fellowship from the Fondation pour la Recherche Médicale (France). This work was funded by grants from the National Science and Engineering Research Council of Canada (#434942) and the CIHR (MOP-111142) to J.-C.L., who holds the Canada Research Chair in Cell Division and Differentiation. IRIC is supported in part by the Canadian Center of Excellence in Commercialization and Research, the Canada Foundation for Innovation, and the FRQS. The authors declare no competing financial interests.

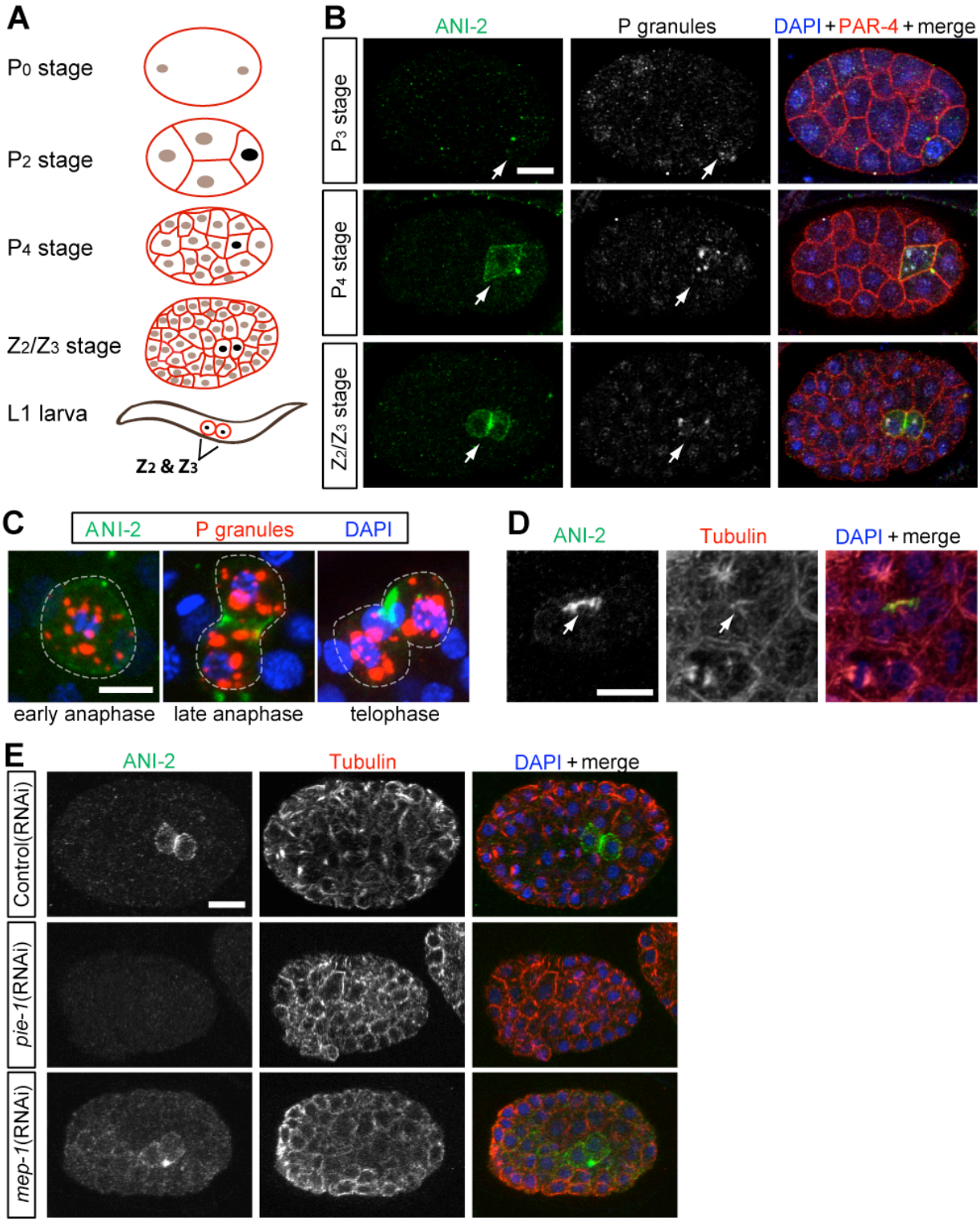
A
P0 stage
P2 stage
P4 stage
Z2/Z3 stage
L1 larva
Z2 & Z3
B
ANI-2
P granules
DAPI + PAR-4 + merge
P3 stage
P4 stage
Z2/Z3 stage
C
ANI-2
P granules
DAPI
early anaphase
late anaphase
telophase
D
ANI-2
Tubulin
DAPI + merge
E
ANI-2
Tubulin
DAPI + merge
Control(RNAi)
pie-1(RNAi)
mep-1(RNAi)

Figure 3.1.1.

Figure 3.1.1: ANI-2 stably accumulates at the midbody between the two primordial germ cells.

(A) Schematic representation of germ cell specification (black nuclei) during embryonic development. The primordial germ cells Z2 and Z3 are born from the P4 blastomere and do not undergo further division until hatching. (B) Mid-section confocal images of fixed wild-type embryos immunostained with ANI-2 (green), P-granules (PGL-1, gray), PAR-4 (to label the cortex, red) and DAPI (blue). Arrows point to the germline blastomeres. Scale bar, 10 μm. (C) Confocal projections of the dividing P4 blastomere in fixed wild-type embryos immunostained with ANI-2 (green), P-granules (PGL-1, red) and DAPI (blue). The white dashed line delineates the cell membrane. Scale bar, 5 μm. (D) Mid-section confocal images of the primordial germ cells of a fixed wild-type embryo immunostained with ANI-2 (green), alpha-tubulin (red), and DAPI (blue). Arrows point to the midbody. Scale bar, 5 μm. (E) Mid-section confocal images of fixed wild-type (top), *pie-1*(RNAi) (middle) and mep-1(RNAi) (bottom) embryos immunostained with ANI-2 (green), alpha-tubulin (red), and DAPI (blue). In all frames, anterior is to the left. Scale bar, 10 μm.

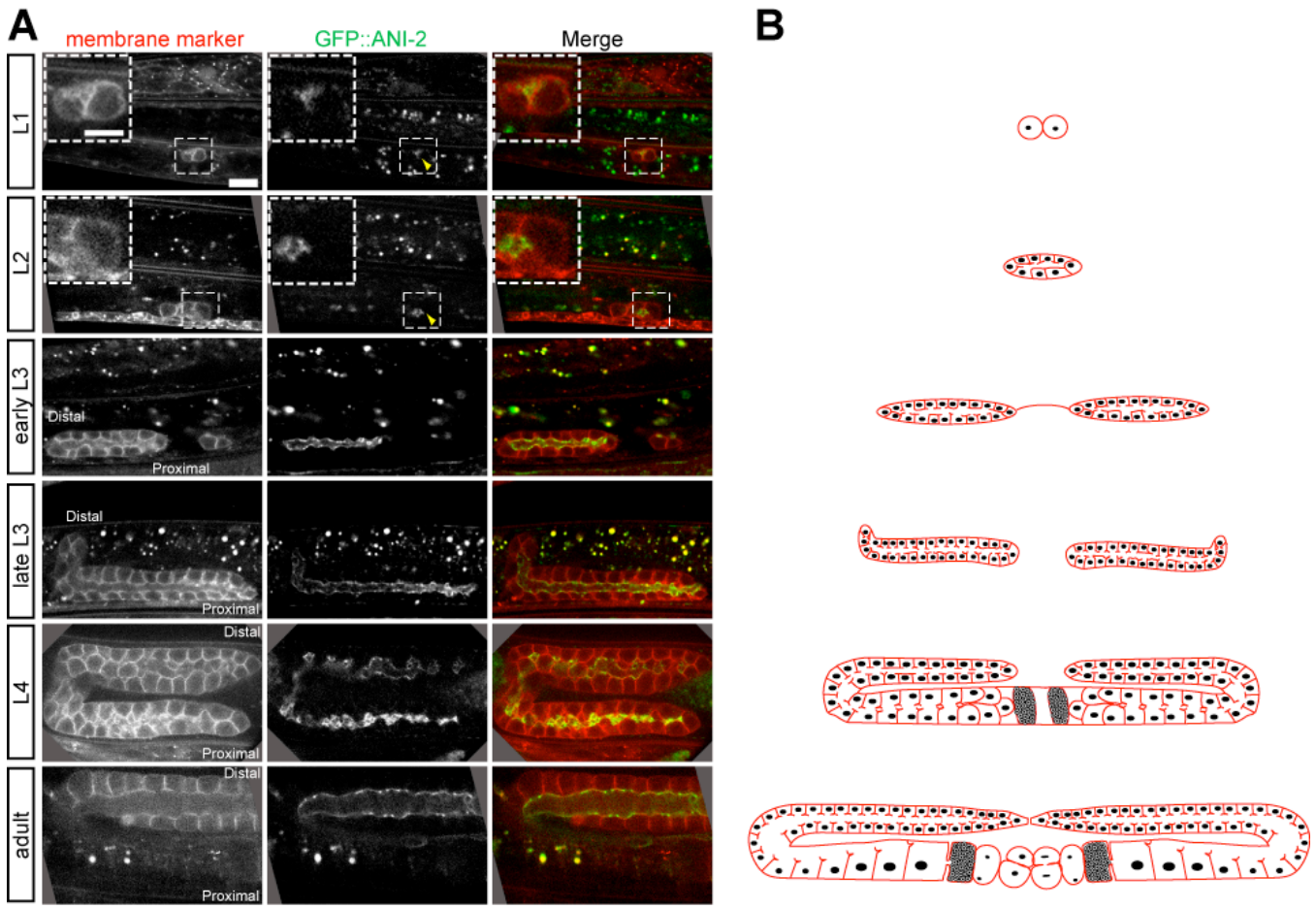

Figure 3.1.2.

Figure 3.1.2: ANI-2 is found at the rachis bridge of all germ cells throughout larval development.

(A) Mid-section confocal images of the germline of wild-type hermaphrodites expressing GFP::ANI-2 (green, yellow arrowheads) and a membrane marker (red) at various stages of development. For simplicity, only one gonad arm is shown from the L3 stage onward. In all frames, anterior is to the left. Scale bar, 10 µm. The regions delineated by the white dashed squares are magnified in inset (scale bar for insets, 5 µm). (B) Schematic representation of germline development at the developmental stages shown in panel E. Germ cells undergo proliferation and differentiation during larval growth until animals reach adulthood. For simplicity, only the germline is depicted.

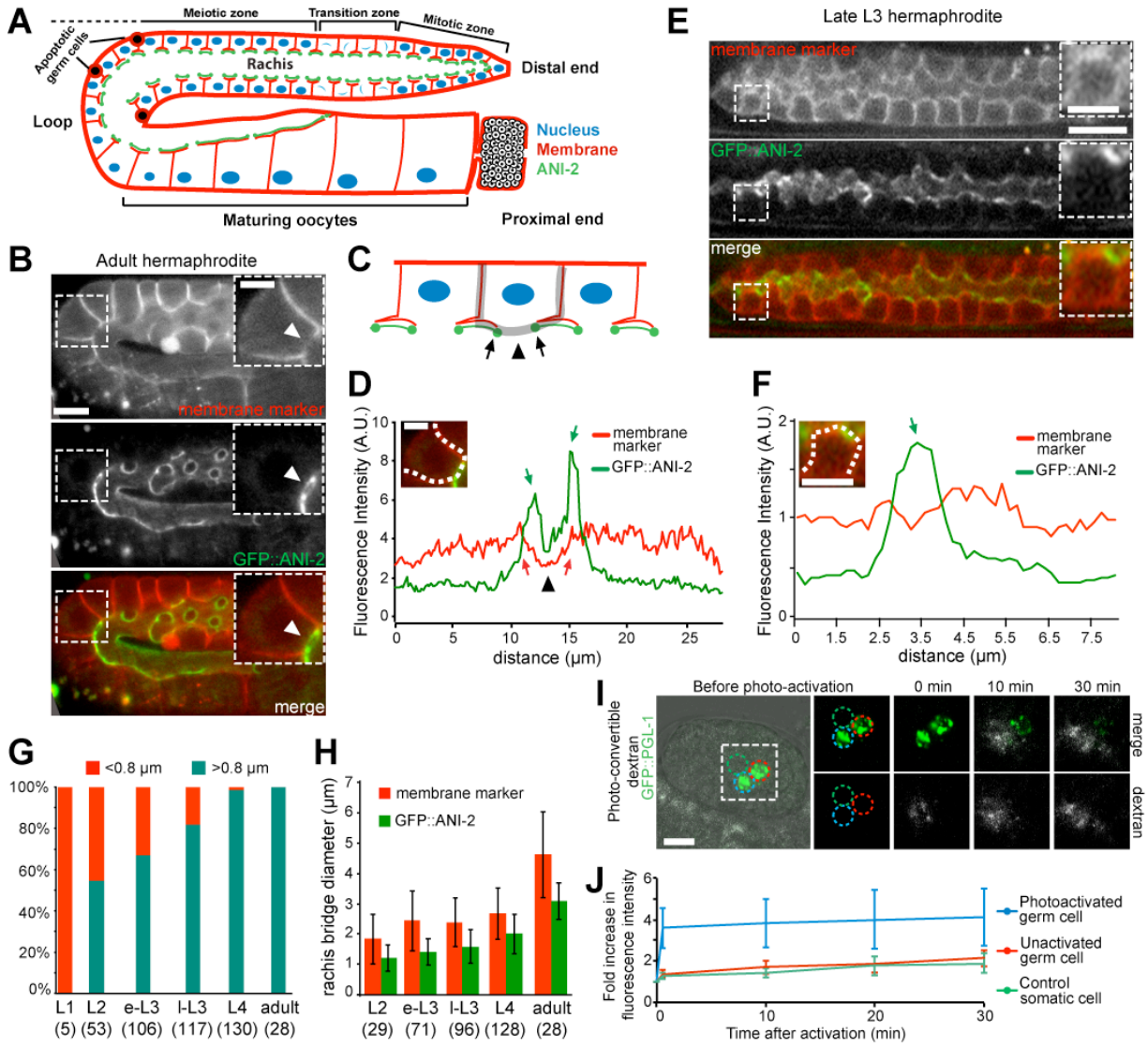

Figure 3.1.3.

Figure 3.1.3: Germ cell rachis bridge formation arises progressively during larval development.

(A) Schematic representation of the adult hermaphrodite germline. ANI-2 (green) lines up at the periphery of the central rachis and is enriched at rachis bridges, and it is delocalized upon oocyte cellularization. (B & E) Mid-section confocal images of the germline of a wild-type adult (B) and L3 (E) hermaphrodites expressing GFP::ANI-2 (green) and a membrane marker (red). Scale bar, 10 μm. The regions delineated by the white dashed square are magnified in inset (scale bar for insets, 5 μm). In panel B, the white arrowhead points to the germ cell

opening to the rachis. (C) Schematic representation of germ cells as in (A) depicting the method for measuring rachis bridge organization. Fluorescence intensity is measured along the lateral and apical cortices (line shown in black). Arrows point to the position of the rachis bridge as seen in mid-section images, and the arrowhead points to the germ cell opening to the rachis. (D & F) Measured fluorescence intensities (in arbitrary units) for each fluorescent marker along the lateral and apical cortices (white dotted line, as shown in insets; scale bar for insets, 5 μm) of the germ cell magnified in panel B and E, respectively. Red and green arrows point to peaks of membrane marker and GFP::ANI-2 fluorescence intensities, respectively. Both peaks border a minimum in fluorescence intensity (black arrowhead) that corresponds to the germ cell opening to the rachis. (G) Proportion of germ cells showing rachis bridges with a diameter >0.8 μm (turquoise) or <0.8 μm (red) throughout larval development, as measured by fluorescent marker distribution. (H) Maximal rachis bridge diameter in germ cells throughout larval development, as measured with GFP::ANI-2 (green) or membrane (red) fluorescence distribution. Error bars represent standard deviation. In panels G and H the numbers in brackets represent the total number of germ cells analyzed. (I) Mid-section confocal images of an embryo expressing GFP::PGL-1 (green) exogenously supplied with photo-convertible rhodamine-dextran (gray). Time is relative to fluorescence photo-activation (at time 0) in one of the two primordial germ cells (blue dashed circle). The sister cell is delineated by a red dashed circle and the green dashed circle delineates a nearby somatic cell. Scale bar, 10 μm. (J) Fold-increase (from time 0) in fluorescence intensity over time measured in each cell shown in panel I. Error bars represent standard deviation over 13 embryos.

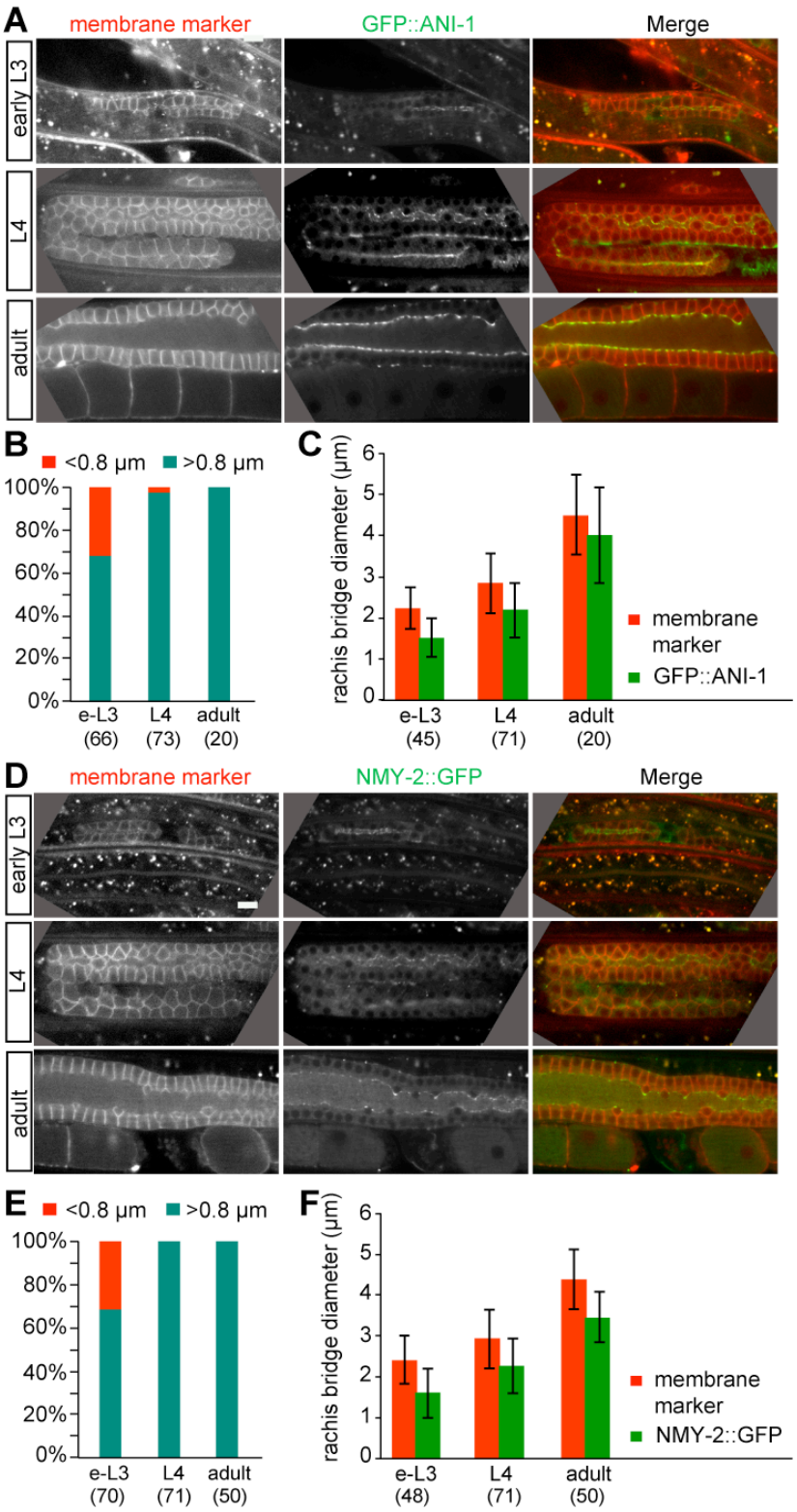
A
membrane marker
GFP::ANI-1
Merge
early L3
L4
adult
B
<0.8 µm
>0.8 µm
100%
80%
60%
40%
20%
0%
e-L3 (66)
L4 (73)
adult (20)
C
rachis bridge diameter (µm)
membrane marker
GFP::ANI-1
e-L3 (45)
L4 (71)
adult (20)
D
membrane marker
NMY-2::GFP
Merge
E
F
NMY-2::GFP
e-L3 (70)
L4 (71)
adult (50)
e-L3 (48)

Figure 3.1.4.

Figure 3.1.4: ANI-1 and NMY-2 localize to the rachis of wild-type hermaphrodites and report on rachis bridge organization.

(A & D) Mid-section confocal images of the germline of wild-type early L3 (top), L4 (middle) and adult (bottom) hermaphrodites co-expressing a membrane marker and GFP::ANI-1 (A) or NMY-2::GFP (D). In all frames, anterior is to the left. Scale bars, 10 μm. (B & E) Proportion of germ cells showing rachis bridges with a diameter >0.8 μm (turquoise) or <0.8 μm (red) throughout development, as measured by GFP::ANI-1 (B) and NMY-2::GFP (E) fluorescence distribution. (C & F) Maximal rachis bridge diameter in germ cells of animals in various developmental stages, as measured with fluorescence distribution of the membrane marker (red) and GFP::ANI-1 (C, green) or NMY-2::GFP (F, green). Error bars represent standard deviation. In panels B, C, E and F the numbers in brackets represent the total number of germ cells analyzed. The results on rachis bridges organization obtained with these markers are identical to those obtained after analysis of GFP::ANI-2 (Figure 2).

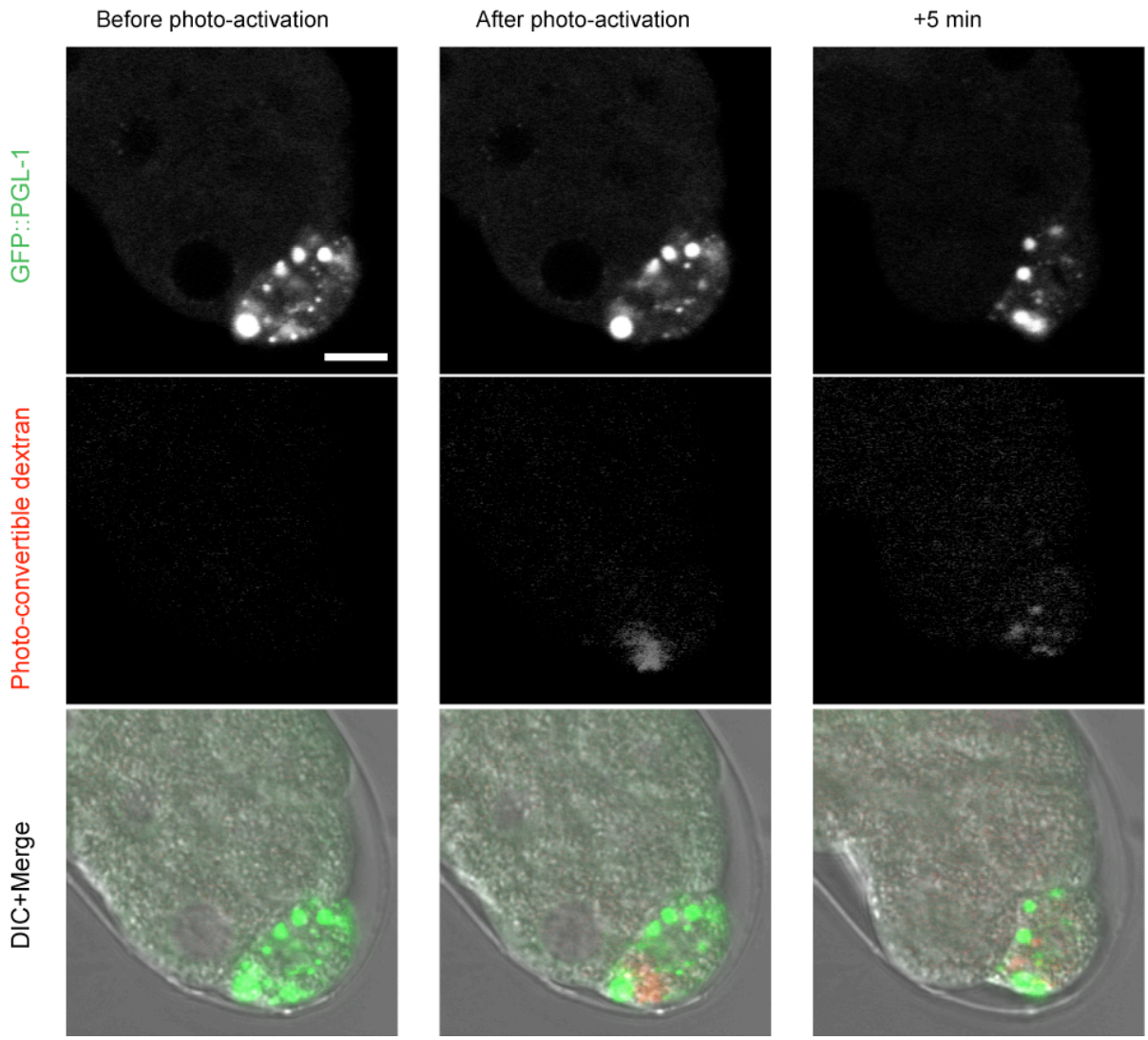

Figure 3.1.5.

Figure 3.1.5: Molecule diffusion in the cytoplasm of embryonic blastomeres.

Mid-section confocal images of an embryo expressing GFP::PGL-1 exogenously supplied with photo-convertible rhodamine-dextran. Following photo-activation in part of the P_3 blastomere, the fluorescent signal rapidly spread throughout the cell. Scale bar, 10 µm.

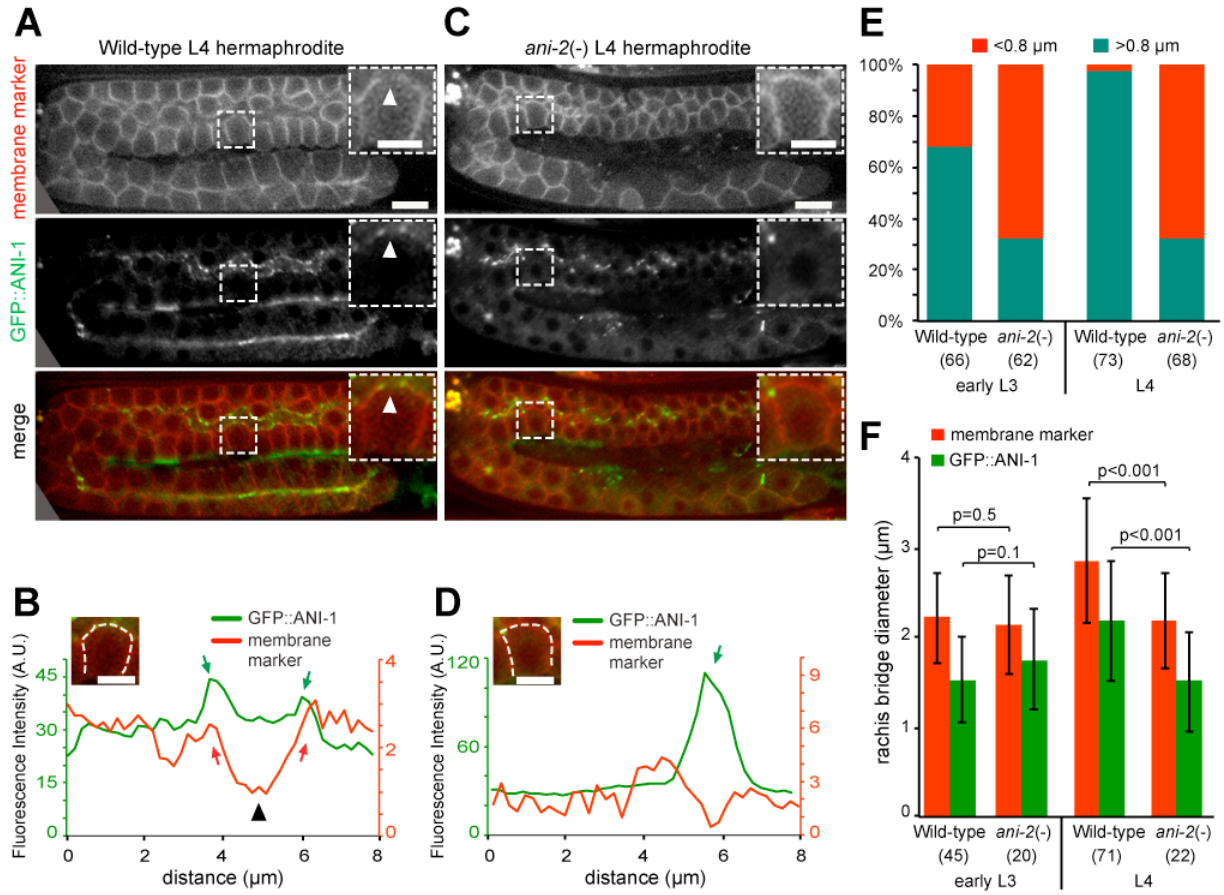

Figure 3.1.6.

Figure 3.1.6: ANI-2 is required for rachis bridge stabilization.

(A & C) Mid-section confocal images of the germline of a wild-type (A) and an *ani-2*(-) (C) L4 hermaphrodite expressing a membrane marker (red) and GFP::ANI-1 (green). Scale bar, 10 µm. The regions delineated by the white dashed square are magnified in inset (scale bar for insets, 5 µm). In panel A, the white arrowhead points to the germ cell opening to the rachis. (B & D) Measured fluorescence intensities (in arbitrary units specific to each curve) for each fluorescent marker along the lateral and apical cortices (white dotted line, as shown in insets; scale bar for insets, 5 µm) of the germ cell magnified in panel A and C, respectively. Red and green arrows point to peaks of membrane marker and GFP::ANI-1 fluorescence intensities,

respectively, and the black arrowhead points to the intensity minimum. (E) Proportion of germ cells showing rachis bridges with a diameter >0.8 μm (turquoise) or <0.8 μm (red) in wild-type and *ani-2*(-) mutant animals at the L3 and L4 larval stages, as measured by fluorescent marker distribution. (F) Maximal rachis bridge diameter in germ cells of wild-type and *ani-2*(-) animals at the L3 and L4 larval stages, as measured with membrane (red) or GFP::ANI-1 (green) fluorescence distribution. Rachis bridges that are <0.8 μm in diameter are excluded from this analysis. Error bars represent standard deviation. In panels E and F the numbers in brackets represent the total number of germ cells analyzed.

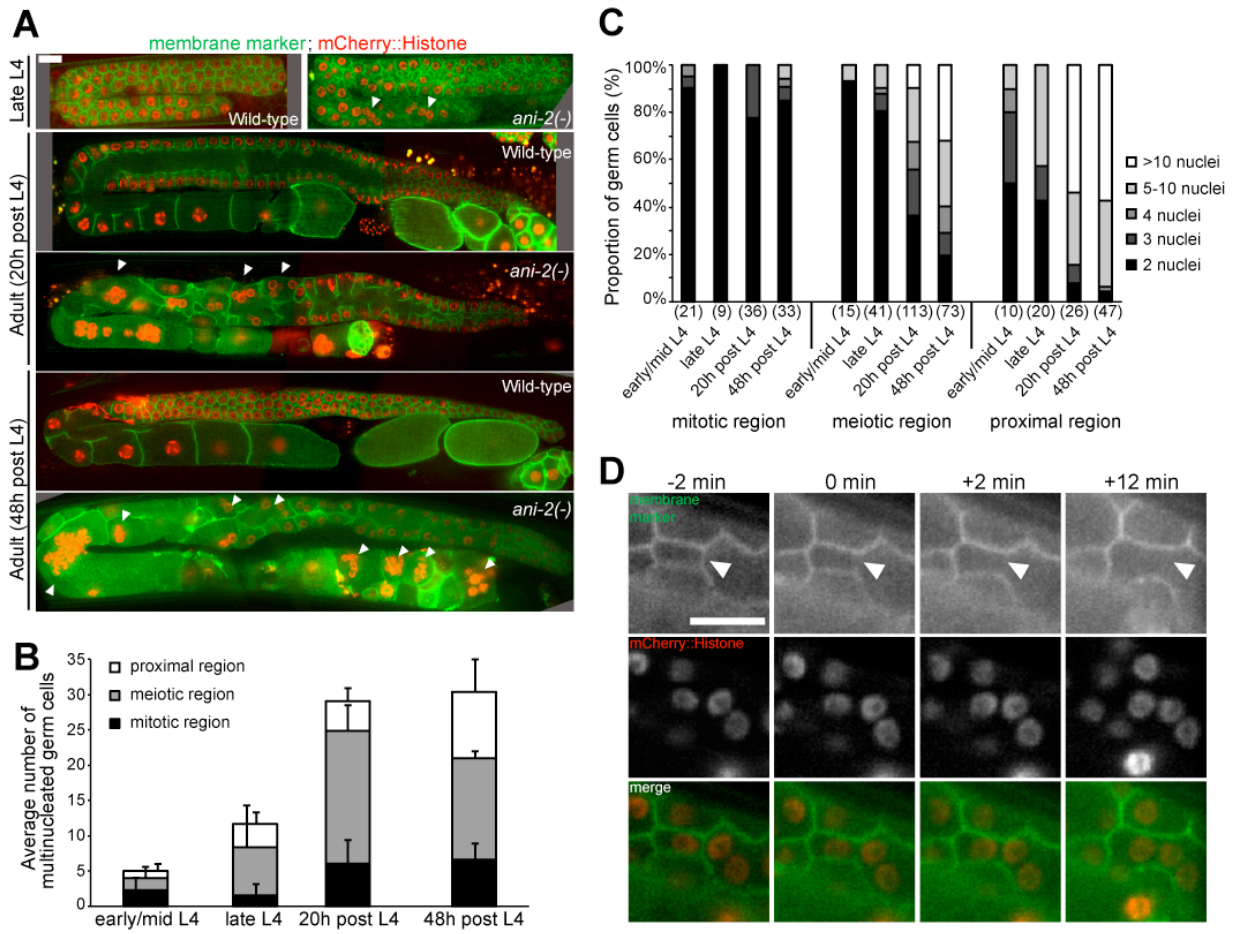

Figure 3.1.7.

Figure 3.1.7: Loss of ANI-2 causes germ cell multinucleation and collapse of membrane partitions.

(A) Mid-section confocal images of the germline of wild-type and *ani-2*(-) hermaphrodite animals at various stages of development expressing a membrane marker (green) and mCherry::Histone H2B (red). Each image was assembled from multiple acquisitions of the same animal. Arrowheads point to multinucleated germ cells. (B) Average number of multinucleated germ cells in various germline regions of *ani-2*(-) mutant hermaphrodites at the specified stage. Multinucleation was never observed in control animals at any stage. Error bars represent standard deviation over 5-9 animals at each stage. (C) Proportion of multinucleated

germ cells with 2, 3, 4, 5-10 and >10 nuclei in various germline regions of *ani-2*(-) hermaphrodites at the specified stage. The number of germ cells analyzed is shown for each condition. (D) Mid-section confocal time-lapse images of germ cells of an *ani-2*(-) hermaphrodite expressing a membrane marker (green) and mCherry::Histone H2B (red) captured during the collapse of a membrane partition (arrowhead). The stages examined and reported are early-mid L4 larvae, late L4 larvae, 20h post L4 stage and 48h post L4 stage. Scale bars, 10 μm.

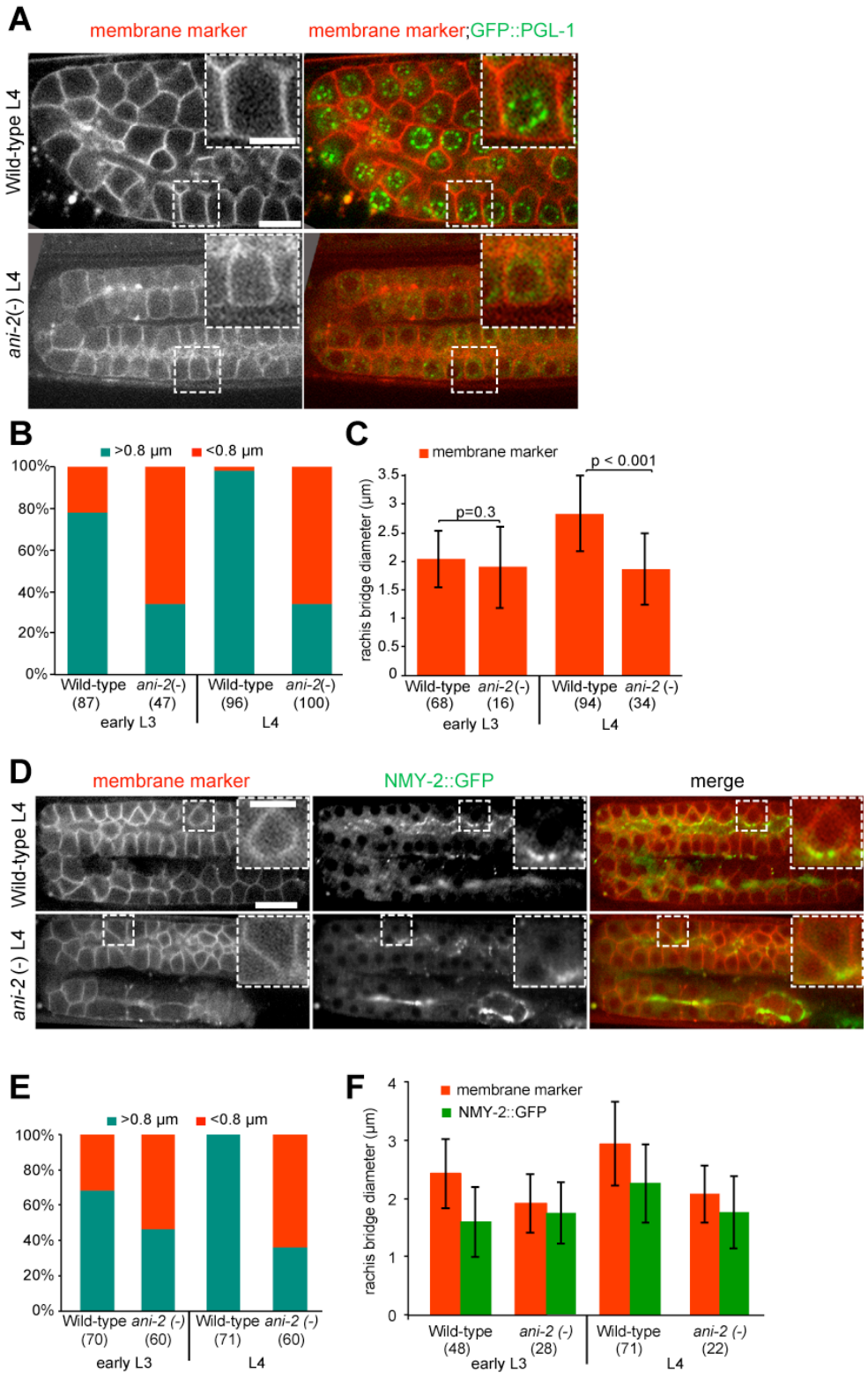
A
membrane marker
membrane marker;GFP::PGL-1
Wild-type L4
ani-2(-) L4
B
>0.8 µm
<0.8 µm
100%
80%
60%
40%
20%
0%
Wild-type (87)
ani-2(-) (47)
Wild-type (96)
ani-2(-) (100)
early L3
L4
C
membrane marker
p < 0.001
p=0.3
rachis bridge diameter (µm)
3.5
3
2.5
2
1.5
1
0.5
0
Wild-type (68)
ani-2 (-) (16)
Wild-type (94)
ani-2 (-) (34)
early L3
L4
D
membrane marker
NMY-2::GFP
merge
Wild-type L4
ani-2 (-) L4
E
>0.8 µm
<0.8 µm
100%
80%
60%
40%
20%
0%
Wild-type (70)
ani-2 (-) (60)
Wild-type (71)
ani-2 (-) (60)
early L3
L4
F
membrane marker
NMY-2::GFP
rachis bridge diameter (µm)
4
3
2
1
0
Wild-type (48)
ani-2 (-) (28)
Wild-type (71)
ani-2 (-) (22)
early L3
L4

Figure 3.1.8.

Figure 3.1.8: ANI-2 is required for rachis bridge stability.

(A & D) Mid-section confocal images of the germline of a wild-type and an *ani-2*(-) L4 hermaphrodite expressing a membrane marker (red) and GFP::PGL-1 (A, green) or NMY-2::GFP (D, green). Scale bar, 10 μm. The regions delineated by the white dashed square are magnified in inset (scale bar for insets, 5 μm). (B & E) Proportion of germ cells showing rachis bridges with a diameter >0.8 μm (turquoise) or <0.8 μm (red) in wild-type and *ani-2*(-) animals at the L3 and L4 larval stages, as measured by distribution of the membrane marker alone (B) or together with NMY-2::GFP (E). (C & F) Maximal rachis bridge diameter in germ cells of wild-type and *ani-2*(-) animals at the L3 and L4 larval stages, as measured with distribution of the membrane marker alone (red) or together with NMY-2::GFP (green). Rachis bridges that are <0.8 μm in diameter are excluded from this analysis. Error bars represent standard deviation. In panels B, C, E and F the numbers in brackets represent the total number of germ cells analyzed. The results on rachis bridges organization obtained with these markers are identical to those obtained after analysis of GFP::ANI-1 (Figure 3).

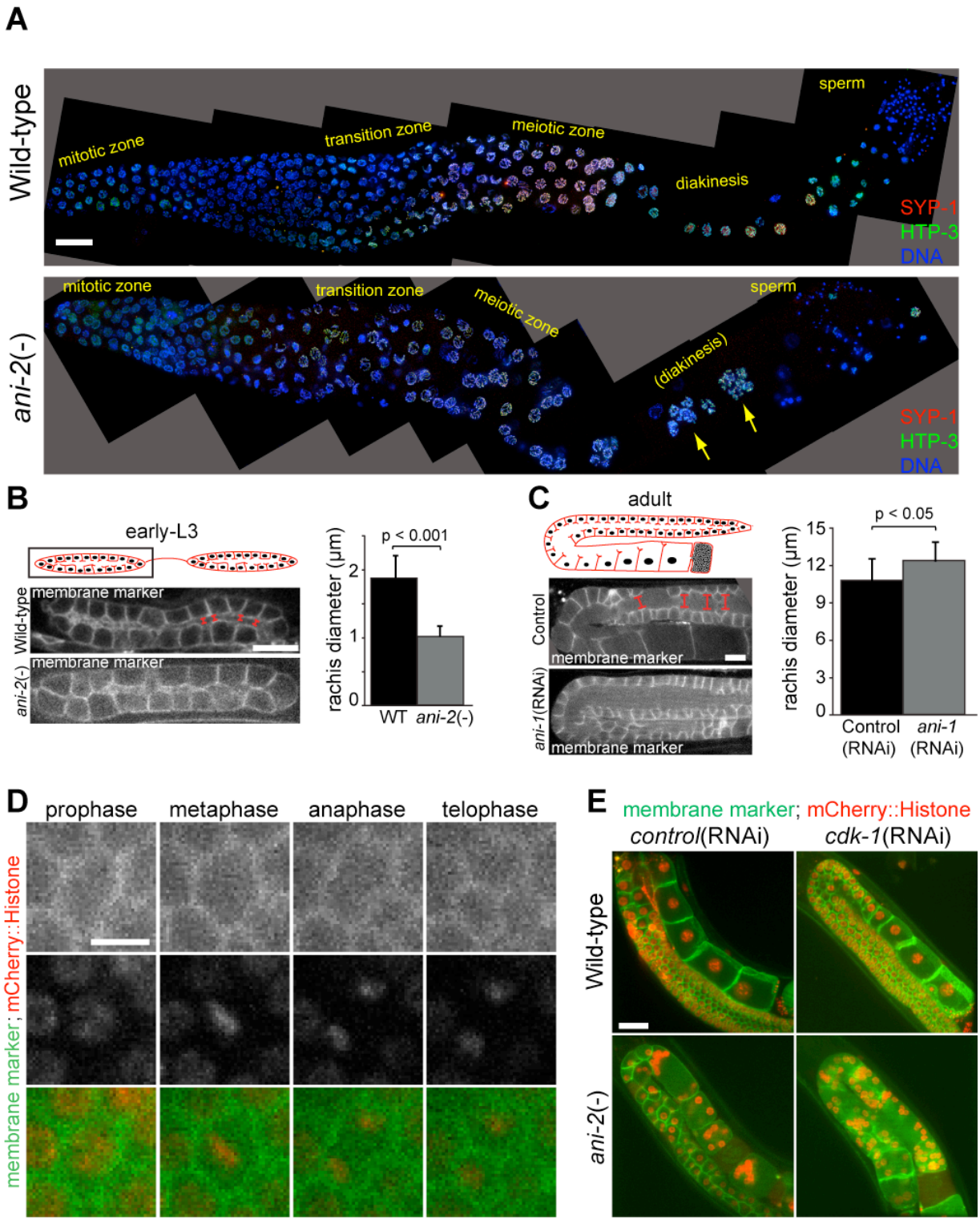
A
Wild-type
mitotic zone
transition zone
meiotic zone
diakinesis
sperm
SYP-1
HTP-3
DNA
ani-2(-)
mitotic zone
transition zone
meiotic zone
(diakinesis)
sperm
SYP-1
HTP-3
DNA
B
early-L3
membrane marker
Wild-type
membrane marker
ani-2(-)
p < 0.001
rachis diameter (µm)
WT
ani-2(-)
C
adult
Control
membrane marker
ani-1(RNAi)
membrane marker
p < 0.05
rachis diameter (µm)
Control (RNAi)
ani-1 (RNAi)
D
prophase
metaphase
anaphase
telophase
membrane marker; mCherry::Histone
E
membrane marker; mCherry::Histone
control(RNAi)
cdk-1(RNAi)
Wild-type
ani-2(-)

Figure 3.1.9.

Figure 3.1.9: Phenotypic analysis of *ani-2* mutants.

(A) Projected image stacks of fixed extruded gonads from wild-type (left) and *ani-2*(-) young adult hermaphrodites immunostained with SYP-1 (red), HTP-3 (green) and DAPI (blue). Arrows point to germ cells with defect in diakinesis. Each image was assembled from multiple acquisitions of the same gonad. Scale bar, 20 μm. (B) Schematic representation of the gonad and images of one gonad in wild-type and *ani-2*(-) mutant early L3 stage larvae. Rachis diameter was measured in multiple regions and confocal sections of the gonad (red line). The graph represents the average diameter of the rachis in wild-type and *ani-2*(-) mutant L3 stage larvae. Rachis diameter is significantly reduced in *ani-2*(-) mutants compared to wild type. (C) Schematic representation of the gonad and images of one gonad in control and *ani-1(RNAi)* adult animals. Figure elements are as in panel B. Rachis diameter is significantly increased in *ani-1(RNAi)* animals compared to control. (D) Time-lapse confocal images of a germline stem cell dividing in the gonad of an *ani-2*(-) hermaphrodite. The cell properly progresses through all stages of M phase. Scale bar, 5 μm. (E) Mid-section confocal images of the germline of wild-type and *ani-2*(-) adult hermaphrodites expressing a membrane marker (green) and mCherry::Histone H2B (red). Blocking cell cycle progression with *cdk-1(RNAi)* (right) did not preclude germ cell multinucleation, indicating that it is not a consequence of inappropriate re-entry into the cell cycle. Scale bar, 10 μm.

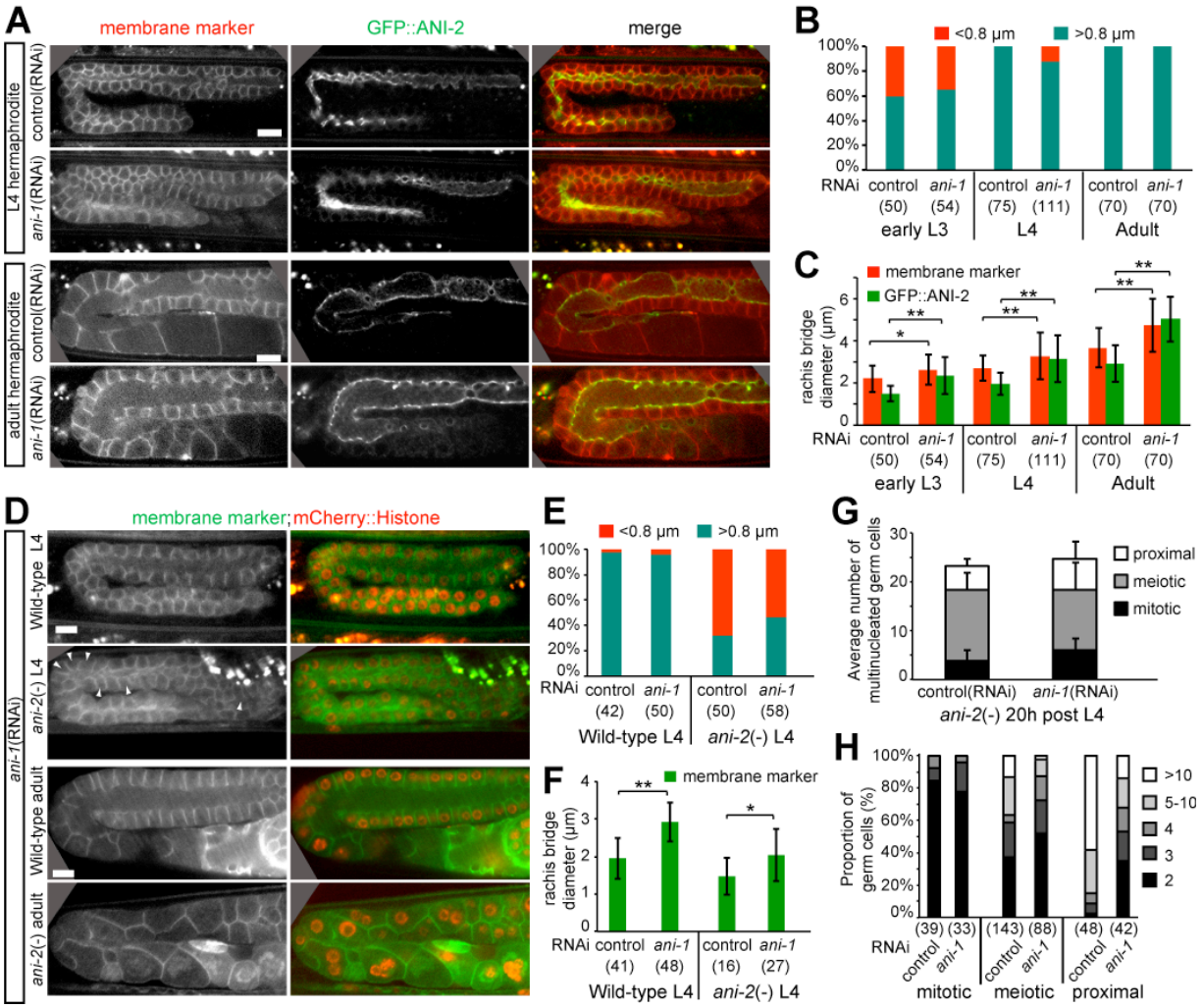

Figure 3.1.10.

Figure 3.1.10: ANI-2 and ANI-1 have opposing activities in germline organization

(A) Mid-section confocal images of the germline of wild-type L4 (top) and adult (bottom) hermaphrodites, treated with control(RNAi) or *ani-1*(RNAi), and expressing GFP::ANI-2 (green) and a membrane marker (red). (B) Proportion of germ cells showing rachis bridges with a diameter >0.8 µm (turquoise) or <0.8 µm (red) in animals of the specified condition, as measured by fluorescent marker distribution. (C) Maximal rachis bridge diameter in germ cells of animals of the specified condition, as measured with membrane (red) or GFP::ANI-2 (green) fluorescent distribution. (D) Mid-section confocal images of the germline of wild-type

and *ani-2*(-) young adult hermaphrodites (20h post L4), treated with *ani-1*(RNAi), and expressing a membrane marker (green) and mCherry::Histone H2B (red). (E) Proportion of germ cells showing rachis bridges with a diameter >0.8 μm (turquoise) or <0.8 μm (red) in animals of the specified condition, as measured by fluorescent marker distribution. (F) Maximal rachis bridge diameter in germ cells of animals of the specified condition, as measured with membrane fluorescent distribution. (G) Average number of multinucleated germ cells in various germline regions of *ani-2*(-) mutant hermaphrodites (20h post L4) treated with control(RNAi) or *ani-1*(RNAi). Error bars represent standard deviation over 10-17 animals at each stage. (H) Proportion of multinucleated germ cells with 2, 3, 4, 5-10 and >10 nuclei in various germline regions of *ani-2*(-) hermaphrodites (20h post L4) treated with control(RNAi) or *ani-1*(RNAi). In panels B, C, E, F and H, the numbers in brackets represent the total number of germ cells analyzed. Scale bars, 10 μm. *$p < 0.01$. **$p < 0.001$.

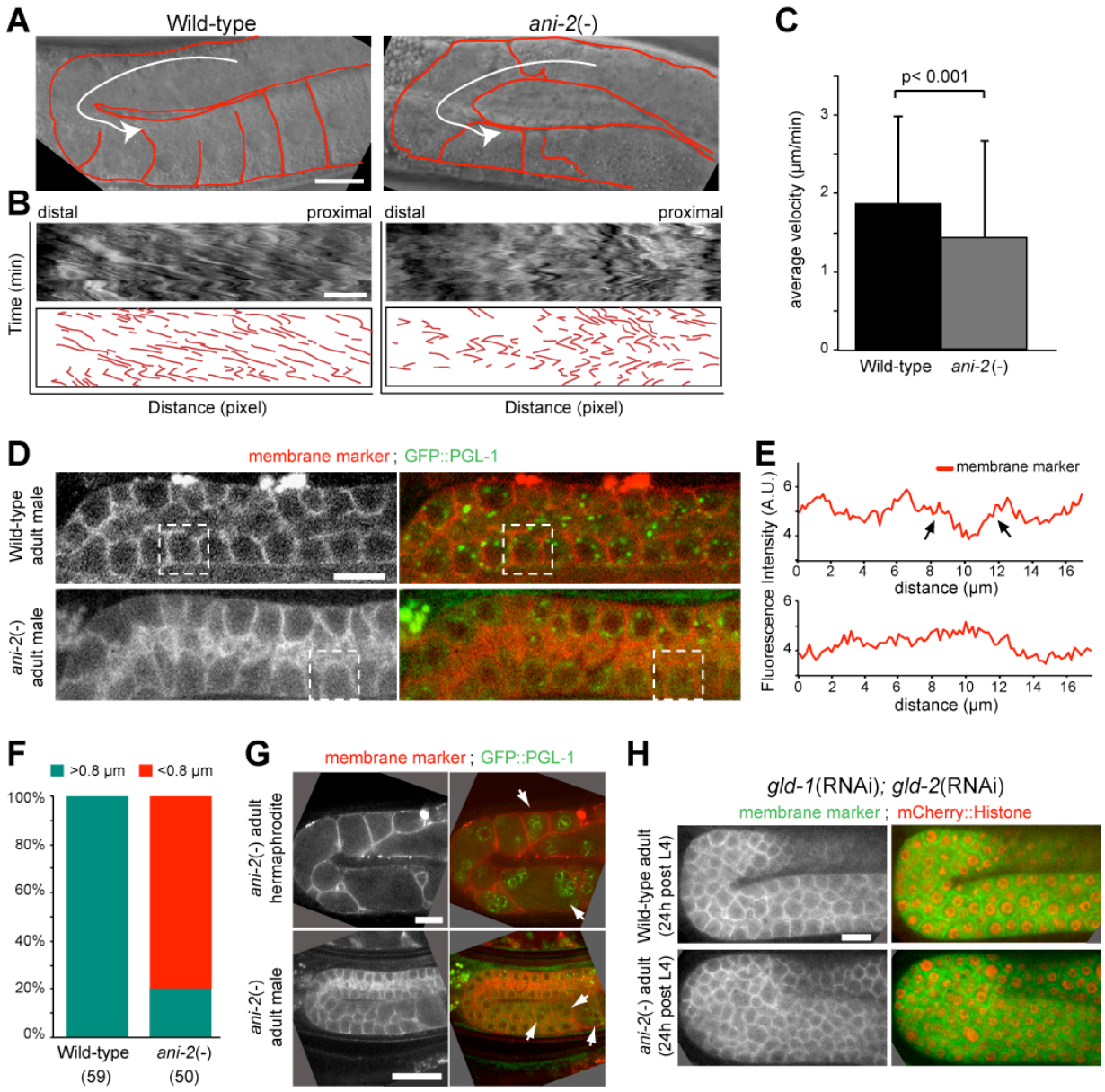

Figure 3.1.11.

Figure 3.1.11: Cytoplasmic streaming in the rachis may be responsible for germline disorganization in *ani-2* mutants

(A) DIC images of the germlines of wild-type (left) and *ani-2*(-) (right) young adult animals. Some membrane partitions are outlined in red. The white arrow depicts the direction of

cytoplasmic streaming. (B) DIC images (top) and schematic representations (bottom) of kymographs of cytoplasmic streaming in the gonads of animals depicted in panel A. Kymographs were made along the white line shown in panel A. The total duration of the movie is 45 min. (C) Average velocity of cytoplasmic streaming in the rachis of wild-type (black) and *ani-2*(-) (gray) animals. Error bars represent standard deviation over 9 animals analyzed for each genotype. (D) Mid-section confocal images of a wild-type (top) and an *ani-2*(-) (bottom) male adult germlines expressing a membrane marker (red) and GFP::PGL-1 (green). (E) Measured fluorescence intensities (in arbitrary units) for the membrane marker along the lateral and apical cortices of the germ cells of each male genetic background delineated by a dashed square in panel D. Arrows point to peaks of membrane marker fluorescence intensity bordering a minimum. (F) Proportion of germ cells showing rachis bridges with a diameter >0.8 μm (turquoise) or <0.8 μm (red) in wild-type and *ani-2*(-) animals at the adult stage, as measured by membrane marker distribution. The numbers in brackets represent the total number of germ cells analyzed. (G) Mid-section confocal images of the germlines of an *ani-2*(-) adult hermaphrodite (top) and an *ani-2*(-) adult male (bottom) expressing a membrane marker (red) and GFP::PGL-1 (green). Arrowheads point to multinucleated germ cells, whose number is significantly reduced in *ani-2*(-) males. (H) Mid-section confocal images of the gonads of wild-type (top) and *ani-2*(-) (bottom) adult hermaphrodites expressing a membrane marker (green) and mCherry::Histone H2B (red) and depleted of GLD-1 and GLD-2 by RNAi. Scale bars, 10 μm.

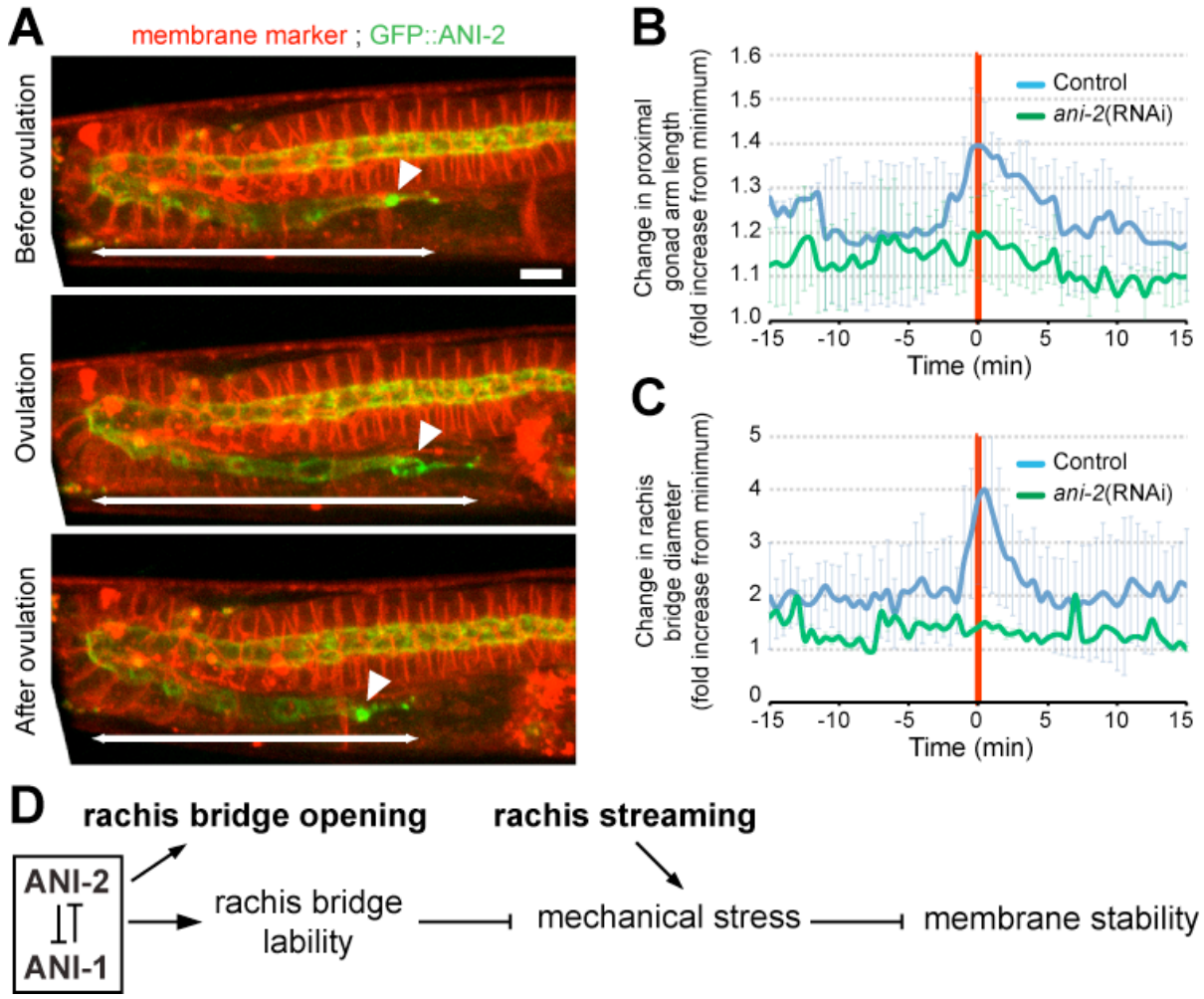

Figure 3.1.12.

Figure 3.1.12: ANI-2 permits elastic deformation of the adult hermaphrodite gonad and rachis bridges.

(A) Time-lapse confocal image projections of the gonad of a wild-type hermaphrodite expressing GFP::ANI-2 (green) and a membrane marker (red) captured before (top), during (middle) and after (bottom) ovulation. Arrowheads point to the most proximal rachis bridge. Double-headed arrows indicate the length of the GFP::ANI-2-enriched portion of the proximal gonad arm. Scale bar, 10 μm. See also Movies S1 and S2. (B & C) Measured fold-increase (as compared to minimum measurement) in proximal gonad arm length (B) and rachis bridge

diameter (C) over time in the gonads of control (blue, n=6), and *ani-2*(RNAi) (green, n=5) adult hermaphrodite animals undergoing ovulation. Time 0 corresponds to the point of oocyte entry into the spermatheca. Error bars represent standard deviation. (D) Proposed model depicting ANI-1 and ANI-2 function in promoting rachis bridge opening during larval development and relieving mechanical stress upon oogenesis in adult animals.

Strain #	Genotype
N2	Wild-type Bristol strain
VC703	*ani-2(ok1147)/mIn1[mIs14 dpy-10(e128)] II*
OD95	*unc-119(ed3) III; ltIs37 [Ppie-1::mCherry::his-58; unc-119(+)] IV; ltIs38 [Ppie-1::gfp::PH(PLC1delta1); unc-119(+)]*
UM185	*unc-119(ed3) III; ltIs44 [Ppie-1::mCherry::PH(PLC1delta1); unc-119(+)] IV; axIs1720 [Ppie-1::gfp::pgl-1::pgl-1 3'; unc-119(+)]*
UM186	*ani-2(ok1147)/mIn1[mIs14 dpy-10(e128)] II; ltIs44 [Ppie-1::mCherry::PH(PLC1delta1); unc-119(+)] IV; axIs1720 [Ppie-1::gfp::pgl-1::pgl-1 3'; unc-119(+)]*
UM208	*unc-119(ed3) III; ltIs81 [Ppie-1::gfp-TEV-Stag::ani-2; unc-119 (+)]; ltIs44 [Ppie-1::mCherry::PH(PLC1delta1); unc-119(+)] IV*
OD182	*unc-119(ed3) III; ltIs28 [Ppie-1::gfp-TEV-Stag::ani-1; unc-119 (+)]; ltIs44 [Ppie-1::mCherry::PH(PLC1delta1); unc-119(+)] IV*
UM341	*ani-2(ok1147)/mIn1[mIs14 dpy-10(e128)] II; unc-119(ed3) III; ltIs28 [Ppie-1::gfp-TEV-Stag::ani-1; unc-119 (+)]; ltIs44 [Ppie-1::mCherry::PH(PLC1delta1); unc-119(+)] IV*
OD183	*unc-119(ed3) III; ltIs44 [Ppie-1::mCherry::PH(PLC1delta1); unc-119(+)] IV; zuIs45 [Pnmy-2::nmy-2::gfp; unc-119 (+)] V*
UM342	*ani-2(ok1147)/mIn1[mIs14 dpy-10(e128)] II; unc-119(ed3) III; ltIs44 [Ppie-1::mCherry::PH(PLC1delta1); unc-119(+)] IV; zuIs45 [Pnmy-2::nmy-2::gfp; unc-119 (+)] V*
JH2107	*unc-119(ed3) III; axIs1720 [Ppie-1::gfp::pgl-1::pgl-1 3'; unc-119(+)]*
UM209	*ani-2(ok1147)/mIn1[mIs14 dpy-10(e128)] II; ltIs37 [Ppie-1::mCherry::his-58; unc-119(+)] IV; ltIs38 [Ppie-1::gfp::PH(PLC1delta1); unc-119(+)]*
JK2879	*gld-2(q497) gld-1(q485) I/hT2[qIs48] (I;III)*
UM230	*gld-2(q497) gld-1(q485) I/hT2[qIs48] (I;III); ; ani-2(ok1147)/mIn1[mIs14 dpy-10(e128)] II; ltIs37 [Ppie-1::mCherry::his-58; unc-119(+)] IV; ltIs38 [Ppie-1::gfp::PH(PLC1delta1); unc-119(+)]*

Table 3.1.1: *C. elegans* strains used in this study

3.2. Article 2

Formation of the two C. elegans primordial germ cells occurs by incomplete cytokinesis

Rana Amini, Alexandre St-Pierre-See and Jean-Claude Labbé

This manuscript is ready for submission as a report.

I jointly conceived this study with J.C.L. and designed all experiments. I executed all experiments and data analysis except for the following figure: Figures 3.2.7. and 3.2.8., performed and analyzed by A.S.P.S., Université de Montréal. I wrote the first draft of the manuscript.

Formation of the two C. elegans primordial germ cells occurs by incomplete cytokinesis

Rana Amini [1], Alexandre St-Pierre-See[1] and Jean-Claude Labbé [1,2]

[1] Institute of Research in Immunology and Cancer, and [2] Department of Pathology and Cell Biology, Université de Montréal, Montréal, QC, Canada.

Keywords: abscission, Cytokinesis, germ cell rachis ring, midbody, midbody ring, PGC, Syncytium formation

Abstract

Cytokinesis consists in the physical separation of the two daughter cells, after mitosis. However, during development of certain tissues, mitotic division is followed by incomplete cytokinesis, giving rise to interconnected cells in a shared cytoplasm, or syncytium. Syncytial structures have been repeatedly described in female and male germlines in species ranging from insects to humans. Nevertheless, the mechanism of syncytium formation is poorly characterized. To understand the mechanism of syncytium formation, we monitored the dynamics of P_4 cytokinesis. The P_4 blastomere divides into the two primordial germ cells (PGCs) during embryogenesis and eventually gives rise to all GCs of the germline. We find that P_4, similar to its somatic neighbors, goes normally through the first phase of cytokinesis, also known as cytoplasmic isolation. Interestingly however, unlike somatic blastomeres, P_4 fails to complete the second phase of cytokinesis wherein the midbody ring (MBR) is released from the cell-cell boundary. While the MBRs of somatic cells disappear soon after their cortical release, the MBR connecting the two PGCs remains tightly associated to the cortex throughout embryogenesis. We further show that MB/MBR components; ANI-1, ANI-2, NMY-2, UNC-59^{Septin}, CYK-7, ZEN-4^{Mklp1}, RHO-1^{RhoA} and ECT-2^{RhoGEF} are localized to GC rings throughout germline development from the L1 stage to adulthood, suggesting that GC rings are derived from MBRs. Interestingly, while RHO-1^{RhoA} and ECT-2^{RhoGEF} are also localized to GC cortices, the other MBR components are solely enriched at GC rings, indicating that they might play different roles in syncytium maintenance during gonad development. Our findings support a model in which incomplete cytokinesis of the P_4 blastomere results in persistence of the MBR between the two PGCs, thus forming a stable bridge that, in turn, promotes syncytium biogenesis.

Introduction

Cytokinesis, the last step of cell division, is a spatiotemporally controlled event that occurs in multiple steps to ensure reliable cell separation (Eggert et al., 2006; Glotzer, 2005; Green et al., 2012). Cytokinesis begins by formation of a dynamic actomyosin-based contractile ring beneath the plasma membrane at the cell equator (Eggert et al., 2006; Green et al., 2012). The cytokinetic contractile ring (CR) is composed of many cytoskeletal proteins, including actin, myosin II, anillin, septins, and their regulators and as such undergoes constriction during anaphase (Eggert et al., 2006; Green et al., 2012; Wu and Pollard, 2005). Constriction of the CR, partitions the cytoplasm at the center of the mitotic spindle, generating an intercellular bridge (ICB) that transiently interconnects the two daughter cells (Barr and Gruneberg, 2007; Eggert et al., 2006; Glotzer, 2005; Glotzer, 2009b; Green et al., 2012; Pollard, 2010). As cytokinesis proceeds, the CR undergoes further constriction, until it contacts the central spindle and forms a highly dense structure known as the midbody (MB) (Straight et al., 2003). The MB is derived from the central spindle and is therefore composed of microtubules and various central spindle proteins including the Mitotic kinesin-like protein (Mklp1) and the Rho GTPase activating protein (RhoGAP) CYK-4 (Green et al., 2012; White and Glotzer, 2012). As the constriction nears completion, the CR shrinks in diameter and eventually matures into the midbody ring (MBR), a dense structure that forms around the center of the MB (Green et al., 2012). It has been shown that in *Drosophila* S2 cells, MBR maturation requires the septin (Peanut)/citron kinase (Sticky)-dependent retention of anillin within the structure (El Amine et al., 2013; Kechad et al., 2012). The mature MBR contains several CR components, including myosin II, anillin, the septins, citron kinase, and RhoA (Kechad et al., 2012) and connects the dividing cells for up to several hours until it is finally severed through an event known as abscission, generating two fully separated sibling cells (Agromayor and Martin-Serrano, 2013; Barr and Gruneberg, 2007; Eggert et al., 2006; Mullins and Biesele, 1977; Pollard, 2010; Schweitzer and D'Souza-Schorey, 2004; Steigemann and Gerlich, 2009). Abscission is a complex, tightly regulated process required for disassembly of the MBR and physical separation of the two daughter cells. One key component of the abscission machinery is the ESCRT (endosomal sorting complex required

for transport) complex, which promotes recruitment of spastin, a microtubule-severing enzyme and induces membrane scission (Schiel et al., 2012; Yang et al., 2008). It has been previously proposed that the MB and its microtubules function as a targeting platform to recruit the ESCRT complex and the membrane trafficking machinery to coordinate abscission (Agromayor and Martin-Serrano, 2013; Fededa and Gerlich, 2012; Schiel and Prekeris, 2013). Despite this general conviction, work in the *C. elegans* embryo has provided convincing evidence that depletion of MB microtubules does not prevent abscission, suggesting that the MBR is the key regulator of abscission dynamics (Green et al., 2013). Because cytokinesis occurs through a coordinated series of interdependent steps, problems at any step of this cascade may cause failure in cytokinesis, with several deleterious consequences such as polyploidy, which can lead to the increase in gene expression and cytoskeletal disorganization that are characteristic of many cancers or other pathologies (Ganem and pellman, 2007; Lacroix and Maddox, 2012).

During development of certain tissues however, the transient MBR is not severed through abscission but instead matures into a stable structure that persists for a long period of time, thus connecting the daughter cells in a syncytium (Haglund et al., 2011). Syncytial structures have been repeatedly described in different somatic tissues including human hepatocytes and *Drosophila* ovarian follicle cells (Airoldi et al., 2011; Clubb and Bishop, 1984; Gupta, 2000; Lacroix and Maddox, 2012), but perhaps the most studied syncytial tissues are the female and male germlines of a large number of animals (Amini et al., 2014; Dym and Fawcett, 1971; Fawcett et al., 1959; Haglund et al., 2011; Hime et al., 1996; Kloc et al., 2004; Ong and Tan, 2010; Pepling et al., 1999). Classically, germline syncytia have been proposed either to function in gametogenesis and gamete fertility, to provide the behavioral synchrony of interconnected cells at critical stages during development (e.g. synchronous sperm differentiation) or to mediate nutrient or signal sharing among the connected germ cells (GCs) that have different ploidies (Greenbaum et al., 2006; Haglund et al., 2011; Hime et al., 1996; Robinson and Cooley, 1996).

Despite the general occurrence of germline syncytia and their important role in the propagation of various species, the mechanism by which persistent MBRs are formed is poorly characterized. One established model is that regulated failure at distinct stages of cytokinesis contributes to syncytiogenesis. A compelling example of this type of syncytium formation came from *in vivo* and biochemical evidence during mammalian spermatogenesis, wherein it has been shown that the enrichment of the GC-specific, ankyrin-kinase protein TEX14 in the ring canals of male mice prevents progression of abscission, and thereby generates a syncytium (Greenbaum et al., 2007; Greenbaum et al., 2006). Past work mainly on the *Drosophila* germline proposed a similar scenario, wherein distinct protein composition of the syncytium-forming cells could function to stabilize their MBRs and thereby protect them from abscission (Cooley, 1998; Fawcett et al., 1959; Haglund et al., 2011; Pepling et al., 1999). Despite this, how germline syncytia are formed is still not fully understood.

The syncytial *C. elegans* hermaphrodite gonad represents an experimentally accessible system to address mechanisms of syncytium formation *in vivo*. All GCs in the *C. elegans* gonad originate from a single embryonic germline precursor blastomere termed P_4 (Wang and Seydoux, 2013). During gastrulation, P_4 migrates to the interior of the embryo, wherein it divides symmetrically along the antero-posterior (AP) axis to give rise to the primordial germ cells (PGCs) Z_2 and Z_3 (Deppe et al., 1978; Sulston, 1983).

Eventually, Z_2 moves toward the dorsal side while Z_3 remains almost stationary until both PGCs are positioned perpendicular to the AP axis. Z_2 and Z_3 remain mitotically quiescent during embryogenesis and initiate proliferation after hatching, at the mid-L1 larval stage. The number of GCs drastically expands during larval development, eventually generating the ~1000 GCs in both gonad arms of the hermaphrodite adult. The germline of a hermaphrodite adult C. elegans is organized in two U-shaped gonad arms that form tubular epithelia, in which all GCs surround a central cytoplasm core, termed rachis. Each GC is connected to the rachis through a stable opening, here referred to as GC rachis ring. While GC rachis rings connect the apical side of GCs to the rachis in the center of the gonad, all GC nuclei are otherwise

confined within a plasma membrane that precludes a direct connection with each other. The molecular composition, formation and maintenance of GC rachis rings in *C. elegans* are not well defined.

To elucidate the mechanism of syncytium biogenesis, we monitored the division of germline founder cells in the *C. elegans* embryo. We found that while P_4 completes the first stage of cytokinesis known as cytoplasmic isolation, similar to its somatic neighbors, it fails to accomplish the subsequent abscission-dependent MBR release, which leads to maintenance of the MBR between its two daughter cells Z_2 and Z_3 throughout the rest of embryogenesis. Our further characterization of GC rachis rings throughout gonad development revealed that three known MB/MBR components, UNC-59, CYK-7 (a novel MBR component) and ZEN-4^{Mklp1} (a centralspindlin component) are enriched at GC rachis rings from the first larval stage, suggesting that the *C. elegans* GC rachis rings are derived from the MBRs that are stably formed during embryogenesis. This work offers new insight into the composition, organization, and mechanism of GC syncytium formation in *C. elegans*.

Results and Discussion:

Contractility regulators are properly recruited to the cleavage furrow of the P_4 blastomere during C. elegans embryogenesis

To ensure the faithful propagation of the genome, several distinct steps of cytokinesis must be spatiotemporally regulated. An important step among these is assembly of the actomyosin-based CR beneath the plasma membrane as failure in proper assembly of CR causes incomplete cytokinesis. To gain insight into molecular mechanism of germline syncytium formation in *C. elegans*, we first asked whether the syncytial *C. elegans* germline is formed through incomplete cytokinesis caused by defects in CR assembly during P_4 division. To address this question, we monitored localization of a set of contractility regulators during P_4 cytokinesis; myosin II heavy chain (NMY-2::GFP), canonical anillin (ANI-1::GFP) and a septin (UNC-59::GFP), all known components of both CR and MBR (Green et al., 2013,

Singh and Pohl, 2014a). We observed that during anaphase, all 3 components were enriched at the cleavage furrow (Figure 3.2.1 A, B & C, white arrowheads), suggesting that CR assembly occurs properly upon P_4 division.

Assembly of CR does not guarantee a successful cytokinesis, as a non-functional or defective CR that is not capable of ingression could result in cytokinesis failure. To assess whether the P_4 possess a functional CR, we monitored ingression dynamics of CR in P_4 blastomere by tracking NMY-2::GFP during P_4 cytokinesis. We found that the CR diameter progressively narrowed during constriction (Figure 3.2.1 A, B & C, bottom rows in all panels), indicating that a functional CR is assembled at the cleavage furrow during P_4 division. Altogether, these results indicate that NMY-2, ANI-1 and UNC-59 are all properly localized to the division plane upon P_4 division and that the germline syncytium is not formed due to defects in CR assembly/formation or ingression.

Cytoplasmic isolation occurs during P_4 division

Cytokinesis of the *C. elegans* 1-cell embryo was previously shown to occur in two temporally different stages (Green et al., 2013). During the first stage known as cytoplasmic isolation, the cytokinetic ring ingresses and closes around the MB and eventually matures and transforms itself into another structure termed the MBR, thus precluding cytoplasmic exchange between the dividing daughter cells. During the second stage, septins and ESCRT proteins act on the plasma membrane and MBR at the cell-cell interface to severe the MBR, generating two physically separated daughter cells (Green et al., 2013).

To understand whether the syncytial architecture of *C. elegans* GCs is born out of incomplete cytokinesis, we asked if P_4 accomplishes the first stage of cytokinesis, cytoplasmic isolation followed by CR-to-MBR transition. In order to follow CR closure, we used embryos expressing NMY-2::GFP and developed an assay to measure CR diameter over time (Figure 3.2.2 B). Because somatic blastomeres undergo complete conventional cytokinesis (Green et

al., 2013), we first used them as control to document the division dynamics of randomly selected somatic cells (n=14) (Figure 3.2.2 A and 3.2.3 A). We observed that at the onset of ingression, the CR was 6.6 μm in diameter and that it typically constricted to a diameter of <0.4 μm on average in 8.3 minutes (Figure 3.2.2 D). The timing of somatic CR closure was highly variable and, on average, longer than the time reported previously for the 1-cell *C. elegans* embryo (4.6 minutes) (Green et al., 2013). This difference could be due to different imaging conditions, the different strains we used or innate developmental dissimilarities between the 1-cell stage embryo and later-stage somatic blastomeres, including their lineage as well as positioning in the embryo. Despite this discrepancy, we were able to define CR closure timing and MBR formation in somatic blastomeres using our assay.

We then used our assay to monitor dynamics of CR closure in the P_4 blastomere (Figure 3.2.2 C and 3.2.3 C) and observed that the initial diameter of the CR at furrow initiation was 5.4 μm and that it progressively narrowed until it reached <0.4 μm in diameter (n=7) (Figure 3.2.2 D), indicating that P_4 undergoes proper constriction with very similar kinetics to their somatic neighboring cells (Figure 3.2.2 D). The only difference is that the CR closure, after onset of furrowing, took slightly longer in P_4 than in the embryonic somatic blastomeres (Figure 3.2.3 C). Nevertheless, our data shows that P_4, similar to its somatic neighboring cells, possesses a functional CR that can contract until it eventually matures and converts itself into a MBR (Figure 3.2.3 D), showing that the syncytial structure of *C. elegans* GCs does not arise from defects in cytoplasmic isolation. In support of this, we previously found that there is no cytoplasmic exchange between Z_2 and Z_3 shortly after P_4 division, suggesting that the embryonic PGCs are not syncytial at least immediately after P_4 division (Amini et al., 2014).

The MBR is not released during P_4 cytokinesis

We showed that P_4 completes the first stage of cytokinesis, wherein the CR closure results in cytoplasmic isolation. Thus, we asked whether the second stage of cytokinesis, known as abscission, occurs properly in P_4. To this end, we performed time-lapse fluorescence

imaging and tracked the MBR during P_4 division by monitoring NMY-2::GFP, a stable MBR component (Green et al., 2013; Singh and Pohl, 2014a) (Figure 3.2.4). We then developed an assay based on location dynamics of NMY-2::GFP foci to examine the dynamics of membrane and MB/MBR shedding as readout of abscission. The assay relies on determining the position of the MBR over time, by measuring the distance between the fluorescence intensity peak of the membrane marker and NMY-2::GFP along a line positioned perpendicular to the MBR at the cell-cell border (Figure 3.2.4 B and C). To confirm that this assay accurately reflected on abscission, we first imaged MBR dynamics in somatic blastomeres, which are known to undergo complete abscission (Figure 3.2.4 B). Soon after CR closure and its maturation into MBR, the peaks of fluorescence intensity for both membrane and NMY-2::GFP overlap at the center (Figure 3.2.4 B, white arrow at 0' and Graph on top), consistent with the nascent MBR having not yet dissociated from the membrane between the dividing cells. The MBRs in somatic cells persisted at the cell-cell boundary on average 8.5 minutes after CR closure (n=10 embryos). We considered the MBR as released, when the distance between the intensity peaks of NMY-2::GFP and membrane marker was >0.4 μm (Figure 3.2.4 B, yellow arrowhead and graph in bottom) and found that the MBR was released in somatic cells on average 9 minutes after CR closure (Figure 3.2.4 D). The observation that the MBR is not released immediately upon CR closure is in agreement with previous studies showing that MBRs in P_0 cell (Green et al., 2013) as well as in somatic cells persist at the membrane between the dividing daughter cells in the early *C. elegans* embryo (Green et al., 2013; Singh and Pohl, 2014a).

We further tracked MBRs after their release from the membrane and monitored their path in somatic cells (Figure 3.2.5 A, white arrowhead). We found that in most cases (n=14/18 embryos), the MBR freely moved within the same cell before it disappeared. In others (n=2/18 embryos), the MBR moved within the same cell before it joined the CR of either the cell's granddaughter or a neighboring cell. In 2/18 embryos, a neighboring non-sister cell internalized the MBR. In addition, we also calculated the MBR lifetime after their release in somatic cells and found that the timing of MBR degradation is variable between cells (Figure 3.2.5 C). We also calculated the maximum distance between cell-cell interface and the post-

released MBR before its disappearance. Our results showed that the maximum distance that MBRs could travel from the cell-cell interface also varied from one cell to another (Figure 3.2.5 D) and that some MBRs could travel significantly longer distances after their release compared to others (Figure 3.2.5 D, red arrow). Altogether, our results show that we could detect the MBR release using our assay and that the timing of MBR release and degradation as well as the path traveled by MBRs after their release varies between cells. It has been shown that the MBR fate after abscission varies depending on cell type and that and instance the MBR release into a neighboring cell correlates with the cortical tension along the AP axis of the embryo (Singh and Pohl, 2014a). The observed variations in the timing of MBR release or behavior could thus be explained by local differences in the tension of neighboring cells. Overall, our results indicate that MBR release occurs in all somatic cells, on average 9.0 minutes after the completion of cytoplasmic isolation, and that their fate and trajectories are highly variable after they are released from the plasma membrane.

We then asked if MBR release occurs within the same time frame in P_4 as in its somatic counterparts. Strikingly, we observed that the MBR in P_4 was never released from the plasma membrane (Figure 3.2.4 C, white arrow and 3.2.4 D) during the time that somatic MBRs were typically discarded (Figure 3.2.4 B, yellow arrowhead). We found that the MBR, as were assessed by NMY-2::GFP, remained associated to the plasma membrane between the PGCs for at least 46 minutes, well above the typical 9 minutes required for the MBR release in somatic cells (Figure 3.2.5 B, white arrows). P_4 was previously shown to divide with a significant delay compared to its sister somatic blastomere, D (Harrell and Goldstein, 2011; Sulston, 1983), but this delay could not account for the prolonged association between the MBR and the plasma membrane. Similar MBR dynamics were obtained after imaging two other MBR components, UNC-59::GFP and ANI-1::GFP (data not shown). Altogether, we conclude that the last stage of cytokinesis, which consists in the ESCRT/Septin-dependent MBR release, does not occur in PGCs, suggesting that abscission and thus cytokinesis fails to complete during PGC division.

NMY-2 persists at the membrane between PGCs throughout embryogenesis

Persistence of NMY-2::GFP between Z_2 and Z_3 may reflect MBR stabilization. To understand if this is the case, we monitored PGCs for longer periods throughout the course of embryogenesis and measured the fate of the MBR, by measuring the kinetic profiles of NMY-2::GFP max fluorescence intensities upon CR closure (Figure 3.2.6 B and C). Our quantification revealed that the fluorescence intensity levels of NMY-2::GFP in PGCs remained high up to two hours after CR closure during different stages of embryonic development (Figure 3.2.6 C), suggesting that NMY-2 foci persisted as a coherent structure at the membrane between the two daughter cells throughout embryogenesis. During the migration of Z_2 toward the dorsal side of the embryo, the NMY-2::GFP focus (and thus presumably the MBR) underwent reorganization and, as such, was transformed from a spherical structure at the membrane boundary between the Z_2 and Z_3 cells to a bar-shaped structure that extended perpendicular to the cell-cell interface (Figure 3.2.6 B, yellow arrowhead). This indicates that the MBR of PGCs is dynamic despite being stably anchored between the two cells throughout embryogenesis. Altogether, our results indicate that while the MBR in somatic cells disappears soon after abscission, it remains stably associated to the cell-cell interface of PGCs long after the completion of mitosis. This observation further suggests that MBR stabilization in PGCs prevents them from undergoing complete abscission.

C. elegans GC rachis rings may be derived from the MBR of PGCs

Persistence of the MBR between PGCs throughout embryogenesis raised the possibility that its further maturation during either later embryonic stages or during the L1 stage could give rise to the GC rachis rings. As a step to assess this possibility, we asked whether the known CR/MBR components, namely UNC-59, CYK-7, ZEN-4 and RHO-1 (Green et al., 2013; Maddox et al., 2005b; Nguyen et al., 2000; Zhou et al., 2013) are found at GC rachis rings of newly-hatched L1 larvae. Using a live-imaging assay that we have previously developed to visualize GC rachis ring openings (Amini et al., 2014), we observed that GFP::UNC-59, GFP::CYK-7, GFP::RHO-1 (Figures 3.2.7 A-C, top panels), mCherry::ZEN-4, CYK-4::GFP and ECT-2::GFP (data not shown) are enriched between Z_2

and Z_3 upon hatching of the L1 larva. Because the L1 larva hatches on average 7 hours after the division of P_4 into Z_2 and Z_3, this result further supports the notion that the MBR anchored between the two PGCs is stable.

We then asked whether these MBR components remain stably associated to GC rachis rings at later stages of development. We observed that GFP::UNC-59, GFP::CYK-7 and GFP::RHO-1 remain enriched at GC rachis rings throughout larval development and in adult hermaphrodites (Figure 3.2.7 A-C). In addition, mCherry::ZEN-4 is also localized to GC rachis rings throughout gonad development (3.2.8 A in L-L3 animals and data not shown). This is in agreement with our previous finding that three other CR/MBR components, GFP::ANI-2, GFP::ANI-1 and NMY-2::GFP, are enriched at GC rachis rings at all stages of animal development (Amini et al., 2014). However, the localization pattern of these seven regulators in GCs was dissimilar. CYK-7 and ZEN-4 localized in a pattern very similar to that of the *bona fide* GC rachis ring components ANI-1 and ANI-2 (Amini et al., 2014) (Figure 3.2.7 B and Figure 3.2.8 A). While, UNC-59 was also found at the basal and lateral membranes of GCs (yellow arrowheads, Figure 3.2.7 A), in a pattern similar to that of NMY-2. This suggests that ANI-1, ANI-2, CYK-7 and ZEN-4 may specifically function at GC rachis rings, while UNC-59 and NMY-2 have additional functions in other cortical compartments. Interestingly, both RHO-1 (Figure 3.2.7 C) and its GEF ECT-2 (data not shown) were equally present at GC rachis rings and at basal and lateral GC cortices at all stages of development. These results indicate that all known CR/MBR components are found at GC rachis rings throughout hermaphrodite development, supporting the notion that the GC rachis rings are stable structures that are derived from the CR/MBRs. Consistent with this, the presence of the CR/MBR components has also been observed in somatic and germline syncytial ring canals in *Drosophila*, and this has been proposed to contribute to syncytium formation (Airoldi et al., 2011; Haglund et al., 2011).

Altogether, our findings support a model (Figure 3.2.9 D) in which GC rachis rings are derived from a stable MBR that is formed via incomplete cytokinesis upon P_4 division, during

embryogenesis. While P_4 initiates cytokinesis similar to somatic cells, it fails to complete abscission, leaving a stable MBR between Z_2 and Z_3 instead of releasing and degrading it. This MBR persists between PGCs and undergoes a dynamic reorganization later during embryogenesis that successively transforms it into a bar-like structure and a ring-like structure by the L1 stage. This would effectively allow the PGCs to remain interconnected throughout embryogenesis, perhaps initiating syncytium formation. As all GCs contain a rachis ring, a corollary of this model posits that the stable MBR that is formed during embryogenesis duplicates and that each duplicated structure is inherited by one PGC.

Stabilized MBRs are conserved features of germline syncytia in other animals and have previously been proposed to promote syncytium formation (Haglund et al., 2011). Past efforts, mainly concentrated on the *Drosophila* germline, proposed that stabilization of the MBRs transform them into ring canals that interconnect GCs, thus forming a syncytium (Cooley, 1998; Fawcett et al., 1959; Haglund et al., 2011; Hime et al., 1996; Pepling et al., 1999). In addition, it has been shown that maintenance and stabilization of the MBR is key to prevent completion of cytokinesis in *Drosophila* follicular cells (Airoldi et al., 2011), suggesting that MBR stabilization and incomplete cytokinesis could be an evolutionary conserved feature for syncytium formation. In this regard, the PGCs of the *C. elegans* embryo more closely resemble what has been observed in other germline (Haglund et al., 2011) or somatic (Airoldi et al., 2011) syncytia. Thus it could be possible that NMY-2 persistence and thereby MBR stabilization functions as a nucleating factor for syncytium formation during *C. elegans* embryogenesis.

Materials and Methods:

C. elegans Strains and Culture

All strains were maintained at 20°C according to standard protocols as described by Brenner (1974) (Brenner, 1974) and are listed in Table 4.1.

Worm Mounting

Time-lapse imaging of embryos: Embryos were obtained after cutting open gravid hermaphrodites in 6-8 μl of egg buffer with two 25-gauge needles. Using mouth pipet, embryos were then mounted on a 3% agarose pad and covering them with a 0.1% poly-L-lysine coated coverslip. The chamber was backfilled with egg buffer and sealed using either Vaseline or VaLaP (1:1:1 Vaseline, lanolin, and paraffin).

Fluorescence imaging of germlines: Synchronized animals of a desired developmental stage were anaesthetized in 0.04% tetramisole (Sigma) in M9 buffer and transferred to a 3% agarose pad and covering them with a 0.1% poly-L-lysine coated coverslip. The chamber was backfilled with M9 buffer containing 0.04% tetramisole and sealed using either Vaseline or VaLaP (1:1:1 Vaseline, lanolin, and paraffin).

Fluorescence live imaging of embryos

Images were acquired with a spinning disk confocal microscope system. A 63×/1.4 NA Plan Apochromat oil objective with 2 × 2 binning was used to acquire the images. More detailed settings of imaging is listed below: to visualize PGC behavior, 20 confocal sections (separated by 1 μm) were captures every 5 min. For monitoring PGC cytokinesis (Figure 3.2.3), timing of MBR release (Figure 3.2.5) and MBR trajectory after release, 15-20 confocal sections (separated by 0.5 μm) were captures every 35 sec. To track MBRs in PGCs during later stages of embryogenesis, 19 confocal sections (separated by 0.5 μm) were filmed every 10 minutes for 2-3 hrs.

Analysis of CR closure timing

Using ImageJ, we draw a 3-pixel width line along the cleavage furrow and obtained the fluorescence intensity profile of both membrane and NMY-2::GFP along the line in 3 consecutive Zs in the middle (Figure 3.2.2). All measurements were then done on max projection images of these Zs. The CR diameter was assessed by measuring the distance between the two distinct fluorescence intensity peaks of each marker during embryogenesis. We considered the first time point wherein we observed CR furrowing as our t0 or "furrow ingression onset". The CR was considered as closed when the distance between the two peaks was >0.4 μm (Figure 3.2.2). Analysis of CR diameter overtime was carried out in Excel.

Analyses of MBR release timing and MBR trajectory after release

We draw a line (width 3 pixels), using ImageJ, we draw a line perpendicular to the MBR at the cell-cell border along the cleavage furrow and obtained the fluorescence intensity profile of both membrane and NMY-2::GFP along that line in 3 consecutive Zs in the middle (Figure 3.2.4 B and C). All measurements were then done on max projection images of these Zs. CR closure was assigned as t0. The MBR was considered as released when it was positioned more than 0.4 μm away from the cell-cell interface. Analyses of MBR release timing and MBR trajectory after abscission were carried out in Excel.

MBR SUM and Max fluorescence intensity measurements

Fluorescence intensities were measured by defining a small square region of interest in ImageJ around the MBR. MBR signals were background subtracted using another square with the same dimensions (Figure 3.2.6).

Fluorescence live imaging of germlines and GC ring diameter analysis

To visualize GC ring components, a swept field microscope was used. The 35-μm slit and 60×/1.4 NA or 100×/1.4 NA objectives were used to acquire confocal sections (separated by 0.5 μm) spanning the entire rachis as described previously (Amini et al., 2014). To monitor rachis bridges, six consecutive confocal sections were analyzed independently using ImageJ, by measuring fluorescence intensity of expressed fluorescent markers along a 3-pixel-thick

line drawn along the lateral and apical cortex, as described previously (Amini et al., 2014).

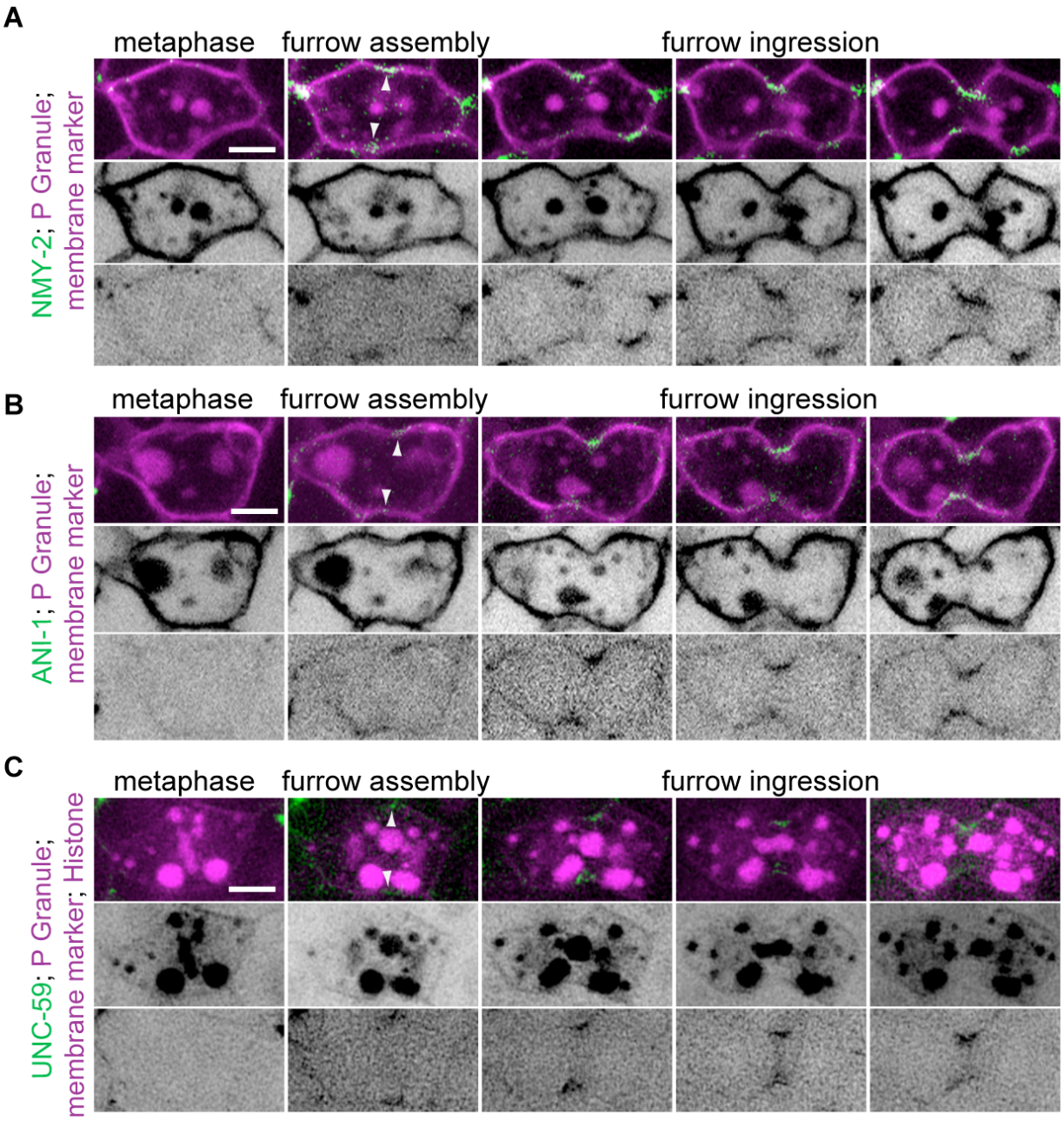

Figure 3.2.1.

Figure 3.2.1: Contractility regulators are assembled properly to the division plane of PGC division in the *C. elegans* embryo.

Time-lapse montage of the division plane from confocal images of wild-type embryo

expressing membrane marker (magenta) and PGL-1, a germ cell marker (magenta) and three known contractility regulators: **(A)** NMY-2::GF (green) **(B)** ANI-1::GFP and **(C)** UNC-59::GFP and histone. For each panel the merge is shown on top, the membrane in the middle and the contractility regulators in the bottom. All three contractility components are assembled properly to the cleavage furrow (arrowheads) and are capable of furrowing.

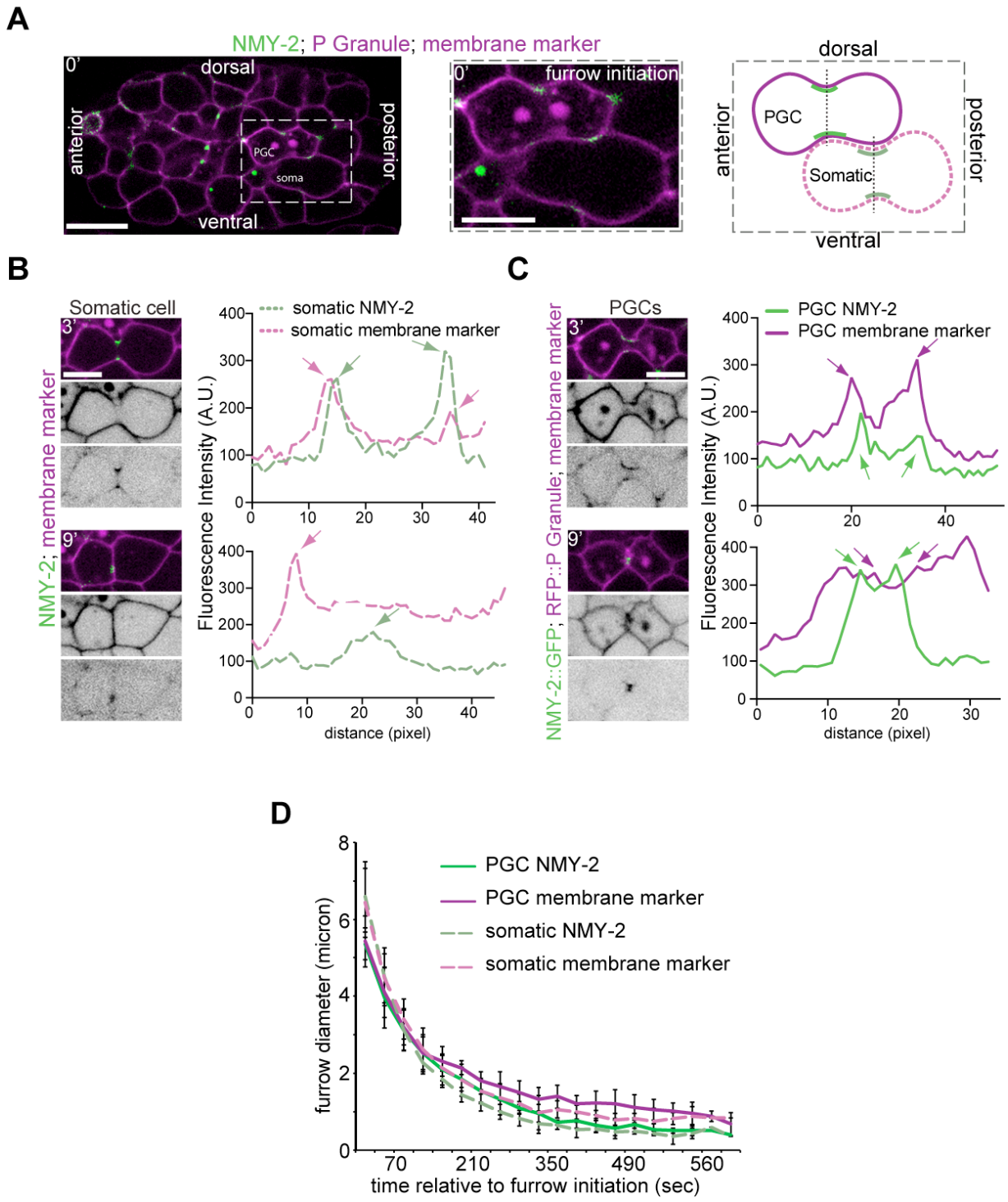
A
NMY-2; P Granule; membrane marker
0'
dorsal
anterior
posterior
PGC
soma
ventral
0'
furrow initiation
dorsal
PGC
anterior
posterior
Somatic
ventral
B
Somatic cell
NMY-2; membrane marker
3'
9'
somatic NMY-2
somatic membrane marker
Fluorescence Intensity (A.U.)
distance (pixel)
C
PGCs
NMY-2::GFP; RFP::P Granule; membrane marker
PGC NMY-2
PGC membrane marker
Fluorescence Intensity (A.U.)
distance (pixel)
D
PGC NMY-2
PGC membrane marker
somatic NMY-2
somatic membrane marker
furrow diameter (micron)
time relative to furrow initiation (sec)

Figure 3.2.2.

Figure 3.2.2: Assay to quantify CR diameter upon furrow initiation.

(A) Mid-section confocal images of wild-type embryo expressing NMY-2::GFP (green) and membrane marker (magenta) and PGL-1, a germ cell marker (magenta). The region delineated by the white dashed square is magnified in inset (scale bar for insets, 5 μm) and shows a somatic cell and PGC during CR closure (middle). Schematic illustrates the method for monitoring diameter of CR overtime, which was determined and compared by line scans (gray dotted lines) draw perpendicularly on the division plane of both somatic and PGC. **(B)** A somatic cell shown in (A) at different time points. Measured fluorescence intensities (in arbitrary units specific to each curve) for each time point is shown next to it. Light purple and magenta arrows point to peaks of membrane marker in somatic and. Light green and green arrows point to peaks of NMY-2::GFP intensities in somatic and PGCs respectively. CR was considered as closed when the distance between the NMY-2 peak and membrane peak was more than 0.4 micron. **(C)** Graph showing the kinetics of CR closure in somatic (n= 14 embryos) and PGCs (n= 7 embryos). Error bars= standard deviation.

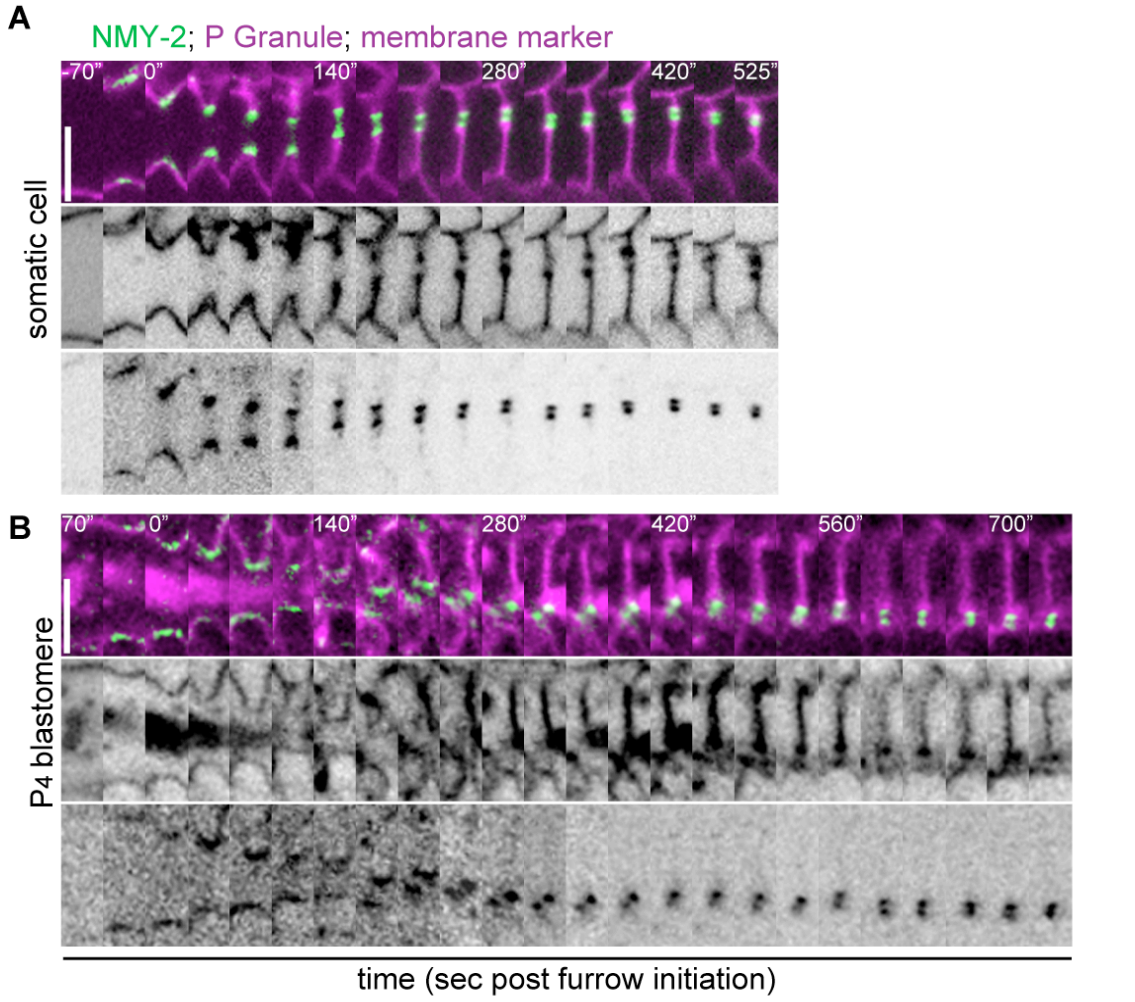
A
NMY-2; P Granule; membrane marker
-70"
0"
140"
280"
420"
525"
somatic cell
B
-70"
0"
140"
280"
420"
560"
700"
P4 blastomere
time (sec post furrow initiation)
C
ns
p= 0.087
time to reach cytoplasmic isolation (min)
15
10
5
0
somatic cells
P4
D
CR-to-MBR maturation in soma and P4
furrow ingression
CR-MBR transition
nascent MBR
plasma membrane, CR, MBR

Figure 3.2.3.

Figure 3.2.3: Cytoplasmic isolation occurs during PGC division in the *C. elegans* embryo.

Time-lapse montage of the division plane from confocal images of wild-type embryo expressing NMY-2::GFP (green) and membrane marker and PGL-1, a germ cell marker (magenta) **(A)** a somatic cell and **(B)** a PGC. **(C)** Graph showing that CR closure occurs with a slight delay in PGCs. Data was compared using a student ttest (^{ns} p=0.87). **(D)** Schematic showing that in PGCs similar to somatic cells, CR closes and undergoes maturation to transform into MBR in the embryo.

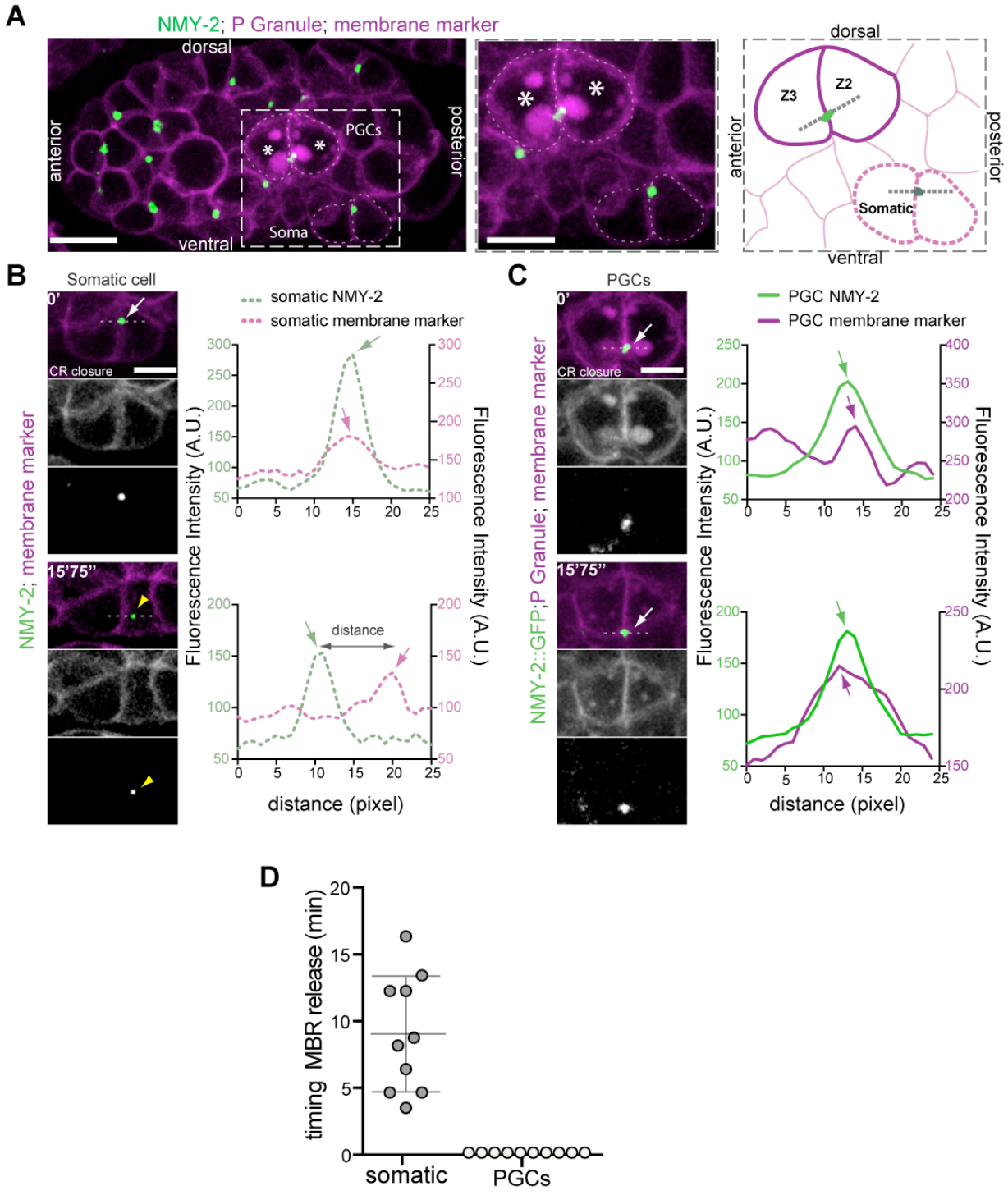
A
NMY-2; P Granule; membrane marker
dorsal
anterior
posterior
ventral
PGCs
Soma
dorsal
Z3
Z2
anterior
posterior
Somatic
ventral
B
Somatic cell
0'
CR closure
15'75"
NMY-2; membrane marker
somatic NMY-2
somatic membrane marker
Fluorescence Intensity (A.U.)
distance
distance (pixel)
C
PGCs
PGC NMY-2
PGC membrane marker
NMY-2::GFP;P Granule; membrane marker
D
timing MBR release (min)
somatic
PGCs

Figure 3.2.4

Figure 3.2.4: MBR of PGCs is not released.

Mid-section confocal images of wild-type embryo expressing NMY-2::GFP (green) and membrane marker (magenta) and PGL-1, a germ cell marker (magenta) (left). The region delineated by the white dashed square is magnified in inset (scale bar for insets, 5 μm) and shows a somatic cell and PGC during CR closure (middle). Stars point to Z_2 and Z_3. Schematic illustrates the method for monitoring the MB release, which was determined and compared by line scans (gray dotted lines) (right). **(B and C)** Central plane confocal images of **(B)** a somatic cell and **(C)** a PGC shown in (A) at different time points. Measured fluorescence intensities (in arbitrary units specific to each curve) for each time point is shown next to it. Light purple and magenta arrows point to peaks of membrane marker in somatic and PGCs respectively. Light green and green arrows point to peaks of NMY-2::GFP intensities in somatic and PGCs respectively. MBR was considered as released when the distance between the NMY-2 peak and membrane peak was more than 0.4 micron. NMY-2::GFP and membrane peaked at the same position at t0 (CR closure) in somatic cells and during both time points in PGCs. White arrows point to MBR at the cell-cell boundary. Yellow arrowhead points to a released MBR. **(D)** Graph showing MBR release timing in somatic cells vs. PGCs.

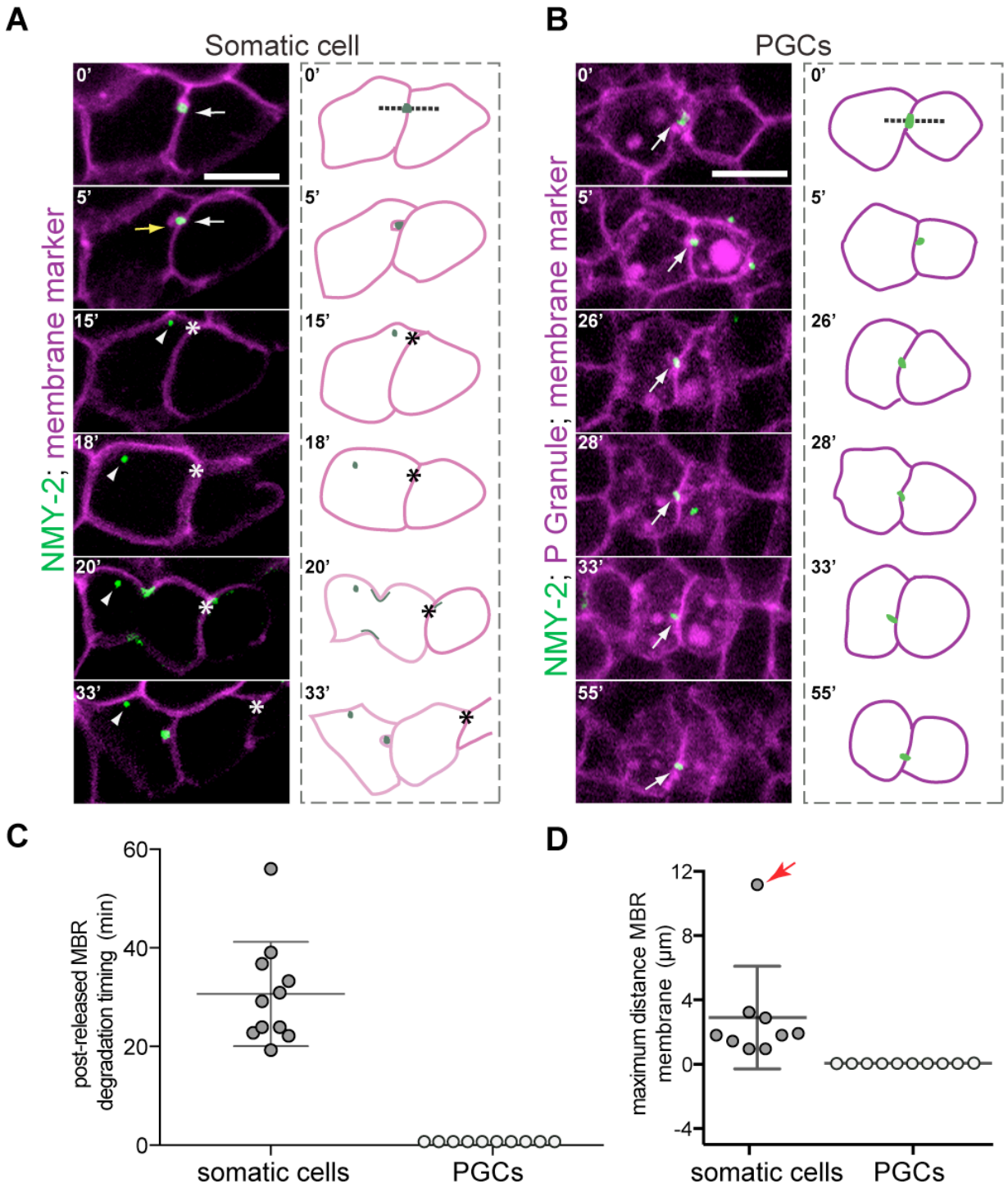
A
Somatic cell
NMY-2; membrane marker
0'
5'
15'
18'
20'
33'
B
PGCs
NMY-2; P Granule; membrane marker
0'
5'
26'
28'
33'
55'
C
post-released MBR degradation timing (min)
60
40
20
0
somatic cells
PGCs
D
maximum distance MBR membrane (µm)
12
8
4
0
-4
somatic cells
PGCs

Figure 3.2.5.

Figure 3.2.5: MBR trajectory in soma *vs.* PGCs.

Mid-section confocal sequential frames of wild-type embryos expressing NMY-2::GFP (green) and membrane marker (magenta) and PGL-1, a germ cell marker (magenta) in **(A)** a somatic cell and **(B)** PGCs. The representing illustrations are next to each image. The gray dotted line shows the position wherein the intensity profile of membrane and NMY-2::GFP was measured. The white arrow points to the embedded MB in the cortex. The yellow arrow points to membrane shedding in somatic cell. The white arrowheads point to the MBR upon release at sequential frames and the white star points to the membrane from which MBR was released. **(C)** The graph shows the distance between the MBR and cortex as was measured from a line intensity profile plotted along the MBR on the side that is about to break over time in somatic cells (n= 8 embryos). The red dotted line represents dynamics of MBR path upon release of the cell shown in A. **(D)** Graph shows the maximum distance (micron) that somatic MBR travels after being released from the membrane. The red arrow represents the maximum distance travelled by the cell shown in (A). MBR in PGCs is never released.

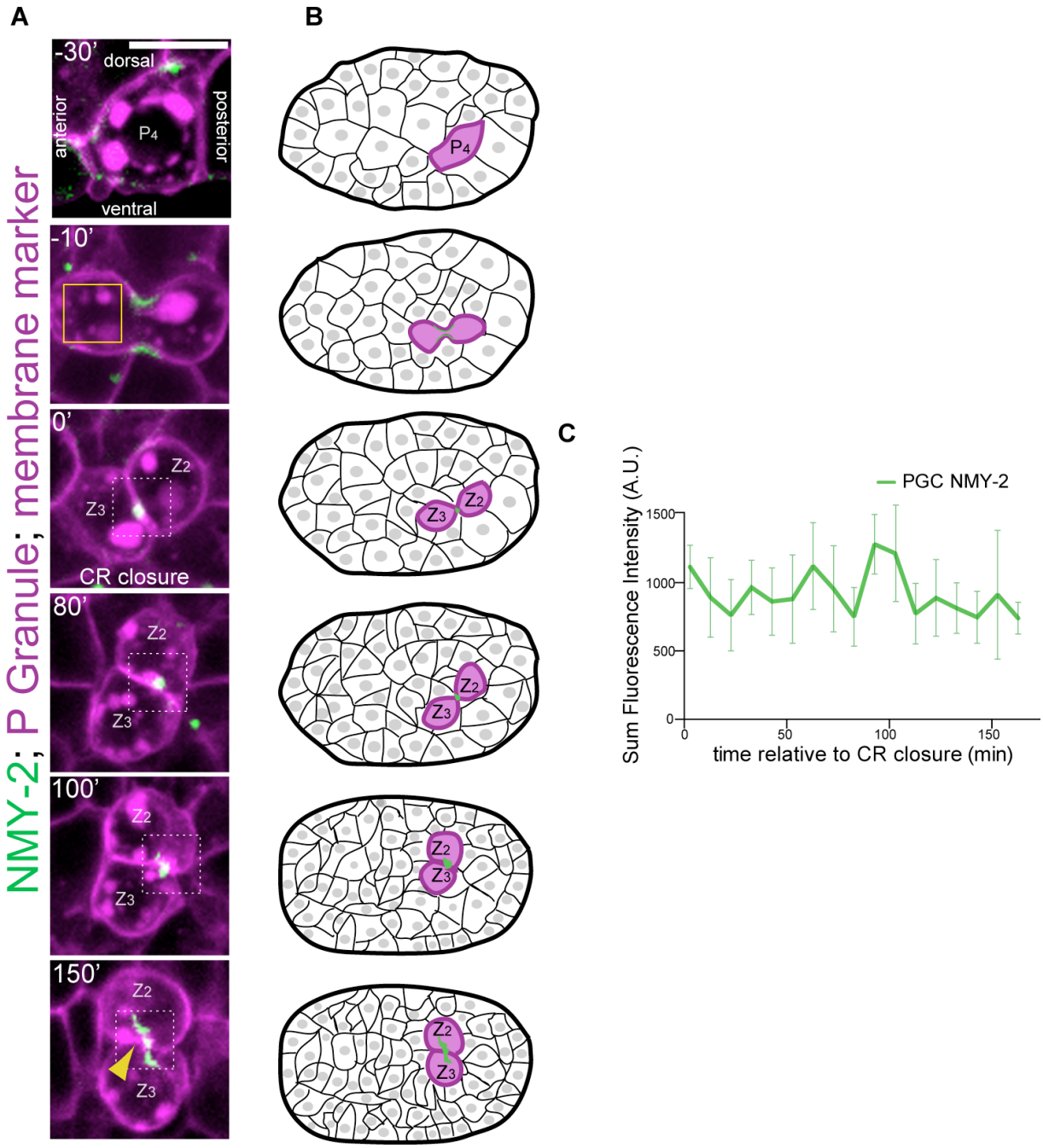
A
B
C
NMY-2; P Granule; membrane marker
-30'
dorsal
anterior
posterior
ventral
P4
-10'
0'
Z2
Z3
CR closure
80'
100'
150'
PGC NMY-2
Sum Fluorescence Intensity (A.U.)
1500
1000
500
0
50
100
150
time relative to CR closure (min)

Figure 3.2.6.

Figure 3.2.6: MB/MBR is stabilized in PGCs.

(A) Schematic representing the PGC behavior dynamics during *C. elegans* embryogenesis. P_4 undergoes division and generate Z_2 at the posterior and Z_3 at the anterior. Z_2 undergoes a 90° rotation toward the dorsal side of the embryo and thus the PGCs become perpendicular to the antero-posterior axis. **(B)** Mid-section confocal sequential frames of wild-type PGCs expressing NMY-2::GFP; RFP::P Granule; membrane marker. The dotted yellow square points the position wherein the max intensity profile of NMY-2::GFP were measured. The yellow square points to a region with the same size in the cytoplasm as background. These values were then subtracted from NMY-2::GFP Max intensities. The yellow arrows point to MBR when it undergoes structural reorganization **(C)** Graph shows the max fluorescence intensity of the NMY-2::GFP in PGCs does not decrease upon CR closure.

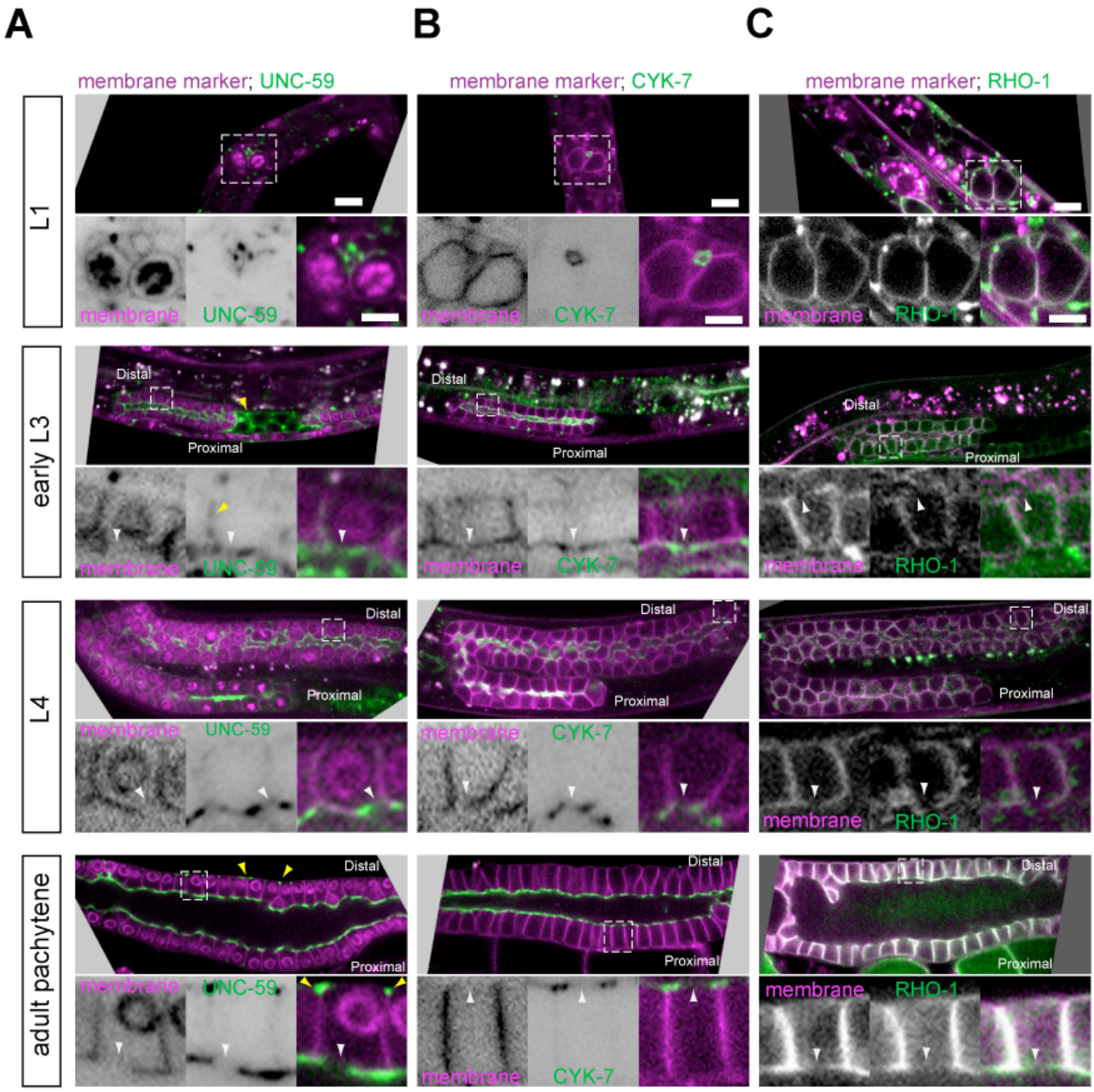
A
B
C
membrane marker; UNC-59
membrane marker; CYK-7
membrane marker; RHO-1
L1
early L3
L4
adult pachytene
membrane
UNC-59
CYK-7
RHO-1
Distal
Proximal

Figure 3.2.7.

Figure 3.2.7: Cytoskeletal proteins are enriched at GC rachis rings throughout larval development.

(A-C) Mid-section confocal images of the germline of wild-type hermaphrodites expressing **(A)** GFP::UNC-59 and a membrane marker (magenta), **(B)** GFP::CYK-7 and a membrane marker (magenta) and **(C)** GFP::RHO-1, membrane marker (magenta). The regions delineated by the white dashed squares are magnified in inset (scale bar for insets, 5 μm). White arrowheads point to GC bridge openings membranes. Yellow arrowheads in A point to non-GC bridge GFP::UNC-59 to lateral membrane in E-L3, to somatic gonad in L-L3 and to basal membrane in adults. For simplicity, only one gonad arm is shown from the L3 stage onward. In all frames, anterior is to the left. Scale bar, μm.

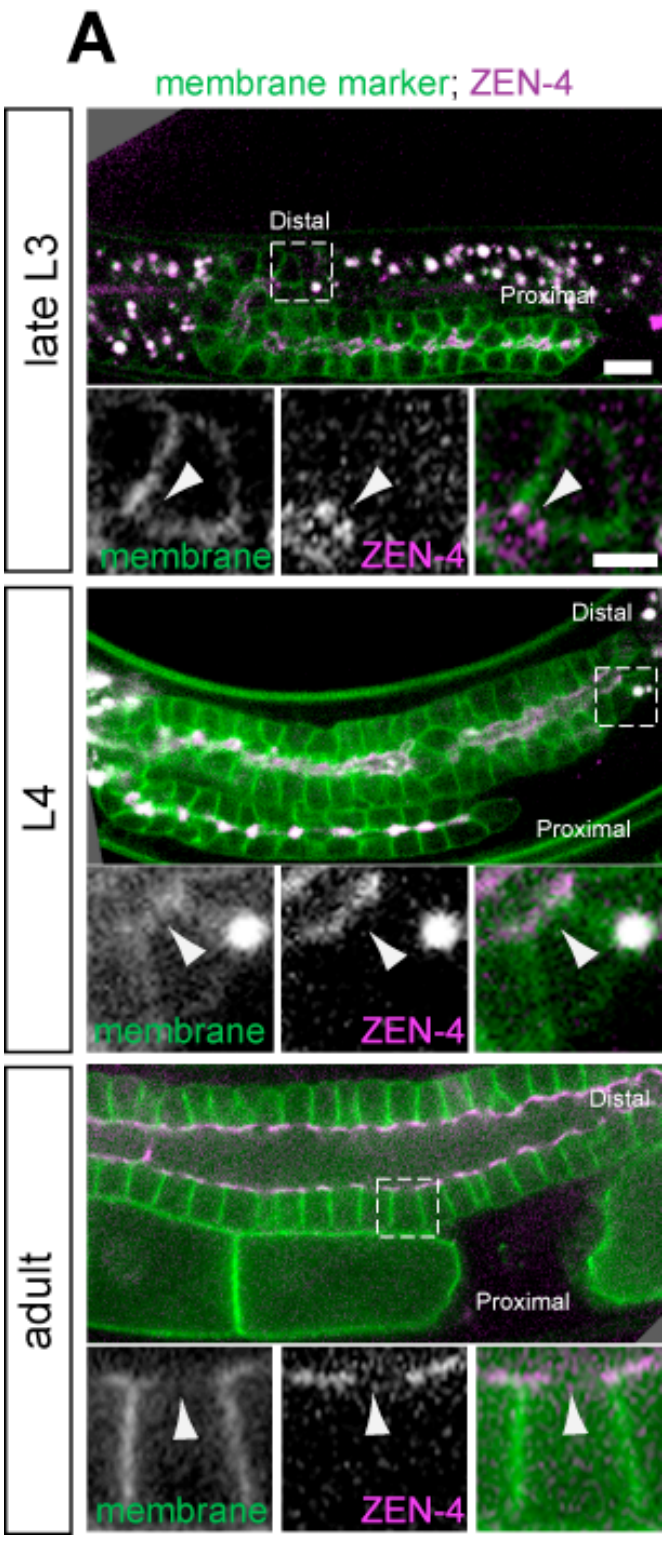
A
membrane marker; ZEN-4
late L3
Distal
Proximal
membrane
ZEN-4
L4
Distal
Proximal
membrane
ZEN-4
adult
Distal
Proximal
membrane
ZEN-4

Figure 3.2.8.

Figure 3.2.8: Centralspindlin protein ZEN-4 is enriched at GC rachis rings throughout larval development.

Mid-section confocal images of the germline of wild-type of late-L3, L4 and Adult hermaphrodites expressing mCherry::ZEN-4 (Mklp-1) (magenta) and a membrane marker (green). ZEN-4 is a *bona fide* GC rachis ring marker, wherein it remains enriched throughout germline development.

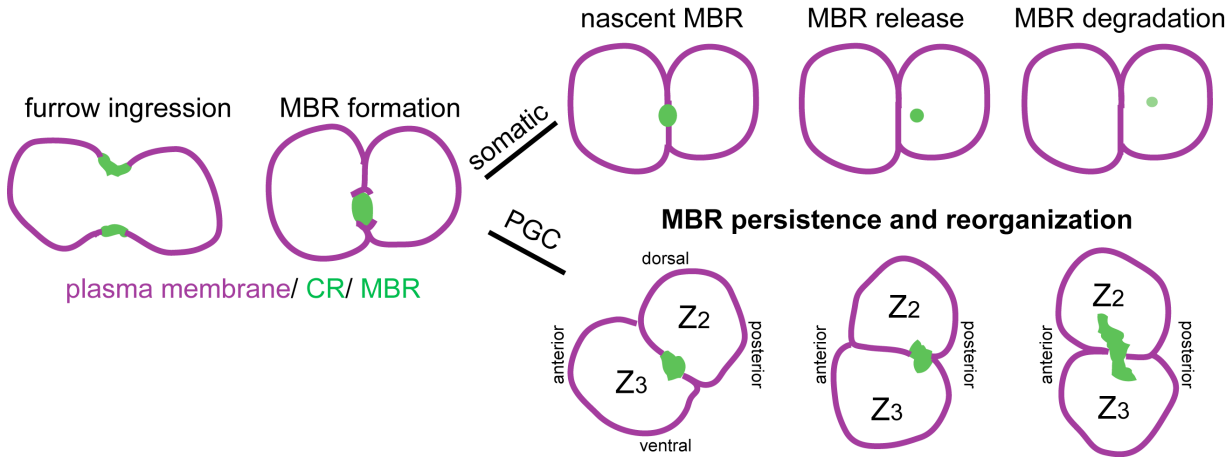

Figure 3.2.9.

Figure 3.2.9: A model for germline syncytium nucleation during PGC division in the *C. elegans* embryo.

The initial steps of cytokinesis, the CR assembly, CR constriction, CR closure and MBR formation occur properly in PGCs. However, the MBR of PGCs remain stably associated to the membrane between the two dividing daughter cells. While, the MBRs are released in somatic blastomeres, they undergo reorganization at the boundary between Z_2 and Z_3, wherein they remain enriched for the rest of animals life.

Strain #	Genotype
N2	Wild-type Bristol strain
OD297	*OD56 (mCherry::histone H2B);unc-119(ed3) III; ltIs20 [pASM10; pie-1/GFP::unc-59; unc-119 (+)]ltIs44 [pAA173; pie-1/mCherry::PH(PLC1delta1); unc-119(+)*
OD449	*unc-119(ed3) III; ltIs44 [pAA173; pie-1/mCherry::PH(PLC1delta1); unc-119 (+)]; ltIs154 [pOD539(pBG3); pie-1::C08C3.4::GFP; unc-119 (+)]*
OD1268	*unc-119(ed3) III; HzIs169 [pie-1/mCherry:ZEN-4; unc-119 (+)] ; ltIs38 [pAA1; pie- 1/GFP::PH(PLC1delta1); unc-119 (+)]*
UM319	*unc-119(ed3) III; tjIs1 [pie-1::GFP::rho-1 + unc-119(+)] ; ltIs44 [pAA173; pie-1/mCherry::PH(PLC1delta1); unc-119 (+)]*
UM405	*(mCherry::histone H2B);unc-119(ed3) III; ltIs20 [pASM10; pie-1/GFP::unc-59;unc-119 (+)]ltIs44 [pAA173; pie-1/mCherry::PH(PLC1 delta1); zuls244 [nmy-2::PGL-1::mRFP-1];unc-119 (ed3)*
UM456	*unc-119(ed3) III; ltIs86 [pASM65; pie-1::ANI-1 (fl cDNA)::GFP; unc-119 (+)]; cpSi20[Pmex-5::TAGRFPT::PH::tbb-2 3'UTR + unc-119 (+)] I; unc-119(ed3) III; zuls244 [nmy-2::PGL-1::mRFP-1];unc-119 (ed3)*
UM458	*cp13[nmy-2::gfp + LoxP]) I; cpSi20[Pmex-5::TAGRFPT::PH::tbb-2 3'UTR + unc-119 (+)] I; unc-119(ed3) III; zuls244 [nmy-2::PGL-1::mRFP-1];unc-119(ed3)*

Table 3.2.1: *C. elegans* strains used in this study

4. DISCUSSION

Over a century after their discovery, syncytial tissues still remain intriguing to scientists and we are only just beginning to understand the mechanisms involved in syncytia formation and their function and, as such, many important questions remain to be answered. Most attempts to characterize formation and maintenance of syncytial tissues have been performed predominantly in the *Drosophila* germline and occasionally in mammalian germline. While these studies had success in understanding the molecular composition of these fascinating structures and some insight into their formation and function, they are unlikely to reflect the physiological and developmental significance of all syncytial tissues and their exact mode of formation as well as their maintenance strategies. Our current study reveals additional biological insight into the exciting new paradigm of syncytiogenesis, from nucleation to maturation, and provides evidence for an alternative function for this type of tissue architecture, apart from more traditional roles that are currently associated with syncytia. In addition, studying how syncytia are formed and maintained provides a unique opportunity to better understand altered outcome of cytokinesis in multiple contexts, which could significantly contribute to a better understanding of the cytokinesis itself. I start the discussion by a published commentary, wherein we have previously discussed the results from *Article 1* (see *Section 4.1.*). Then I will discuss mechanism of syncytium nucleation/formation (see *Section 4.2.*), ANI-2 potential role in syncytiogenesis (*Section 4.3.*), how GC rachis rings remain open or close (*Section 4.4.*), role of the somatic gonad (*Section 4.5.*) followed by a discussion on 4.6. On the functional significance of syncytial tissues (*Section 4.6.*).

4.1. Syncytium biogenesis: Its all about maintaining good connections

Rana Amini [1], Nicolas T. Chartier [2], Jean-Claude Labbé [1,3]

Published in *Worm*, 2015 4:1, e992665, DOI: 10.4161/21624054.2014.992665

[1] Institute of Research in Immunology and Cancer, and [3] Department of Pathology and Cell Biology, Université de Montréal, Montréal, QC, H3C 3J7, Canada.[2] Biotechnology Center, Dresden University of Technology, Dresden, Germany.

Dr. N.T.C. and I wrote the first draft of the manuscript together.

Corresponding authors: Nicolas Chartier and Jean-Claude Labbé

Keywords: Cytokinesis, Anillin, Syncytiogenesis, Germline development

Abstract

At the end of mitosis, cells typically complete their division with cytokinesis. In certain tissues however, incomplete cytokinesis can give rise to cells that remain connected by intercellular bridges, thus forming a syncytium. Examples include the germline of many species, from fruitfly to humans, yet the mechanisms regulating syncytial formation and maintenance is unclear, and the biological relevance of syncytial organization remains largely speculative. To better understand these processes, we recently used the germline of *Caenorhabditis elegans* as a model for syncytium development. Analysis of the germline syncytial architecture throughout development revealed that it arises progressively during larval growth and that it relies on the activity of 2 actomyosin scaffold proteins of the Anillin family. Our work also showed that the gonad can sustain elastic deformation when under mechanical stress and that this property may be conferred by the malleability of syncytial openings. We suggest that elasticity and resistance to mechanical stress constitutes a general property of syncytial tissues.

Introduction

Healthy mammalian cells are typically mononucleated and physically separate their duplicated DNA and cytoplasmic content into the 2 daughter cells after mitosis. This step, termed cytokinesis, depends on the synchronized activities of cell cycle regulators, microtubules and the cortical actin cytoskeleton to build and localize an equatorial actomyosin contractile ring, the cytokinetic ring. Ingression of the cytokinetic ring between the 2 segregated sets of chromosomes allows the separation of the daughter cells. In some cases however, cells do not complete cytokinesis and thus form a syncytium, as in germ cells in many species and some physiologically polyploid cells such as mammalian hepatocytes (Haglund et al., 2011; Margall-Ducos et al., 2007). Impaired cytokinesis and polyploidy are also often observed in cancer cells where they are thought to favor genetic instability (Davoli and de Lange, 2012; Fujiwara et al., 2005; Ganem and Pellman, 2007). One important challenge in cell biology is to understand the physiological mechanisms by which some animal cells undergo controlled incomplete cytokinesis without deleterious consequences such as aneuploidy. Here we discuss our recent findings on syncytial organization using the Caenorhabditis elegans gonad as a model (Amini et al., 2014). Our work revealed the importance of balancing the activities of 2 proteins of the Anillin- family of actin scaffold proteins to stabilize contractile rings in an open form and suggested a novel interesting role in the resistance of syncytial structures to mechanical stress.

The C. elegans Gonad as a Model for Syncytium Formation and Organization

During development of the *C. elegans* embryo, the unique germline precursor blastomere, termed P_4, divides at approximately the 100 cells stage to give birth to the 2 primordial germ cells (GCs) Z_2 and Z_3. These cells remain mitotically quiescent until the mid-L1 larval stage, when they start to proliferate. GC mitotic proliferation is sustained throughout larval development until animals complete the last larval stage, when GCs initiate meiosis and gametogenesis. The germline of an adult *C. elegans* hermaphrodite consists of more than 1000 nuclei organized in 2 gonad arms that form tubular syncytia, in which all GCs surround a

central cytoplasm core, termed rachis. Each GC is connected to the rachis through a stable opening, referred to as rachis bridge that is stabilized by a ring (Figure 4.1.1). As is the case for other syncytia, rachis bridge rings are enriched in the actomyosin regulators that are typically involved in cytokinetic ring formation and ingression such as the non-muscle myosin NMY-2, the 2 Anillin proteins ANI-1 and ANI-2, and the centralspindlin complex components CYK-4 and ZEN-4 (Amini et al., 2014; Maddox et al., 2005; Zhou et al., 2013). Interestingly, depletion of some of these proteins and other regulators of actomyosin contractility results in severe disorganization of gonad architecture, such as absence of GC partitions and multinucleation (Green et al., 2011). This suggests parallels in the organization of stable rachis bridge rings and cytokinetic rings.

Our recent work in *C. elegans* revealed that the Anillin proteins ANI-1 and ANI- 2 participate in cytokinesis of somatic blastomeres and biogenesis of the germ- line syncytium (Amini et al., 2014; Chartier et al., 2011). The nematode protein ANI-1 possesses all the motifs of *Drosophila* and mammalian Anillin and could, in principle, bind actin, myosin and all the other regulators mentioned above; it is thus considered as the *C. elegans* canonical Anillin. ANI-2 is a shorter Anillin isoform that lacks the N-terminal domains predicted to bind actin and myosin, but still possesses the C-terminal domains predicted to interact with RhoA, CYK-4, ECT-2, microtubules and septins. While ANI-1 is localized at the cytokinetic ring of all somatic cells and is required for proper asymmetric cytokinetic ring ingression, ANI-2 is mainly enriched at rachis bridges and its levels are minimal in embryonic somatic blastomeres (Figure 4.1.1) (Amini et al., 2014; Maddox et al., 2005). This led us to investigate in more details the role of ANI-2 in the development of the syncytial germline.

Syncytium Biogenesis: From Nucleation to Maturation

During cytokinesis, dividing cells typically form a transient intercellular bridge, known as the midbody, that gets pinched off during cellular abscission. In cells undergoing incomplete cytokinesis however, abscission does not complete and the midbody matures into a

stable bridge interconnecting the 2 daughter cells (Greenbaum et al., 2007). The spatiotemporal analysis of ANI-2 localization during *C. elegans* embryonic development revealed that it is undetectable in early blastomeres and becomes enriched specifically in the P_4 germline blastomere. Interestingly, upon division of P_4, ANI-2 accumulates and persists at the mid- body, suggesting that its loading and stabilization between the 2 primordial GCs serves as nucleating event in syncytial organization. Despite this early accumulation of ANI-2, we could not detect exchange of a fluorescent marker between Z_2 and Z_3, suggesting that the 2 cells do not share cytoplasm and, thus, are not syncytial at this stage. This indicates that if rachis bridges are nucleated upon P_4 division, they require further maturation to allow cytoplasmic exchange. This is compatible with the observation, made by electron microscopy, that syncytial organization of the germline only becomes apparent at the second larval stage (Hirsh et al., 1976).

Analysis of ANI-2 localization during larval development revealed that it remains enriched at the apical side of GCs and at rachis bridge rings at all stages, including in adult animals. Interestingly, we found that rachis bridge diameter increases as animals progress through larval stages. These results suggest that rachis bridge maturation occurs progressively during larval development and is independent from rachis bridge nucleation. Such decoupling could be analogous to *Drosophila*, where ring canals and cytoplasmic bridges connecting GCs increase in diameter as GCs progress through gametogenesis (Tilney et al., 1996). While an increase in cell size could in principle account for the increase in rachis bridge diameter, we found that the size of *C. elegans* GCs remains largely constant during larval development (unpublished results). It will be interesting to determine the mechanism that allows the increase of rachis bridge diameter, as this may inform on the regulation of their maturation. It has been shown that the tight bundling of actin filaments to one another is key to ring canal expansion and stabilization during *Drosophila* oogenesis (Tilney et al., 1996). While there are similarities of com- position between *C. elegans* cytokinetic rings and rachis bridge rings, whether a process such as this promotes rachis bridge maturation has yet to be determined.

The presence of ANI-2 at the onset of germline formation and its persistence at rachis bridges throughout larval development suggested that it plays a role in rachis bridge nucleation and/or maturation. Analysis of rachis bridge organization in *ani-2* mutant animals revealed that the majority of GCs had no detectable rachis bridge. A minority of GCs (30%) had well defined rachis bridges but, as opposed to controls, their diameter did not increase during larval development. This suggests that ANI-2 is not essential for rachis bridge nucleation but that its presence is crucial during rachis bridge maturation to promote their opening.

Syncytial Maintenance Depends on a Balance Between Anillin Activities

Phenotypic analysis of early embryonic development previously suggested that ANI-2, lacking the predicted N-terminal actin- and myosin-binding domains found in ANI-1, may function as negative regulator of contractility (Chartier et al., 2011). ANI-1, like ANI- 2, is enriched at GC rachis bridges throughout *C. elegans* development suggesting that the 2 Anillin proteins function in germline organization. As reported in our recent article (Amini et al., 2014), we observed that depletion of ANI-1 by RNAi did not cause severe defects in gonad organization but resulted in an increase in the diameter of rachis bridges, an increase in rachis width and a delay in oocyte cellularization (Figure 4.2.2). Interestingly, these defects are opposite to those observed in *ani-2* mutants and many of the phenotypes of *ani-2* mutants were partly suppressed by RNAi depletion of ANI-1. This suggests that the defects in *ani-2* mutant animals result from an increase in ANI-1 activity and that the 2 Anillin proteins counteract each other to regulate the rachis bridge stability and germline syncytial organization. What regulates the balance of activity between the 2 Anillins is currently unclear. The two proteins do not control each other's accumulation at rachis bridges, and thus this balance may rely on the potential capacity of ANI-2 to "titrate" one or many actomyosin regulators required for ANI-1 function in organizing or stabilizing contractile networks. Interestingly, phenotypic profiling screens in the *C. elegans* gonad have shown that depletion of several proteins, including known regulators of actomyosin contractility, results in defects reminiscent of those observed in *ani-2* mutants (Green et al., 2011). Whether these proteins work with ANI-2 to regulate syncytial organization is not known, but future analyses of the

molecular composition of rachis bridge rings and of the mutual dependence of these proteins for their proper localization will enhance our understanding of rachis bridge nucleation/maturation and of syncytial organization.

The Syncytial Architecture of the Gonad Favors Resistance to Mechanical Stress

One of the striking phenotypes associated with the loss of *ani-2* is a germ cell multinucleation defect that initiates upon entry into adulthood and progresses in severity from then on. This is a striking phenotype as the germline of *ani-2* mutants is largely morphologically normal until then, except for a decrease in rachis bridge diameter and in rachis width. Our analysis revealed that the multinucleation defect results from a collapse of GC partitions and is not a consequence of severe endoreplication or cytokinetic failure, suggesting that it is of non-cell autonomous origin.

One of the processes that begins when hermaphrodites enter adulthood is oogenesis, an event during which oocyte growth is sustained by cytoplasmic streaming in the rachis (Wolke et al., 2007). We found that multinucleation is dependent on oogenesis, as multi- nucleated compartments were reduced in conditions where oogenesis was absent, such as in male gonads (which form only sperm) and in gonads depleted of GLD-1/ 2 (which contain only mitotic GCs). We postulated that the cytoplasmic streaming that occurs during oogenesis could generate mechanical stress at rachis bridges, and that in absence of ANI-2 this stress could be sufficient to provoke the collapse of partitions between GCs. To test this hypothesis, we imaged adult hermaphrodite gonads during ovulation, when entry of the oocyte into the spermatheca is accompanied by an important deformation and stretching of the rachis. Interestingly, we found that this stretching is transient and is accompanied by an equally transient increase in the diameter of the most proximal rachis bridge. This indicates that the gonad has elastic properties and further suggests that rachis bridges account for its elastic deformation. Importantly, this elastic response upon ovulation was lost in animals partially depleted of ANI-2, suggesting that ANI-2 is important to confer elastic properties to the gonad. Our results suggest a model in which the presence of ANI-2 at rachis bridge rings

allows their deformation, which in turns, confers elastic properties to the whole tissue and allows it to sustain deformation and thus compensate for mechanical stress. Tissue elasticity and resistance to mechanical stress could be a conserved feature of syncytia. For instance, recent work on murine syncytiotrophoblasts grown in culture revealed that their cortex is more elastic than that of the mononucleated trophoblasts from which they are derived (Zeldovich et al., 2013). While much remains to be done to fully understand the precise mechanism by which syncytia are formed and maintained, our work suggests that the differential expression and/ or regulation of contractility regulators such as ANI-1 and ANI-2 may provide the necessary tools to begin addressing this important question.

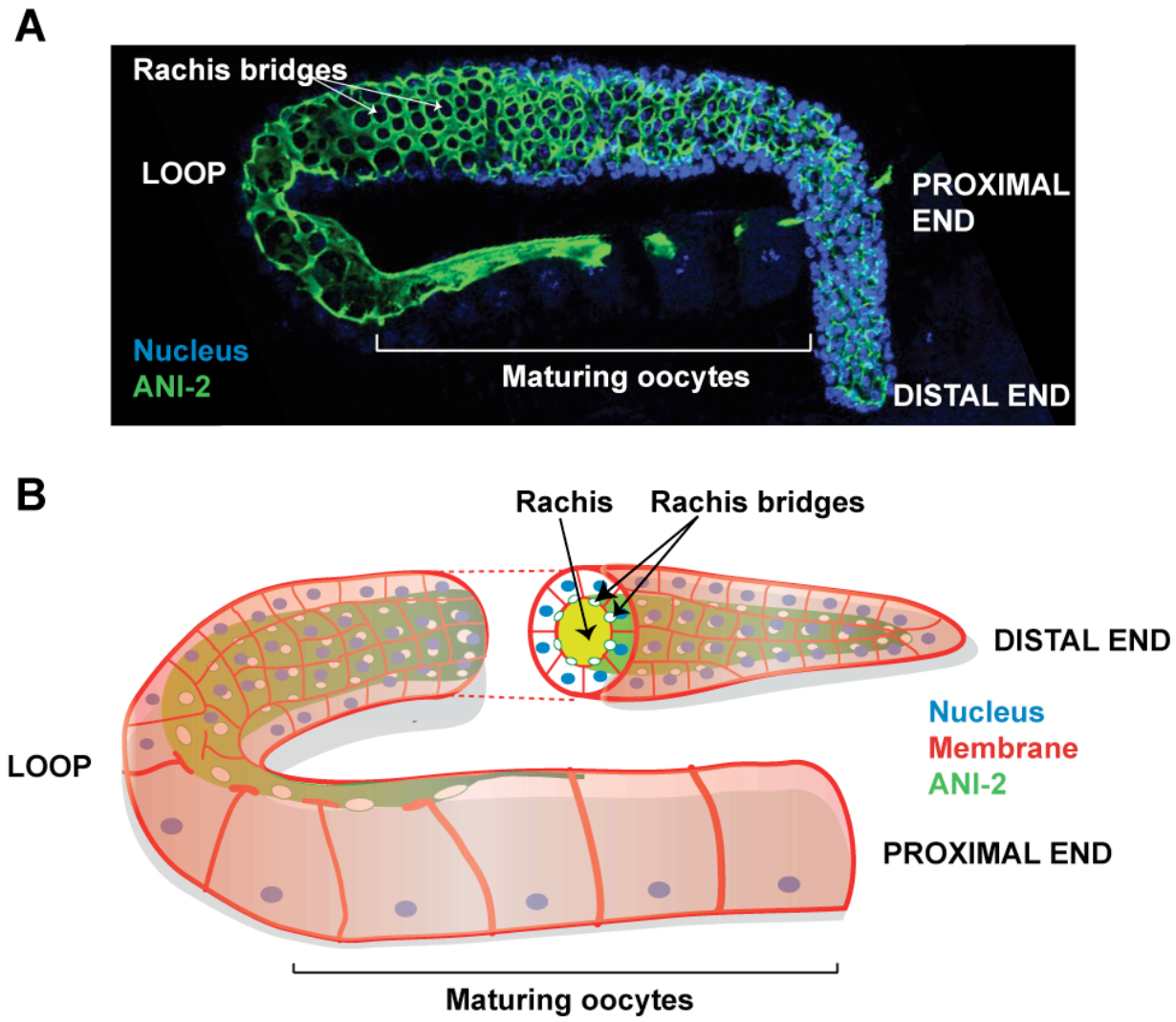

Figure 4.1.1

Figure 4.1.1: Organization of the *C. elegans* hermaphrodite gonad.

(A) Confocal projection of a fixed wild-type hermaphrodite *C. elegans* gonad arm stained with ANI-2 (highlighting the rachis in green) and DAPI (highlighting DNA in blue). Each rachis bridge is open to the rachis and is stabilized by a ring enriched in ANI-2 and other contractility regulators. **(B)** Schematic representation of a wild-type hermaphrodite gonad arm. A virtual transverse section of the germline is depicted, showing the rachis and its delineating ANI-2-enriched cortex.

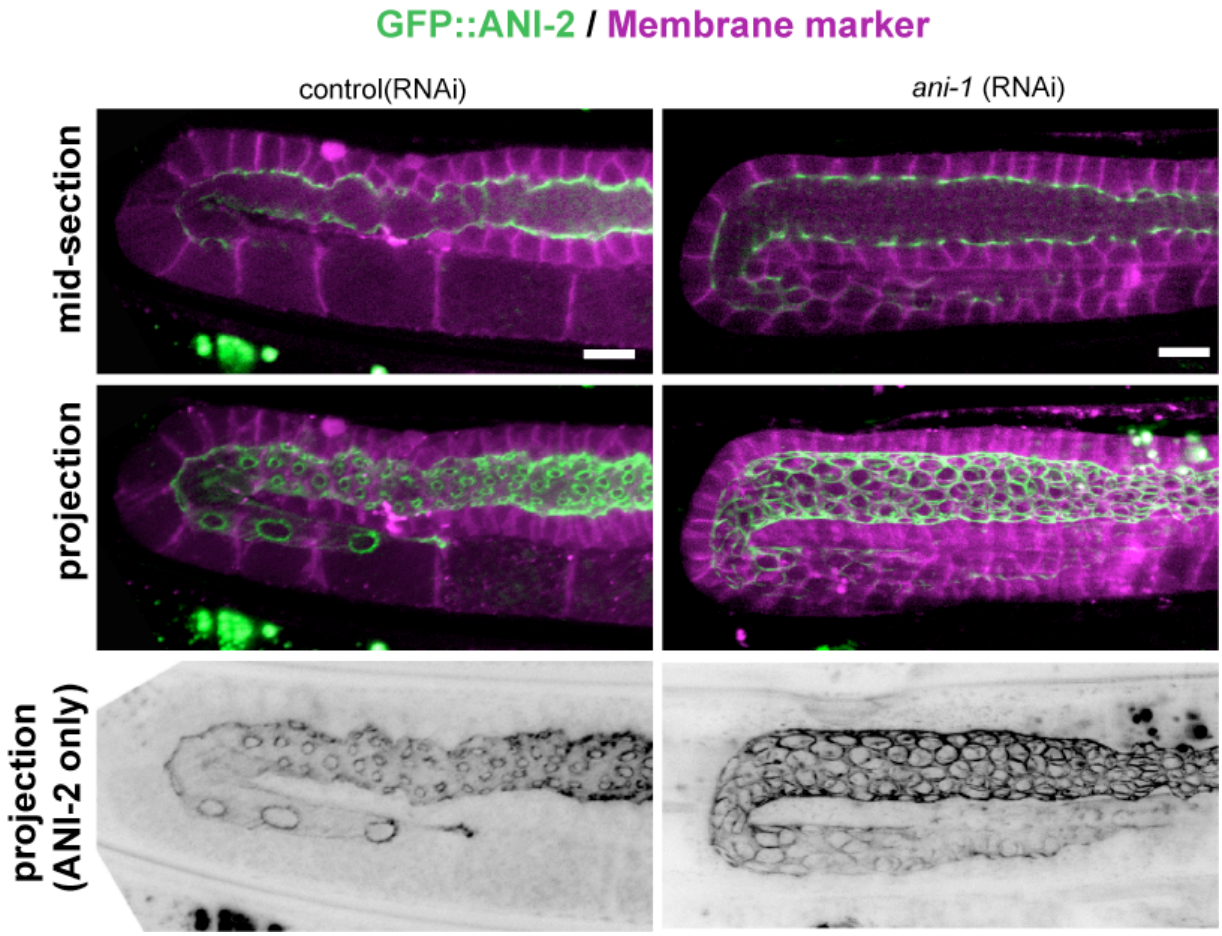

Figure 4.1.2

4.1.2. ANI-2 localization in control and ANI-1-depleted animals.

Confocal mid-sections and projections of live wild-type adult hermaphrodite gonads treated with control(RNAi) or *ani-1*(RNAi) and expressing GFP::ANI-2 (green) and a membrane marker (magenta). Rachis diameter is significantly increased and GC rings are significantly larger in *ani-1*(RNAi) animals compared to control. Scale bars, 10 mm.

4.2. When failure is success: syncytiogenesis of the *C. elegans* germline by incomplete cytokinesis

Syncytia occur during normal development of a wide range of cell types and species. Up to now, studies revealed that in many cases, syncytiogenesis is coupled closely with altered cytokinesis or cytokinesis failure. Consistent with this, our data shows that the *C. elgans* germline syncytiogenesis is also achieved through cytokinesis failure. Our results, together with findings in other models, underline the evolutionary conservation of cytokinesis failure in syncytium formation. Yet, the molecular mechanism of incomplete cytokinesis in germline syncytiogenesis in *C. elegans* and other systems remains mysterious. Nevertheless, in light of our data, I propose a model for germline syncytial formation in *C. elegans* as follows: **1)** nucleation of syncytium (the MBR stabilization and abscission failure), **2)** MBR maturation and transformation into GC rachis rings and ultimately the MBR/GC rachis ring duplication. These stages of germline syncytium formation are distinct but not necessarily independent and they could either all take place within the *C. elegans* embryo or initiate in the embryo and continue further rearrangements in the *C. elegans* L1 larva. For the moment, the model is speculative and intended to inspire hypotheses and discussions of its biological implications. Further imaging of dynamics of syncytium formation as well as analyses of genes important for this important event, combined with studies on the mechanisms of conventional cytokinesis, could shed light on this important stage of *C. elegans* germline development.

Nucleation of the C. elegans germline syncytium by incomplete cytokinesis

The syncytium could in principle arise from a failure in furrow assembly, ingression, or abscission. Here, we showed that early stages of cytokinesis occur properly in P_4. However, the MBR is not severed from the cell-cell boundary between Z_2 and Z_3 and instead remains stably associated to the PGCs, suggesting that abscission, the last stage of cytokinesis by which the MBR is removed to achieve truly separated daughter cells, does not take place. Altogether, given the knowledge of all the requirements for successful cytokinesis, a logical interpretation of these results is that formation of the GC rachis rings in the *C. elegans*

germline is nucleated during embryogenesis and result from either the MBR stabilization or cytokinesis failure at the abscission stage, or both, rather than alterations of cytokinesis at earlier stages. These could include modification of abscission machinery to accomplish incomplete cytokinesis and coordinated expression and recruitment of proteins that will stabilize the MBR. It is important to note that it is not clear from our results whether MBR stabilization is the cause or consequence of abscission failure. Nevertheless here, for convenience of discussion I will first discuss the MBR stabilization, followed by mechanism of abscission failure.

The MBR stabilization appears to play important roles during syncytium formation as altering the MBR fate transforms it into a stable ICB rather than discarding it via abscission in several different syncytia (Haglund et al., 2011). During conventional cytokinesis, the MBR functions as a transient ICB connecting the two dividing cells. In syncytial tissues of *Drosophila* and other insects however, this transient bridge is stabilized, partly as result of formation of a distinctive cytoplasmic zone known as the fusome, as well as accumulation of an electron dense material lining the outer rim of ICB (Weber and Russell, 1987). These structures could function in stabilizing the transient MBR connection between the dividing daughter cells until they become mature ring canals. Likewise, in *C. elegans* PGCs, the MBR stabilization could also contribute to maintenance of the MBR at the Z_2-Z_3 boundary and thereby promotion and/or maintenance of incomplete cytokinesis. Before our work, based on published data, there was not much known about the temporal or spatial organization of GC rachis rings during gonad development. We showed that contractility regulators such as myosin II, ANI-1, ZEN-4 (Pavarotti/MKLP-1) and UNC-59 (septin) localize at the GC rachis rings at all times during germline development. The presence of a fusome-like or an electron dense structure in *C. elegans* PGCs has not been confirmed, and thus it remains unclear whether syncytium formation always depends on such structure. However, one might reasonably expect that other PGC-specific components are involved in converting the stable MBR into GC rachis ring in *C. elegans*.

For instance, given the persistence of the CR/MBR components such as myosin II, ANI-1, ZEN-4 and CYK-7 and UNC-59 at the MBR between Z_2 and Z_3 at all times, throughout both embryogenesis and germline development, it is tempting to speculate that the PGC MBR is transformed into stable GC rachis rings and that at least some of these components are needed to stabilize the MBR by anchoring it to the membrane. This would preclude the completion of cytokinesis and promote syncytium formation by keeping the connection between Z_2 and Z_3 open, albeit it may be very small or blocked. While it will be important to investigate the role of these components, two of them appear to be good candidates; Anillin and the centralspindlin protein ZEN-4. Anillin, a stable component of both *Drosophila* male germline and somatic stable ICBs, is a membrane binding PH domain (anillin in human and *S. pombe* has three membrane-associating elements that anchor it at the cleavage furrow, Sun et al., 2015), that presumably links the CR and the MBR to the plasma membrane during cytokinesis and thus was repeatedly proposed to function in the MBR stability (Haglund et al., 2011). In addition, given that ZEN-4 is a conserved component of stable ICBs in several types of syncytia including the syncytial *C. elegans* germline (Zhou et al., 2013) and *Section4. Article 1*), ZEN-4 could also play a role in stabilizing the MBR during syncytium formation in *C. elegans*. Interestingly, we showed that ANI-2 is required for the stability and maintenance of GC rachis rings in the germlines of L4 larvae and adult animals (see *Section 4., Article 1*), suggesting that the GC-specific ANI-2 protein might also play a role to stabilize the MBR during syncytium formation. Altogether, the MBR stability may physically impede the progress of cytokinesis by blocking abscission.

But by what mechanisms could a stabilized MBR perturb abscission? One possibility is that PGC-specific components of the MBR are actively involved in impeding either recruitment of the abscission components to abscission sites or activity of abscission factors (e.g., ESCRTs or microtubule severing enzymes), to favor incomplete cytokinesis. Undoubtedly, the first step toward understanding which of the above scenarios happens during *C. elegans* syncytium formation is to investigate whether abscission factors are present at the MBR of PGCs, in comparison to their somatic counterparts, and monitoring whether their dynamics during PGC division is different from that of their somatic counterparts during embryogenesis.

Interestingly, *in vivo* and biochemical evidence from studies in the mouse testis supports a model of cytokinesis failure through inhibiting the assembly of abscission components. As I described before, according to this model, in germline tissues, TEX-14 competes with the ESCRT-I proteins ALiX and TSG101 for binding to CEP55 at the MB and prevents targeting of ESCRT-III to the abscission site, to ultimately block the progression of abscission (Morita et al., 2007). However, due to the apparent absence CEP55 and TEX-14 homologues in *C. elegans*, this model may not translate easily to this system. While, it will be important to consider whether any of the PGC MB components in *C. elegans* serve a corresponding physiological role to TEX-14, evidence from our studies suggests that one interesting potential candidate could be ANI-2 (this will be expanded in *Section 4.3.*).

MBR maturation and transformation into GC rachis ring

Nucleation of the *C. elegans* germline syncytium through incomplete cytokinesis of P_4 does not necessarily mean that the PGCs immediately become syncytial. Interestingly, this notion is supported by our result from *Article 1* (See *Section 3.1.*), wherein we could not detect exchange of a fluorescent cytoplasmic marker between Z_2 and Z_3, suggesting that the two cells do not share cytoplasm and thus are not syncytial at this stage. One interpretation of this result is that Z_2 and Z_3 are linked by a stable MBR that either has a very small diameter and/or is blocked by some material (e.g. microtubule). Instead, further MBR maturation could be required for transforming it into an open GC rachis ring and allow the formation of a connection, and thereby cytoplasmic exchange, between Z_2 and Z_3.

This arises an important question of when the Z_2 and Z_3 cells become syncytial. One possibility is that the MBR-to-GC rachis ring conversion occurs during post-embryonic development of Z_2 and Z_3, for instance at L1. It could be also that the MBR is converted into a GC rachis ring during later stages of embryonic development. In *Article 2*, we observed that the stable MBR at the membrane boundary between Z_2 and Z_3 undergoes reorganization during embryogenesis and as such, is transformed from a spherical structure to a bar-shaped structure that extended perpendicular to the cell-cell interface (Figure 3.2.6). This indicates

that the MBR of PGCs is dynamic despite being stably anchored between the two cells throughout embryogenesis, suggesting that at least some steps of MBR-to-GC rachis ring transformation could occur during embryonic development. Nevertheless, our data does not show whether MBR undergoes further maturation in the embryo and/or L1 and when the MBR-to-GC ring conversion occurs. Unfortunately, we could not resolve this question by performing live imaging during the complete course of embryogenesis because of the rapid movement of the embryo inside its eggshell during the late stages of embryogenesis. This could be tested by examining the dynamics of MBR in less-mobile embryos taking advantage of mutants with defective muscle contraction. Likewise, live imaging of the first division of PGCs at L1 could also give informative insight into the process of GC ring formation and maturation.

Moreover, our results show that at least four proteins commonly present in the CRs/MBRs; Myosin II, ANI-1, UNC-59 and CYK-7 are also stable components of the GC rachis rings throughout the *C. elegans* germline development, arguing that GC rachis rings may be derived from the arrested CRs or stabilized MBRs. In consistent with this, based on the persistent of the CR/MBR components at the somatic and germline syncytial ring canals in *Drosophila* (Airoldi et al., 2011; Haglund et al., 2011) and the male mice GC ICBs (Greenbaum et al., 2011; Greenbaum et al., 2007), it has been suggested that these syncytial structures are derived from CR/MBRs (Cooley, 1998; Fawcett et al., 1959; Haglund et al., 2011; Hime et al., 1996; Pepling et al., 1999). While these similarities could suggest that the process of GC rachis ring formation and maturation may actually be analogous to the processes in the above-mentioned syncytial tissues, future studies will be needed to verify whether this is also the case in *C. elegans* and dissect the potential molecular machineries involved in this process.

But how does CR/MBR maturation and transformation into GC rachis ring could occur? Septins have the intrinsic ability to organize into rings as observed *in vitro.* A mammalian septin complex of SEPT2/6/7 can self-assemble into rings with a diameter of ~0.6 μm in the absence of actin (Kinoshita *et al.,* 2002). We showed that a *C. elegans* septin homolog UNC-

59 is enriched in the stabilized MBR as well as GC rachis rings, raising the possibility that septin together with other cytoskeletal components could organize this transformation in a way similar to the organization of septin rings at the yeast bud neck (nelson 2003). In addition, in *Drosophila* egg chambers, for instance the ring canal maturation occurs via sequential addition of several different proteins including phosphotyrosine epitopes (Robinson et al., 1994), actin, HTS. It is not known whether *C. elegans* syncytium formation is also accompanied by such events, but spatiotemporal investigation of the molecular composition of the MBR/GC rachis rings in the *C. elegans* could provide informative insights into this. Another interesting question that arises from our studies is how and when the GC rachis ring between Z_2 and Z_3 is duplicated into two GC rachis rings so that each GC inherits a GC rachis ring. We showed in *Article 1* and *Article 2* that all GCs in the *C. elegans* germline contain a GC rachis ring, suggesting that the stable MBR that is formed during embryogenesis must either duplicate during late embryogenesis or in the newly-hatched. Dynamic monitoring of the late embryo as well as L1 will tell us will tell us which scenario occurs.

4.3. ANI-2 potential role in syncytiogenesis

In *Section 3.2., Article 2*, we showed that during *C. elegans* embryonic development, ANI-2 is undetectable in somatic blastomeres and only becomes cortically enriched in the P_4 germline blastomere. Interestingly, upon P_4 division, ANI-2 accumulates and persists at the MBR between the two PGCs, Z_2 and Z_3. Given ANI-2's exclusive localization at PGCs and its scaffolding abilities to interact with several distinct proteins, it is tempting to speculate that ANI-2 could function to promote incomplete cytokinesis. Our results from Chapter 3.1 indicate that ANI-2 would not physically block constriction of the CR during division of P_4 blastomere, but instead could either physically stabilize the MBR or preclude the targeting of ESCRTs and in particular ESCRT-III to abscission sites or both, which would serve as a nucleating event for syncytium formation. Upon CR closure, the CR undergoes maturation and thereby is transformed into an MBR that, according to our results, persists at the cell-cell interface between Z_2 and Z_3 during the course of embryogenesis, suggesting that it is a stable

structure. It has been previously shown that in the *Drosophila* S2 cells, the MBR must be anchored to the plasma membrane so as to stabilize the close connection between the daughter cells and that anillin function to prevent the MBR from regressing during later stages of cytokinesis (El Amine et al., 2013; Kechad et al., 2012). Based on this and given the GC-specific accumulation of ANI-2 at the MBR of PGCs, one hypothesis could be that MBR maintenance at the Z_2-Z_3 boundary depends on ANI-2. Alternatively, or in addition, ANI-2 might serve to stabilize other structural proteins present at the MBR including septin to form the nascent GC rachis rings or to maintain the already formed rings between PGC during embryogenesis. Given that ANI-2 is a scaffolding protein containing the PH-binding domain, it is possible that ANI-2 might accomplish this by cooperating with septins (see above) or by binding additional structural or regulatory GC rachis ring components and thereby could serve role as an anchor of MBR-plasma membrane to stabilize interactions between the MBRs and the plasma membrane.

In a second scenario, ANI-2 could function in abscission failure by inhibiting the abscission factor recruitment or activity or a combination of both. As I described before, in human cells anillin, RhoA and septin localize to the two abscission sites on each side of the MB (Renshaw et al., 2014). This particular localization pattern was proposed to prime these sites for the future recruitment of ESCRT-III machinery during abscission. Interestingly, it was shown that the septin-dependent anillin dissipation from the presumptive abscission sites is a prerequisite for ESCRT-III recruitment and ultimately completion of cytokinesis (Renshaw et al., 2014). Even though much still needs to be understood about the molecular details of abscission in *C. elegans*, in light of our data, a model based on competition between ANI-1 and ANI-2 could explain the failure of abscission in PGCs. Our results from *Article 1*, show that ANI-1 and ANI-2 compete each other for the regulation of contractility. Therefore the presence of ANI-2 at the MBR may locally counteract ANI-1 activity, perhaps by uncoupling it from one or more of its regulators or effectors including septin. This competition could potentially result in persistence of ANI-1 at the presumptive abscission site and thereby precludes ESCRT-III from being recruited. In such scenario, ANI-2 has an analogous role to TEX-14. Alternatively, ANI-

2 could also function by inhibiting the activity of abscission components. In addition, ANI-2 could also contribute to MBR maturation and its transformation into GC rachis ring.

Altogether, regardless of the exact mechanism of abscission failure and exact role of ANI-2, an important hypothesis that stems from our results (based on ANI-2 localization at the MBR of PGCs) is that ANI-2, in one way or another, may contribute to syncytium formation of the *C. elegans* germline. Clearly, this notion could be followed up by depletion of ANI-2 in the *C. elegans* PGCs, to gain insight into how ANI-2 contributes to syncytium formation and how ANI-2 modifies the MBR and/or abscission machinery to regulate germline syncytium formation by scoring the defects associated with ANI-2 depletion. This brings many additional questions such as whether and how ANI-2 couples MBR stability to abscission failure and maintains MBR-plasma membrane anchoring during syncytium formation. One way to study this could involve using domain analysis of ANI-2 to determine how ANI-2 mediates its presumptive role in syncytiogenesis. While the N-terminal region of ANI-2 lacks obvious actin- and myosin-binding domains, its central and C- terminal regions contain AHD and PH domains, respectively. To identify the role of ANI-2 domains in germline syncytium formation during *C. elegans* embryonic development, truncated forms of ANI-2 with specific domain deletions could be generated to determine whether these truncated proteins can localize properly to the cortex of P_4 germline blastomeres followed by enrichment at the MBR, MBR-persistence and reorganization in PGCs of the embryo of *C. elegans*. In addition, localization of other contractility regulators to the MBR of PGCs could also be tested. Such careful phenotypic analysis should unravel whether and how ANI-2 acts during P_4 cytokinesis, MBR-persistence and reorganization in the embryo of *C. elegans*, to determine the stage during which ANI-2 functions to regulate syncytiogenesis.

Overall, the scenarios mentioned above are not mutually exclusive and ANI-2 may contribute to one or all of them. ANI-2 as one of the basic structural elements of the *C. elegans* PGC MBR and GC rachis rings might be needed not only during syncytium nucleation, but also during its growth and maturation, by anchoring other proteins of the MBR to the plasma

membrane. At this time, there is no evidence to suggest any such role for ANI-2 and more studies will be required to understand ANI-2 function in syncytium formation. More insight into molecular mechanisms controlling how the abscission machinery is modified in different cellular contexts will give valuable information about mechanisms controlling complete versus incomplete cytokinesis *in vivo*.

4.4. GC rachis rings: to contract or not to contract

GCs in the distal arm of the *C. elegans* germline undergo proliferation and thereby cytokinesis with an open GC rachis ring. Interestingly, all major components of the cytokinetic machinery are present at the GC rachis rings but they do not trigger the closure of the rings in the distal germline. It is puzzling why during normal cytokinesis, these components promote the final closure, whereas during GC divisions presence of these proteins could not promote the GC rachis ring closure and thereby all GCs remain connected to the rachis. One possibility for maintenance of open rings is that a regulated inhibitory mechanism is imposed on the cytokinetic machinery present at GC rachis rings to preclude closure of the GC rachis ring. This might be achieved either through indirect inhibition of the actomyosin contractility through inhibition of Rho-1 activity or direct inhibition of myosin itself. Interestingly, the latter scenario has been previously reported in the *Drosophila* female germline, wherein dephosphorylation of myosin II results in arrest of constriction in the ring canals and thus maintenance of the syncytial organization of the germline (Ong et al., 2010). Investigations of the activity of RhoA and myosin are important to dissect the underlying mechanisms of this germline feature.

When considering the impact and significance of GC rachis rings for gonad organization and propagation of the animal, another important question that emerges is how the GC rachis rings are maintained open during the course of gonad development. Although, it sounds logical that the same components that inhibit contraction of the GC rachis ring could also function in maintaining the ring as an open structure, it could be that two different mechanisms contribute

to this event. Based on our results, we proposed a model wherein the balance of activity between the two *C. elegans* anillins, ANI-1 and ANI-2, is required for stability and ultimately maintenance of GC rachis rings (see *Section 4., Article 1* and *Section 5.1.*). In addition, localization of other contractility regulators at GC rachis rings and/or at GC membranes argues in favor of their potential role in mediating syncytial maintenance. Consistent with this, phenotypic profiling screens in the *C. elegans* gonad have shown that depletion of several proteins (17 proteins), including 7 distinct known regulators of actomyosin contractility (myosin II, UNC-45, LET-502, CYK-4, ACT-4, ECT-2 and Rho-1), results in defects reminiscent of those observed in *ani-2* mutants (Green et al., 2011), suggesting that they might function in GC rachis ring maintenance either directly or via retaining ANI-2 at those structure throughout germline development. This could be tested by monitoring ANI-2 localization and GC rachis ring structure in animals depleted for each of the 7 contractility regulators. This will identify the critical regulators of maintenance at GC rachis rings and ANI-2 assembly to them and thus provide mechanistic information regarding the structure, formation and/or maintenance of GC rachis rings. Given that there are many contractility regulators that display a similar terminal phenotype as ANI-2 depletion, it is tempting to speculate that maintenance of the germline syncytial structure requires recruitment of downstream regulators of contractility.

Another interesting potential candidate protein for GC syncytial maintenance, based on its localization pattern and function, is HIM-4, a conserved extracellular matrix (ECM) hemicentin protein with orthologs in all vertebrate species (Hodgkin et al., 1979). At the L1 larval stage, HIM-4 accumulates in the extracellular space between GCs but gradually disappears from the lateral membrane of GCs and instead becomes enriched at the GC rachis rings on the apical side of GCs (Vogel and Hedgecock, 2001), where ANI-2 is also enriched. Interestingly, depletion of HIM-4 results in destabilization/weakening of lateral membranes between GCs and formation of multinucleated GCs and oocytes, which in turn results in gonad disorganization and sterility (Vogel and Hedgecock, 2001), suggesting that HIM-4 is required for the stability of GC membranes and ultimately maintaining syncytial integrity of GCs in the

gonad. But how might an ECM protein contribute to maintenance of syncytium? One possibility is that HIM-4 may anchor the GC rachis ring to the ECM outside of the cell and as such may provide additional stability to the GC rachis rings. Future attempts will uncover whether and how HIM-4 links the GC rachis rings to the extracellular matrix to stabilize GC rachis rings and maintain their syncytial architecture.

While GCs in the distal arm of the *C. elegans* gonad should maintain their GC rachis rings open to remain connected to the rachis, in the proximal germline, GCs undergo cellularization and are severed from the rachis upon oocyte formation. Hence even if we answer the questions of how GC rachis rings become and remain open in the distal arm of the germline, one enduring mystery of the field still remains unanswered: What promotes oocyte cellularization in the proximal gonad? In other words, while the more proximally-located GCs are contractile and thereby are capable of closing their GC rachis rings to ultimately separate oocytes from rachis, the distally-located GCs lack such ability and remain non-contractile, suggesting that contractility of GC rachis rings is spatially regulated within the germline.

It could be that persistence of the contractility regulators (e.g., myosin II) at GC rachis rings serves the primary role of completion of cytokinesis in the proximal gonad, but that contraction of the GC rachis rings is inhibited probably by the negative regulators of contractility in the distal region, whereas removal of these negative regulators is likely to promote oocyte cellularization in the proximal region of the gonad. Several genes with important functions in conventional cytokinesis are also required for oocyte cellularization, including the Rho-binding kinase *let-502* (Piekny and Mains, 2002) and an actin regulator *cyk-1* (Swan et al., 1998). Nonetheless, there is no answer in the field as to how the transition from open (non-contractile) to cellularized (contractile) happens. Our study hints at a potential role for anillins in mediating this transition in a spatiotemporally manner. ANI-2 is removed from the cortex upon oocyte cellularization and its depletion by RNAi results in precocious closure of rachis rings and thereby early oocyte individualization (see Section4., *Article* 1, our unpublished data and Maddox et al., 2005), suggesting that ANI-2 is a likely candidate to

inhibit contraction of GC rachis rings. On the other hand, our *ani-1* RNAi depleted animals exhibit late oocyte cellularization (see *Section 4., Article 1*). Altogether, our results suggest that a balance between these two anillins might function to either directly or indirectly regulate spatiotemporal organization of the germline contractility network to favor oocyte cellularization only in the proximal arm of the gonad. What regulates this balance is yet to be determined, but given the scaffolding capacity of anillins, one possibility is that ANI-2 interacts with binding partners of ANI-1, thereby inhibiting their interaction with ANI-1 and as such functions to restrict complete cytokinesis of oocytes. In this scenario, a spatiotemporal control of either assembly/disassembly or activity/inactivity (or both) of contractility regulators in the distal and proximal regions during gonad development is a prerequisite for the transition from the distally non-contractile to proximally contractile rings. A thorough analysis of the distribution and dynamics of proteins throughout gonad, during and after oocyte cellularization, followed by their genetic disruption, could be helpful to identify *bona fide* components of GC rachis rings *vs.* cellularized oocytes and could allow the dissection of the spatiotemporal function of these components in orchestrating the non-contractile to contractile transition of GC rachis rings during *C. elegans* development.

4.5. The role of the somatic gonad in the regulation of syncytium formation

Interactions between different cell types play crucial roles in tissue and organ development and architecture, raising an interesting question as to whether this type of cell-cell interaction also impinges on the regulation of germline syncytiogenesis during gonad primordium formation in the *C. elegans* embryo. As described in *Section 1.7.2.1.*, the gonad primordium is a simple organ consisting of just four cells – two PGCs (Z_2 and Z_3), and two somatic gonadal precursor cells (SGPs) (Z_1 and Z_4) (Sulston et al., 1983). During the process of gonadal primordium formation the two SGPs migrate posteriorly along the endoderm, turn and recognize the PGCs, and finally wrap themselves almost completely around them (Rohrschneider and Nance, 2013; Sulston et al., 1983). This process could contribute to

syncytium formation during gonadal primordium formation in the *C. elegans* embryo. Previously, it was shown that ablation of SGP precursor cells, prior to gonad primordium formation, results in PGCs death, whereas PGCs survive but cannot proliferate if the two SGPs are ablated after gonad primordium formation (Kimble and White, 1981), suggesting that SGPs control PGC survival and proliferation during embryogenesis. Nevertheless, it is not known whether this unique interaction between SGPs and PGCs also contributes to the process of syncytium formation during the *C. elegans* embryonic development. This could be tested using a combination of fluorescence imaging and embryological manipulations such as laser ablations to monitor distinct stages of syncytium formation including P_4 division, abscission failure, MBR persistent and reorganization and ultimately MBR to GC rachis ring conversion, to determine whether and how interactions between SGPs (Z_1 and Z_4) and PGCs (Z_2 and Z_3) directs the germline syncytiogenesis. Alternatively, morphogenetic movements of the neighboring endoderm or other adjacent somatic blastomeres could indirectly promote syncytiogenesis in PGCs. It could be that the syncytiogenesis of PGCs is a GC-specific intrinsically controlled event. These different processes are not mutually exclusive and a combination of all of them could also direct the overall behavior of PGCs during syncytium formation in the embryo. Isolation of P_4 and monitoring its division *in vitro* could help discriminate between these scenarios.

We showed that the diameter of GC rachis rings progressively increased during subsequent stages of larval development (see *Section3, Article 1* and Figure 3.2). It is currently unclear whether the progressive opening of GC rachis rings is a passive or active process. In the previous section (*Section 5.5.*) I discussed the possible role of contractility regulators localized at GC rachis rings in actively controlling the syncytial structure of the germline during gonad development. However, another possibility is that the syncytial GC structure is passively regulated by the somatic gonad. For instance, the distal tip cell (DTC) migration during larval development could mechanically induce opening of the GC rachis rings. I tested this notion by perturbing the DTC migration and thus the gonad positioning by either blocking DTC migration (*gon-1* and *ppn-1* RNAi) or by enhancing the DTC migration (*ccdc-55* RNAi) and I

could not detect differences in GC rachis ring size and opening in these animals (Unpublished data), suggesting that the DTC migration does not contribute to GC rachis ring formation in the gonad. More studies must be done to understand which scenario controls the syncytium formation and/or maintenance during embryogenesis and germline development.

4.6. On the functional significance of syncytial tissues

As described throughout this thesis, syncytia are a characteristic feature of several tissues in the human body including GCs, hepatocytes, cardiomyocytes and megakaryocytes. our work provides a glimpse into the mechanisms that can result in controlled incomplete cytokinesis and, as such, could enhance our understanding of heart disease and liver regeneration. Thus, understanding how these syncytial tissues are formed and maintain and may reveal new perspectives in a number of congenital and chronic diseases in which syncytial cells and incomplete cytokinesis appear to play a key role.

Polyploidy have been also observed in different human cancers (Coward and Harding, 2014; Gentric and Desdouets, 2014; Lacroix and Maddox, 2012). Almost 100 years ago, Theodor Boveri in his seminal work "*Zur Frage der Entstehung maligner Tumoren"* (Concerning the origin of human tumors), proposed that cytokinesis failure could give rise to multiple centrosomes, leading to tetraploidy which in turn causes genomic instability and cancer. Since then, cytokinesis failure and generation of multinucleated, polyploid and aneuploid cells have been correlated with tumorogenesis. To date, several studies directly demonstrated the significance of cytokinesis failure in tumorigenesis (Castillo et al., 2007; Fujiwara et al., 2005; Sotillo et al., 2007). In addition, cytokinesis failure in certain human cancer cells, such as prostate cancer, results in formation of abnormal stable ICBs (Vidulescu et al., 2005). One problem in cancer treatment is that while the majority of giant polyploid cells die, a small subset of them acquire resistance toward anti-cancer treatments (Coward and Harding, 2014; Zhang et al., 2014b). Thus, our work may help understand how polyploid cells can survive in tumorous populations and help develop new therapeutic strategies that target polyploid tumor

cells to maintain patient tumors in a drug sensitive state.

Understanding the normal function of syncytial tissues could have some clinical and therapeutic implications. Nonetheless, determining function of syncytia has received little attention over the years. In this work, we showed that the syncytial architecture of *C. elegans* germline confers elastic properties to the whole tissue, allowing it to sustain mechanical deformation and, perhaps, balance mechanical stress. Interestingly, it was shown that polyploidization and syncytiogenesis are two strategies used by mammalian and *Drosophila* epithelial tissues for wound healing (Galko and Krasnow, 2004; Losick et al., 2013; Singer and Clark, 1999). It was proposed that the large syncytial tissue formed at the wound site provides more robust cytoskeletal structure necessary to generate an appropriate mechanical environment to restore tissue integrity and thereby to heal the scar (Losick et al., 2013; Tamori and Deng, 2013). Our results, together with these findings in these *Drosophila* tissues bear striking similarity to the elasticity and the unusual cytoskeletal organization of the murine syncytiotrophoblasts and their ability to resist physical deformation and pathogen entry in both humans and mice (Zeldovich et al., 2013). Altogether, these results and ours from *Section 3.1, Article 1*, suggest that various tissues might have adapted syncytium formation as a strategy to resist against cellular and mechanical stresses cellular stresses.

It will be interesting to determine if tissue elasticity and mechanical resistance is a conserved feature of all syncytia and if anillin contributes in mechanical elasticity in other syncytial tissues as well. This could offer novel paradigms for considering mechanisms in wound healing or tissue regeneration. Consequently, the establishment of a model system for studying the control of incomplete cytokinesis and syncytium formation is likely to provide insight to questions of wide significance. Advances in modern tools such as tissue engineering will potentially enable us to broaden our perspective far beyond limitations of these early works. We are still in the early stages of understanding the factors contributing to the origin and establishment of syncytia and their roles but increasing awareness on diverse functions of syncytia has begun to unravel how these fascinating phenomena contribute to normal

physiology and disease.

5. CONCLUDING REMARKS

Although *C. elegans* is a well-studied model, how the syncytial germline is formed was uncharacterized before our study. In summary, data presented here establish ANI-2 as a *bona fide* component of MBR of PGCs during embryogenesis as well as the GC rachis rings throughout germline development. Our major contributions include: 1) the germline syncytium is nucleated via abscission failure of P_4, 2) the MBR formed at the cell-cell boundary between PGCs remains stably associated to the PGCs throughout the course of embryogenesis and is present in GC rachis rings throughout germline development, 3) Known contractility regulators are enriched at the GC rachis rings throughout germline development, 4) ANI-2 as a *bona fide* component of GC rachis rings throughout germline development 5) GC syncytial architecture arises progressively, and this depends on ANI-2, 6) Two Anillin proteins, the canonical ANI-1 and the short ANI-2, have opposing actions on syncytial organization; and 7) GC rachis rings confer elasticity to the syncytial germline under mechanical stress, a novel function for these structures and that ANI-2 is required to mediate this. Our work is the first thorough analysis of the cellular mechanisms underlying syncytial formation and maintenance and will significantly contribute to understand how this process occurs in other tissues or organisms. Together, our work has opened new insights for the possible similar functions of Anillins and/or ICBs in higher organisms. Aside from providing great insights into mechanism of controlled incomplete cytokinesis, these studies hold the potential to lead to targeted therapies in treating diseases such as cancer.

REFERENCES:

Abmayr, S.M., S. Zhuang, and E.R. Geisbrecht. 2008. Myoblast fusion in Drosophila. *Methods in molecular biology*. 475:75-97.

Agromayor, M., and J. Martin-Serrano. 2013. Knowing when to cut and run: mechanisms that control cytokinetic abscission. *Trends in cell biology*. 23:433-441.

Airoldi, S.J., P.F. McLean, Y. Shimada, and L. Cooley. 2011. Intercellular protein movement in syncytial Drosophila follicle cells. *Journal of cell science*. 124:4077-4086.

Alastalo, T.P., M. Lonnstrom, S. Leppa, K. Kaarniranta, M. Pelto-Huikko, L. Sistonen, and M. Parvinen. 1998. Stage-specific expression and cellular localization of the heat shock factor 2 isoforms in the rat seminiferous epithelium. *Experimental cell research*. 240:16-27.

Amano, M., M. Ito, K. Kimura, Y. Fukata, K. Chihara, T. Nakano, Y. Matsuura, and K. Kaibuchi. 1996. Phosphorylation and activation of myosin by Rho-associated kinase (Rho-kinase). *The Journal of biological chemistry*. 271:20246-20249.

Amini, R., E. Goupil, S. Labella, M. Zetka, A.S. Maddox, J.C. Labbe, and N.T. Chartier. 2014. C. elegans Anillin proteins regulate intercellular bridge stability and germline syncytial organization. *The Journal of cell biology*. 206:129-143.

Anderson, E., and E. Huebner. 1968. Development of Oocyte and Its Accessory Cells of Polychaete Diopatra Cuprea (Bosc). *J Morphol*. 126:163-&.

Arnold, J.M. 1969. Cleavage furrow formation in a telolecithal egg (Loligo pealii). I. Filaments in early furrow formation. *The Journal of cell biology*. 41:894-904.

Arnold, J.M. 1974. Intercellular bridges in somatic cells: cytoplasmic continuity of blastoderm cells of Loligo pealei. *Differentiation; research in biological diversity*. 2:335-341.

Asano, S., K. Hamao, and H. Hosoya. 2009. Direct evidence for roles of phosphorylated regulatory light chain of myosin II in furrow ingression during cytokinesis in HeLa cells. *Genes to cells : devoted to molecular & cellular mechanisms*. 14:555-568.

Bailly, A., and A. Gartner. 2013. Germ cell apoptosis and DNA damage responses. *Advances in experimental medicine and biology*. 757:249-276.

Barr, F.A., and U. Gruneberg. 2007. Cytokinesis: placing and making the final cut. *Cell*. 131:847-860.

Bastos, R.N., and F.A. Barr. 2010. Plk1 negatively regulates Cep55 recruitment to the midbody to ensure orderly abscission. *The Journal of cell biology*. 191:751-760.

Bate, M. 1990. The embryonic development of larval muscles in Drosophila. *Development*. 110:791-804.

Bate, M., and E. Rushton. 1993. Myogenesis and muscle patterning in Drosophila. *Comptes rendus de l'Academie des sciences. Serie III, Sciences de la vie*. 316:1047-1061.

Baylies, M.K., M. Bate, and M. Ruiz Gomez. 1998. Myogenesis: a view from Drosophila. *Cell*. 93:921-927.

Bement, W.M., H.A. Benink, and G. von Dassow. 2005. A microtubule-dependent zone of active RhoA during cleavage plane specification. *Journal of Cell Biology*. 170:91-101.

Bement, W.M., A.L. Miller, and G. von Dassow. 2006. Rho GTPase activity zones and transient contractile arrays. *Bioessays*. 28:983-993.

Berlin, A., A. Paoletti, and F. Chang. 2003. Mid2p stabilizes septin rings during cytokinesis in fission yeast. *The Journal of cell biology*. 160:1083-1092.

Birkenfeld, J., P. Nalbant, B.P. Bohl, O. Pertz, K.M. Hahn, and G.M. Bokoch. 2007. GEF-H1 modulates localized RhoA activation during cytokinesis under the control of mitotic kinases. *Developmental cell*. 12:699-712.

Bloor, J.W., and D.P. Kiehart. 2002. Drosophila RhoA regulates the cytoskeleton and cell-cell adhesion in the developing epidermis. *Development*. 129:3173-3183.

Bogart, J.P., R.P. Elinson, and L.E. Licht. 1989. Temperature and sperm incorporation in polyploid salamanders. *Science*. 246:1032-1034.

Bohrmann, J., and K. Biber. 1994. Cytoskeleton-Dependent Transport of Cytoplasmic Particles in Previtellogenic to Mid-Vitellogenic Ovarian Follicles of Drosophila - Time-Lapse Analysis Using Video-Enhanced Contrast Microscopy. *Journal of cell science*. 107:849-858.

Bonaccorsi, S., M.G. Giansanti, and M. Gatti. 1998. Spindle self-organization and cytokinesis during male meiosis in asterless mutants of Drosophila melanogaster. *The Journal of cell biology*. 142:751-761.

Braun, R.E., R.R. Behringer, J.J. Peschon, R.L. Brinster, and R.D. Palmiter. 1989. Genetically haploid spermatids are phenotypically diploid. *Nature*. 337:373-376.

Brenner, S. 1974. The genetics of Caenorhabditis elegans. *Genetics*. 77:71-94.

Brill, J.A., G.R. Hime, M. Scharer-Schuksz, and M.T. Fuller. 2000. A phospholipid kinase regulates actin organization and intercellular bridge formation during germline cytokinesis. *Development*. 127:3855-3864.

Bringmann, H., and A.A. Hyman. 2005. A cytokinesis furrow is positioned by two consecutive signals. *Nature*. 436:731-734.

Brown, E.H., and R.C. King. 1964. Studies on the Events Resulting in the Formation of an Egg Chamber in Drosophila Melanogaster. *Growth*. 28:41-81.

Burgos, M.H., and D.W. Fawcett. 1955. Studies on the fine structure of the mammalian testis. I. Differentiation of the spermatids in the cat (Felis domestica). *The Journal of biophysical and biochemical cytology*. 1:287-300.

Burton, K., and D.L. Taylor. 1997. Traction forces of cytokinesis measured with optically modified elastic substrata. *Nature*. 385:450-454.

Buszczak, M., S. Paterno, D. Lighthouse, J. Bachman, J. Planck, S. Owen, A.D. Skora, T.G. Nystul, B. Ohlstein, A. Allen, J.E. Wilhelm, T.D. Murphy, R.W. Levis, E. Matunis, N. Srivali, R.A. Hoskins, and A.C. Spradling. 2007. The Carnegie protein trap library: A versatile tool for Drosophila developmental studies. *Genetics*. 175:1505-1531.

Campbell, R.E., G. Gaidamaka, S.K. Han, and A.E. Herbison. 2009. Dendro-dendritic bundling and shared synapses between gonadotropin-releasing hormone neurons. *Proceedings of the National Academy of Sciences of the United States of America*. 106:10835-10840.

Canman, J.C. 2009. Cytokinetic astralogy. *Journal of Cell Biology*. 187:757-759.

Cao, L., W. Yu, Y. Wu, and L. Yu. 2009. The evolution, complex structures and function of septin proteins. *Cellular and molecular life sciences : CMLS*. 66:3309-3323.

Cao, L.G., and Y.L. Wang. 1996. Signals from the spindle midzone are required for the stimulation of cytokinesis in cultured epithelial cells. *Molecular biology of the cell*. 7:225-232.

Carlsson, A.E. 2006. Contractile stress generation by actomyosin gels. *Physical review. E, Statistical, nonlinear, and soft matter physics*. 74:051912.

Carlton, J.G., M. Agromayor, and J. Martin-Serrano. 2008. Differential requirements for Alix

and ESCRT-III in cytokinesis and HIV-1 release. *Proceedings of the National Academy of Sciences of the United States of America*. 105:10541-10546.
Carlton, J.G., and J. Martin-Serrano. 2007. Parallels between cytokinesis and retroviral budding: a role for the ESCRT machinery. *Science*. 316:1908-1912.
Carmena, M., M.G. Riparbelli, G. Minestrini, A.M. Tavares, R. Adams, G. Callaini, and D.M. Glover. 1998. Drosophila polo kinase is required for cytokinesis. *The Journal of cell biology*. 143:659-671.
Carmena, M., M. Wheelock, H. Funabiki, and W.C. Earnshaw. 2012. The chromosomal passenger complex (CPC): from easy rider to the godfather of mitosis. *Nature reviews. Molecular cell biology*. 13:789-803.
Castillo, A., H.C. Morse, 3rd, V.L. Godfrey, R. Naeem, and M.J. Justice. 2007. Overexpression of Eg5 causes genomic instability and tumor formation in mice. *Cancer research*. 67:10138-10147.
Castrillon, D.H., and S.A. Wasserman. 1994. Diaphanous is required for cytokinesis in Drosophila and shares domains of similarity with the products of the limb deformity gene. *Development*. 120:3367-3377.
Chalfie, M., Y. Tu, G. Euskirchen, W.W. Ward, and D.C. Prasher. 1994. Green fluorescent protein as a marker for gene expression. *Science*. 263:802-805.
Chang, Y.C., Y.J. Chen, C.H. Wu, Y.C. Wu, T.C. Yen, and P. Ouyang. 2010. Characterization of centrosomal proteins Cep55 and pericentrin in intercellular bridges of mouse testes. *Journal of cellular biochemistry*. 109:1274-1285.
Cheeseman, I.M., S. Niessen, S. Anderson, F. Hyndman, J.R. Yates, 3rd, K. Oegema, and A. Desai. 2004. A conserved protein network controls assembly of the outer kinetochore and its ability to sustain tension. *Genes & development*. 18:2255-2268.
Chen, C.T., A.W. Ettinger, W.B. Huttner, and S.J. Doxsey. 2013. Resurrecting remnants: the lives of post-mitotic midbodies. *Trends in cell biology*. 23:118-128.
Chen, E.H., E. Grote, W. Mohler, and A. Vignery. 2007. Cell-cell fusion. *Febs Lett*. 581:2181-2193.
Cho, W. 2001. Membrane targeting by C1 and C2 domains. *The Journal of biological chemistry*. 276:32407-32410.
Clubb, F.J., Jr., and S.P. Bishop. 1984. Formation of binucleated myocardial cells in the neonatal rat. An index for growth hypertrophy. *Laboratory investigation; a journal of technical methods and pathology*. 50:571-577.
Conradt, B., and D. Xue. 2005. Programmed cell death. *WormBook : the online review of C. elegans biology*:1-13.
Cooley, L. 1998. Drosophila ring canal growth requires Src and Tec kinases. *Cell*. 93:913-915.
Coward, J., and A. Harding. 2014. Size Does Matter: Why Polyploid Tumor Cells are Critical Drug Targets in the War on Cancer. *Frontiers in oncology*. 4:123.
Crittenden, S.L., E.R. Troemel, T.C. Evans, and J. Kimble. 1994. GLP-1 is localized to the mitotic region of the C. elegans germ line. *Development*. 120:2901-2911.
D'Avino, P.P. 2009. How to scaffold the contractile ring for a safe cytokinesis - lessons from Anillin-related proteins. *Journal of cell science*. 122:1071-1079.
D'Avino, P.P., T. Takeda, L. Capalbo, W. Zhang, K.S. Lilley, E.D. Laue, and D.M. Glover. 2008. Interaction between Anillin and RacGAP50C connects the actomyosin contractile ring with spindle microtubules at the cell division site. *Journal of cell science*. 121:1151-1158.

Davoli, T., and T. de Lange. 2012. Telomere-driven tetraploidization occurs in human cells undergoing crisis and promotes transformation of mouse cells. *Cancer cell*. 21:765-776.

de Cuevas, M., M.A. Lilly, and A.C. Spradling. 1997. Germline cyst formation in Drosophila. *Annual review of genetics*. 31:405-428.

de Cuevas, M., and A.C. Spradling. 1998. Morphogenesis of the Drosophila fusome and its implications for oocyte specification. *Development*. 125:2781-2789.

De Veylder, L., J.C. Larkin, and A. Schnittger. 2011. Molecular control and function of endoreplication in development and physiology. *Trends in plant science*. 16:624-634.

deCuevas, M., J.K. Lee, and A.C. Spradling. 1996. alpha-spectrin is required for germline cell division and differentiation in the Drosophila ovary. *Development*. 122:3959-3968.

Deppe, U., E. Schierenberg, T. Cole, C. Krieg, D. Schmitt, B. Yoder, and G. von Ehrenstein. 1978. Cell lineages of the embryo of the nematode Caenorhabditis elegans. *Proceedings of the National Academy of Sciences of the United States of America*. 75:376-380.

Dickinson, D.J., J.D. Ward, D.J. Reiner, and B. Goldstein. 2013. Engineering the Caenorhabditis elegans genome using Cas9-triggered homologous recombination. *Nat Methods*. 10:1028-+.

Doberstein, S.K., R.D. Fetter, A.Y. Mehta, and C.S. Goodman. 1997. Genetic analysis of myoblast fusion: blown fuse is required for progression beyond the prefusion complex. *The Journal of cell biology*. 136:1249-1261.

Dubreuil, V., A.M. Marzesco, D. Corbeil, W.B. Huttner, and M. Wilsch-Brauninger. 2007. Midbody and primary cilium of neural progenitors release extracellular membrane particles enriched in the stem cell marker prominin-1. *The Journal of cell biology*. 176:483-495.

Dym, M., and D.W. Fawcett. 1971. Further observations on the numbers of spermatogonia, spermatocytes, and spermatids connected by intercellular bridges in the mammalian testis. *Biology of reproduction*. 4:195-215.

Echard, A., G.R. Hickson, E. Foley, and P.H. O'Farrell. 2004. Terminal cytokinesis events uncovered after an RNAi screen. *Current biology : CB*. 14:1685-1693.

Edgar, L.G. 1995. Blastomere culture and analysis. *Methods in cell biology*. 48:303-321.

Egelhoff, T.T., R.J. Lee, and J.A. Spudich. 1993. Dictyostelium myosin heavy chain phosphorylation sites regulate myosin filament assembly and localization in vivo. *Cell*. 75:363-371.

Eggert, U.S., A.A. Kiger, C. Richter, Z.E. Perlman, N. Perrimon, T.J. Mitchison, and C.M. Field. 2004. Parallel chemical genetic and genome-wide RNAi screens identify cytokinesis inhibitors and targets. *PLoS biology*. 2:e379.

Eggert, U.S., T.J. Mitchison, and C.M. Field. 2006. Animal cytokinesis: from parts list to mechanisms. *Annual review of biochemistry*. 75:543-566.

Eikenes, A.H., A. Brech, H. Stenmark, and K. Haglund. 2013. Spatiotemporal control of Cindr at ring canals during incomplete cytokinesis in the Drosophila male germline. *Developmental biology*. 377:9-20.

Eikenes, A.H., L. Malerod, A.L. Christensen, C.B. Steen, J. Mathieu, I.P. Nezis, K. Liestol, J.R. Huynh, H. Stenmark, and K. Haglund. 2015. ALIX and ESCRT-III coordinately control cytokinetic abscission during germline stem cell division in vivo. *PLoS genetics*. 11:e1004904.

El Amine, N., A. Kechad, S. Jananji, and G.R.X. Hickson. 2013. Opposing actions of septins and Sticky on Anillin promote the transition from contractile to midbody ring. *Journal of Cell Biology*. 203:487-504.

Elia, N., R. Sougrat, T.A. Spurlin, J.H. Hurley, and J. Lippincott-Schwartz. 2011. Dynamics of endosomal sorting complex required for transport (ESCRT) machinery during cytokinesis and its role in abscission. *Proceedings of the National Academy of Sciences of the United States of America*. 108:4846-4851.

Engel, F.B., M. Schebesta, and M.T. Keating. 2006. Anillin localization defect in cardiomyocyte binucleation. *Journal of molecular and cellular cardiology*. 41:601-612.

Estey, M.P., C. Di Ciano-Oliveira, C.D. Froese, M.T. Bejide, and W.S. Trimble. 2010. Distinct roles of septins in cytokinesis: SEPT9 mediates midbody abscission. *The Journal of cell biology*. 191:741-749.

Ettinger, A.W., M. Wilsch-Brauninger, A.M. Marzesco, M. Bickle, A. Lohmann, Z. Maliga, J. Karbanova, D. Corbeil, A.A. Hyman, and W.B. Huttner. 2011. Proliferating versus differentiating stem and cancer cells exhibit distinct midbody-release behaviour. *Nat Commun*. 2:503.

Fawcett, D.W. 1961. Intercellular bridges. *Experimental cell research*. Suppl 8:174-187.

Fawcett, D.W. 1970. A comparative view of sperm ultrastructure. *Biology of reproduction*. 2:Suppl 2:90-127.

Fawcett, D.W. 1973. Observations on the organization of the interstitial tissue of the testis and on the occluding cell junctions in the seminiferous epithelium. *Advances in the biosciences*. 10:83-99.

Fawcett, D.W., S. Ito, and D. Slautterback. 1959. The occurrence of intercellular bridges in groups of cells exhibiting synchronous differentiation. *The Journal of biophysical and biochemical cytology*. 5:453-460.

Fededa, J.P., and D.W. Gerlich. 2012. Molecular control of animal cell cytokinesis. *Nat Cell Biol*. 14:440-447.

Felix, M.A., and F. Duveau. 2012. Population dynamics and habitat sharing of natural populations of Caenorhabditis elegans and C. briggsae. *BMC biology*. 10:59.

Field, C.M., and B.M. Alberts. 1995. Anillin, a contractile ring protein that cycles from the nucleus to the cell cortex. *The Journal of cell biology*. 131:165-178.

Field, C.M., M. Coughlin, S. Doberstein, T. Marty, and W. Sullivan. 2005. Characterization of anillin mutants reveals essential roles in septin localization and plasma membrane integrity. *Development*. 132:2849-2860.

Fielding, A.B., E. Schonteich, J. Matheson, G. Wilson, X. Yu, G.R. Hickson, S. Srivastava, S.A. Baldwin, R. Prekeris, and G.W. Gould. 2005. Rab11-FIP3 and FIP4 interact with Arf6 and the exocyst to control membrane traffic in cytokinesis. *The EMBO journal*. 24:3389-3399.

Fiil, A. 1978. Follicle Cell Bridges in Mosquito Ovary - Syncytia Formation and Bridge Morphology. *Journal of cell science*. 31:137-143.

Fire, A., S. Xu, M.K. Montgomery, S.A. Kostas, S.E. Driver, and C.C. Mello. 1998. Potent and specific genetic interference by double-stranded RNA in Caenorhabditis elegans. *Nature*. 391:806-811.

Fishkind, D.J., and Y.L. Wang. 1993. Orientation and three-dimensional organization of actin filaments in dividing cultured cells. *The Journal of cell biology*. 123:837-848.

Foor, W.E. 1967. Ultrastructural aspects of oocyte development and shell formation in Ascaris lumbricoides. *The Journal of parasitology*. 53:1245-1261.
Fotopoulos, N., D. Wernike, Y. Chen, N. Makil, A. Marte, and A. Piekny. 2013. Caenorhabditis elegans anillin (ani-1) regulates neuroblast cytokinesis and epidermal morphogenesis during embryonic development. *Developmental biology*. 383:61-74.
Francis, R., M.K. Barton, J. Kimble, and T. Schedl. 1995. gld-1, a tumor suppressor gene required for oocyte development in Caenorhabditis elegans. *Genetics*. 139:579-606.
Fujiwara, T., M. Bandi, M. Nitta, E.V. Ivanova, R.T. Bronson, and D. Pellman. 2005. Cytokinesis failure generating tetraploids promotes tumorigenesis in p53-null cells. *Nature*. 437:1043-1047.
Fukuyama, M., A.E. Rougvie, and J.H. Rothman. 2006. C. elegans DAF-18/PTEN mediates nutrient-dependent arrest of cell cycle and growth in the germline. *Current biology : CB*. 16:773-779.
Gachet, Y., S. Tournier, J.B. Millar, and J.S. Hyams. 2004. Mechanism controlling perpendicular alignment of the spindle to the axis of cell division in fission yeast. *The EMBO journal*. 23:1289-1300.
Galko, M.J., and M.A. Krasnow. 2004. Cellular and genetic analysis of wound healing in Drosophila larvae. *PLoS biology*. 2:E239.
Ganem, N.J., and D. Pellman. 2007. Limiting the proliferation of polyploid cells. *Cell*. 131:437-440.
Gao, P., and J. Zheng. 2011. Oncogenic virus-mediated cell fusion: new insights into initiation and progression of oncogenic viruses--related cancers. *Cancer letters*. 303:1-8.
Gao, Y., E. Smith, E. Ker, P. Campbell, E.C. Cheng, S. Zou, S. Lin, L. Wang, S. Halene, and D.S. Krause. 2012. Role of RhoA-specific guanine exchange factors in regulation of endomitosis in megakaryocytes. *Developmental cell*. 22:573-584.
Geddis, A.E., and K. Kaushansky. 2006. Endomitotic megakaryocytes form a midzone in anaphase but have a deficiency in cleavage furrow formation. *Cell cycle*. 5:538-545.
Gentric, G., and C. Desdouets. 2014. Polyploidization in liver tissue. *The American journal of pathology*. 184:322-331.
Gentric, G., C. Desdouets, and S. Celton-Morizur. 2012. Hepatocytes polyploidization and cell cycle control in liver physiopathology. *International journal of hepatology*. 2012:282430.
Giorgi, F. 1978. Intercellular bridges in ovarian follicle cells of Drosophila melanogaster. *Cell and tissue research*. 186:413-422.
Glass, N.L., D.J. Jacobson, and P.K. Shiu. 2000. The genetics of hyphal fusion and vegetative incompatibility in filamentous ascomycete fungi. *Annual review of genetics*. 34:165-186.
Glotzer, M. 1997a. Cytokinesis. *Current biology : CB*. 7:R274-276.
Glotzer, M. 1997b. The mechanism and control of cytokinesis. *Current opinion in cell biology*. 9:815-823.
Glotzer, M. 2001. Animal cell cytokinesis. *Annual review of cell and developmental biology*. 17:351-386.
Glotzer, M. 2005. The molecular requirements for cytokinesis. *Science*. 307:1735-1739.
Glotzer, M. 2009a. The 3Ms of central spindle assembly: microtubules, motors and MAPs. *Nat Rev Mol Cell Bio*. 10:9-20.
Glotzer, M. 2009b. Cytokinesis: GAP gap. *Current biology : CB*. 19:R162-165.

Gondos, B., and L.A. Conner. 1973. Ultrastructure of developing germ cells in the fetal rabbit testis. *The American journal of anatomy*. 136:23-42.

Goodyer, W., S. Kaitna, F. Couteau, J.D. Ward, S.J. Boulton, and M. Zetka. 2008. HTP-3 links DSB formation with homolog pairing and crossing over during C. elegans meiosis. *Developmental cell*. 14:263-274.

Green, R.A., H.L. Kao, A. Audhya, S. Arur, J.R. Mayers, H.N. Fridolfsson, M. Schulman, S. Schloissnig, S. Niessen, K. Laband, S. Wang, D.A. Starr, A.A. Hyman, T. Schedl, A. Desai, F. Piano, K.C. Gunsalus, and K. Oegema. 2011. A high-resolution C. elegans essential gene network based on phenotypic profiling of a complex tissue. *Cell*. 145:470-482.

Green, R.A., J.R. Mayers, S.H. Wang, L. Lewellyn, A. Desai, A. Audhya, and K. Oegema. 2013. The midbody ring scaffolds the abscission machinery in the absence of midbody microtubules. *Journal of Cell Biology*. 203:505-520.

Green, R.A., E. Paluch, and K. Oegema. 2012. Cytokinesis in animal cells. *Annual review of cell and developmental biology*. 28:29-58.

Greenbaum, M.P., N. Iwamori, J.E. Agno, and M.M. Matzuk. 2009. Mouse TEX14 is required for embryonic germ cell intercellular bridges but not female fertility. *Biology of reproduction*. 80:449-457.

Greenbaum, M.P., T. Iwamori, G.M. Buchold, and M.M. Matzuk. 2011. Germ cell intercellular bridges. *Cold Spring Harbor perspectives in biology*. 3:a005850.

Greenbaum, M.P., L. Ma, and M.M. Matzuk. 2007. Conversion of midbodies into germ cell intercellular bridges. *Developmental biology*. 305:389-396.

Greenbaum, M.P., W. Yan, M.H. Wu, Y.N. Lin, J.E. Agno, M. Sharma, R.E. Braun, A. Rajkovic, and M.M. Matzuk. 2006. TEX14 is essential for intercellular bridges and fertility in male mice. *Proceedings of the National Academy of Sciences of the United States of America*. 103:4982-4987.

Gregory, S.L., S. Ebrahimi, J. Milverton, W.M. Jones, A. Bejsovec, and R. Saint. 2008. Cell division requires a direct link between microtubule-bound RacGAP and Anillin in the contractile ring. *Current biology : CB*. 18:25-29.

Gromley, A., C. Yeaman, J. Rosa, S. Redick, C.T. Chen, S. Mirabelle, M. Guha, J. Sillibourne, and S.J. Doxsey. 2005. Centriolin anchoring of exocyst and SNARE complexes at the midbody is required for secretory-vesicle-mediated abscission. *Cell*. 123:75-87.

Guidotti, J.E., O. Bregerie, A. Robert, P. Debey, C. Brechot, and C. Desdouets. 2003. Liver cell polyploidization: a pivotal role for binuclear hepatocytes. *The Journal of biological chemistry*. 278:19095-19101.

Guizetti, J., L. Schermelleh, J. Mantler, S. Maar, I. Poser, H. Leonhardt, T. Muller-Reichert, and D.W. Gerlich. 2011. Cortical Constriction During Abscission Involves Helices of ESCRT-III-Dependent Filaments. *Science*. 331:1616-1620.

Guo, G.Q., and G.C. Zheng. 2004. Hypotheses for the functions of intercellular bridges in male germ cell development and its cellular mechanisms. *Journal of theoretical biology*. 229:139-146.

Gupta, S. 2000. Hepatic polyploidy and liver growth control. *Seminars in cancer biology*. 10:161-171.

Haglund, K., I.P. Nezis, D. Lemus, C. Grabbe, J. Wesche, K. Liestol, I. Dikic, R. Palmer, and H. Stenmark. 2010. Cindr interacts with anillin to control cytokinesis in Drosophila

melanogaster. *Current biology : CB*. 20:944-950.
Haglund, K., I.P. Nezis, and H. Stenmark. 2011. Structure and functions of stable intercellular bridges formed by incomplete cytokinesis during development. *Communicative & integrative biology*. 4:1-9.
Hall, D.H., V.P. Winfrey, G. Blaeuer, L.H. Hoffman, T. Furuta, K.L. Rose, O. Hobert, and D. Greenstein. 1999. Ultrastructural features of the adult hermaphrodite gonad of Caenorhabditis elegans: relations between the germ line and soma. *Developmental biology*. 212:101-123.
Hanson, P.I., R. Roth, Y. Lin, and J.E. Heuser. 2008. Plasma membrane deformation by circular arrays of ESCRT-III protein filaments. *Journal of Cell Biology*. 180:389-402.
Harrell, J.R., and B. Goldstein. 2011. Internalization of multiple cells during C. elegans gastrulation depends on common cytoskeletal mechanisms but different cell polarity and cell fate regulators. *Developmental biology*. 350:1-12.
Hickson, G.R., and P.H. O'Farrell. 2008a. Anillin: a pivotal organizer of the cytokinetic machinery. *Biochemical Society transactions*. 36:439-441.
Hickson, G.R.X., and P.H. O'farrell. 2008b. Rho-dependent control of anillin behavior during cytokinesis. *Journal of Cell Biology*. 180:285-294.
Hime, G.R., J.A. Brill, and M.T. Fuller. 1996. Assembly of ring canals in the male germ line from structural components of the contractile ring. *Journal of cell science*. 109 (Pt 12):2779-2788.
Hipp, J., and A. Atala. 2004. Tissue engineering, stem cells, cloning, and parthenogenesis: new paradigms for therapy. *Journal of experimental & clinical assisted reproduction*. 1:3.
Hirsh, D., D. Oppenheim, and M. Klass. 1976. Development of the reproductive system of Caenorhabditis elegans. *Developmental biology*. 49:200-219.
His, W., Ueber Zellen und Syncytienbildung. Studien an Salamander Keim. Abhandl. der Math.-Physik. Classe der Kgl. Sach. Gesells. der Wissen-schaften, Bd. XXIV, 1898.
Hodgkin, J., H.R. Horvitz, and S. Brenner. 1979. Nondisjunction Mutants of the Nematode CAENORHABDITIS ELEGANS. *Genetics*. 91:67-94.
Hu, C.K., M. Coughlin, and T.J. Mitchison. 2012. Midbody assembly and its regulation during cytokinesis. *Molecular biology of the cell*. 23:1024-1034.
Hubbard, E.J., and D. Greenstein. 2000. The Caenorhabditis elegans gonad: a test tube for cell and developmental biology. *Developmental dynamics : an official publication of the American Association of Anatomists*. 218:2-22.
Huckins, C., and E.F. Oakberg. 1978. Morphological and quantitative analysis of spermatogonia in mouse testes using whole mounted seminiferous tubules. II. The irradiated testes. *The Anatomical record*. 192:529-542.
Huppertz, B., H.G. Frank, J.C.P. Kingdom, F. Reister, and P. Kaufmann. 1998. Villous cytotrophoblast regulation of the syncytial apoptotic cascade in the human placenta. *Histochem Cell Biol*. 110:495-508.
Issman-Zecharya, N., and O. Schuldiner. 2014. The PI3K class III complex promotes axon pruning by downregulating a Ptc-derived signal via endosome-lysosomal degradation. *Developmental cell*. 31:461-473.
Iwamori, T., N. Iwamori, L. Ma, M.A. Edson, M.P. Greenbaum, and M.M. Matzuk. 2010. TEX14 interacts with CEP55 to block cell abscission. *Molecular and cellular biology*.

30:2280-2292.
Jaglarz, M.K., and K.R. Howard. 1995. The active migration of Drosophila primordial germ cells. *Development*. 121:3495-3503.
Jantsch-Plunger, V., P. Gonczy, A. Romano, H. Schnabel, D. Hamill, R. Schnabel, A.A. Hyman, and M. Glotzer. 2000. CYK-4: A Rho family gtpase activating protein (GAP) required for central spindle formation and cytokinesis. *The Journal of cell biology*. 149:1391-1404.
Jaramillo-Lambert, A., M. Ellefson, A.M. Villeneuve, and J. Engebrecht. 2007. Differential timing of S phases, X chromosome replication, and meiotic prophase in the C. elegans germ line. *Developmental biology*. 308:206-221.
Jimenez, A.J., P. Maiuri, J. Lafaurie-Janvore, S. Divoux, M. Piel, and F. Perez. 2014. ESCRT machinery is required for plasma membrane repair. *Science*. 343:1247136.
Jimenez, G., A. Gonzalez-Reyes, and J. Casanova. 2002. Cell surface proteins Nasrat and Polehole stabilize the Torso-like extracellular determinant in Drosophila oogenesis. *Genes & development*. 16:913-918.
Joo, E., M.C. Surka, and W.S. Trimble. 2007. Mammalian SEPT2 is required for scaffolding nonmuscle myosin II and its kinases. *Developmental cell*. 13:677-690.
Kamath, R.S., M. Martinez-Campos, P. Zipperlen, A.G. Fraser, and J. Ahringer. 2001. Effectiveness of specific RNA-mediated interference through ingested double-stranded RNA in Caenorhabditis elegans. *Genome biology*. 2:RESEARCH0002.
Katzmann, D.J., M. Babst, and S.D. Emr. 2001. Ubiquitin-dependent sorting into the multivesicular body pathway requires the function of a conserved endosomal protein sorting complex, ESCRT-I. *Cell*. 106:145-155.
Kaufman, M.H. 1991. New Insights into Triploidy and Tetraploidy, from an Analysis of Model Systems for These Conditions. *Hum Reprod*. 6:8-16.
Kawasaki, I., Y.H. Shim, J. Kirchner, J. Kaminker, W.B. Wood, and S. Strome. 1998. PGL-1, a predicted RNA-binding component of germ granules, is essential for fertility in C. elegans. *Cell*. 94:635-645.
Kechad, A., S. Jananji, Y. Ruella, and G.R.X. Hickson. 2012. Anillin Acts as a Bifunctional Linker Coordinating Midbody Ring Biogenesis during Cytokinesis. *Current Biology*. 22:197-203.
Kim, J.H., Y.X. Ren, W.P. Ng, S. Li, S.M. Son, Y.S. Kee, S.L. Zhang, G.F. Zhang, D.A. Fletcher, D.N. Robinson, and E.H. Chen. 2015. Mechanical Tension Drives Cell Membrane Fusion. *Developmental cell*. 32:561-573.
Kim, S., K. Shilagardi, S.L. Zhang, S.N. Hong, K.L. Sens, J. Bo, G.A. Gonzalez, and E.H. Chen. 2007. A critical function for the actin cytoskeleton in targeted exocytosis of prefusion vesicles during myoblast fusion. *Developmental cell*. 12:571-586.
Kim, S., C. Spike, and D. Greenstein. 2013. Control of oocyte growth and meiotic maturation in Caenorhabditis elegans. *Advances in experimental medicine and biology*. 757:277-320.
Kimble, J., and S.L. Crittenden. 2007. Controls of germline stem cells, entry into meiosis, and the sperm/oocyte decision in Caenorhabditis elegans. *Annual review of cell and developmental biology*. 23:405-433.
Kimble, J., and D. Hirsh. 1979. The postembryonic cell lineages of the hermaphrodite and male gonads in Caenorhabditis elegans. *Developmental biology*. 70:396-417.
Kimble, J.E., and J.G. White. 1981. On the control of germ cell development in

Caenorhabditis elegans. *Developmental biology*. 81:208-219.
Kimura, K., T. Tsuji, Y. Takada, T. Miki, and S. Narumiya. 2000. Accumulation of GTP-bound RhoA during cytokinesis and a critical role of ECT2 in this accumulation. *The Journal of biological chemistry*. 275:17233-17236.
Kinoshita, M. 2003. Assembly of mammalian septins. *Journal of biochemistry*. 134:491-496.
Kloc, M., S. Bilinski, M.T. Dougherty, E.M. Brey, and L.D. Etkin. 2004. Formation, architecture and polarity of female germline cyst in Xenopus. *Developmental biology*. 266:43-61.
Knudsen, K.A., and A.F. Horwitz. 1977. Tandem events in myoblast fusion. *Developmental biology*. 58:328-338.
Kocherlakota, K.S., J. Wu, J. McDermott, and S.M. Abmayr. 2009. Analysis of the Cell Adhesion Molecule Sticks-and-Stones Reveals Multiple Redundant Functional Domains, Protein-Interaction Motifs and Phosphorylated Tyrosines That Direct Myoblast Fusion in Drosophila melanogaster (vol 178, pg 1371, 2008). *Genetics*. 183:755-755.
Kramerova, I.A., and A.A. Kramerov. 1999. Mucinoprotein is a universal constituent of stable intercellular bridges in Drosophila melanogaster germ line and somatic cells. *Developmental dynamics : an official publication of the American Association of Anatomists*. 216:349-360.
Kudryavtsev, B.N., M.V. Kudryavtseva, G.A. Sakuta, and G.I. Stein. 1993. Human hepatocyte polyploidization kinetics in the course of life cycle. *Virchows Archiv. B, Cell pathology including molecular pathology*. 64:387-393.
Kuo, T.C., C.T. Chen, D. Baron, T.T. Onder, S. Loewer, S. Almeida, C.M. Weismann, P. Xu, J.M. Houghton, F.B. Gao, G.Q. Daley, and S. Doxsey. 2011. Midbody accumulation through evasion of autophagy contributes to cellular reprogramming and tumorigenicity (vol 13, pg 1214, 2011). *Nat Cell Biol*. 13:1467-1467.
Lacroix, B., and A.S. Maddox. 2012. Cytokinesis, ploidy and aneuploidy. *The Journal of pathology*. 226:338-351.
Lafaurie-Janvore, J., P. Maiuri, I. Wang, M. Pinot, J.B. Manneville, T. Betz, M. Balland, and M. Piel. 2013. ESCRT-III assembly and cytokinetic abscission are induced by tension release in the intercellular bridge. *Science*. 339:1625-1629.
Lemmon, M.A. 2004. Pleckstrin homology domains: not just for phosphoinositides. *Biochemical Society transactions*. 32:707-711.
Lemmon, M.A., K.M. Ferguson, and C.S. Abrams. 2002. Pleckstrin homology domains and the cytoskeleton. *Febs Lett*. 513:71-76.
Leys, S.P., E. Cheung, and N. Boury-Esnault. 2006. Embryogenesis in the glass sponge Oopsacas minuta: Formation of syncytia by fusion of blastomeres. *Integr Comp Biol*. 46:104-117.
Li, F., X. Wang, J.M. Capasso, and A.M. Gerdes. 1996. Rapid transition of cardiac myocytes from hyperplasia to hypertrophy during postnatal development. *Journal of molecular and cellular cardiology*. 28:1737-1746.
Li, F., X. Wang, and A.M. Gerdes. 1997. Formation of binucleated cardiac myocytes in rat heart: II. Cytoskeletal organisation. *Journal of molecular and cellular cardiology*. 29:1553-1565.
Lin, H., and A.C. Spradling. 1993. Germline stem cell division and egg chamber development in transplanted Drosophila germaria. *Developmental biology*. 159:140-152.

Lin, H., and A.C. Spradling. 1995. Fusome asymmetry and oocyte determination in Drosophila. *Developmental genetics*. 16:6-12.
Lin, H., L. Yue, and A.C. Spradling. 1994. The Drosophila fusome, a germline-specific organelle, contains membrane skeletal proteins and functions in cyst formation. *Development*. 120:947-956.
Liu, J., G.D. Fairn, D.F. Ceccarelli, F. Sicheri, and A. Wilde. 2012. Cleavage furrow organization requires PIP(2)-mediated recruitment of anillin. *Current biology : CB*. 22:64-69.
Loncle, N., M. Agromayor, J. Martin-Serrano, and D.W. Williams. 2015. An ESCRT module is required for neuron pruning. *Scientific reports*. 5:8461.
Lord, M., E. Laves, and T.D. Pollard. 2005. Cytokinesis depends on the motor domains of myosin-II in fission yeast but not in budding yeast. *Molecular biology of the cell*. 16:5346-5355.
Lordier, L., A. Jalil, F. Aurade, F. Larbret, J. Larghero, N. Debili, W. Vainchenker, and Y. Chang. 2008. Megakaryocyte endomitosis is a failure of late cytokinesis related to defects in the contractile ring and Rho/Rock signaling. *Blood*. 112:3164-3174.
Losick, V.P., D.T. Fox, and A.C. Spradling. 2013. Polyploidization and cell fusion contribute to wound healing in the adult Drosophila epithelium. *Current biology : CB*. 23:2224-2232.
Lu, J., W.L. Dentler, and E.A. Lundquist. 2008. FLI-1 Flightless-1 and LET-60 Ras control germ line morphogenesis in C. elegans. *BMC developmental biology*. 8:54.
Lui, D.Y., and M.P. Colaiacovo. 2013. Meiotic development in Caenorhabditis elegans. *Advances in experimental medicine and biology*. 757:133-170.
Ma, X., M. Kovacs, M.A. Conti, A. Wang, Y. Zhang, J.R. Sellers, and R.S. Adelstein. 2012. Nonmuscle myosin II exerts tension but does not translocate actin in vertebrate cytokinesis. *Proceedings of the National Academy of Sciences of the United States of America*. 109:4509-4514.
MacQueen, A.J., M.P. Colaiacovo, K. McDonald, and A.M. Villeneuve. 2002. Synapsis-dependent and -independent mechanisms stabilize homolog pairing during meiotic prophase in C. elegans. *Genes & development*. 16:2428-2442.
Madaule, P., M. Eda, N. Watanabe, K. Fujisawa, T. Matsuoka, H. Bito, T. Ishizaki, and S. Narumiya. 1998. Role of citron kinase as a target of the small GTPase Rho in cytokinesis. *Nature*. 394:491-494.
Maddox, A.S., B. Habermann, A. Desai, and K. Oegema. 2005a. Distinct roles for two *C. elegans* anillins in the gonad and early embryo. *Development*. 132:2837-2848.
Maddox, A.S., B. Habermann, A. Desai, and K. Oegema. 2005b. Distinct roles for two C. elegans anillins in the gonad and early embryo. *Development*. 132:2837-2848.
Maddox, A.S., L. Lewellyn, A. Desai, and K. Oegema. 2007. Anillin and the septins promote asymmetric ingression of the cytokinetic furrow. *Developmental cell*. 12:827-835.
Mahajan-Miklos, S., and L. Cooley. 1994. Intercellular cytoplasm transport during Drosophila oogenesis. *Developmental biology*. 165:336-351.
Mahowald, A.P., and Strasshe.Jm. 1970. Intercellular Migration of Centrioles in Germarium of Drosophila-Melanogaster - an Electron Microscopic Study. *Journal of Cell Biology*. 45:306-&.
Mandato, C.A., and W.M. Bement. 2001. Contraction and polymerization cooperate to assemble and close actomyosin rings around Xenopus oocyte wounds. *The Journal of*

cell biology. 154:785-797.
Margall-Ducos, G., S. Celton-Morizur, D. Couton, O. Bregerie, and C. Desdouets. 2007. Liver tetraploidization is controlled by a new process of incomplete cytokinesis. *Journal of cell science*. 120:3633-3639.
Massarwa, R., S. Carmon, B.Z. Shilo, and E.D. Schejter. 2007. WIP/WASp-based actin-polymerization machinery is essential for myoblast fusion in Drosophila. *Developmental cell*. 12:557-569.
Masterson, J. 1994. Stomatal size in fossil plants: evidence for polyploidy in majority of angiosperms. *Science*. 264:421-424.
Matsumura, F. 2005. Regulation of myosin II during cytokinesis in higher eukaryotes. *Trends in cell biology*. 15:371-377.
Matuliene, J., and R. Kuriyama. 2002. Kinesin-like protein CHO1 is required for the formation of midbody matrix and the completion of cytokinesis in mammalian cells. *Molecular biology of the cell*. 13:1832-1845.
Matuliene, J., and R. Kuriyama. 2004. Role of the midbody matrix in cytokinesis: RNAi and genetic rescue analysis of the mammalian motor protein CHO1. *Molecular biology of the cell*. 15:3083-3094.
Maupin, P., and T.D. Pollard. 1986. Arrangement of actin filaments and myosin-like filaments in the contractile ring and of actin-like filaments in the mitotic spindle of dividing HeLa cells. *Journal of ultrastructure and molecular structure research*. 94:92-103.
McCarter, J., B. Bartlett, T. Dang, and T. Schedl. 1999. On the control of oocyte meiotic maturation and ovulation in Caenorhabditis elegans. *Developmental biology*. 205:111-128.
McDonald, B., and J. Martin-Serrano. 2009. No strings attached: the ESCRT machinery in viral budding and cytokinesis. *Journal of cell science*. 122:2167-2177.
McLean, P.F., and L. Cooley. 2014. Bridging the divide: illuminating the path of intercellular exchange through ring canals. *Fly*. 8:13-18.
Mello, C.C., J.M. Kramer, D. Stinchcomb, and V. Ambros. 1991. Efficient gene transfer in C.elegans: extrachromosomal maintenance and integration of transforming sequences. *The EMBO journal*. 10:3959-3970.
Mendell, J.E., K.D. Clements, J.H. Choat, and E.R. Angert. 2008. Extreme polyploidy in a large bacterium. *Proceedings of the National Academy of Sciences of the United States of America*. 105:6730-6734.
Mendes Pinto, I., B. Rubinstein, and R. Li. 2013. Force to divide: structural and mechanical requirements for actomyosin ring contraction. *Biophysical journal*. 105:547-554.
Meola, S.M., H.H. Mollenhauer, and J.M. Thompson. 1977. Cytoplasmic Bridges within Follicular-Epithelium of Ovarioles of 2 Diptera, Aedes-Aegypti and Stomoxys-Calcitrans. *J Morphol*. 153:81-85.
Merritt, C., D. Rasoloson, D. Ko, and G. Seydoux. 2008. 3' UTRs are the primary regulators of gene expression in the C. elegans germline. *Current biology : CB*. 18:1476-1482.
Mierzwa, B., and D.W. Gerlich. 2014. Cytokinetic abscission: molecular mechanisms and temporal control. *Developmental cell*. 31:525-538.
Miller, K.G., C.M. Field, and B.M. Alberts. 1989. Actin-binding proteins from Drosophila embryos: a complex network of interacting proteins detected by F-actin affinity chromatography. *The Journal of cell biology*. 109:2963-2975.
Minestrini, G., E. Mathe, and D.M. Glover. 2002. Domains of the Pavarotti kinesin-like

protein that direct its subcellular distribution: effects of mislocalisation on the tubulin and actin cytoskeleton during Drosophila oogenesis. *Journal of cell science*. 115:725-736.

Mishima, M., S. Kaitna, and M. Glotzer. 2002. Central spindle assembly and cytokinesis require a kinesin-like protein/RhoGAP complex with microtubule bundling activity. *Developmental cell*. 2:41-54.

Morales, C.R., S. Lefrancois, V. Chennathukuzhi, M. El-Alfy, X. Wu, J. Yang, G.L. Gerton, and N.B. Hecht. 2002. A TB-RBP and Ter ATPase complex accompanies specific mRNAs from nuclei through the nuclear pores and into intercellular bridges in mouse male germ cells. *Developmental biology*. 246:480-494.

Morita, E., V. Sandrin, H.Y. Chung, S.G. Morham, S.P. Gygi, C.K. Rodesch, and W.I. Sundquist. 2007. Human ESCRT and ALIX proteins interact with proteins of the midbody and function in cytokinesis. *The EMBO journal*. 26:4215-4227.

Mullins, J.M., and J.J. Biesele. 1977. Terminal phase of cytokinesis in D-98s cells. *The Journal of cell biology*. 73:672-684.

Nakeff, A., and B. Maat. 1974. Separation of megakaryocytes from mouse bone marrow by velocity sedimentation. *Blood*. 43:591-595.

Narbonne, P., V. Hyenne, S. Li, J.C. Labbe, and R. Roy. 2010. Differential requirements for STRAD in LKB1-dependent functions in C. elegans. *Development*. 137:661-670.

Neujahr, R., C. Heizer, and G. Gerisch. 1997. Myosin II-independent processes in mitotic cells of Dictyostelium discoideum: redistribution of the nuclei, re-arrangement of the actin system and formation of the cleavage furrow. *Journal of cell science*. 110 (Pt 2):123-137.

Nguyen, H.G., and K. Ravid. 2006. Tetraploidy/aneuploidy and stem cells in cancer promotion: The role of chromosome passenger proteins. *Journal of cellular physiology*. 208:12-22.

Nguyen, T.Q., H. Sawa, H. Okano, and J.G. White. 2000. The C. elegans septin genes, unc-59 and unc-61, are required for normal postembryonic cytokineses and morphogenesis but have no essential function in embryogenesis. *Journal of cell science*. 113 Pt 21:3825-3837.

Nishimura, Y., and S. Yonemura. 2006. Centralspindlin regulates ECT2 and RhoA accumulation at the equatorial cortex during cytokinesis. *Journal of cell science*. 119:104-114.

Nystul, T., and A. Spradling. 2007. An epithelial niche in the Drosophila ovary undergoes long-range stem cell replacement. *Cell stem cell*. 1:277-285.

O'Connell, C.B., S.P. Wheatley, S. Ahmed, and Y.L. Wang. 1999. The small GTP-binding protein rho regulates cortical activities in cultured cells during division. *The Journal of cell biology*. 144:305-313.

Ong, S., C. Foote, and C. Tan. 2010. Mutations of DMYPT cause over constriction of contractile rings and ring canals during Drosophila germline cyst formation. *Developmental biology*. 346:161-169.

Ong, S., and C. Tan. 2010. Germline cyst formation and incomplete cytokinesis during Drosophila melanogaster oogenesis. *Developmental biology*. 337:84-98.

Oren-Suissa, M., and B. Podbilewicz. 2010. Evolution of Programmed Cell Fusion: Common Mechanisms and Distinct Functions. *Dev Dynam*. 239:1515-1528.

Otto, S.P., and J. Whitton. 2000. Polyploid incidence and evolution. *Annual review of*

genetics. 34:401-437.
Paix, A., Y. Wang, H.E. Smith, C.Y. Lee, D. Calidas, T. Lu, J. Smith, H. Schmidt, M.W. Krause, and G. Seydoux. 2014. Scalable and versatile genome editing using linear DNAs with microhomology to Cas9 Sites in Caenorhabditis elegans. *Genetics*. 198:1347-1356.
Pastey, M.K., T.L. Gower, P.W. Spearman, J.E. Crowe, Jr., and B.S. Graham. 2000. A RhoA-derived peptide inhibits syncytium formation induced by respiratory syncytial virus and parainfluenza virus type 3. *Nature medicine*. 6:35-40.
Paweletz, N. 2001. Walther Flemming: pioneer of mitosis research. *Nature reviews. Molecular cell biology*. 2:72-75.
Pazdernik, N., and T. Schedl. 2013. Introduction to germ cell development in Caenorhabditis elegans. *Advances in experimental medicine and biology*. 757:1-16.
Pennarossa, G., S. Maffei, G. Tettamanti, T. Congiu, M. deEguileor, F. Gandolfi, and T.A. Brevini. 2015. Intercellular bridges are essential for human parthenogenetic cell survival. *Mechanisms of development*. 136:30-39.
Pepling, M.E., M. de Cuevas, and A.C. Spradling. 1999. Germline cysts: a conserved phase of germ cell development? *Trends in cell biology*. 9:257-262.
Pepling, M.E., and A.C. Spradling. 1998. Female mouse germ cells form synchronously dividing cysts. *Development*. 125:3323-3328.
Pepper, A.S., T.W. Lo, D.J. Killian, D.H. Hall, and E.J. Hubbard. 2003. The establishment of Caenorhabditis elegans germline pattern is controlled by overlapping proximal and distal somatic gonad signals. *Developmental biology*. 259:336-350.
Piekny, A., M. Werner, and M. Glotzer. 2005. Cytokinesis: welcome to the Rho zone. *Trends in cell biology*. 15:651-658.
Piekny, A.J., and M. Glotzer. 2008. Anillin is a scaffold protein that links RhoA, actin, and myosin during cytokinesis. *Current biology : CB*. 18:30-36.
Piekny, A.J., and A.S. Maddox. 2010. The myriad roles of Anillin during cytokinesis. *Seminars in cell & developmental biology*. 21:881-891.
Piekny, A.J., and P.E. Mains. 2002. Rho-binding kinase (LET-502) and myosin phosphatase (MEL-11) regulate cytokinesis in the early Caenorhabditis elegans embryo. *Journal of cell science*. 115:2271-2282.
Piel, M., J. Nordberg, U. Euteneuer, and M. Bornens. 2001. Centrosome-dependent exit of cytokinesis in animal cells. *Science*. 291:1550-1553.
Plachno, B.J., and P. Swiatek. 2011. Syncytia in plants: cell fusion in endosperm-placental syncytium formation in Utricularia (Lentibulariaceae). *Protoplasma*. 248:425-435.
Plachno, B.J., P. Swiatek, H. Sas-Nowosielska, and M. Kozieradzka-Kiszkurno. 2013. Organisation of the endosperm and endosperm-placenta syncytia in bladderworts (Utricularia, Lentibulariaceae) with emphasis on the microtubule arrangement. *Protoplasma*. 250:863-873.
Podbilewicz, B. 2006. Cell fusion. *WormBook : the online review of C. elegans biology*:1-32.
Pollard, T.D. 2004. Ray Rappaport chronology: Twenty-five years of seminal papers on cytokinesis in the Journal of Experimental Zoology. *Journal of experimental zoology. Part A, Comparative experimental biology*. 301:9-14.
Pollard, T.D. 2010. Mechanics of cytokinesis in eukaryotes. *Current opinion in cell biology*. 22:50-56.
Pollarolo, G., J.G. Schulz, S. Munck, and C.G. Dotti. 2011. Cytokinesis remnants define first

neuronal asymmetry in vivo. *Nature neuroscience*. 14:1525-1533.
Potgens, A.J.G., U. Schmitz, P. Bose, A. Versmold, P. Kaufmann, and H.G. Frank. 2002. Mechanisms of syncytial fusion: A review. *Placenta*. 23:S107-S113.
Prokopenko, S.N., A. Brumby, L. O'Keefe, L. Prior, Y. He, R. Saint, and H.J. Bellen. 1999. A putative exchange factor for Rho1 GTPase is required for initiation of cytokinesis in Drosophila. *Genes & development*. 13:2301-2314.
Ramamurty, P.S., and W. Engels. 1977. Occurrence of intercellular bridges between follicle epithelial cells in the ovary of Apis mellifica queens. *Journal of cell science*. 24:195-202.
Rappaport, R. 1961. Experiments Concerning Cleavage Stimulus in Sand Dollar Eggs. *J Exp Zool*. 148:81-&.
Rappaport, R. 1985. Repeated furrow formation from a single mitotic apparatus in cylindrical sand dollar eggs. *J Exp Zool*. 234:167-171.
Rappaport, R., and B.N. Rappaport. 1985. Surface Contractile Activity Associated with Isolated Asters in Cylindrical Sand Dollar Eggs. *J Exp Zool*. 235:217-226.
Rebecchi, M.J., and S. Scarlata. 1998. Pleckstrin homology domains: a common fold with diverse functions. *Annual review of biophysics and biomolecular structure*. 27:503-528.
Reichl, E.M., Y. Ren, M.K. Morphew, M. Delannoy, J.C. Effler, K.D. Girard, S. Divi, P.A. Iglesias, S.C. Kuo, and D.N. Robinson. 2008. Interactions between myosin and actin crosslinkers control cytokinesis contractility dynamics and mechanics. *Current biology : CB*. 18:471-480.
Ren, H.P., and L.D. Russell. 1991. Clonal development of interconnected germ cells in the rat and its relationship to the segmental and subsegmental organization of spermatogenesis. *The American journal of anatomy*. 192:121-128.
Renshaw, M.J., J. Liu, B.D. Lavoie, and A. Wilde. 2014. Anillin-dependent organization of septin filaments promotes intercellular bridge elongation and Chmp4B targeting to the abscission site. *Open biology*. 4:130190.
Reyes, C.C., M. Jin, E.B. Breznau, R. Espino, R. Delgado-Gonzalo, A.B. Goryachev, and A.L. Miller. 2014. Anillin regulates cell-cell junction integrity by organizing junctional accumulation of Rho-GTP and actomyosin. *Current biology : CB*. 24:1263-1270.
Richardson, B.E., K. Beckett, S.J. Nowak, and M.K. Baylies. 2007. SCAR/WAVE and Arp2/3 are crucial for cytoskeletal remodeling at the site of myoblast fusion. *Development*. 134:4357-4367.
Robinson, D.N., K. Cant, and L. Cooley. 1994. Morphogenesis of Drosophila ovarian ring canals. *Development*. 120:2015-2025.
Robinson, D.N., and L. Cooley. 1996. Stable intercellular bridges in development: the cytoskeleton lining the tunnel. *Trends in cell biology*. 6:474-479.
Robinson, D.N., and L. Cooley. 1997. Genetic analysis of the actin cytoskeleton in the Drosophila ovary. *Annual review of cell and developmental biology*. 13:147-170.
Rohrschneider, M.R., and J. Nance. 2013. The union of somatic gonad precursors and primordial germ cells during Caenorhabditis elegans embryogenesis. *Developmental biology*. 379:139-151.
Rosenblatt, J., M.C. Raff, and L.P. Cramer. 2001. An epithelial cell destined for apoptosis signals its neighbors to extrude it by an actin- and myosin-dependent mechanism. *Current biology : CB*. 11:1847-1857.

Rossman, K.L., C.J. Der, and J. Sondek. 2005. GEF means go: turning on RHO GTPases with guanine nucleotide-exchange factors. *Nature reviews. Molecular cell biology*. 6:167-180.

Ruchaud, S., M. Carmena, and W.C. Earnshaw. 2007. Chromosomal passengers: conducting cell division. *Nature reviews. Molecular cell biology*. 8:798-812.

Ruiz-Gomez, M., N. Coutts, A. Price, M.V. Taylor, and M. Bate. 2000. Drosophila dumbfounded: a myoblast attractant essential for fusion. *Cell*. 102:189-198.

Rumyantsev, P.P. 1977. Interrelations of the proliferation and differentiation processes during cardiact myogenesis and regeneration. *International review of cytology*. 51:186-273.

Rushton, E., R. Drysdale, S.M. Abmayr, A.M. Michelson, and M. Bate. 1995. Mutations in a novel gene, myoblast city, provide evidence in support of the founder cell hypothesis for Drosophila muscle development. *Development*. 121:1979-1988.

Russell, L.D., A.W. Vogl, and J.E. Weber. 1987. Actin localization in male germ cell intercellular bridges in the rat and ground squirrel and disruption of bridges by cytochalasin D. *The American journal of anatomy*. 180:25-40.

Salles-Passador, I., A. Moisand, V. Planques, and M. Wright. 1991. Physarum plasmodia do contain cytoplasmic microtubules! *Journal of cell science*. 100 (Pt 3):509-520.

Salmon, E.D. 1989. Cytokinesis in animal cells. *Current opinion in cell biology*. 1:541-547.

Sanger, J.M., M.B. Pochapin, and J.W. Sanger. 1985. Midbody sealing after cytokinesis in embryos of the sea urchin Arabacia punctulata. *Cell and tissue research*. 240:287-292.

Sapir, A., J. Choi, E. Leikina, O. Avinoam, C. Valansi, L.V. Chernomordik, A.P. Newman, and B. Podbilewicz. 2007. AFF-1, a FOS-1-regulated fusogen, mediates fusion of the anchor cell in C-elegans. *Developmental cell*. 12:683-698.

Satterwhite, L.L., and T.D. Pollard. 1992. Cytokinesis. *Current opinion in cell biology*. 4:43-52.

Schafer, G., S. Weber, A. Holz, S. Bogdan, S. Schumacher, A. Muller, R. Renkawitz-Pohl, and S.F. Onel. 2007. The Wiskott-Aldrich syndrome protein (WASP) is essential for myoblast fusion in Drosophila. *Developmental biology*. 304:664-674.

Schicktanz, S., and M. Schweda. 2009. "One man's trash is another man's treasure": exploring economic and moral subtexts of the "organ shortage" problem in public views on organ donation. *Journal of medical ethics*. 35:473-476.

Schiel, J.A., C. Childs, and R. Prekeris. 2013. Endocytic transport and cytokinesis: from regulation of the cytoskeleton to midbody inheritance. *Trends in cell biology*. 23:319-327.

Schiel, J.A., and R. Prekeris. 2011. ESCRT or endosomes?: Tales of the separation of two daughter cells. *Communicative & integrative biology*. 4:606-608.

Schiel, J.A., and R. Prekeris. 2013. Membrane dynamics during cytokinesis. *Current opinion in cell biology*. 25:92-98.

Schiel, J.A., G.C. Simon, C. Zaharris, J. Weisz, D. Castle, C.C. Wu, and R. Prekeris. 2012. FIP3-endosome-dependent formation of the secondary ingression mediates ESCRT-III recruitment during cytokinesis. *Nat Cell Biol*. 14:1068-1078.

Schmidt, K., and B.J. Nichols. 2004. A barrier to lateral diffusion in the cleavage furrow of dividing mammalian cells. *Current biology : CB*. 14:1002-1006.

Schroeder, T.E. 1972. The contractile ring. II. Determining its brief existence, volumetric changes, and vital role in cleaving Arbacia eggs. *The Journal of cell biology*. 53:419-434.

Schweitzer, J.K., and C. D'Souza-Schorey. 2004. Finishing the job: cytoskeletal and membrane events bring cytokinesis to an end. *Experimental cell research*. 295:1-8.

Seglen, P.O. 1997. DNA ploidy and autophagic protein degradation as determinants of hepatocellular growth and survival. *Cell Biol Toxicol*. 13:301-315.

Sellitto, C., and R. Kuriyama. 1988. Distribution of a Matrix Component of the Midbody during the Cell-Cycle in Chinese-Hamster Ovary Cells. *Journal of Cell Biology*. 106:431-439.

Selman, G.G., and M.M. Perry. 1970. Ultrastructural changes in the surface layers of the newt's egg in relation to the mechanism of its cleavage. *Journal of cell science*. 6:207-227.

Sens, K.L., S.L. Zhang, P. Jin, R. Duan, G.F. Zhang, F.B. Luo, L. Parachini, and E.H. Chen. 2010. An invasive podosome-like structure promotes fusion pore formation during myoblast fusion. *Journal of Cell Biology*. 191:1013-1027.

Shandala, T., S.L. Gregory, H.E. Dalton, M. Smallhorn, and R. Saint. 2004. Citron kinase is an essential effector of the Pbl-activated Rho signalling pathway in Drosophila melanogaster. *Development*. 131:5053-5063.

Shi, Y.R., K. Barton, A. De Maria, J.M. Petrash, A. Shiels, and S. Bassnett. 2009. The stratified syncytium of the vertebrate lens. *Journal of cell science*. 122:1607-1615.

Singer, A.J., and R.A.F. Clark. 1999. Mechanisms of disease - Cutaneous wound healing. *New Engl J Med*. 341:738-746.

Singh, D., and C. Pohl. 2014a. Coupling of rotational cortical flow, asymmetric midbody positioning, and spindle rotation mediates dorsoventral axis formation in C. elegans. *Developmental cell*. 28:253-267.

Singh, D., and C. Pohl. 2014b. A function for the midbody remnant in embryonic patterning. *Communicative & integrative biology*. 7:e28533.

Skop, A.R., H.B. Liu, J. Yates, B.J. Meyer, and R. Heald. 2004. Dissection of the mammalian midbody proteome reveals conserved cytokinesis mechanisms. *Science*. 305:61-66.

Slautterback, D.B., and D.W. Fawcett. 1959. The development of the cnidoblasts of Hydra; an electron microscope study of cell differentiation. *The Journal of biophysical and biochemical cytology*. 5:441-452.

Smith, B.E., and R.E. Braun. 2012. Germ cell migration across Sertoli cell tight junctions. *Science*. 338:798-802.

Somers, W.G., and R. Saint. 2003. A RhoGEF and Rho family GTPase-activating protein complex links the contractile ring to cortical microtubles at the onset of cytokinesis. *Developmental cell*. 4:29-39.

Somma, M.P., B. Fasulo, G. Cenci, E. Cundari, and M. Gatti. 2002. Molecular dissection of cytokinesis by RNA interference in Drosophila cultured cells. *Molecular biology of the cell*. 13:2448-2460.

Sotillo, R., E. Hernando, E. Diaz-Rodriguez, J. Teruya-Feldstein, C. Cordon-Cardo, S.W. Lowe, and R. Benezra. 2007. Mad2 overexpression promotes aneuploidy and tumorigenesis in mice. *Cancer cell*. 11:9-23.

Steigemann, P., and D.W. Gerlich. 2009. Cytokinetic abscission: cellular dynamics at the midbody. *Trends in cell biology*. 19:606-616.

Steigemann, P., C. Wurzenberger, M.H. Schmitz, M. Held, J. Guizetti, S. Maar, and D.W. Gerlich. 2009. Aurora B-mediated abscission checkpoint protects against tetraploidization. *Cell*. 136:473-484.

Straight, A.F., A. Cheung, J. Limouze, I. Chen, N.J. Westwood, J.R. Sellers, and T.J. Mitchison. 2003. Dissecting temporal and spatial control of cytokinesis with a myosin II Inhibitor. *Science*. 299:1743-1747.

Straight, A.F., C.M. Field, and T.J. Mitchison. 2005. Anillin binds nonmuscle myosin II and regulates the contractile ring. *Molecular biology of the cell*. 16:193-201.

Strome, S. 1986. Fluorescence visualization of the distribution of microfilaments in gonads and early embryos of the nematode Caenorhabditis elegans. *The Journal of cell biology*. 103:2241-2252.

Sulston, J.E. 1983. Neuronal cell lineages in the nematode Caenorhabditis elegans. *Cold Spring Harbor symposia on quantitative biology*. 48 Pt 2:443-452.

Sulston, J.E., and H.R. Horvitz. 1977. Post-embryonic cell lineages of the nematode, Caenorhabditis elegans. *Developmental biology*. 56:110-156.

Sulston, J.E., E. Schierenberg, J.G. White, and J.N. Thomson. 1983. The embryonic cell lineage of the nematode *Caenorhabditis elegans*. *Dev Biol*. 100:64-119.

Sun, L.F., R.F. Guan, I.J. Lee, Y.J. Liu, M.R. Chen, J.W. Wang, J.Q. Wu, and Z.C. Chen. 2015. Mechanistic Insights into the Anchorage of the Contractile Ring by Anillin and Mid1. *Developmental cell*. 33:413-426.

Swan, K.A., A.F. Severson, J.C. Carter, P.R. Martin, H. Schnabel, R. Schnabel, and B. Bowerman. 1998. cyk-1: a C. elegans FH gene required for a late step in embryonic cytokinesis. *Journal of cell science*. 111 (Pt 14):2017-2027.

Tan, C., B. Stronach, and N. Perrimon. 2003. Roles of myosin phosphatase during Drosophila development. *Development*. 130:671-681.

Tatsumoto, T., X. Xie, R. Blumenthal, I. Okamoto, and T. Miki. 1999. Human ECT2 is an exchange factor for Rho GTPases, phosphorylated in G2/M phases, and involved in cytokinesis. *The Journal of cell biology*. 147:921-928.

Tatusova, T.A., and T.L. Madden. 1999. BLAST 2 Sequences, a new tool for comparing protein and nucleotide sequences. *FEMS microbiology letters*. 174:247-250.

Tcherkezian, J., and N. Lamarche-Vane. 2007. Current knowledge of the large RhoGAP family of proteins. *Biology of the cell / under the auspices of the European Cell Biology Organization*. 99:67-86.

Thomas, J.H., and E. Wieschaus. 2004. src64 and tec29 are required for microfilament contraction during Drosophila cellularization. *Development*. 131:863-871.

Tian, D., M. Diao, Y. Jiang, L. Sun, Y. Zhang, Z. Chen, S. Huang, and G. Ou. 2015. Anillin Regulates Neuronal Migration and Neurite Growth by Linking RhoG to the Actin Cytoskeleton. *Current biology : CB*. 25:1135-1145.

Tilney, L.G., M.S. Tilney, and G.M. Guild. 1996. Formation of actin filament bundles in the ring canals of developing Drosophila follicles. *The Journal of cell biology*. 133:61-74.

Triplet, C.V., M.J. Garcia, H.H. Bik, D. Beaudet, and A. Piekny. 2014. Anillin interacts with microtubules and is part of the astral pathway that defines cortical domains. *Journal of cell science*. 127:3699-3710.

Tse, Y.C., A. Piekny, and M. Glotzer. 2011. Anillin promotes astral microtubule-directed cortical myosin polarization. *Molecular biology of the cell*. 22:3165-3175.

Unhavaithaya, Y., and T.L. Orr-Weaver. 2012. Polyploidization of glia in neural development links tissue growth to blood-brain barrier integrity. *Genes & development*. 26:31-36.

Urbisz, A.Z., L. Chajec, and P. Swiatek. 2015. The Ovary of Tubifex tubifex (Clitellata, Naididae, Tubificinae) Is Composed of One, Huge Germ-Line Cyst that Is Enriched

with Cytoskeletal Components. *PloS one*. 10:e0126173.
Vale, R.D., J.A. Spudich, and E.R. Griffis. 2009. Dynamics of myosin, microtubules, and Kinesin-6 at the cortex during cytokinesis in Drosophila S2 cells. *The Journal of cell biology*. 186:727-738.
Ventela, S., J. Toppari, and M. Parvinen. 2003. Intercellular organelle traffic through cytoplasmic bridges in early spermatids of the rat: mechanisms of haploid gene product sharing. *Molecular biology of the cell*. 14:2768-2780.
Vidulescu, C.F., S. Clejan, and K. O'Connor. 2005. Vesicle traffic through intercellular bridges in DU145 human prostate cancer cells. *Faseb J*. 19:A822-A822.
Vitrat, N., K. Cohen-Solal, C. Pique, J.P. Le Couedic, F. Norol, A.K. Larsen, A. Katz, W. Vainchenker, and N. Debili. 1998. Endomitosis of human megakaryocytes are due to abortive mitosis. *Blood*. 91:3711-3723.
Vogel, B.E., and E.M. Hedgecock. 2001. Hemicentin, a conserved extracellular member of the immunoglobulin superfamily, organizes epithelial and other cell attachments into oriented line-shaped junctions. *Development*. 128:883-894.
von Dassow, G., K.J.C. Verbrugghe, A.L. Miller, J.R. Sider, and W.M. Bement. 2009. Action at a distance during cytokinesis. *Journal of Cell Biology*. 187:831-845.
von Schwedler, U.K., M. Stuchell, B. Muller, D.M. Ward, H.Y. Chung, E. Morita, H.E. Wang, T. Davis, G.P. He, D.M. Cimbora, A. Scott, H.G. Krausslich, J. Kaplan, S.G. Morham, and W.I. Sundquist. 2003. The protein network of HIV budding. *Cell*. 114:701-713.
Wang, J.T., and G. Seydoux. 2013. Germ cell specification. *Adv Exp Med Biol*. 757:17-39.
Watanabe, N., T. Kato, A. Fujita, T. Ishizaki, and S. Narumiya. 1999. Cooperation between mDia1 and ROCK in Rho-induced actin reorganization. *Nat Cell Biol*. 1:136-143.
Watson, E.D., and J.C. Cross. 2005. Development of structures and transport functions in the mouse placenta. *Physiology*. 20:180-193.
Weber, J.E., and L.D. Russell. 1987. A study of intercellular bridges during spermatogenesis in the rat. *The American journal of anatomy*. 180:1-24.
Weng, J., D.N. Krementsov, S. Khurana, N.H. Roy, and M. Thali. 2009. Formation of syncytia is repressed by tetraspanins in human immunodeficiency virus type 1-producing cells. *Journal of virology*. 83:7467-7474.
Werner, M., and M. Glotzer. 2008. Control of cortical contractility during cytokinesis. *Biochemical Society transactions*. 36:371-377.
Werner, M., E. Munro, and M. Glotzer. 2007. Astral signals spatially bias cortical myosin recruitment to break symmetry and promote cytokinesis. *Current biology : CB*. 17:1286-1297.
White, E.A., and M. Glotzer. 2012. Centralspindlin: At the Heart of Cytokinesis. *Cytoskeleton*. 69:882-892.
White, J.G. 1985. The Astral Relaxation Theory of Cytokinesis Revisited. *Bioessays*. 2:267-272.
Wilson, G.M., A.B. Fielding, G.C. Simon, X. Yu, P.D. Andrews, R.S. Hames, A.M. Frey, A.A. Peden, G.W. Gould, and R. Prekeris. 2005. The FIP3-Rab11 protein complex regulates recycling endosome targeting to the cleavage furrow during late cytokinesis. *Molecular biology of the cell*. 16:849-860.
Wilson, R.K. 1999. How the worm was won. The C. elegans genome sequencing project. *Trends in genetics : TIG*. 15:51-58.
Witkin, J.W., H. O'Sullivan, and A.J. Silverman. 1995. Novel associations among

gonadotropin-releasing hormone neurons. *Endocrinology*. 136:4323-4330.
Wolke, U., E.A. Jezuit, and J.R. Priess. 2007. Actin-dependent cytoplasmic streaming in C. elegans oogenesis. *Development*. 134:2227-2236.
Wollert, T., C. Wunder, J. Lippincott-Schwartz, and J.H. Hurley. 2009a. Membrane scission by the ESCRT-III complex. *Nature*. 458:172-U172.
Wollert, T., D. Yang, X.F. Ren, H.H. Lee, Y.J. Im, and J.H. Hurley. 2009b. The ESCRT machinery at a glance. *Journal of cell science*. 122:2163-2166.
Wolpert, L. 1960. The Mechanics and Mechanism of Cleavage. *International Review of Cytology-a Survey of Cell Biology*. 10:163-216.
Woodruff, R.I., and L.G. Tilney. 1998. Intercellular bridges between epithelial cells in the Drosophila ovarian follicle: a possible aid to localized signaling. *Developmental biology*. 200:82-91.
Wu, J.Q., and T.D. Pollard. 2005. Counting cytokinesis proteins globally and locally in fission yeast. *Science*. 310:310-314.
Xu, X., and B.E. Vogel. 2011. A secreted protein promotes cleavage furrow maturation during cytokinesis. *Current biology : CB*. 21:114-119.
Yamamoto, S., V. Bayat, H.J. Bellen, and C. Tan. 2013. Protein phosphatase 1ss limits ring canal constriction during Drosophila germline cyst formation. *PloS one*. 8:e70502.
Yang, D., N. Rismanchi, B. Renvoise, J. Lippincott-Schwartz, C. Blackstone, and J.H. Hurley. 2008. Structural basis for midbody targeting of spastin by the ESCRT-III protein CHMP1B. *Nature structural & molecular biology*. 15:1278-1286.
Yonemura, S., K. Hirao-Minakuchi, and Y. Nishimura. 2004. Rho localization in cells and tissues. *Experimental cell research*. 295:300-314.
Yoshizaki, H., Y. Ohba, M.C. Parrini, N.G. Dulyaninova, A.R. Bresnick, N. Mochizuki, and M. Matsuda. 2004. Cell type-specific regulation of RhoA activity during cytokinesis. *The Journal of biological chemistry*. 279:44756-44762.
Yuce, O., A. Piekny, and M. Glotzer. 2005. An ECT2-centralspindlin complex regulates the localization and function of RhoA. *Journal of Cell Biology*. 170:571-582.
Yue, L., and A.C. Spradling. 1992. hu-li tai shao, a gene required for ring canal formation during Drosophila oogenesis, encodes a homolog of adducin. *Genes & development*. 6:2443-2454.
Yumura, S., M. Ueda, Y. Sako, T. Kitanishi-Yumura, and T. Yanagida. 2008. Multiple mechanisms for accumulation of myosin II filaments at the equator during cytokinesis. *Traffic*. 9:2089-2099.
Zak, R. 1974. Development and proliferative capacity of cardiac muscle cells. *Circulation research*. 35:suppl II:17-26.
Zamboni, L., and B. Gonndos. 1968. Intercellular bridges and synchronization of germ cell differentiation during oogenesis in the rabbit. *The Journal of cell biology*. 36:276-282.
Zang, J.H., G. Cavet, J.H. Sabry, P. Wagner, S.L. Moores, and J.A. Spudich. 1997. On the role of myosin-II in cytokinesis: division of Dictyostelium cells under adhesive and nonadhesive conditions. *Molecular biology of the cell*. 8:2617-2629.
Zeldovich, V.B., C.H. Clausen, E. Bradford, D.A. Fletcher, E. Maltepe, J.R. Robbins, and A.I. Bakardjiev. 2013. Placental syncytium forms a biophysical barrier against pathogen invasion. *PLoS pathogens*. 9:e1003821.
Zhang, H., Y. Wang, J.J. Wong, K.L. Lim, Y.C. Liou, H. Wang, and F. Yu. 2014a. Endocytic pathways downregulate the L1-type cell adhesion molecule neuroglian to promote

dendrite pruning in Drosophila. *Developmental cell*. 30:463-478.
Zhang, L., and A.S. Maddox. 2010. Anillin. *Current biology : CB*. 20:R135-136.
Zhang, S., I. Mercado-Uribe, Z. Xing, B. Sun, J. Kuang, and J. Liu. 2014b. Generation of cancer stem-like cells through the formation of polyploid giant cancer cells. *Oncogene*. 33:116-128.
Zhao, W.M., and G. Fang. 2005. Anillin is a substrate of anaphase-promoting complex/cyclosome (APC/C) that controls spatial contractility of myosin during late cytokinesis. *The Journal of biological chemistry*. 280:33516-33524.
Zhao, W.M., A. Seki, and G. Fang. 2006. Cep55, a microtubule-bundling protein, associates with centralspindlin to control the midbody integrity and cell abscission during cytokinesis. *Molecular biology of the cell*. 17:3881-3896.
Zhou, K., M.M. Rolls, and W. Hanna-Rose. 2013. A postmitotic function and distinct localization mechanism for centralspindlin at a stable intercellular bridge. *Developmental biology*. 376:13-22.
Zhou, M., and Y.L. Wang. 2008. Distinct pathways for the early recruitment of myosin II and actin to the cytokinetic furrow. *Molecular biology of the cell*. 19:318-326.